MULTI PHASE NUMERICAL MODELLING OF THICKENING AND SEDIMENTATION

BY

CHRISTOPHER JOHN BAILEY
BSc (Honours)

Thesis submitted to the Council for National Academic Awards in partial fulfilment of the requirements for the Degree of Doctor of Philosophy.

Centre for Numerical Modelling and Process Analysis
School of Mathematics, Statistics and Computing
Thames Polytechnic
London.

In collaboration with
Department of Trade and Industry, Warren Springs Laboratories.

JULY 1988

CONTENTS

ABSTRACT

Phenomena that involve the settling of particulates in a host fluid are encountered in many practical systems which find applications in many areas of industry. A numerical model has been developed to simulate the settlement of non-flocculated and flocculated particulate suspensions in batch sedimentation. The non flocculated mode of the model is extended to predict the performance of a continuous gravity thickener.

The various particle species within the particulate suspension are represented as separate phases with distinct concentrations and velocities. A multiphase representation of the settling process gives greater detail of the interactions present between the particulates. The build up of the sediment as well as a prediction of the compression point, for flocculated suspensions, is modelled using a revised version of packing theory. The build up of flocs in the free settling region is incorporated via population balances.

Also, as well as the above theoretical work, experimentwal work has been undertaken to obtain data for non-flocculated suspensions. For batch sedimentation this data is in the form of density profiles and for the continuous thickener it is in the form of concentration profiles. The proposed model compares favourably with this experimental data and gives closer predictions than does a model representing the state of the art, at this point in time, for non-flocculated batch sedimentation.

ACKNOWLEDGEMENTS

I would like to express my gratitude to Professor Mark Cross and Dr Dilwyn Edwards for their help and guidance throughout this project.

I also wish to thank Dr Peter Tucker and Phil Parsonage who helped me with the experimental work. I would also like to acknowledge the financial and experimental support of Warren Spring Laboratory through a SERC-CASE studentship.

My sincerest thanks go to my family and friends for all their help and encouragement.

Finally, many thanks to Edie McFall for the typing of this thesis.

CHAPTER ONE

INTRODUCTION

1.1 Sedimentation and Thickening

Solid-liquid separation has widespread applications in the industrial world. Examples of some processes which involve solid-liquid separation are:-

1) Sedimentation and thickening.
2) Centrifugation.
3) Hydrocyclones.
4) Flotation.

All the above processes involve the movement of solids and liquid due to an applied force acting on these phases. The process of importance with regards to this thesis is "Sedimentation and Thickening". Sedimentation involves the movement of particulates in a host fluid due to the action of gravity. Thickening involves sedimentation and compaction taking place in a large circular tank containing a particulate slurry. The compaction occurs in the sediment region, at the base of the tank, which may be compressible or incompressible depending on the nature of the particulate slurry. To increase the rate of thickening and to enable very fine particulates to settle, flocculants are used. Flocculants are chemicals which break down the repulsive forces between particles and build bridges linking the particles. This enables particles to agglomerate and settle as larger masses known as flocs. Thickening is a favoured method of large scale dewatering because of its cost and simplicity. The main design requirement of a thickener is its surface area, this must be large enough to enable solids throughput so that solids do not build up in the thickener and, hence, appear in the overflow. To enable greater compaction of the sediment, depth is also said to be important. Over the last ten years major advances have taken place in this field which include; improvements in synthetic

flocculants, better thickener designs and a greater understanding of the principles involved.

1.2 Literature Review

There have been numerous experimental and theoretical investigations into the sedimentation of particles in a fluid. The first analysis was by Stokes (1851) who observed the rate of fall of a single spherical particle in a quiescent Newtonian fluid at low Reynolds number which led to his well-known law:

$$U_t = \frac{d^2(\rho_s - \rho_f)g}{18\mu_f} \qquad (1.1)$$

where U_t is the terminal velocity of a sphere, d its diameter, ρ_s its density, ρ_f the fluid density, μ_f the fluid viscosity and g the gravitational constant. For solid concentrations, by volume, above 1% the average settling velocity of the monodispersed suspension will be noticeably lower than that predicted by equation (1.1). This is due to a phenomena known as hindered settling. This effect is incorporated by multiplying equation (1.1) by a hindered settling function to give the solids velocity. Two of the most widely used empirical functions are those by Richardson and Zaki (1954) and Barnea (1973). Richardson and Zaki proposed the following correlation between μ_t and solids velocity, U_s;

$$\frac{U_s}{U_t} = (1-S)^n \qquad (1.2)$$

where S is solids concentration and n is a value dependent on Reynolds number. Barnea (1973) gave the following explanation for hindrance:

1) HYDROSTATIC EFFECT: The suspension density is greater than that of the fluid alone and consequently the buoyancy force is greater. Therefore the suspension density should be used in equation (1.1.) instead of the fluid density.

2) MOMENTUM TRANSFER EFFECT: The presence of other particles effects the transfer of momentum between each particle and the fluid. This effect is related to the "apparent" bulk viscosity of the suspension.

Barnea (1973) related solids velocity and terminal velocity using the above effects. The momentum transfer effect is incorporated by using a relationship between suspension and fluid viscosities.

The majority of particulate mixtures are not monodispersed as they contain particles of different sizes, density and shape. These polydispersed mixtures have been modelled by Lockett and Al-Habbooby (1973, 1974) who carried out experiments on binary particulate mixtures. They used the monodispersed Richardson and Zaki (1954) correlation to predict the solids velocity of each phase where the total particle concentration is used to correct the terminal velocity of each phase as predicted by equation (1.1). Mirza and Richardson (1979) extended the Lockett and Al-Habbooby model to predict the sedimentation of multisized particle systems. They compared their model predictions with experimental results in the form of velocity against voidage plots. As with the Lockett and Al-Habbooby comparisons they found that the model overpredicted sedimentation velocities. To remedy this effect they applied a correction factor of $(\text{voidage})^{0.4}$ to the velocities, this gave satisfactory comparisons with their experimental results. In a similar study Selim et al (1983) proposed that the Stokes velocity of phase i, say, should be modified by replacing the fluid density in equation (1.1)

by the average density of a suspension consisting of fluid and particles of size smaller than i. Obviously this is only valid for multisized systems but Selim obtained good comparisons between his experimental results and model predictions. For a polydisperse system the settling of the suspension will result in the formation of distinct zones. The lowest zone just above the sediment containing all particulate phases at their initial concentrations, with each successive region above containing one fewer phase than the zone below (i.e. fastest settling phase. The above models use the Richardson and Zaki empirical correlation and mass balances to calculate, iteratively, the velocity and solids concentrations of each phase in each zone. In these models no account is taken of the sediment build up at the base. In a short communication Masliyah (1979) extended the governing equation for hindered settling to incorporate different densities as well as sizes. He proposed the use of the total suspension density instead of the fluid density in the buoyancy term and suggested the use of the Richardson and Zaki (1954) or the Barnea (1973) correlations for the momentum transfer effects. Unfortunately no detailed comparisons with experimental data was made but the use of the suspension density instead of the fluid density is obviously a correct assumption. This has been a debating point in the literature for many years but its obvious that the buoyancy is not caused by the density difference between the suspended particles and surrounding fluid, but is the result of the imbalance between the pressures exerted on each of the settling units by the fluid, which is a verticle hydraulic pressure gradient. In a suspension this gradient is determined by the suspension density and not by the fluid density. The effect of buoyancy is less than that of structure which is determined essentially by the suspension viscosity. Barnea (1973) gave a detailed review of suspension viscosity models and also proposed his own which is used in this thesis.

The design of thickeners is based on calculating the unit area. This is the surface area of a thickener required to handle unit weight of solids in unit time, or simply the area per unit throughout required to give a specified dewatering. The principle investigators into thickener design were Coe and Clevenger (1916). The objective of their work was to present a method to calculate the area of a thickener from batch sedimentation tests. This test consists of filling a glass tube with slurry at known concentration and letting the solids settle. For steady state continuous thickening Coe and Clevenger derived the following formula:

$$G = \frac{U}{\frac{1}{S} - \frac{1}{S_u}} \qquad (1.3)$$

where G is the solids handling capacity or the flux of solids moving towards the underflow, S is the solids concentration of a batch test, U its settling velocity and S_u is the solids concentration at the thickener underflow. The method requires that pulps of various concentrations between the thickener feed and underflow be prepared as batch tests in sedimenting columns. These suspensions are allowed to settle and the rate of fall of the supernatant/pulp interface is noted. Using equation (1.3) a flux against concentration plot can be constructed. The minimum value of flux is taken as the solids handling capacity of the thickener and used in the design. The thickener area can be calculated from this flux value, where flux is defined as thickener feed rate divided by surface area. This approach makes the following assumptions:

1) No segregation occurs.
2) Most flux limiting concentration lies in the free settling zone.

3) Solids velocity is independent of concentration.

The Coe and Clevenger (1916) method held favour for nearly forty years until Kynch (1952) produced his mathematical analysis of the batch settling curve. Kynch based his analysis on the same assumptions as above and concluded that concentrations would propogate upwards from the bottom of a suspension, each at it own constant velocity equal to the tangent of the batch-flux curve at that concentration. He further showed that the settling velocities of higher concentrations could be obtained from the batch settling curve of a suspension initially at a uniform lower concentration. The batch settling curve being a plot of supernatant/pulp interfce height against time. Talmage and Fitch (1955) used Kynch's mathematics to estimate thickener area from a batch settling curve. The curve is obtained from a batch test whose initial slurry concentration is equal to that of the thickener feed. This is a graphical technique which requires locating the compression point on the batch settling curve and drawing a tangent to it. From this both the limiting concentration and its settling velocity can be calculated. Using equation (1.3) the corresponding solids handling capacity is calculated from which the thickener area is estimated. The Talmage and Fitch model shows a definite improvement over Coe and Clevenger in that it is experimentally simpler with all data being obtained from one batch settling curve. The concensus of opinion, Pearce (1977), is that the Talmage and Fitch procedure overpredicts thickener area while the Coe and Clevenger method underpredicts thickener area. Therefore it is safer to use Talmage and Fitch's methods as this ensures throughput and no presence of solids in the overflow of the thickener.

Kynch's (1952) analysis has become the basis of the solids flux theory of which graphical techniques based on the batch settling curve (Talmage

and Fitch (1955)), and the batch flux curve, (Yoshioka (1957) and Hassett (1965)), have been proposed. The major drawback with these techniques is that they rely on the assumptions that solids velocity is a unique function of solids concentration. This certainly is not the case with flocculated pulps although it may be true for some metallurgical suspensions, Holdich (1983).

For flocculated suspensions particles collide and some agglomeration may occur causing flocs to form. Michaels and Bolger (1962) correlated experimental data by means of a modified form of the Richardson and Zaki (1954) equation. They assumed that each floc was spherical in shape and that water within the floc moved with it. Based on these assumptions the movement of flocs in the free settling region are expected to follow equation (1.2); but with solids concentration replaced by floc concentration and solids density replaced by floc density. This equation is valid in the free settling region but does not take into account floc formation and is invalid in the compression zone where flocs lose their individual identity and become part of a compressible structure. In the compression region Michaels and Bolger (1962) used a concept similar to the Terzargi soil consolidation model to develop a model predicting the subsidence rate in the compression zone. They assume that the compressing pulp will have a resistivity and compressive yield which are both dependent on solids concentration.

Shirato et al (1970) confirmed experimentally the assumption that solids pressure is dependent on solids concentration only. For permeability he assumed the Kozeny relationship and obtained good comparisons between predicted and measured concentration profiles for ferric oxide and zinc oxide suspensions. Kos (1974) reflected the assumption that permeability was a function of concentration and dynamic pressure. He

also found that solids pressure is approximately proportional to solids concentration.

Gaudin and Fuerstenau (1962) carried out experiments on flocculated Kaolin suspension; for the compression regime they applied Poiseuilles law to the flow of liquid through pores in the pulp. The pores were considered to have a size distribution given by a Schuhmann (1940) distribution. This model requires knowledge of the number and sizes of the pores present in a pulp and is therefore difficult to apply.

Coe and Clevenger (1916) observed the subsidence rate for pulps having concentrations in the compression regime. They deduced that compaction was a function of time; a conclusion which is now known to be invalid, Fitch (1975). Dell and Keleghan (1973) used a cleverly designed pressure measuring method to show that solids velocity was not dependent on solids concentration for flocculated material. They found that the mass of material above a fixed height did not fall off linearly as predicted by Coe and Clevenge (1916) and Kynch (1952), but exponentially. Dick (1967) suggested a deviation factor from ideality, the retardation factor, which varies exponentially with solids concentration. Dick (1972) also emphasised the point that for compressible pulps the effects of sedimentation and compaction must be combined in order to understand performance.

Adorjan (1975) also assumed solids pressure and permeability to be dependent on solids concentration. With the assumption that no segregation is present and that permeability is obtained from compression permeability cell tests, Adorjan used his theory to predict thickener unit areas via numerical integration to obtain height concentration profiles.

Dixon (1977, 1978) proposed the use of a force balance approach as well as mass balances for the fluid and particulate phases present in non-flocculated and flocculated systems. He assumed the presence of only one solid phase and discussed the forces present in the system. He concluded that: "There is no solids flux limitation associated with the free settling zone in a continuous gravity thickener". Holdich (1983) carried out experiments to obtain concentration profiles for the settlement of both flocculated and non-flocculated suspensions. He used the force balance approach proposed by Dixon to assess the relevance and completeness of the constituent terms. He assumed no segregation to take place and proposed an extra term known as transient solids pressure to be present throughout the suspension. This term is introduced to explain why concentration gradients are present in the free settling region. Via his experimental results he concludes that the commonly made assumption of solids pressure being dependent on solids concentration is too simplistic.

Fitch (1983), Tiller (1981) and Concha (1987) revised the classical Kynch theory to be valid for compressible suspensions. Fitch and Tiller both propose alternative graphical procedures to obtain suspension concentrations and their corresponding settling velocities. Concha reports that both the Fitch and Tiller revisions violate the fundamentals of the Kynch theory. Concha used a numerical procedure incorporating a solids pressure term, dependent on solids concentration, beyond the compression regime. Using this procedure he obtains solids concentrations over time throughout a batch vessel. As with all other authors he assumes that no segregation occurs in the free settling region.

Although thickener throughput is controlled by area it is believed that underflow concentration is determined by thickener depth. Talmage and Fitch (1955) extended their graphical procedure to predict thickener depth needed to give a desired underflow. Pearce (1977) reports that this method may give unrealistic results and states the "three foot rule", which states that if the predicted depth is over 3ft then the area is increased so that the depth is equal to 3ft. This gives underflow concentrations closer to those predicted by the Talmage and Fitch (1955) compression test. This is adequate for most metallurgical operations but fails for flocculated suspensions and at this point in time no sound theory for the effects of depth has been developed, Pearce (1977).

As can be deduced from the above review a lot of controversy still exists as to the principles governing sedimentation and thickening, especially for compressible suspensions. Although much research has been undertaken the operation of a thickener remains more of an art than a science and there is still a need for models and techniques which can be used to predict thickener performance.

1.3 Aims of Research

The thickening of a particulate slurry is essentially a multiphased phenomena. Particles of different sizes, shapes and densities may be present and their rate of settlement and compaction characteristics will be dependent on these values. Further, the effect of flocculation will give rise to the formation of flocs which will have distinct sizes, shapes and densities. The work of thickening and sedimentation, to date, has mostly been undertaken to investigate either the free settling region or the sediment region. For batch sedimentation the vast majority of work is based on the empirical correlations between solids

settling velocity and solids terminal velocity. No account in these models is made of where the sediment interface is (i.e. the compression point). Also the internal structure of the sediment and the changes in it during sediment build up are ignored. For flocculated slurries no model exists which predicts floc build up in the free settling zone, it is always assumed that flocs exist of unique size, shape and density. in the case of thickener design the majority of methods are graphical in nature and are based on the batch settling curve. Once again these methods do not predict sediment characteristics and are obviously limited in their use.

The main aim of this research is to develop a numerical model that will represent thickening and sedimentation in much greater detail than models presently used. This is achieved by breaking down the solids distribution in the slurry into a number of distinct phases and also predicting sediment build up using a revised version of packing theory. This model will have three modes of operation:

1) Non Flocculated Batch Sedimentation.
2) Non Flocculated Continuous Gravity Thickening.
3) Flocculated Batch Sedimentation.

The simplest type of model is for mode (1), above, where the other two modes are simply extensions of this model. Using the force balance approach where each solid phase has associated with it equations of mass and momentum, these extensions involve changing and adding terms to the basic transport equations representing each phase present in the system. In addition to the theoretical work, another aim of this research is to obtain good quality experimental data. This will enable verification of the proposed models. Also compared with some of the experimental data

are predictions by the Selim (1983) model which represents one of the better models for batch sedimentation. This model has been extended to cope with multidensity as well as multisized suspensions.

CHAPTER TWO

EXPERIMENTAL METHOD FOR NON FLOCCULATED BATCH SEDIMENTATION

2.1 Introduction

Experimental work into the sedimentation of non-flocculated slurry's has been undertaken by a number of authors, although the amount of useful data especially for this study is limited. Two types of experimental technique can be employed:

1) Direct measurements; where the slurry has to be disturbed.
2) Indirect measurements; where data is recorded without disturbing the slurry.

Direct measurements involve obtaining samples throughout the vessel. This will enable concentrations to be calculated at different locations in the vessel. To understand the full settling behaviour of the slurry undergoing batch sedimentation the experiment must be repeated several times, under identical conditions, so that samples can be obtained at different points in time. This procedure is prone to large errors.

Indirect measurements obtain data (i.e. concentrations, velocities, density changes, etc) predicting the settling behaviour using devices that do not disturb the settling process. A major amount of the experimental work into sedimentation of non-flocculated slurry's has been to obtain the velocities at which each zone in the free settling region descends, see Davies (1968), Mirza (1978) and Selim (1983). This involves colouring each size fraction and recording the rate of fall of each zone (i.e. the velocity of the fastest phase present in each zone) throughout the experiment. Concentration profiles have also been obtained using electrical conductivity, see Holdich (1983). The aim of the following study is to use pressure transducers to obtain density changes during the sedimentation of a multiphase particulate mixture.

2.2 Apparatus used

The experimental setup, see figure 2.1, consists of a perspex tube, eight pressure transducers, a voltmeter, a junction box and a two pen plotter. The perspex tube, see figure 2.2, is of height 60cm and internal diameter 5.2cm. Measuring tape is fixed to the outside of the tube. Before the transducers could be used each was subjected to a vacuum and soaked overnight in water. This eliminates any trapped air, which due to its compressibility would enable the transducer to give erroneous results. The transducers are inserted, using silicon rubber, into holes situated at 5cm intervals from the base of the tube upwards. The front section of each transducer just protruding into the internal part of the tube. A voltage is applied to the circuit via a voltmeter. The juction box acts as a connection between the voltage input, transducers and plotter. The connections inside the junction box were cleaned and re-soldered before being used. The plotter is able to monitor two transducers at a time and is sensitive down to 0.005mV with 0.5mV F.S.D. (full scale deflection).

2.3 Materials used

Four different solids and three different liquids, see table 2.2 are used. The overall size range of each material used is:

Material	Size range (μ)
Glass (soda) Ballontini	20 - 100μ
Glass (lead) Ballontini	30 - 500μ
Copper	30 - 70μ
Quartz	150 - 250μ.

Table 2.1 Size range of solids.

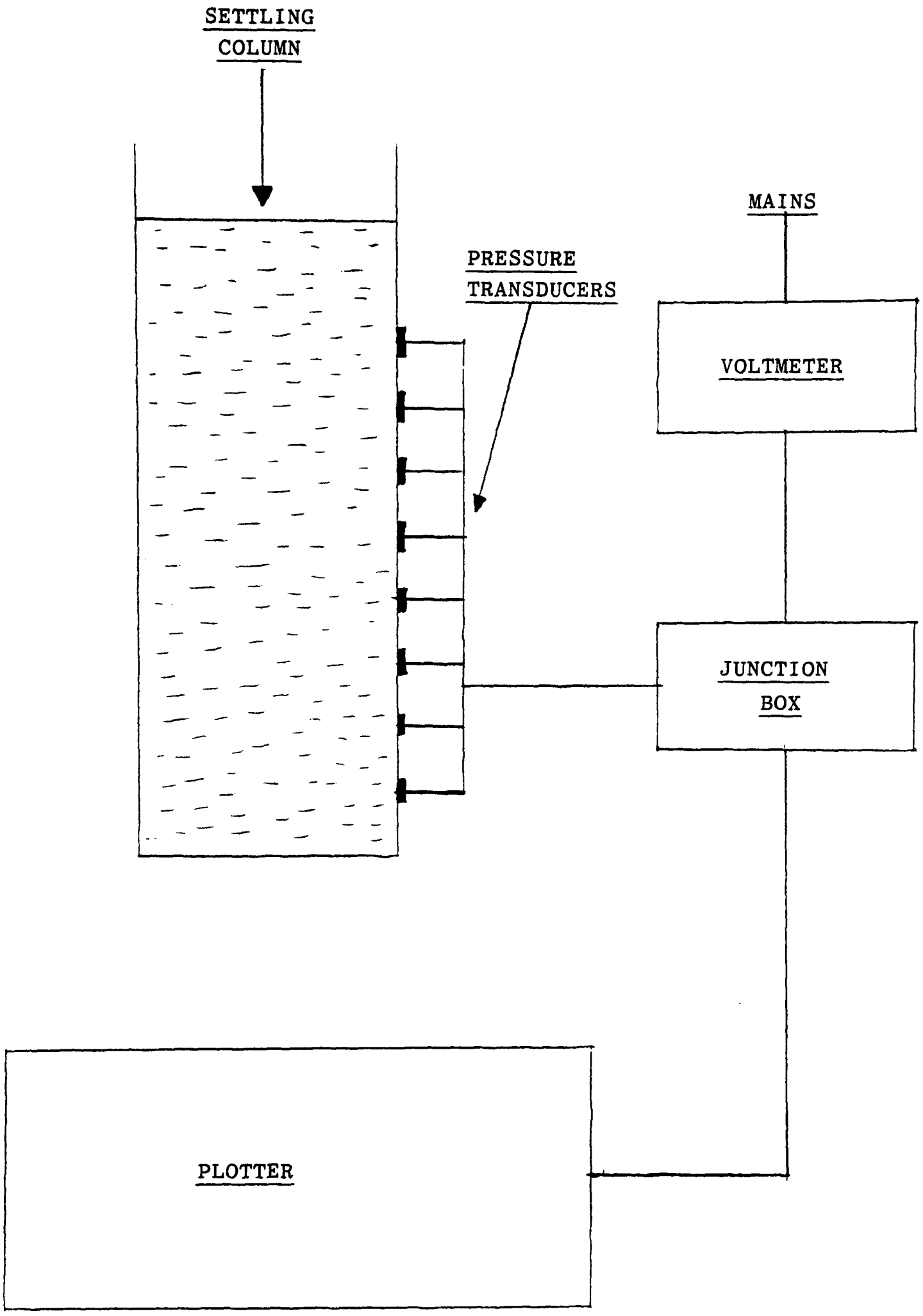

Figure 2.1 Diagram of experimental setup

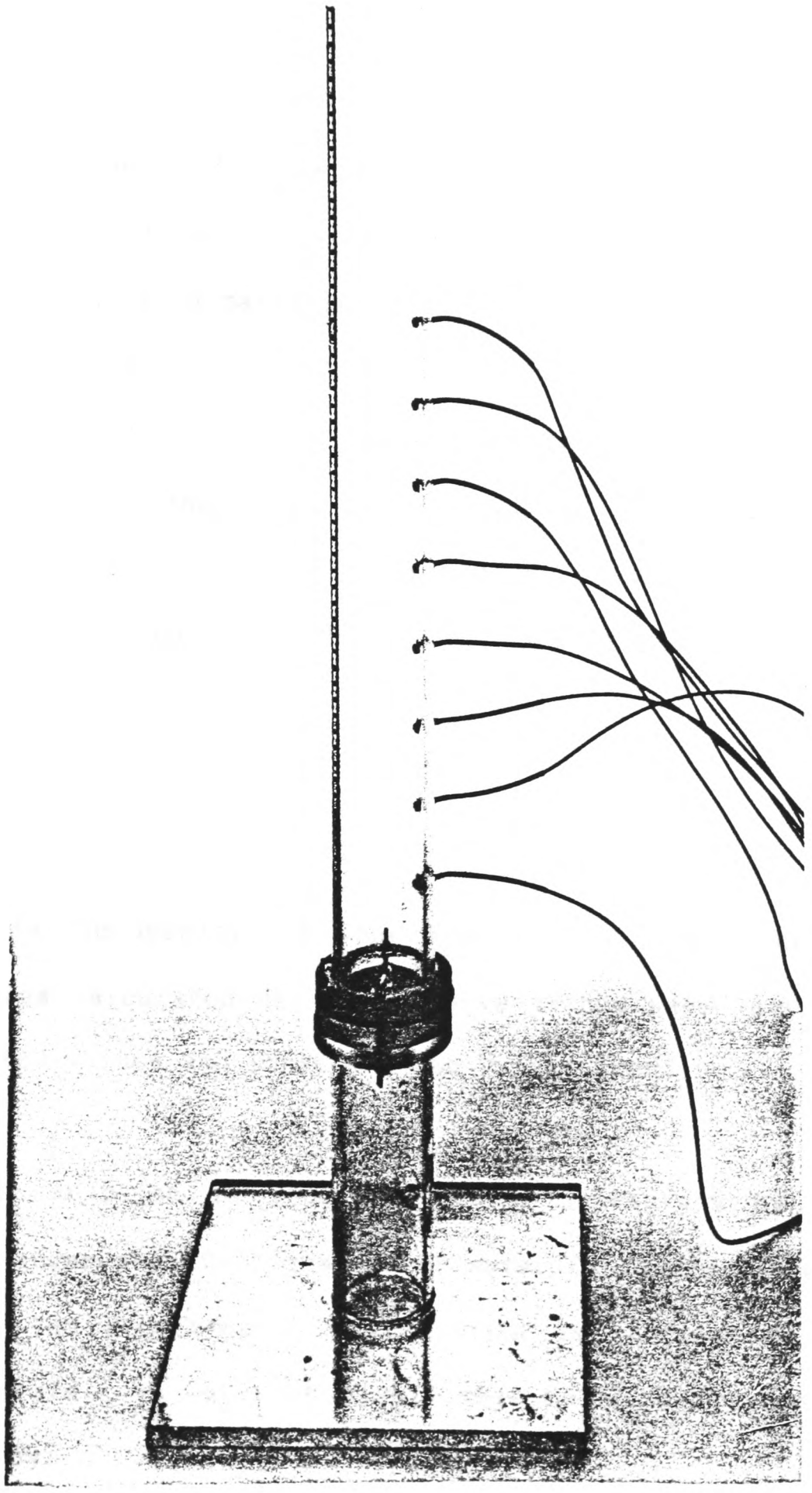

Figure 2.2 Perspex tube with transducers

The shape factor used in this analysis is given by

$$\Phi = \frac{D_e}{D_{AV}} \qquad (2.1)$$

where Φ is the "effective volumetric" shape factor, D_{AV} is the average diameter of the particles and D_e is the diameter of a sphere with volume equal to a particle of diameter D_{AV}. Ballontini and copper are spherical, see figure 2.3, therefore the shape factor is 1·0. Quartz is an angular material and a shape factor commonly used is 0·86, see Cross (1985). The densities for each solid material is calculated using a pycnometer. This device estimates the volume of solid material of known mass in a cup. The density is calculated via

$$\rho = \frac{M}{V} \qquad (2.2)$$

where ρ is the density, M the mass and V the calculated volume. The densities calculated using the above method were very close to the makers quoted values and these are the values used.

The glucose solution is made up in the laboratory by adding 389.8 grammes of sugar and 756.6 grammes of water for every litre of solution required. The densities of each liquid is calculated using a 50cc weighing bottle. The mass of liquid that fully occupies the bottle is calculated by:

Mass of empty bottle = M_1

Mass of full bottle = M_2

Mass of liquid of volume 50cc = $M_2 - M_1$.

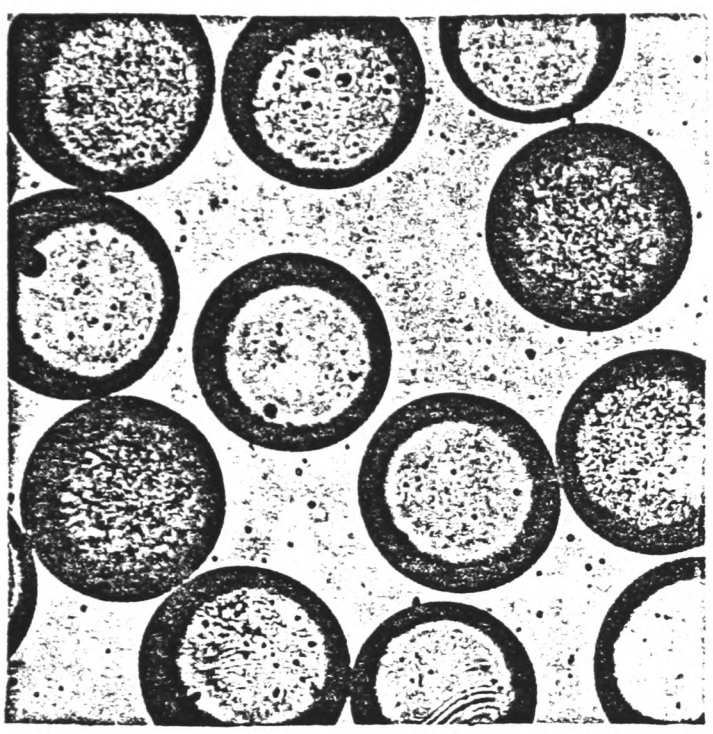

a) Ballontini

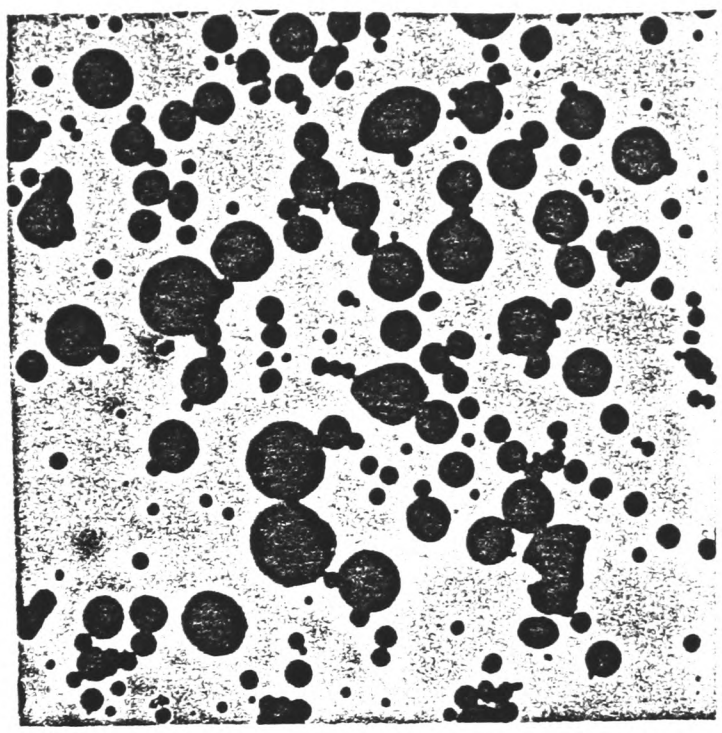

b) Copper

c) Quartz

Figure 2.3 Photomicrographs of solids used for batch sedimentation

The densities are then calculated using equation 2.2. The viscosities are the makers quoted values. All viscosity and density values are at room temperature (i.e. 20°C)

2.4 Experimental procedure

The following procedure will calculate the density changes in the perspex tube due to the movement of the particulates in the fluid particle mixture. For each transducer a linear relationship between pressure and voltage will exist:

$$P = KV + C \tag{2.3}$$

where P is the pressure acting on the transducer, V is the voltage corresponding to this pressure and K,C are constants. The pressure can also be calculated using the effective hydrostatic pressure equation:

$$P = h\rho_B g \tag{2.4}$$

where h is the height of mixture above the transducer, ρ_B the bulk average mixture density and g the gravity constant.

Therefore, given a suspension of uniform concentration (volume fractions) and density throughout, the above relationships, equations (2.3) and (2.4), can be used to find the mixture density above a transducer at different points in time during the settlement of the particulates. The initial mixture density is calculated via:

$$\rho_B = F\rho_f + \sum_{i=1}^{NSOL} S_i\rho_i \tag{2.5}$$

Solid material	Density(Kg/M^3)	Shape factor
Glass (soda) Ballontini	2480	1
Glass (lead) Ballontini	2950	1
Copper	8930	1
Quartz	2600	86

Liquid	Density(Kg/M^3)	Viscosity(Kg/MS)
Water (distilled)	1000	0.001
Diethylene Glycol	1115	0.014
Glucose Solution	1149	0.004

Table 2.2 Material Properties.

where ρ_f is the fluid density and ρ_i is the solid phase density for phase i. F and S_i are the volume fractions for the fluid and solid phases respectively. If the mass of each solid phase in the mixture is M_i and the volume of the fluid, calculated using a 500cc measuring cylinder, is V_F then the total volume of the mixture in the perspex tube is:

$$V_M = V_F + \sum_{i=1}^{NSOL} \frac{M_i}{\rho_i} \qquad (2.6)$$

The solid and fluid volume fractions are calculated via:

$$S_i = \frac{M_i}{\rho_i V_M} \qquad i=1\ldots,NSOL \qquad (2.7)$$

$$F = \frac{V_F}{V_M} \qquad (2.8)$$

Using equations (2.5), (2.6), (2.7) and (2.8) the initial density of the mixture is calculated. The pressure and voltage corresponding to the initial density are calculated using equations (2.3) and (2.4). During the settling process the plotter monitors the decrease in the voltage output from the transducer over time. Using this graphical output and equations (2.3) and (2.4) the decrease in the density of the mixture above the transducer can be calculated.

2.4.1. Calibrations

A 5v voltage is applied to the circuit via the voltmeter for the following calibrations as well as all experimental runs. Each pressure transducer is calibrated to obtain a pressure-voltage relationship.

This involves adding distilled water to the tube and recording the height of water above the transducer as well as the voltage deflection on the plotter. The pressure after each addition of water is calculated using equation (2.4) where ρ_B is the density of water. Applying regression analysis to the pressure, voltage data a linear relationship is obtained, see equation (2.3).

At this point in the analysis it was noticed that only transducers one and four could be measured down to an accuracy of 0.005mv. All other transducers had a measured accuracy down to 0.02mv or higher. This is due to the voltage output being higher for all transducers except one and four. Therefore, to obtain a good degree of accuracy, in interpreting the graphical output, only transducers one and four could be used. For the experimental runs transducer one was exchanged with transducers two and three and recalibrated at these new positions. The pressure-voltage relationships are:

Transducer one:

$$P = 1831V - 11 \qquad (2.9)$$

Transducer one (at second transducer location):

$$P = 1831V - 11 \qquad (2.10)$$

Transducer one (at third transducer location):

$$P = 1781V \qquad (2.11)$$

Transducer four:

$$P = 1818V. \qquad (2.12)$$

2.4.2 Experimental runs

Experimental data has been obtained for a number of one, two and three phase experiments, see tables 2.4, 2.5 and 2.6. Each solid phase is obtained by sieving the solid material. The particle size representing each phase is taken as the mean aperture size of the two sieves used, see table 2.3.

Sieve sizes (μ)	Particle size (μ)	Sieves used
38	41·5	38-45
45	56·5	38-75
63	60	45-75
75	69	63-75
90	76·5	63-90
150	120	90-150
180	200	150-250
250	220	180-250
300	275	250-300
355	302·5	250-355
425	327·5	300-355
500	362·5	300-425
	462·5	425-500.

Table 2.3 Sieve and phase sizes.

ONE PHASE EXPERIMENTS

	SOLID	DIAM(μ)	CONC	LIQUID	TRANSDUCER
Exp one	Glass (lead)	120	0·078	Glycol	one
Exp two	Glass (lead)	275	0·078	Glycol	one
Exp three	Copper	56·5	0·0138	Glycol	two
Exp four	Glass (lead)	275	0·078	Glycol	three
Exp five	Glass (lead)	275	0·1128	Glycol	three
Exp six	Glass (lead)	275	0·25	Glycol	three
Exp seven	Glass (lead)	275	0·35	Glycol	three
Exp eight	Glass (lead)	76·5	0·078	Glycol	three
Exp nine	Glass (lead)	76·5	0·1128	Glycol	three
Exp ten	Glass (lead)	76·5	0·25	Glycol	three
Exp eleven	Glass (lead)	220	0·1	Glycol	three

Table 2.4 Details for one phase experiments

TWO-PHASE EXPERIMENTS

	SOLID	DIAM(μ)	CONC	SOLID	DIAM(μ)	CONC	LIQUID	TRANSDUCER
Exp one	Copper	56·5	0·026	Glass (lead)	76·5	0·076	Glycol	two
Exp two	Copper	56·5	0·0127	Glass (lead)	302.5	0·077	Glycol	two
Exp three	Glass (lead)	327·5	0·0725	Glass (lead)	120	0·0725	Glycol	two
Exp four	Glass (soda)	69	0·1314	Glass (soda)	41·5	0·0497	Water	four
Exp five	Quartz	200	0·0771	Glass (soda)	60	0·1212	Glucose	four
Exp six	Glass (lead)	275	0·039	Glass (lead)	120	0·039	Glycol	one
Exp seven	Copper	56·5	0·034	Glass (lead)	76·5	0·098	Glycol	two
Exp eight	Glass (lead)	302.5	0·039	Glass (lead)	41·5	0·039	Glycol	one
Exp nine	Glass (lead)	220	0·09093	Glass (lead)	76·5	0·09093	Glycol	three

Table 2.5 Details for two phase experiments

THREE-PHASE EXPERIMENTS

	SOLID	DIAM(μ)	CONC	SOLID	DIAM(μ)	CONC	SOLID	DIAM(μ)	CONC	LIQUID	TRANSDUCER
Exp one	Glass (lead)	220	0·0742	Copper	56·5	0·01287	Glass (lead)	76·5	0·0371	Glycol	two
Exp two	Glass (lead	462·5	0·037	Glass(lead)	200	0·0738	Glass (lead)	76·5	0·01845	Glycol	two
Exp three	Glass (lead)	327·5	0·07246	Glass(lead)	200	0·03623	Glass (lead)	76·5	0·03623	Glycol	two
Exp four	Glass (lead)	220	0·11	Copper	56·5	0·019	Glass (lead)	76·5	0·055	Glycol	two
Exp five	Glass (lead)	220	0·164	Copper	56·5	0·028	Glass (lead)	76·5	0·082	Glycol	two
Exp six	Glass (lead)	362·5	0·0195	Glass(lead)	220	0·0402	Glass (lead)	120	0·01833	Glycol	one

Table 2.6 Details for three phase experiments

Approximately 50 grams of particles were sieved at a time and after three or four minutes the sieves were emptied and cleaned with a brush, this was repeated until practically no more particles passed through the sieves. This ensured the appropriate size fractions are obtained. The densities of each size fraction was determined using the pycnometer and was found to be approximately equal to the values given in table 2.2. Each experiment was carried out at 20°C ± 1°C so that extreme changes in viscosities would not occur. The suspensions are formed by adding a known volume of liquid and solids into the perspex tube. Also 5cc of Sodium tri-poly phosphate ($Na_5 P_3 O_{10}$) was added as a dispersent to ensure no flocculation occurs. The tube was then agitated by inserting a bung into the open end and turning the tube up and down for at least five minutes so that a uniform mixture is formed. The suspension is such that the height of the sediment formed never goes above the transducer. This ensured that the pressure changes measured were those transmitted hydrodynamically through the continuous fluid phase and not through solid-solid contacts.

After thorough mixing, the bung is removed and the tube placed vertically on a bench. The plotter is immediately switched on so that the settling process can be monitored. Each experiment was carried out three times to check for reproducibility of the results.

The expected voltage difference for each experiment can be calculated using equations 2.13 and 2.14.

$$V_{INT} = \frac{h\rho_B g - C}{K} \qquad (2.13)$$

$$V_{FIN} = \frac{h\rho_f g - C}{K} \qquad (2.14)$$

where V_{INT} and V_{FIN} are the initial and final voltages respectively. Therefore the expected voltage difference is:

$$V_{DIFF} = V_{INT} - V_{FIN} \quad . \qquad (2.15)$$

For all experiments the voltage difference given by the plotter output was always smaller than the expected value, this is probably due to

1) Effect of circulation currents set up when the suspension is agitated.

2) The time delay in which the plotter takes to respond to the initial voltage output from the pressure transducer.

The correct voltage difference is obtained by interpolating the voltage curve back at the starting point.

Lead ballontini was used in the majority of experiments due to its wide size distribution, see table 2.1. The initial concentrations for all experiments undertaken was in the hindered settling regime, see Bhatty (1986). Also the effect of Brownian motion and the walls should be negligible due to the size of particles used, see Davies (1985). The experimental data for each experiment is given in chapter four where comparisons are made with the proposed model.

CHAPTER THREE

OBTAINING CONTINUOUS GRAVITY THICKENER DATA

3.1 Introduction

A continuous gravity thickener consists of a cylindrical tank of uniform cross-sectional area, although the base may be conical, see figure 3.1. Three streams are associated with a thickener these are:

1) FEED
2) OVERFLOW
3) UNDERFLOW

The operation of the thickener is to obtain a slurry in the underflow stream which has a higher solids content than the feed. As the feed enters the thickener it will encounter essentially two directions of flow, these are:

a) UPFLOW
b) DOWNFLOW

The velocities of the above flows are dependent on the dimensions of the thickener as well as the rates at which the slurry enters and leaves the thickener via the feed and underflow streams respectively. Therefore, particulates from the feed will be incorporated into one of the above flows, depending on their size and density. Particulates in the downflow stream will settle (or consolidate for flocculated slurrys) at the base of the thickener. A rake mechanism is sometimes employed at the base to move the thickened slurry towards the underflow outlet.

Experimental work on thickener performance involves obtaining concentration profiles throughout the thickener for different feed and underflow flow rates. Turner (1976) analysed the thickening of uranium plant slurries using a submersible radioactive density gauge to obtain

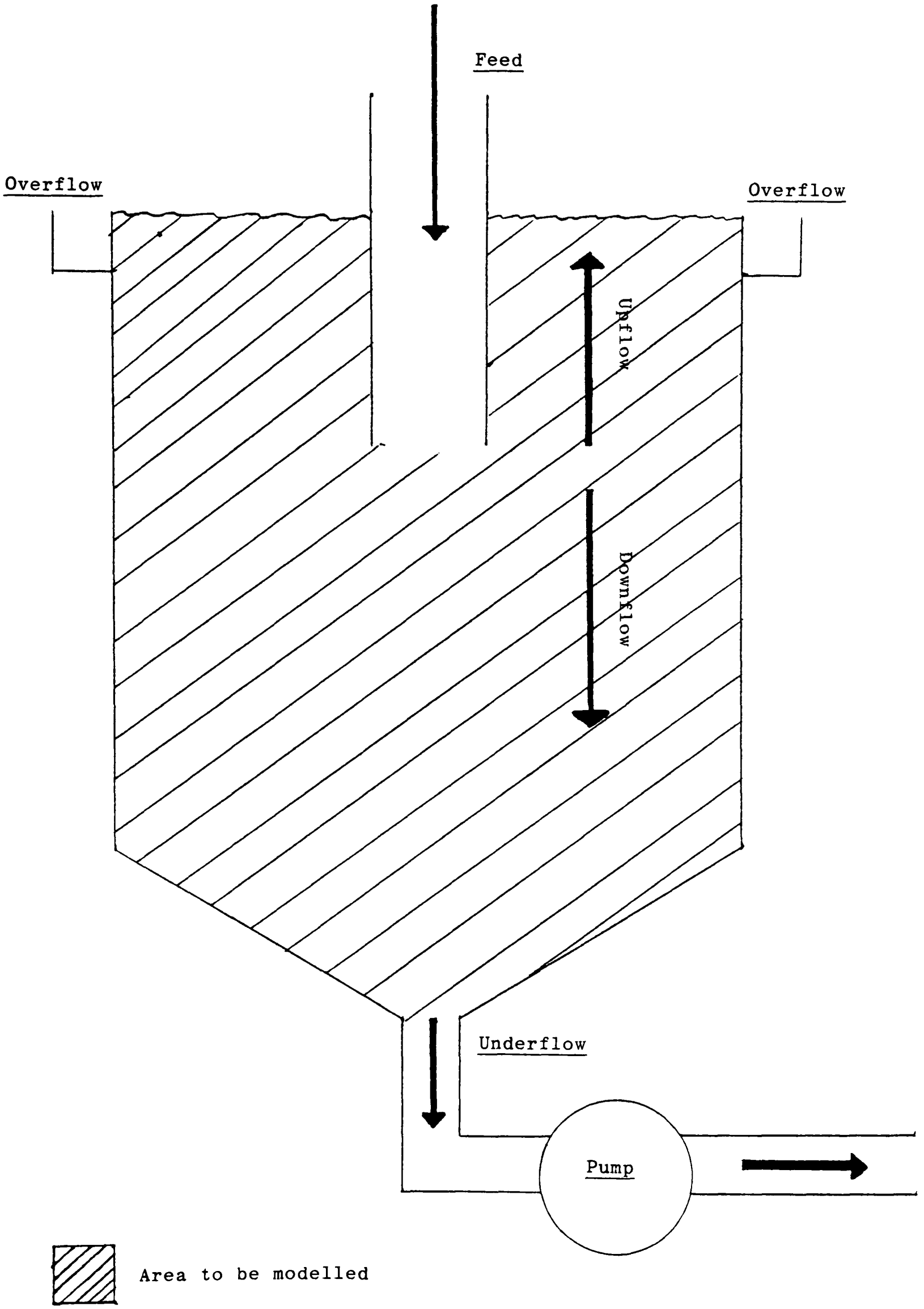

Figure 3.1 Diagram of a continuous thickener

density profiles. Joo-Huia Tay (1983) performed theoretical and experimental studies where velocity and concentration profiles are obtained using a photo-electric principle device. The predictions for concentrations are calculated using a dispersion model used in air pollution studies. Kos (1977) analysed the solids pressure contribution to thickening of flocculated slurries. This involved using a laboratory set-up and obtaininng concentration profiles via sampling ports (taps) situated along the tube representing the thickener. Scott (1968) and Chandler (1983) obtained concentration profiles by analysing grab samples obtained at different depths in the thickener. Unfortunately all the above experimental data did not contain size distributions of the particulate material used. Therefore, the following study was carried out at a minerals processing plant containing three thickeners.

3.2 Apparatus used

One flat bed and two conical bed thickeners were investigated. Forty 200cc plastic sample bottles were used to obtain samples at different depths throughout each thickener and samples of each stream associated with each thickener. Each sample bottle was cleaned and then dried with compressed air. This ensured each sample bottle was thoroughly clean and empty before being used. To obtain samples at different depths a suction process was used. This involved connecting the sample bottle to a pump and a flexible perspex rod which could be lowered into the thickener, see figure 3.2.

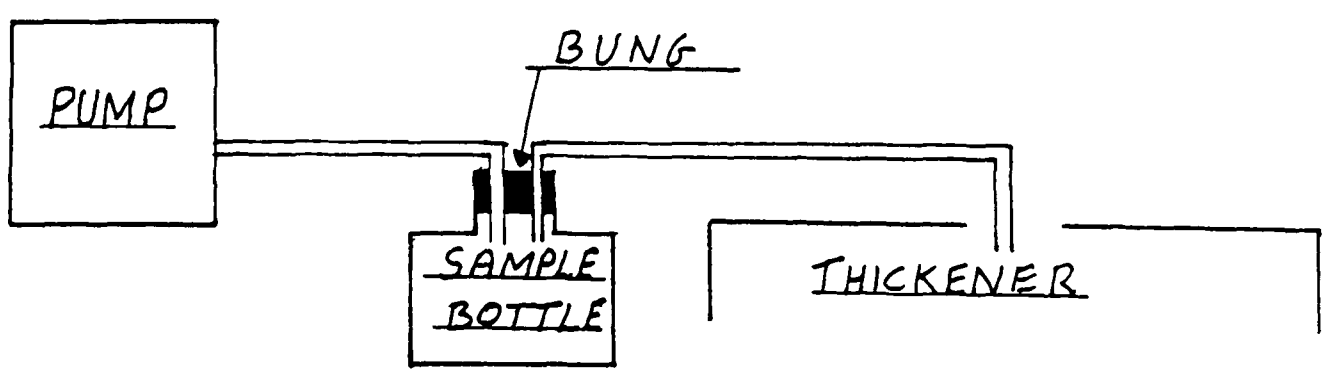

Figure 3.2 Circuit for obtaining depth samples

The perspex rod was of length two meters and was marked at every twenty centimeters using tape. The flow rates of the streams associated with each thickener were measured using a 10 litre bucket and stop watch.

3.3 Experimental procedure

In analysing each thickener the following data is to be obtained.

a) Dimensions of each thickener.

b) Mass flow rates and solids concentrations (weight) associated with each stream.

c) Solids concentrations (weight) throughout each thickener.

A mineral processing plant is concerned with extracting and separating valuable material from a mined ore. The plant at which the three thickeners are located is concerned with extracting Fluorite (Calcium Fluoride, CaF_2), Barytes (Barium sulphide, $BaSO_4$) and Galena (Lead Sulpide, PbS), see figure 3.4. A thickener is used in obtaining each of these materials where the processes associated with each thickener in the mineral processing plant are:

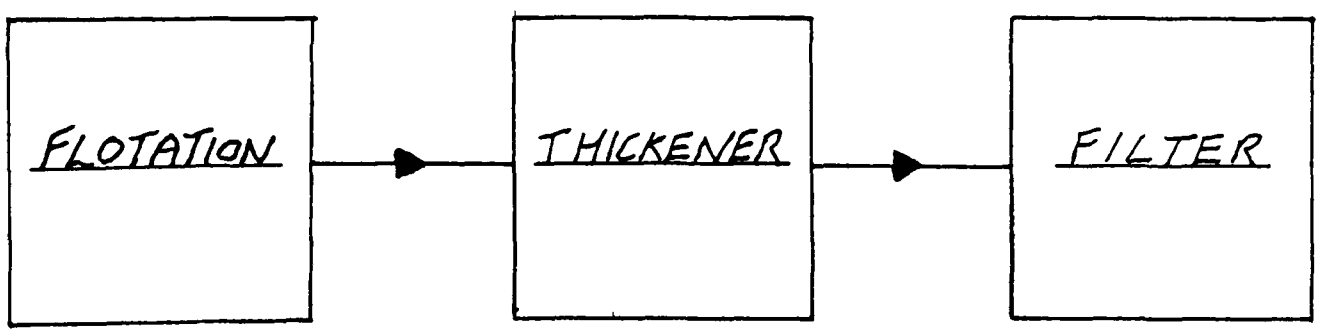

Figure 3.3 Processes associated with each thickener

During the flotation process the Fluorite, Barytes and Galena are separated at very low solids concentrations. The use of thickeners before filtering ensures a higher concentrate enters the filter

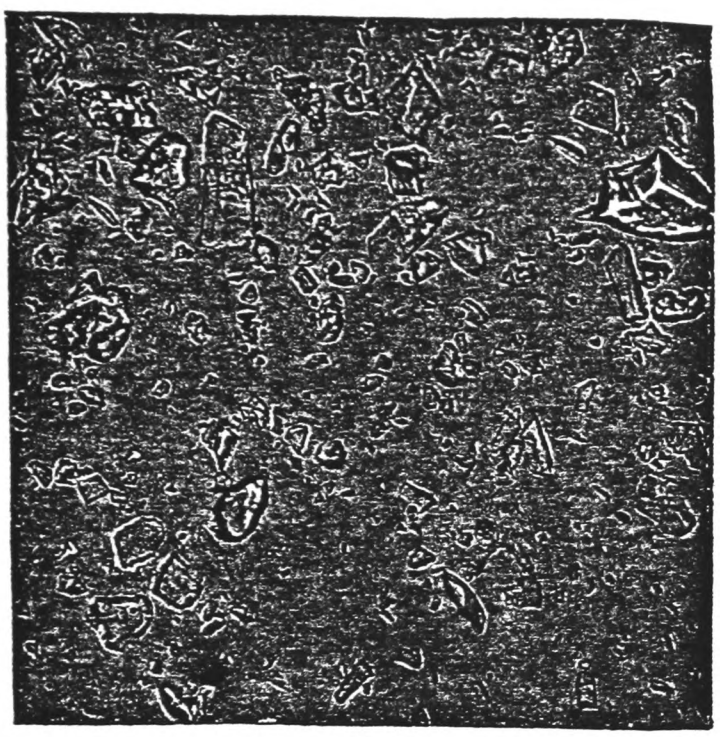

a) Fluorite

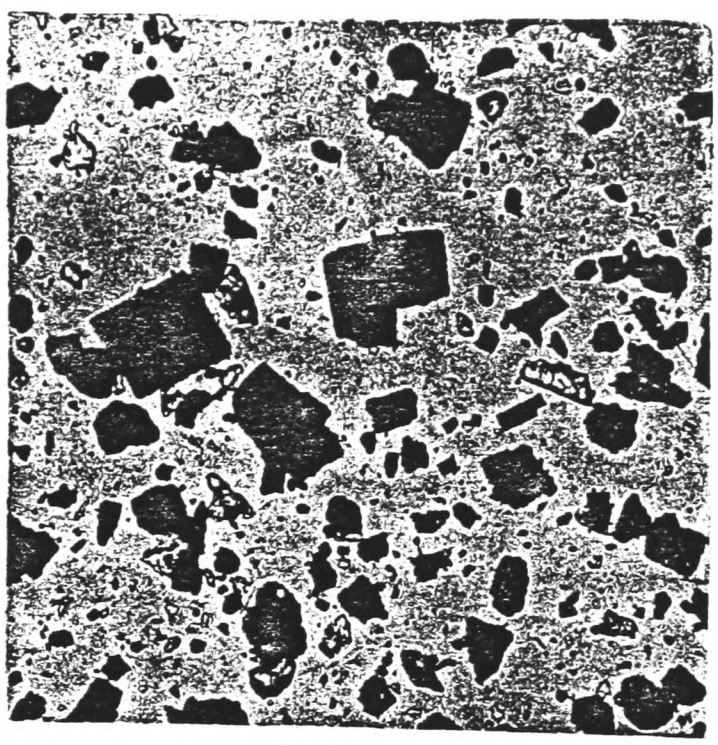

b) Galena

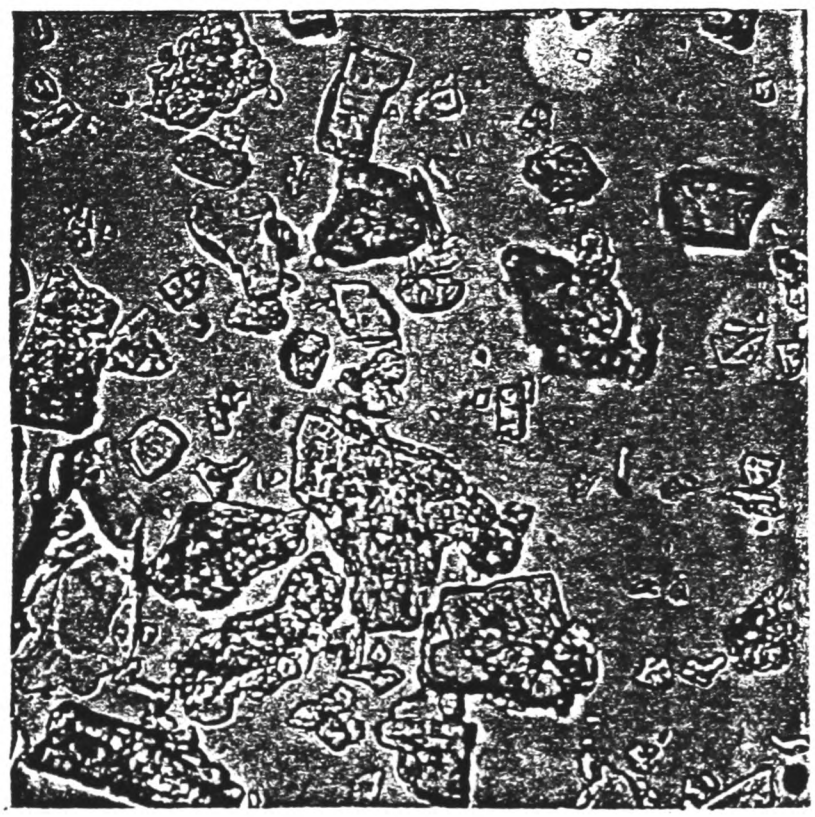

c) Barytes

Figure 3.4 Photomicrographs of solids undergoing thickening

and gives economical and greater use of the filters porous medium. The product from filtering, the filter cake, is then dried giving the required material in powdered form.

To obtain samples at different depths the flexible perspex rod is lowered at 20cm intervals into the slurry occupying the thickener. Once at the required depth the bung, see figure 3.2, is inserted into a used sample bottle. This forces slurry up the perspex rod due to the suction generated. When this used sample bottle becomes full the bung is removed by placing a thumb over the bung entrance to the perspex rod so that the contained slurry in the rod does not travel back into the thickener. The slurry obtained in the used sample bottle is then disposed of. The thumb is then released and the bung quickly inserted into a new sample bottle regenerating the suction at which the sample can be obtained. Gathering samples in the above manner ensures that when the sample is taken the perspex rod contains slurry from the required depth only and not from previous sample depths. Samples and mass flow rates of each stream associated with a thickener are also obtained if possible. To achieve this the pipes representing each stream are located and the outlets found. A sample can then be gathered using a sample bottle. The mass flow rate is calculated by using the 10 litre bucket and stop watch and noting the time it takes for the bucket to become partly full with exiting slurry. The mass of this slurry is then measured by knowing the mass of the bucket. This is repeated several times so that an average mass flow rate can be taken. The obtained samples are analysed in the laboratory to obtain solids concentration and average particle size. Solids concentrations are calculated by the following procedure:

1) Weigh sample bottle with slurry sample (W_1).

2) Remove all contents from sample bottle using excess water and filter these contents. Also note the weight of the filter paper (W_2) and dried sample bottle (W_3).

3) Dry the filter cake by placing it in an oven for 2-3 hours.

4) Weigh dried filter cake with filter paper (W_4).

5) Calculate weight of solids in sample (W_5).

$$W_5 = W_4 - W_2. \tag{3.1}$$

6) Calculate solids concentration (W_6).

$$W_6 = \frac{W_5}{W_1 - W_3} \tag{3.2}$$

The average particle size for each sample is calculated by mixing the sample thoroughly and extracting 10cc of mixed slurry. This is then analysed using the Malvern particle size analyser, which uses the techniques of laser diffraction, to calculate a size distribution. A size distribution was calculated three times for each sample to ensure reproducibility of the results.

Not all streams could be analysed. This was due to the nature and location of the pipes representing these streams. To obtain estimates for these streams a material balance program was used, see Simpson (1988).

3.4 Results

The dimensions of each thickener, see figures 3.6, 3.8 and 3.11, are calculated using an extendable measuring tape. The conical angle for the Fluorite thickener is calculated by measuring the depth at the

perimeter and the depth at an inlet 3·35m in from the perimeter where:

$$\text{Depth at perimeter} = 2{\cdot}15\text{m}$$

$$\text{Depth at inlet} = 2{\cdot}548\text{m}$$

$$\text{Conical angle } \theta = \text{Tan}^{-1}\left[\frac{0{\cdot}398}{3{\cdot}35}\right] = 6^{\circ}\ 47'.$$

The Fluorite thickener was covered with wooden planks, the inlet being a small entrance. The perspex rod was lowered into the slurry via this inlet and depth samples obtained down to a depth of 2·2m. The total feed entering the thickener consisted of the feed from flotation as well as recirculation streams from the filter, see figure 3.5. Samples could be obtained for all streams associated with the Fluorite thickener but mass flow rates could not be calculated for the "feed from flotation" and "thickener underflow" streams. The use of the material balance program estimated these values, see Table 3.8.

The Barytes thickener was covered with fixed metal plates, with no inlet present. Also obtaining an entry point near the feed well was impossible due to lack of space. Therefore depth samples for the Barytes thickener could not be obtained. The conical angle associated with this thickener is assumed to be the same as for the fluorite thickener. Samples of all streams associated with the Barytes thickener, see figure 3.5, could be obtained but the material balance program had to be used to estimate the mass flow rates for "feed from flotation" and "water" streams, see table 3.9.

The total feed into the Barytes and Fluorite thickeners consists of four different streams, "feed from flotation", "filter overflow", "filtrate" and "water". The size distribution and solids concentration for the total feed is calculated by assigning a weighting factor to each stream

in the total feed. This weighting factor represents the proportion of solids that each stream contributes to the overall solids content. Therefore, for the fluorite thickener we have

Streams in total feed	% Solids	Mass flow rate	Weighting factor
Feed from flotation	43·8	9·11	0·8649
Filter overflow	65·0	0·76	0·1071
Filtrate	3·4	3·81	0·028
Water	0	1·91	0

Total mass flow rate of feed = 15·59 Kg/s

Total solids concentration in feed = 29·63%

Table 3.1 Data for total feed in fluorite thickener

Similarly for the Barytes thickener we have:

Streams in total feed	% Solids	Mass flow rate	Weighting factor
Feed from flotation	42·7	3·039	0·625
Filter overflow	58·22	1·275	0·362
Filtrate	2·197	1·209	0·13
Water	0	0·668	0·0

Total mass flow rate of feed = 6·192 Kg/s

Total solids concentration in feed = 33·12%

Table 3.2 Data for total feed in Barytes thickener

Multiplying the size distribution of each stream by its weighting factor and combining all streams present in the feed, the size distribution of

the total feed is obtained see figures 3.7 and 3.9. The total solids concentration is calculated by multiplying the solids concentration of each stream with its weighting factor and combining them.

The Galena thickener circuit, see figure 3.10, consisted of an extra device, a splitter, which restricted the amount of thickened slurry entering the filter. The excess slurry recirculating back to the thickener. The total feed to the Galena thickener consists of five different streams "feed from flotation", "splitter overflow", "filter overflow", "filtrate" and "water". Samples could be obtained for all streams except the "thickener underflow". Also mass flow rates could not be obtained for "feed from flotation", "filter overflow" and "thickener underflow" streams. The use of the material balance program gave estimates for these values, see Table 3.10. The weighting factors associated with streams combining to form the total feed are:

Streams in total feed	% Solids	Mass flow rate	Weighting factor
Feed from flotation	12·7	0·85	0·025
Splitter overflow	74·89	0·12	0·021
Filter overflow	76·31	5·31	0·9439
Filtrate	0·1	0·071	0·00002
Water	0·0	0·614	0·0

Total mass flow rate of feed = 6·965 Kg/s

Total solids concentration of feed = 61·02%

Table 3.3 Data for total feed in Galena thickener

It can be seen that this thickener is essentially a storage device with the vast majority of the feed coming from the "filter overflow" stream.

The size distribution, see figure 3.12, and solids concentration of total feed is calculated as explained above for Fluorite and Barytes. Depth samples could be obtained down to a depth of 1·5m by lowering the perspex rod through an opening just outside the feed well.

Galena is a dark grey material. Analysing the samples it was observed that the overflow consisted of a yellow material as did some of the depth samples. Also the "feed from flotation" stream showed quantities of this material. It was therefore decided to carry out a chemical analysis of the "feed from flotation", thickener overflow" and "thickener underflow" streams to see what solid material is present. The following assays are obtained:

	Galena	Fluorite	Barytes	Other
Feed from flotation	20·44%	15·97%	35·45%	28·14%
Thickener underflow	76·79%	4·11%	6·84%	12·26%
Thickener overflow	38·8%	10·88%	21·45%	28·87%

Table 3.4 Assay values from chemical analysis

The above assays represent the percentage of each material present in each stream. Ignoring "other" material and treating the recirculation streams as one stream the material balance program is used to obtain assay values for the recirculation stream.

	Galena	Fluorite	Barytes
Feed from flotation	28·44%	22·22%	49·33%
Recirculations	88·74%	4·32%	6·94%

Table 3.5 Material balance estimates for recirculation stream

Taking into account the mass flow rates of the above streams, the total feed concentration can be broken down as:

Galena	Flourite	Barytes	Total
53·23%	2·91%	4·88%	61·02%

Table 3.6a Breakdown of Galena Feed

Also the solids concentrations associated with the underflow and overflow are:

	Galena	Flourite	Barytes	Total
Underflow	66·167%	3·546%	5·898%	75·611%
Overflow	0·164%	0·046%	0·09%	0·3%

Table 3.6b Concentrations of Galena Underflow and overflow streams

The density of the Fluorite and Barytes material was calculated using a pycnometer. Due to the presence of other materials in the Galena the density used is the value given in Wills (1985). The density values calculated for the Fluorite and Barytes correspond to the values quoted in Wills, therefore, these are the values used.

	DENSITY	SHAPE FACTOR
GALENA	7500	0·86
FLUORITE	4500	0·86
BARYTES	3200	0·86

Table 3.7 Material properties

The shape factors used are values obtained by noting that the shape of each material is angular, see figure 3.4.

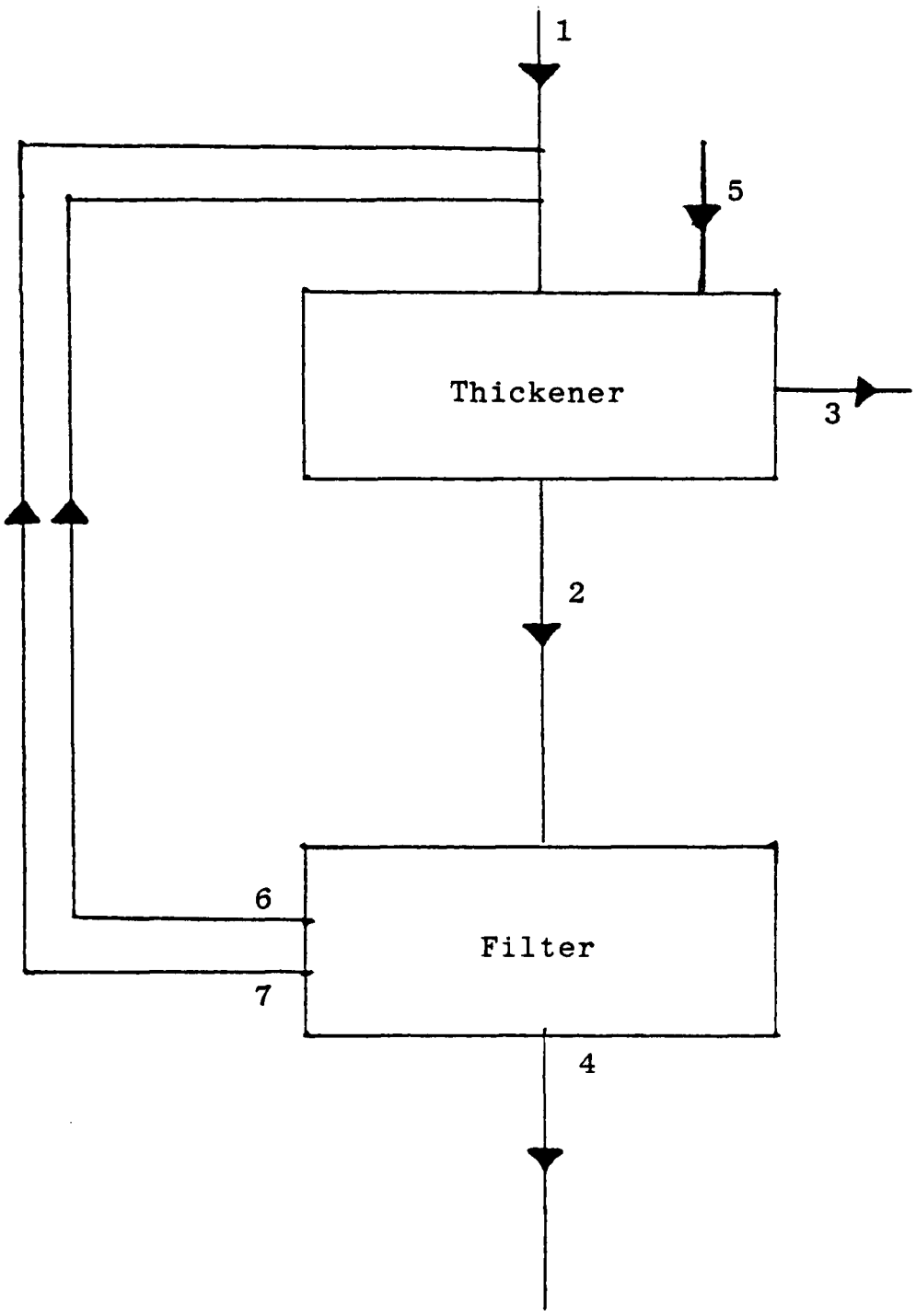

Streams

1 Feed from flotation
2 Thickener underflow
3 Thickener overflow
4 Filter cake
5 Water
6 Filter overflow
7 Filtrate

Figure 3.5 Circuit associated with Fluorite and Barytes thickeners

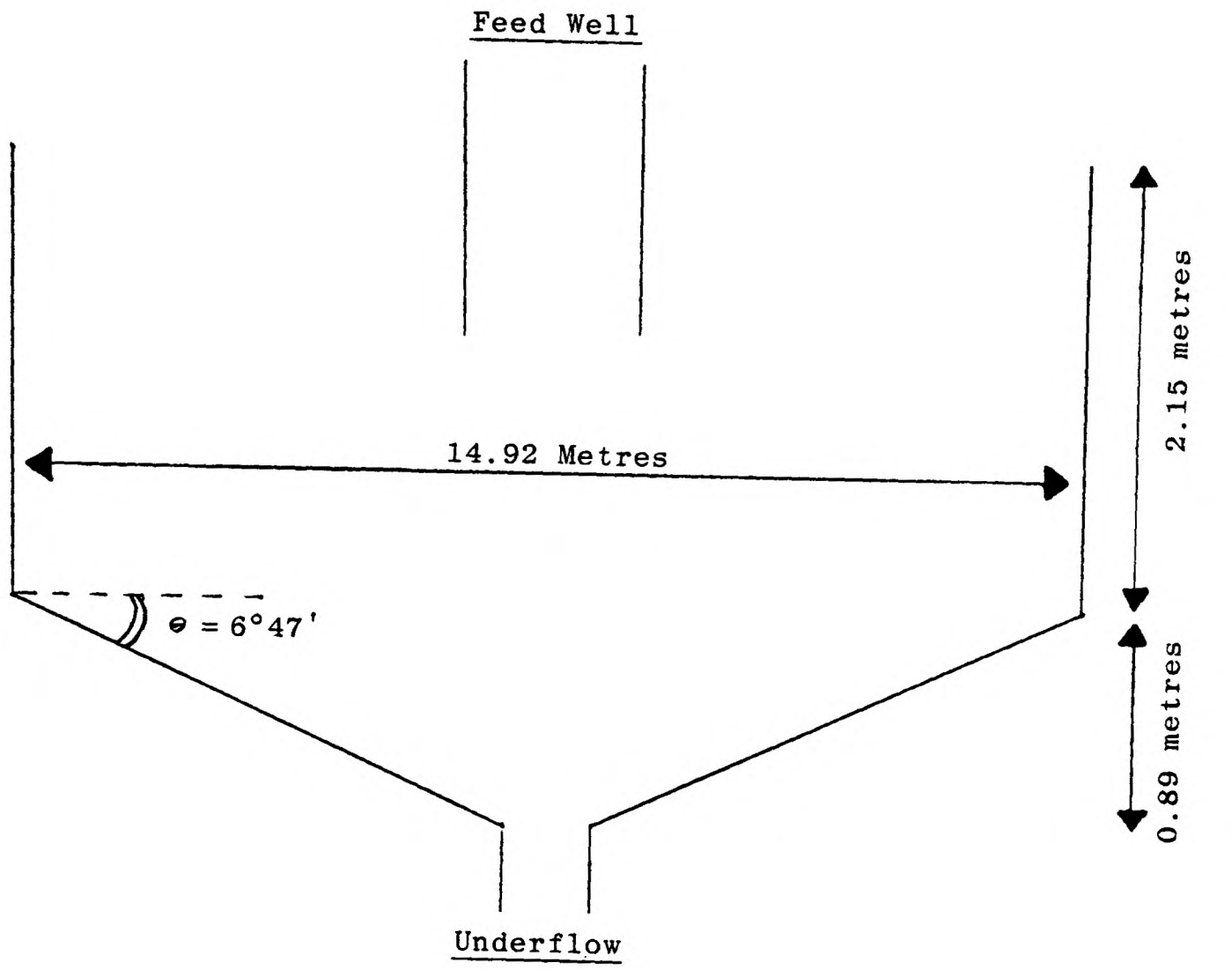

Figure 3.6 Dimensions of Fluorite thickener

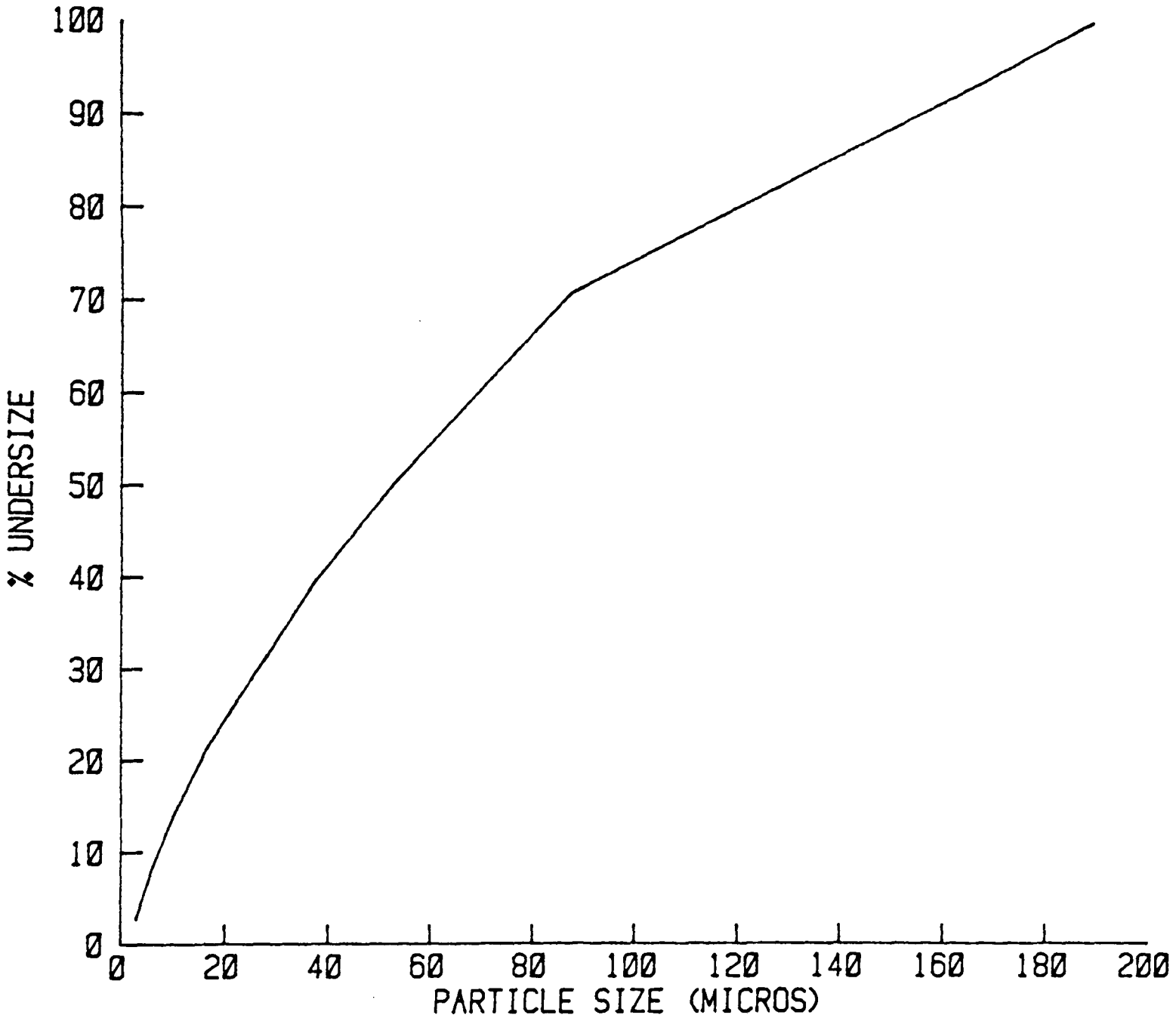

Figure 3.7 Size distribution of Fluorite feed

FLUORITE DATA

Depth below slurry surface (M)	% Solids	Average Particle Diameter (μ)
·1	2·5	6·1
·3	2·1	6·5
·5	2·2	6·5
·7	2·37	7·0
·9	2·3	7·2
1·1	2·4	7·0
1·3	2·44	7·0
1·5	2·74	7·4
1·7	2·86	7·5
1·9	3·53	7·5
2·1	4·05	7·7
2·2	10·63	22·3

	% Solids (WT)	Mass flow rate (kg/s)	Average Particle Diameter (μ)
Thickener feed	43·85	9·11	54
Thickener underflow	52·54	8·56	54
Thickener overflow	1·73	7·03	6·6
Filter overflow	65·05	0·76	54
Filter cake	91·6	4·23	54
Filtrate	3·4	3·81	22
Water sprays	0·0	1·9	-

Table 3.8 Fluorite thickener data

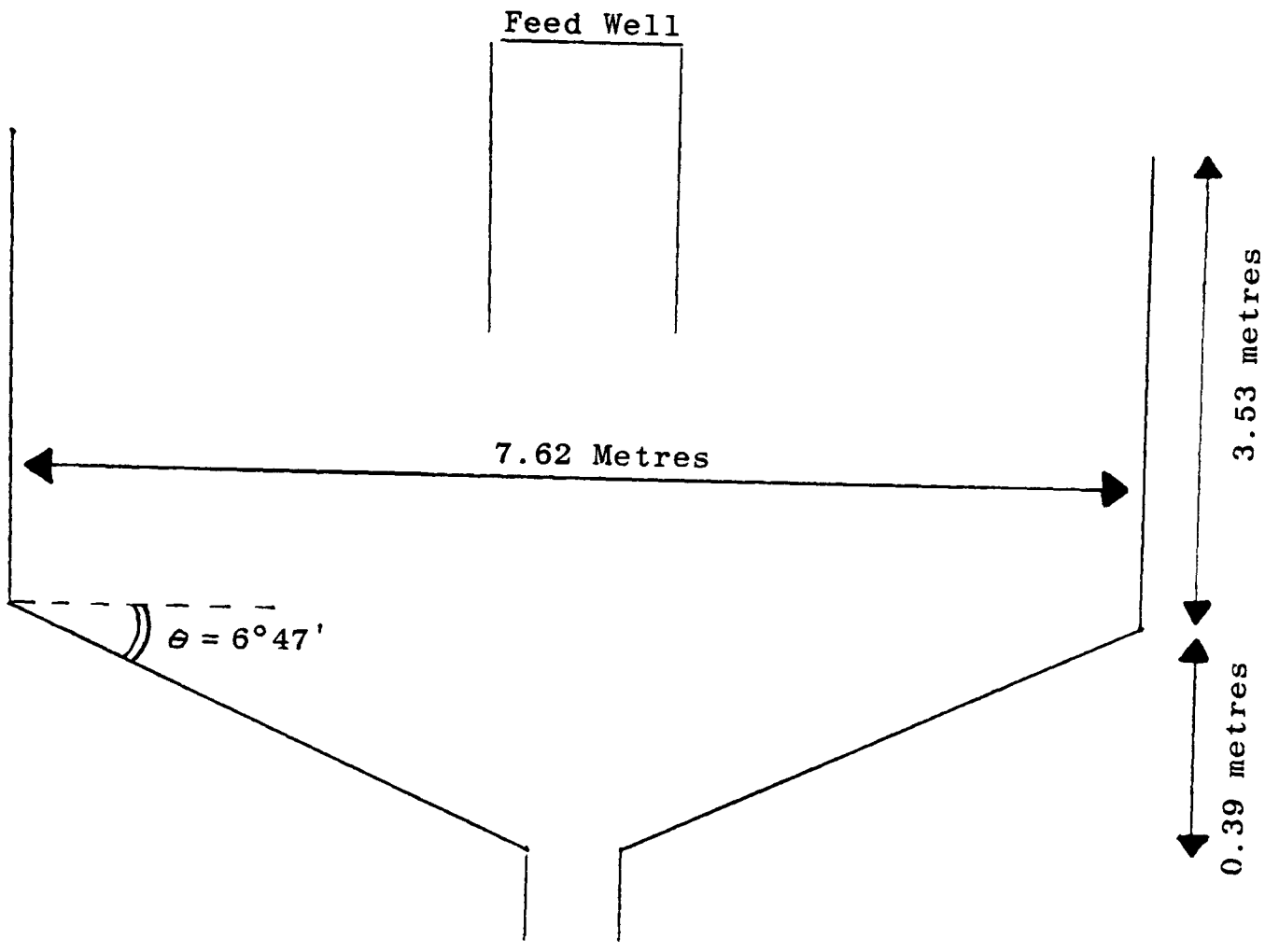

Figure 3.8 Dimensions of Barytes thickener

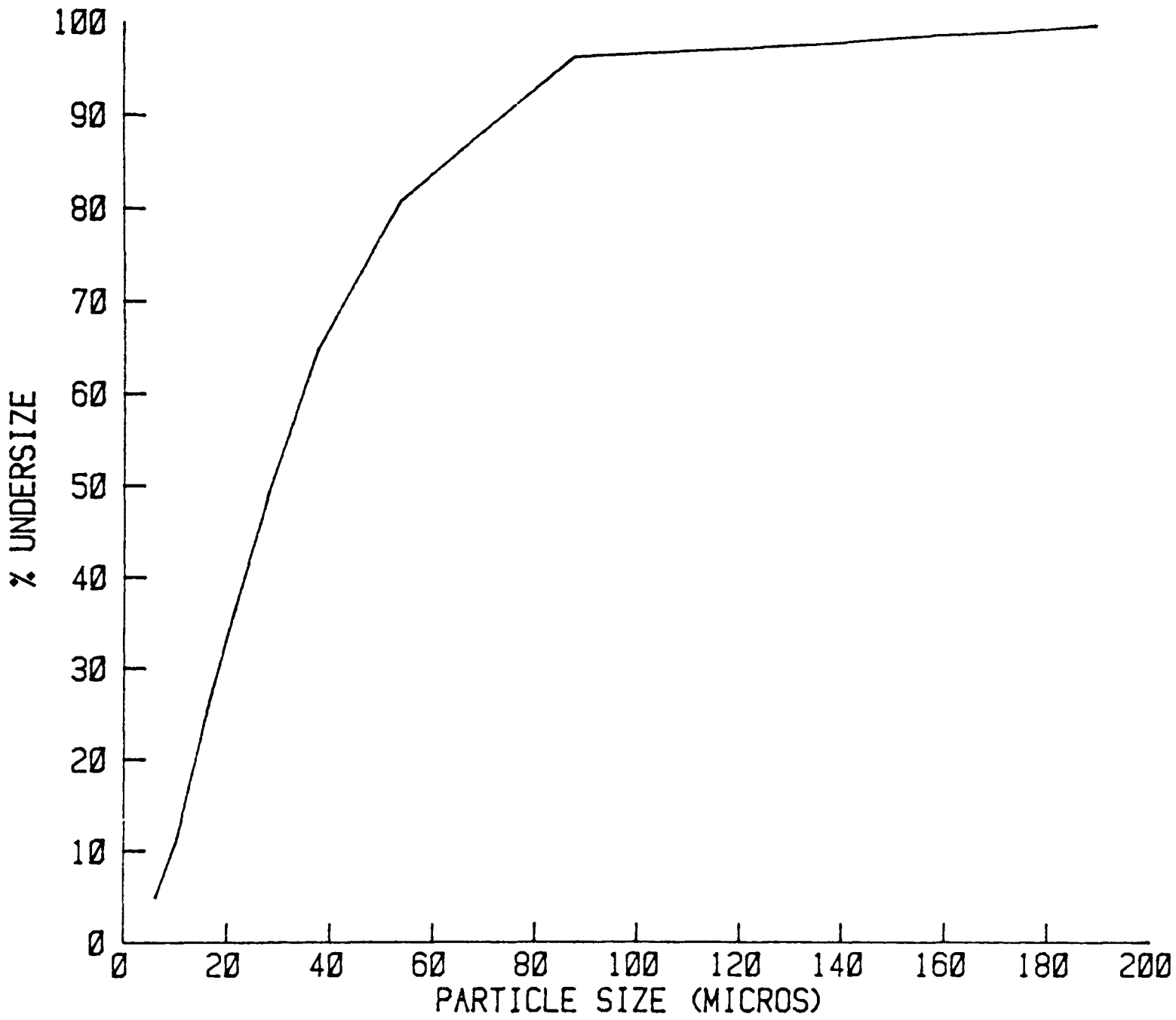

Figure 3.9 Size distribution of Barytes feed

BARYTES DATA

	% Solids (WT)	Mass flow rate (kg/s)	Average Particle Diameter (μ)
Thickener feed	42·17	3·039	8·6
Thickener underflow	52·44	3·9	26·0
Thickener overflow	·2	·29	6·4
Filter overflow	58·22	1·275	28·5
Filter coke	90·193	1·417	-
Filtrate	2·197	1·209	19·5
Water sprays	0·0	·668	-

Table 3.9 Barytes thickener data

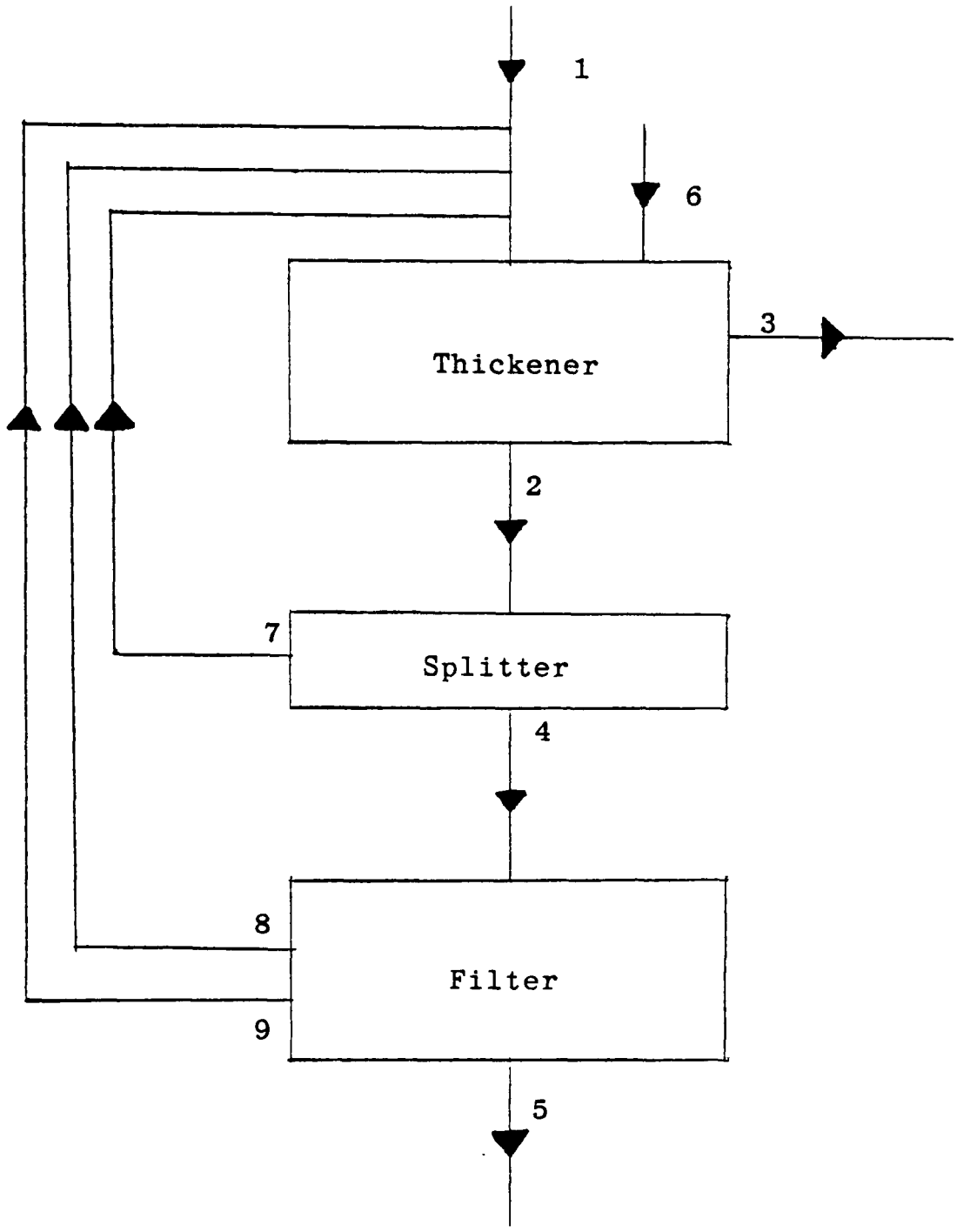

Streams

1 Feed from flotation
2 Thickener underflow
3 Thickener overflow
4 Filter feed
5 Filter cake
6 Water
7 Splitter overflow
8 Filter overflow
9 Filtrate

Figure 3.10 Circuit associated with Galena thickener

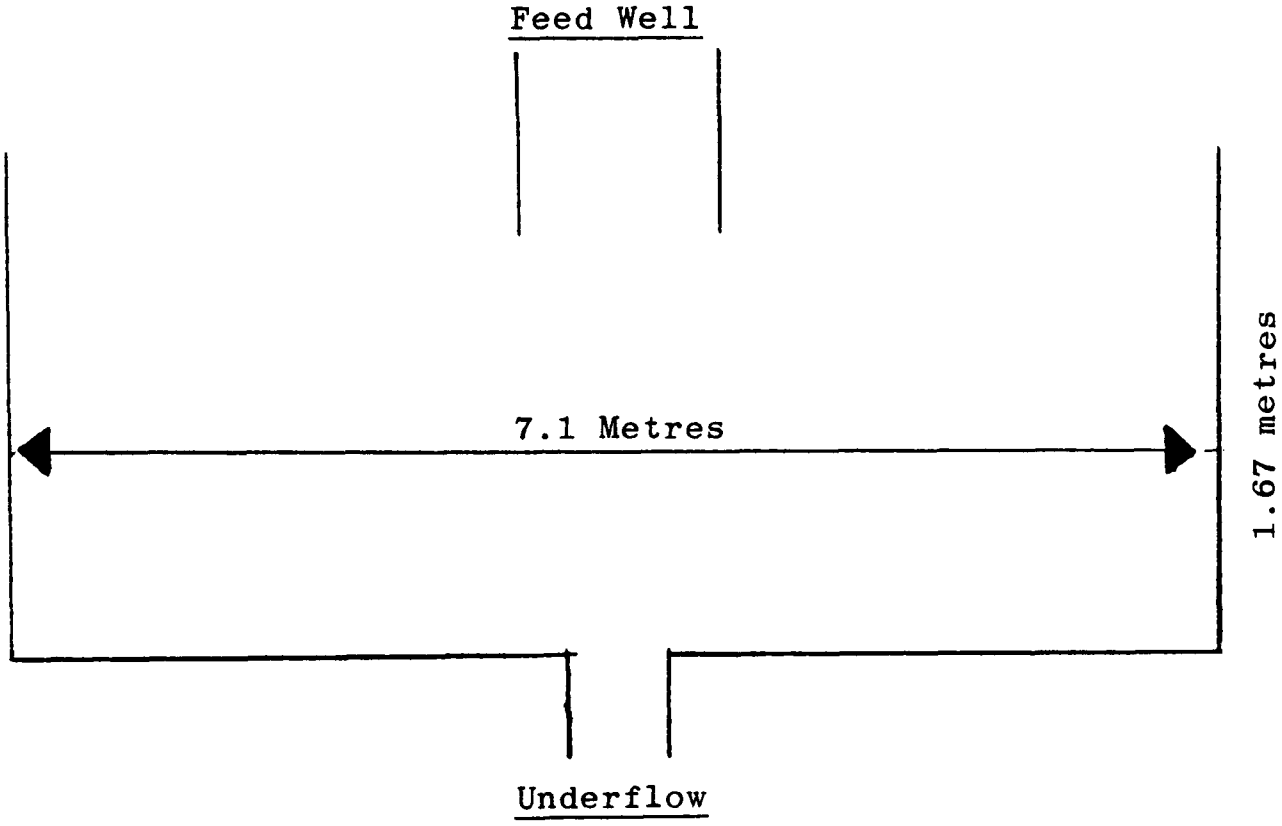

Figure 3.11 Dimensions of Galena Thickener

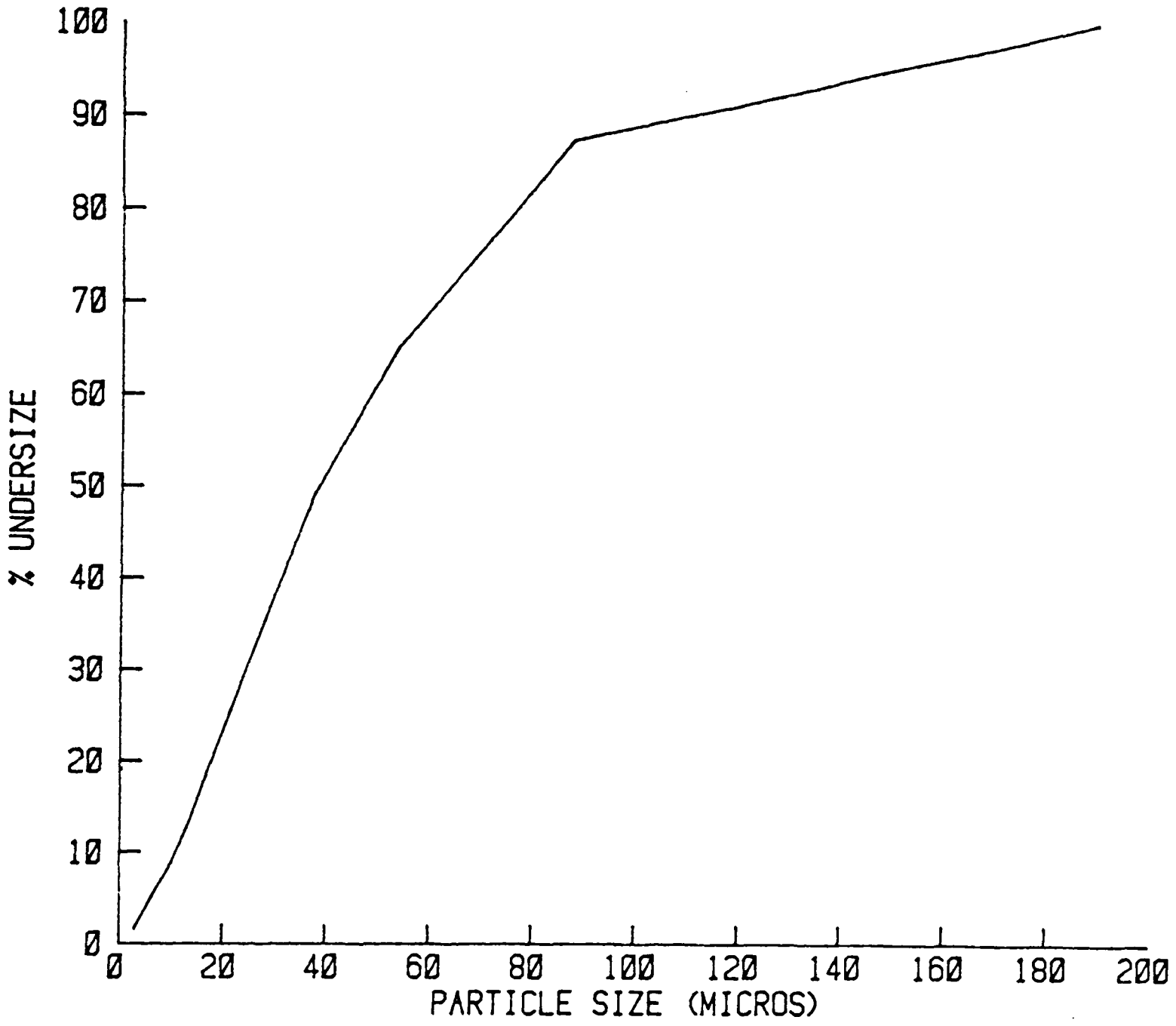

Figure 3.12 Size distribution of Galena feed

GALENA DATA

Depth below slurry surface (M)	% Solids (WT)	Average Particle Diameter (μ)
·1	3·58	8·4
·3	10·3	10·4
·5	12·42	11·2
·7	13·33	12·1
·9	16·0	13·2
1·1	15·55	14·1
1·3	15·7	15·1
1·4	15·85	13·7
1·5	15·9	15·1

	% Solids (WT)	Mass flow rate (kg/s)	Average Particle Diameter (μ)
Thickener overflow	·3	1·35	7·7
Thickener feed	12·7	·85	15·3
Thickener underflow	75·611	5·615	-
Splitter overflow	74·89	·12	32·5
Filter feed	75·626	5·495	33·5
Filter overflow	76·31	5·31	39·0
Filter coke	90·886	·114	-
Filtrate	·17	·071	-
Water sprays	-	·614	-

Table 3.10 Galena thickener data

CHAPTER FOUR

A NUMERICAL MODEL FOR NON-FLOCCULATED BATCH SEDIMENTATION

4.1 Introduction

The movement of particulates in a host fluid, due to the difference in particulate and fluid densities, is essentially a transient one dimensional multiphase problem. Each solid phase being distinct via its density and/or its size and shape.

When non flocculated particulates settle in a fluid two regions are observed, see Figure 4.1, these are;

a) Free settling region

b) Sediment region.

The free settling region consists of particles not in contact with other particles. For a polydisperse suspension this region will contain distinct zones, see Davies (1985). The lowest zone just above the sediment containing all particle phases at their initial concentrations, with each successive zone above containing one fewer phase than the zone below (ie. fastest settling phase). The sediment region for non-flocculated slurries will consist of an incompressible packed structure of particulates. The proposed numerical model makes the following assumptions:

1) The slurry container has uniform cross sectional area.
2) The flow is vertical and horizontally uniform (i.e. negligible wall effects).
3) Forces that can act on the solid particles are gravity (allowing for buoyancy), drag due to the relative motion of the liquid and other particle phases (particle collisions). Also for flocculated material a compressive resistance is present due to floc collapse in the sediment, see chapter six.

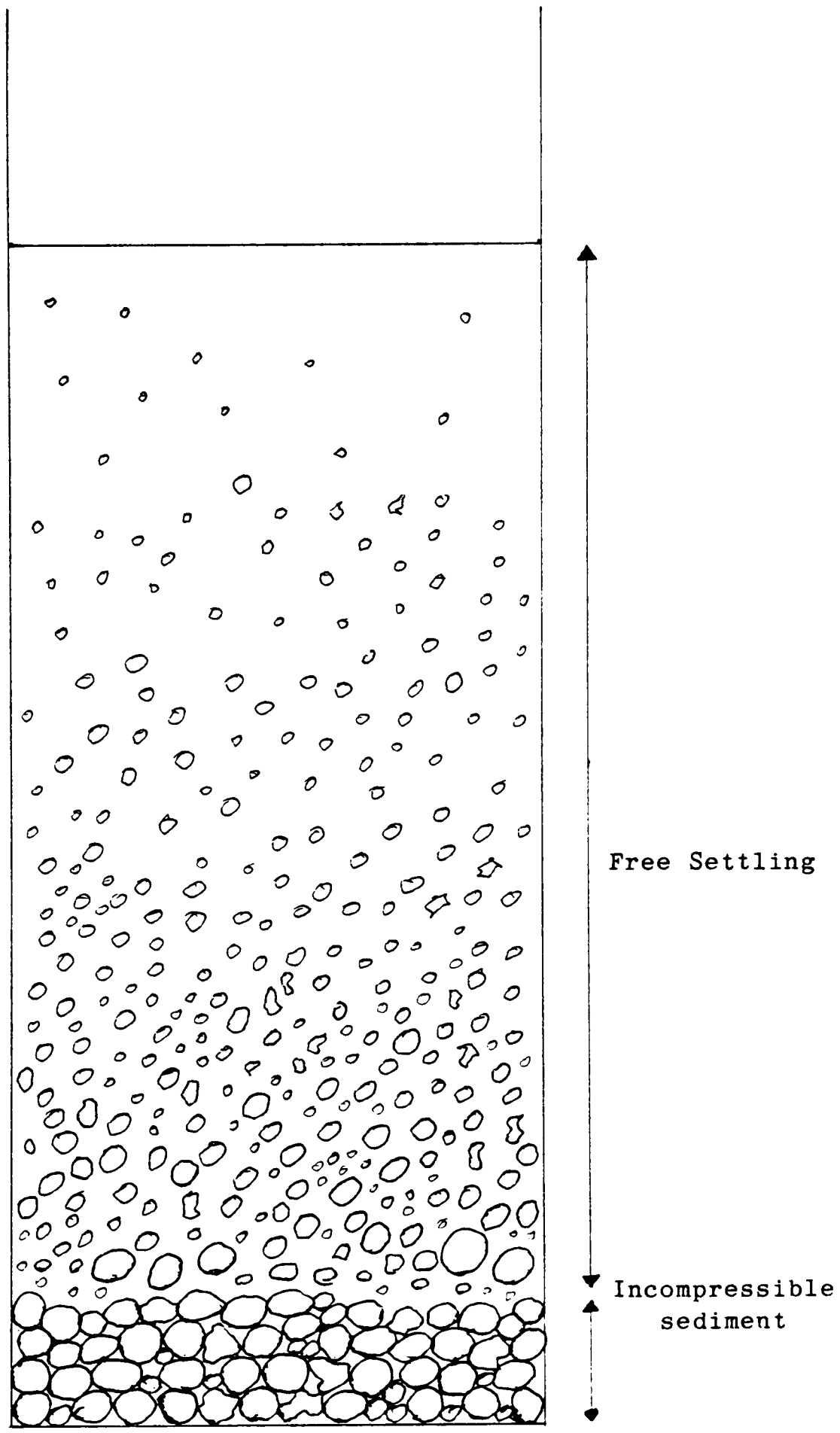

Figure 4.1 Non Flocculated Settling Regions

4) The slurry is treated as a continuum; that is continuous solid and liquid phases that interact with each other.

5) Isothermal conditions are present. Therefore an energy balance is not required.

The problem consists of a set of moving boundaries one for each solid phase and one for the build up of the sediment. The following model predicts concentrations and velocities in the free settling region and also predicts the build up of the sediment region.

4.2 Governing Equations

The differential equations governing the conservation of mass and momentum for each solid phase and the equations for the fluid phase are written in an Eulerian plane of reference. Because of the nature of this particular problem it is essential that each solid phase be represented by a continuity and momentum equation. The forces acting on the solids in an element of thickness dy are:

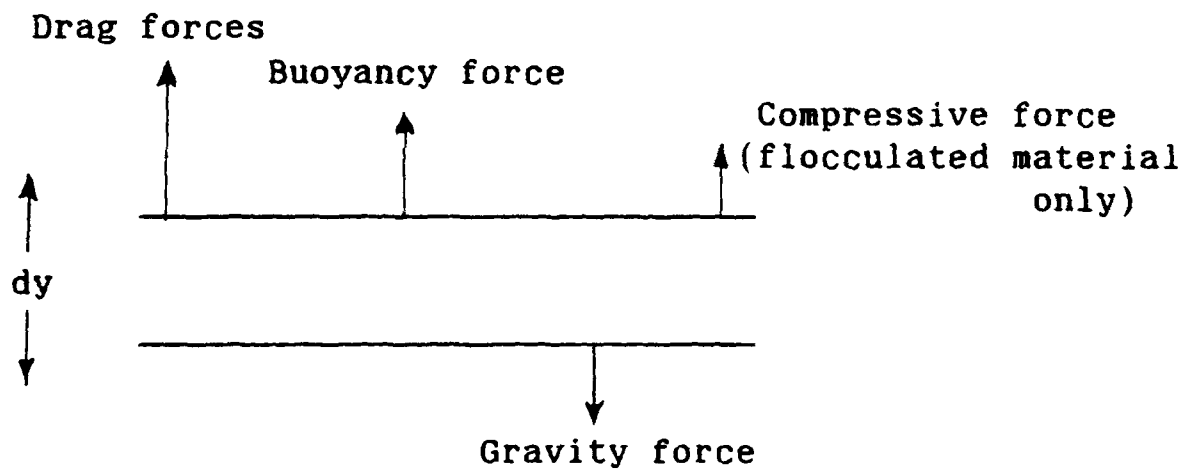

The compressive force is the solids pressure term which becomes dominant in the sediment region for flocculated slurries, see chapter six. The movement of the fluid phase is essentially due to the movement of solids. Therefore in the volume dy fluid is displaced due to the movement of particulates. This movement of the fluid phase can be described by an overall continuity equation, see equation 4.11. This eliminates the need to solve a fluid phase momentum equation, see Appendix.

4.2.1 Solid phase continuity

Associated with each solids phase is a continuity equation. This equation represents the conservation of mass for the relevant solids phase.

$$\frac{\partial(\rho_i S_i)}{\partial t} + \frac{\partial(\rho_i S_i U_i)}{\partial y} = 0 \qquad i=1..NSOL \qquad (4.1)$$

4.2.2 Solid phase momentum

The conservation of momentum for each solid phase is given by the following equation:

$$\frac{\partial}{\partial t}(S_i\rho_i U_i) + \frac{\partial}{\partial y}(S_i\rho_i U_i U_i) = F_D (V-U_i) + \sum_{j=1}^{NSOL} K_{ij} (U_j-U_i)$$

$$- S_i(\rho_i-\rho_m)g \quad i=1..NSOL \qquad (4.2)$$

The two terms on the L.H.S. represent the transient and convection terms respectively. The first term on the R.H.S. represents the fluid particle interaction. This is based on expressions used by Gidaspow (1985), where for flow in the free settling region the interaction term is:

$$F_D = \frac{3}{4} C_D \frac{\rho_f F|V-U_i|S_i}{(d_i\Phi_i)} H \qquad (4.3a)$$

and for flow within the packed structure of the sediment:

$$F_D = \frac{150(1-F)S_i\mu_f}{F(d_i\Phi_i)^2} + \frac{1{\cdot}75\rho_f|V-U_i|S_i}{(d_i\Phi_i)} \qquad (4.3b)$$

where H is the hindered settling effect, due to the presence of other particles, based on the Barnea (1973) correlation

$$H = (1 + (1-F)^{1/3}) \exp\left\{\frac{5(1-F)}{3F}\right\} \tag{4.4}$$

The drag coefficient C_D is given by the Schiller expression

$$C_D = \frac{24}{Re}(1 + 0{\cdot}15\ Re^{0{\cdot}687}) \tag{4.5}$$

where the Reynolds number is

$$Re = d_i \frac{\rho_f |V-U_i|}{\mu_f} F \ . \tag{4.6}$$

The second term represents the particle-particle interaction due to collisions. The interaction coefficient K_{ij} is given by the Nakamura (1976) expression:

$$K_{ij} = \frac{3}{2} \alpha_{ij}(1+e_{ij}) \frac{\rho_i \rho_j S_i S_j (d_i\Phi_i + d_j\Phi_j)^2}{\rho_i (d_i\Phi_i)^3 + \rho_j (d_j\Phi_j)^3} |U_i - U_j| \tag{4.7}$$

The final term represents the force due to gravity and buoyancy acting on the particles. The mixture density term is simply given by:

$$\rho_m = F\rho_f + \sum_{i=1}^{NSOL} \rho_i S_i \tag{4.8}$$

4.2.3 Concentration Balance

The volume fractions are related via the following equation:

$$F + \sum_{i=1}^{NSOL} S_i = 1 \tag{4.9}$$

where F is the fluid volume fraction. This equation states that only

solid phases and the fluid are present in the system.

4.2.4 Total Volumetric Balance.

The continuity equation for the fluid phase is given by:

$$\frac{\partial(\rho_f F)}{\partial t} + \frac{\partial(\rho_f FV)}{\partial y} = 0. \qquad (4.10)$$

As the fluid and solids are assumed to be incompressible, the density terms can be eliminated from equations 4.1 and 4.10. The resulting equations are for volume conservation. These equations can be combined to give the total volumetric balance equation:

$$\frac{\partial(FV)}{\partial y} + \sum_{i=1}^{NSOL} \frac{\partial}{\partial y} (S_i U_i) = 0 \qquad (4.11)$$

4.2.5 Boundary Conditions

Two main boundaries exist, these are at the top of the slurry and at the base of the vessel. The velocities at these boundaries are set to zero. As mentioned earlier other boundaries exist in the slurry (i.e. the sediment-free settling region interface and the interfaces for each solid phase in the free settling region) these will be discussed in the solution procedure, see section 4.5.

4.3 Discretised equations

The vessel is divided into a number of control volumes each of top and bottom area equal to that of the vessel base, and of height Δy, see Figure 4.2. Each of the governing equations are discretised using the fully implicit scheme and finite difference techniques as described by Patankar (1980).

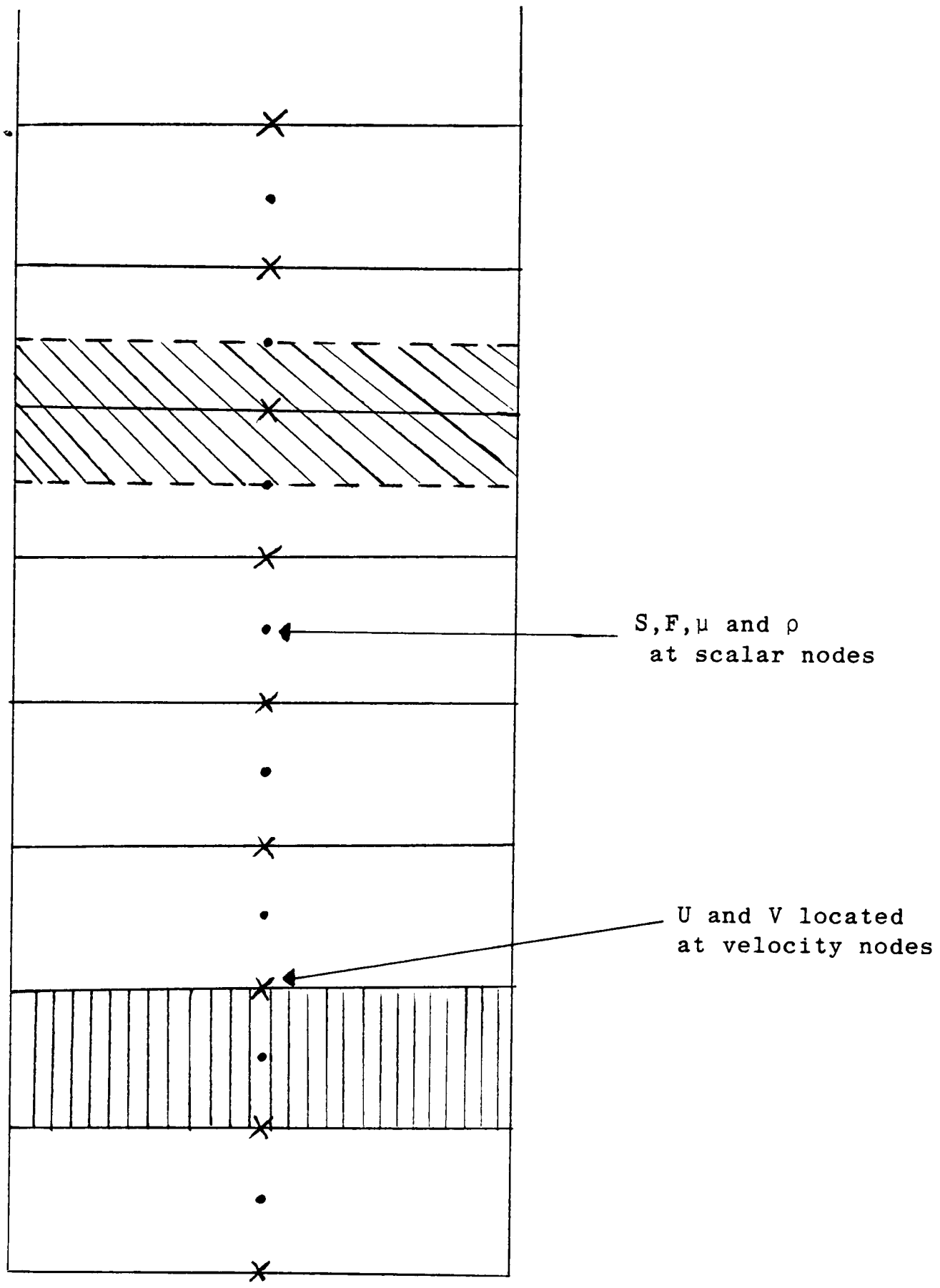

Figure 4.2 Control Volume Specification

The use of a staggered grid, where velocities are located at the interface between scalar cells, eliminates difficulties associated with first order derivatives. The upwind scheme is used as an approximation for first order derivatives, this states that the value of a dependent variable at an interface is equal to the value of that variable at the grid point on the upwind side of the face.

Consider a typical grid point, see Figure 4.3, the discretised equation for the dependent variable Φ at this point can be represented by:

$$AP\Phi_p = AN\Phi_N + AS\Phi_S + b \qquad (4.12)$$

where $\Phi_{P,N,S}$ is the dependent variable at the centre, North and South cells respectively. AN and AS are inflow contribution coefficients and AP is the outflow contribution coefficient. b represents the source term.

4.3.1 Solid Phase Continuity

The continuity equation (4.1) is integrated over the scalar control volume and time. Therefore, referring to Figure 4.3 as scalar control volumes then the integration gives:

$$\rho_i \int_s^n \int_t^{t+\Delta t} \frac{\partial S_i}{\partial t} \, dtdy + \rho_i \int_t^{t+\Delta t} \int_s^n \frac{\partial}{\partial y}(S_i U_i) dydt = 0 \qquad (4.13)$$

which discretises to an equation given by (4.12) where Φ is solids concentration $\dot{S}$ and:

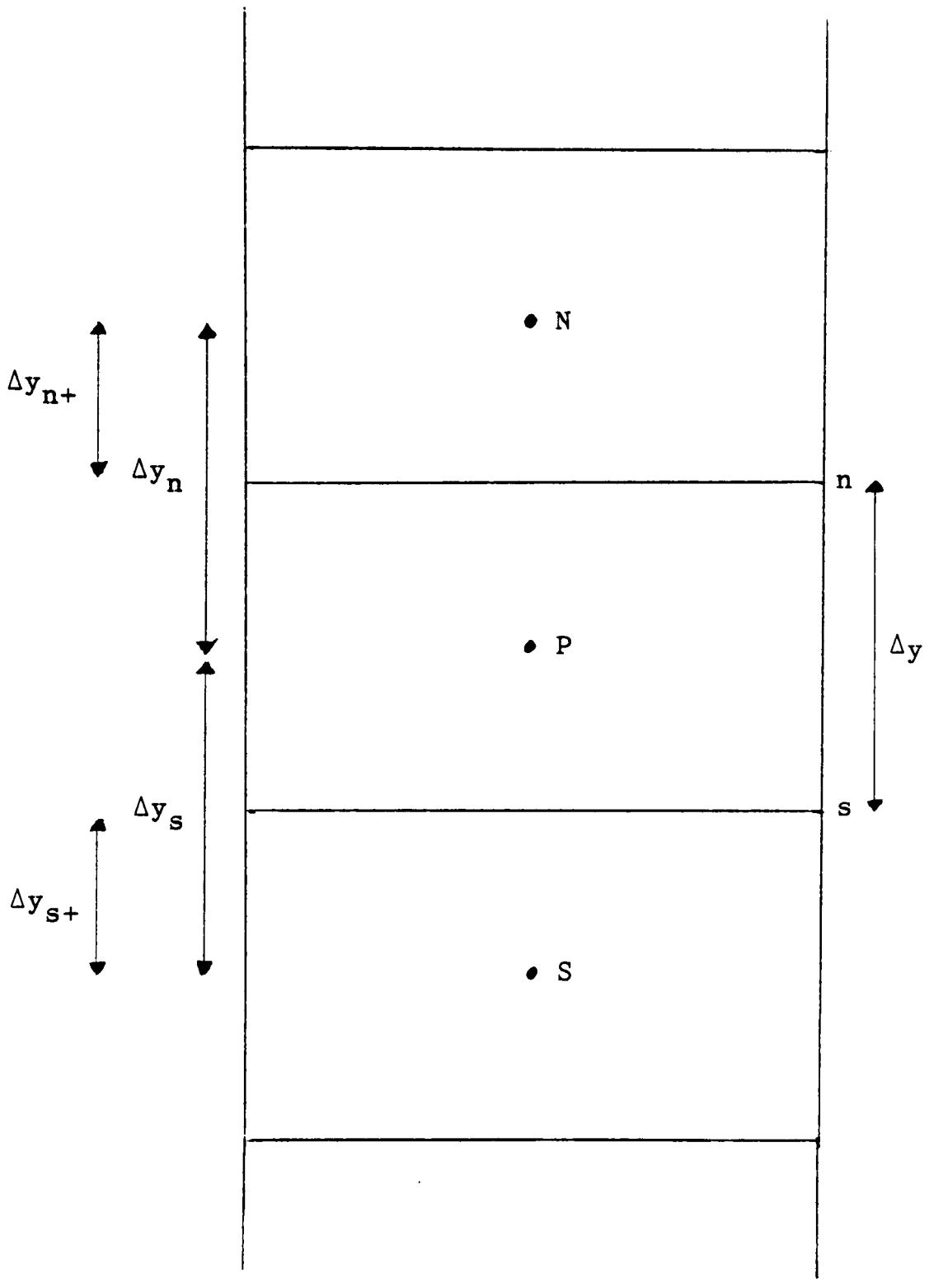

Figure 4.3 Typical Control Volume

$$AN = [\![-U_p, 0]\!] \tag{4.13a}$$

$$AS = [\![U_s, 0]\!] \tag{4.13b}$$

$$AP = \frac{\Delta y}{\Delta t} + [\![U_p, 0]\!] + [\![-U_s, 0]\!] \tag{4.13c}$$

$$b = \frac{\Delta y}{\Delta t} S_p^{OLD} \tag{4.13d}$$

where each of the above variables is for phase i.

4.3.2 Solid phase momentum.

The momentum equation (4.2) is integrated over the velocity control volume and time. Therefore, referring to Figure 4.3 as velocity control volumes then the integration gives:

$$\int_s^n \int_t^{t+\Delta t} \frac{\partial(\rho_i S_i U_i)}{\partial t} dt dy + \int_t^{t+\Delta t} \int_s^n \frac{\partial}{\partial y}(\rho_i S_i U_i U_i) dy dt = \int_t^{t+\Delta t} \int_s^n SOURCE\ dy dt \tag{4.14}$$

where SOURCE contains the gravity, buoyancy, fluid-particle interaction and particle-particle interaction terms. Equation (4.14) discretises to an equation of the form (4.12) where Φ is the solids velocity U and:

$$AN = [\![-\rho_i S_N(\alpha U_p + (1-\alpha)U_N), 0]\!] \tag{4.15a}$$

$$AS = [\![\rho_i S_p(\beta U_s + (1-\beta)U_p), 0]\!] \tag{4.15b}$$

$$AP = AN+AS + \rho_i(\gamma S_p^{OLD} + (1-\gamma)S_N^{OLD}) \frac{\Delta y}{\Delta t} - SP\ \Delta y \tag{4.15c}$$

$$b = U_p^{OLD}\rho_i(\gamma S_p^{OLD} + (1-\gamma)S_N^{OLD}) \frac{\Delta y}{\Delta t} + SC\ \Delta y \tag{4.15d}$$

where

$$\alpha = \frac{\Delta y_{n+}}{\Delta y_n} \tag{4.15e}$$

$$\beta = \frac{\Delta y_{s+}}{\Delta y_s} \tag{4.15f}$$

$$\gamma = \frac{\Delta y_n - \Delta y_{n+}}{\Delta y} \quad . \tag{4.15g}$$

(Note: That 4.15c is valid due to the application of continuity, see Patankar (1980)).

The source term contributions SP and SC are given by:

$$SP = - F_D - \sum_{j=1}^{NSOL} K_{ij} \tag{4.15h}$$

$$SC = F_D V_P + \sum_{j=1}^{NSOL} K_{ij} U_j - S_{INT} (\rho_i - \rho_m) g \tag{4.15i}$$

Where F_D, K_{ij} and ρ_m are given by equations (4.3), (4.7) and (4.8) and the concentration values in these expressions, which are at velocity nodes, are estimated via

$$S_{INT} = (\gamma S_p + (1-\gamma) S_N) \tag{4.15j}$$

where γ is given by equation (4.15g).

4.3.3 Concentration Balance.

The discretised form for this simple relationship is:

$$F_p + \sum_{i=1}^{N} (S_i)p = 1. \tag{4.16}$$

4.3.4 Total Volumetric Balance.

Equation (4.11) is integrated over the scalar control volume. Therefore referring to Figure 4.3 as scalar control volumes then the integration gives:

$$\int_s^n \frac{\partial(FV)}{\partial y}\, dy + \sum_{i=1}^{NSOL} \int_s^n \frac{\partial(S_i U_i)}{\partial y}\, dy = 0 \qquad (4.17)$$

which discretises to an equation of the form (4.12) where Φ is the fluid velocity V and:

$$AN = 0.0 \qquad (4.18a)$$

$$AS = 0.0 \qquad (4.18b)$$

$$AP = \begin{cases} F_N & \text{if } b < 0.0 \\ F_p & \text{if } b \geqslant 0.0 \end{cases} \qquad (4.18c)$$

$$b = \sum_{i=1}^{NSOL} \left\{ \mathbb{I}-(S_i)_N (U_i)_p, 0 \mathbb{I} - \mathbb{I}(S_i)_p, (U_i)_p, 0 \mathbb{I} \right\} \qquad (4.18d)$$

(Note that the values at the south face will already balance as the equations are solved from the base upwards, see solution procedure).

4.4 Incorporating Packing Theory

As particles reach the base of the vessel they will settle and pack to form the sediment, which for non-flocculated material will be incompressible. Due to a size distribution being present the concentration of the packing will depend on what solid phases are present.

4.4.1 Packing Model

During the last few years Ouchiyama (1980,1981,1984,1986) and Cross (1985) have developed a procedure for predicting the packing voidage of particulate size distributions. This model is used in the present study to predict the volume of solids, when treated as a dense packing, in the scalar control volume being packed.

Suppose that $V_C(d_i)$ is the space allocated to each particle of size d_i in the packed sediment. Then the total volume taking into account macropores, see Ouchiyama (1986), would be:

$$V_T = \max_{P} \sum_{i=1}^{P} V_C(d_i)\ N\ f(d_i) \qquad 1 \leqslant P \leqslant NSOL \qquad (4.19)$$

where N and $f(d_i)$ are the total number of particles present and the number fraction of size d_i in a packing consisting of phases 1 to P. Also phases 1 to NSOL represent the largest to the smallest particles respectively.

The main difficulty in solving for V_T is the calculation of $V_C(d_i)$. To estimate this value the following assumptions are made:-

a) Each particle is a sphere.

b) Each particle is surrounded by particles of average diameter $\bar{d}$, where:

$$\bar{d} = \sum_{i=1}^{P} d_i f(d_i) \qquad (4.20)$$

c) A shell $\bar{d}/2$ is imposed over the surface of each particle.

d) The number of notional volumes (particle plus shell) which share the shell space is independent of d_i.

Although the assumption of sphericity has been made, the model is not restricted to spherical particles, see Cross (1985). Figure 4.4 illustrates the model with respect to a particle of size d_i.

The volume of the notional shell that can be shared amongst other shells is:

$$V_M(d_i) = \frac{\pi}{6} \Phi_I^3 \left[(d_i+\bar{d})^3 - (d_i \sim \bar{d})^3\right] \qquad (4.21)$$

where:-

$$d_i - \bar{d} \quad \text{if} \quad d_i > \bar{d}$$

$$d_i \sim \bar{d} =$$

$$0 \quad \text{if} \quad d_i \leqslant \bar{d} \quad .$$

If $\bar{n}$ other notional volumes share $V_M(d_i)$ then the volume of space allocated to a particle of diameter d_i is:

$$V_C(d_i) = \frac{\pi}{6} \Phi_I^3 \left(d_i \sim \bar{d}^3\right) + \frac{V_M(d_i)}{\bar{n}} \qquad (4.22)$$

also the volume of solids in $V_C(d_i)$ is

$$V_S(d_i) = \frac{\pi}{6} \Phi_I^3 (d_i+\bar{d})^3 + [1-E_M(d_i)] \frac{V_M(d_i)}{\bar{n}} \qquad (4.23)$$

where $E_M(d_i)$ is the voidage of the shell.

The void volume of the shell is given by

$$E_M(d_i)V_M(d_i) = \frac{\pi}{6} (d_i+\bar{d})^3 - \frac{\pi}{6} d_i^3 - C(d_i)\frac{\pi}{12} d_i^3 \left\{1 - \frac{3}{8} \frac{\bar{d}}{d_i+\bar{d}}\right\} \qquad (4.24)$$

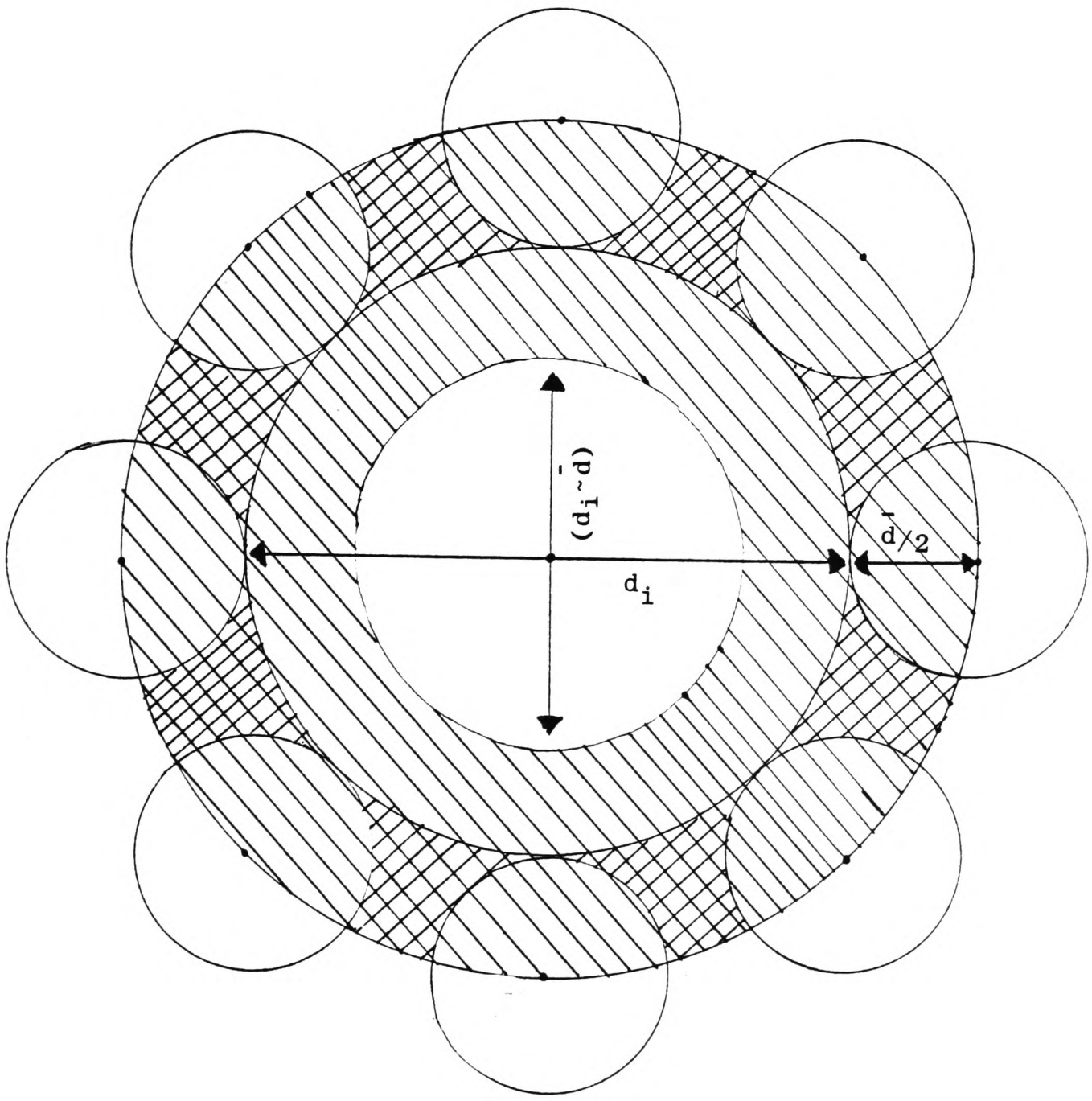

Figure 4.4 Packing Model

where $C(d_i)$ is the coordination number of a sphere,

$$C(d_i) = \frac{32}{13} [7 - 8E(d_i)] \left[\frac{d_i+\bar{d}}{2d}\right]^2 \qquad (4.25)$$

and $E(d_i)$ is the voidage of a packing consisting of particles of size d_i only, see Ouchiyama (1980).

The total solids volume in phases 1 to P is given by:

$$V_S = \sum_{i=1}^{P} \frac{\pi}{6} \Phi_i^3 \, d_i^3 \, N \, f(d_i) \qquad (4.26)$$

and

$$V_S = \sum_{i=1}^{P} V_S(d_i) \, N \, f(d_i). \qquad (4.27)$$

Using the above equations the volume of solids, when treated as a dense packing, in the cell being packed is calculated as follows.

1) Given size fractions d_i and voidages $E(d_i)$ and solids concentrations in cell being packed S_i then evaluate number fractions $f(d_i)$.
2) Using equation (4.20) evaluate $\bar{d}$.
3) Using equations (4.21) and (4.24) evaluate $E_M(d_i)$.
4) Use equations (4.23), (4.26) and (4.27) to evaluate $\bar{n}$.
5) Use equations (4.19) and (4.22) to evaluate V_T.

The calculated value of V_T can be compared with the cell volume Δy to see if the cell is fully packed with particulates.

4.4.2 Further densification of sediment

For non flocculated slurry's the sediment predicted, see section 4.4.1, will contain pores in which small particles may still penetrate and pack, see Kitchener (1977). In order to determine whether or not small particles may penetrate the packed structure forming the sediment an estimate of the size of the open pores is required.

An estimate which is used in this study is the hydraulic diameter, see Gray (1968). This is obtained by assuming the sediment to consist of a set of column channels of constant hydraulic diameter given by:

$$D_H = 4 \frac{\text{Volume of voids}}{\text{Surface area wetted by fluid}} \qquad (4.28a)$$

where:

$$\text{Volume of voids} = F\Delta y \qquad (4.28b)$$

$$\text{Surface area wetted by fluid} = 6\Delta y \sum_{i=1}^{NSOL} S_i/d_i \qquad (4.28c)$$

Therefore given the concentrations in the sediment an estimate of the pore size is given by:

$$D_H = \frac{2}{3} \frac{F}{\sum_{i=1}^{NSOL} \frac{S_i}{d_i}} \qquad (4.28d)$$

If particles exist whose diameter is less than D_H then these particles will penetrate into the sediment increasing the overall solids

concentration which will in turn decrease the hydraulic diameter. This process will continue until the solids diameter is greater than the hydraulic diameter. Also the movement of small particulates into a packed porous structure is governed by a modified form of the Ergun equation representing the fluid particle interaction term, see equation (4.3b).

4.5 Solution procedure

The dependent variables S_i, U_i (i=1...NSOL), F and V are to be solved at different locations throughout the vessel over time, see Figures (4.8). The equations to be solved at each time step are non-linear and highly coupled. Therefore, the finite difference equations (4.12) are solved using an iterative procedure. These finite difference equations are solved at each iteration in the following order:

1) Solid phase momentum and continuity for U_i and S_i respectively i=1...,NSOL.
2) Concentration balance for F.
3) Total volumetric balance for V.

At the next iteration the new value of the fluid velocity, V, will effect the movement of the particulates as it is incorporated into the momentum equation of each solid phase. This in turn will give rise to new values of S_i, U_i and F until convergence has been obtained.

As the variables to be solved are volume fractions and velocities the Jacobi point-by-point iterative procedure is used, see Markatos (1983). Therefore Φ_p is solved from the base upwards for all nodes in the vessel, via:

$$\Phi_P = (AN\Phi_N + AS\Phi_S + b)/AP \qquad (4.29)$$

where the values for Φ_N and Φ_S are from the previous iteration sweep.

The fluid volume fractions are calculated using equation (4.16) where the solid volume fractions are those at the present iteration. The fluid velocities are calculated using equations (4.18) together with (4.12) where the solid volume fractions and velocities in b, equation (4.18d), are those at the present iteration. As the solution procedure is from the base upwards then, when solving for V, the flow across the south face of each scalar control volume will balance and the solution procedure only needs to balance the flow across the north face. This gives rise to equations (4.18).

Each variable is checked for convergence at the end of each iteration. This is achieved by noting the maximum relative error associated with each variable (i.e. RESID) and comparing it with a given tolerance (i.e. TOL). The relative error at each node for variable Φ is obtained, via:

$$RESID = |\Phi - \Phi^*|/|\Phi| \qquad (4.30)$$

where Φ^* is the value of variable Φ at the previous iteration.

The movement of each solid phase boundary in the free settling zone is monitored by noting what scalar control volume the boundary is in initially (i.e. top cell). At the end of each time step the location of this boundary in the cell is calculated, via:

$$\Delta yT = \Delta yT^{*} - [-U_S, 0]\Delta t \qquad (4.31)$$

where ΔyT and ΔyT^{*} are the boundary positions in the cell at the present and previous time steps respectively. U_S is the velocity at the south face, see figure 4.6.

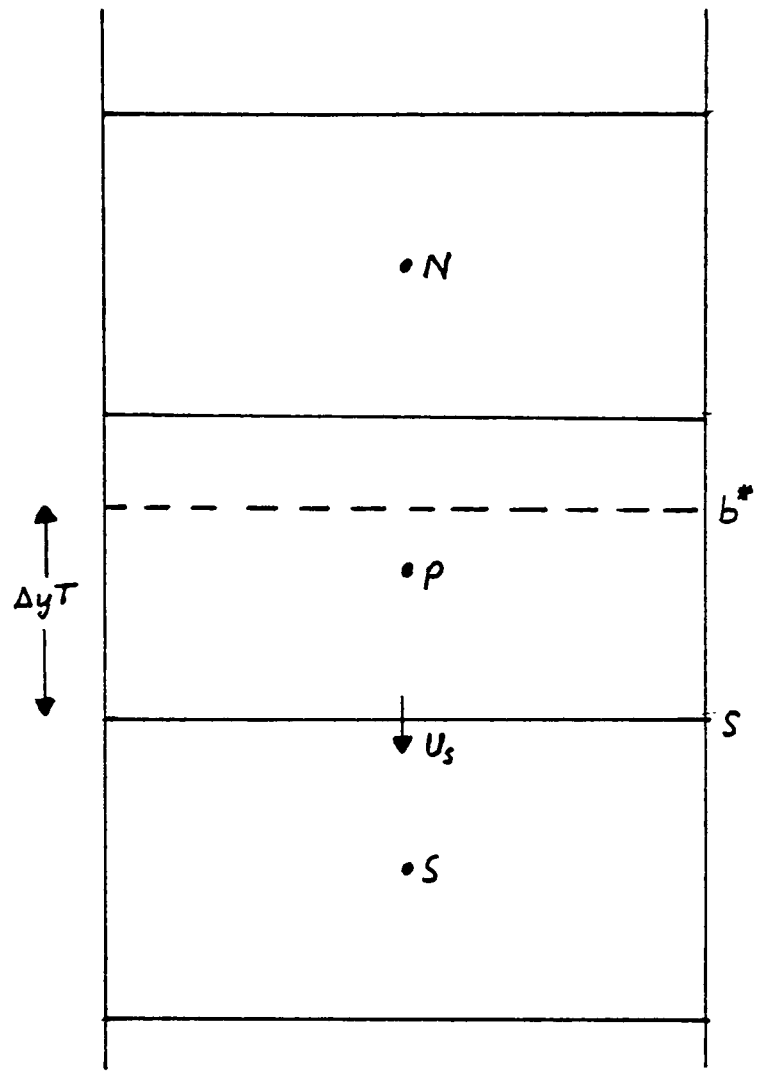

Figure 4.6 The Boundary Cell

The concentration S_{TB} in the boundry cell for phase i is noted when U_S for that phase becomes negative (i.e. downward flow). This concentration is assumed to be uniform throughout the cell. After intervals of time the cell will contain a lesser amount of phase i due to the movement of this phase out of the cell. The concentration of phase i between the boundary b^{*} and the interface S will be S_{TB} but the concentration at P will be for the whole cell. When solving

for U_S and the concentration at node S it is the value of S_{TB} which is used for cell P, not the concentration stored and calculated at P. This avoids a concentration gradient forming due to ignoring the presence of the boundary. When ΔyT becomes negative then the boundary has left the cell and entered the cell below. The concentration in the new boundary cell is adjusted to represent the new boundary position and value of S_{TB}.

The flow of solids into the cell being packed is modelled in a manner similar to the above procedures, see Figure 4.7.

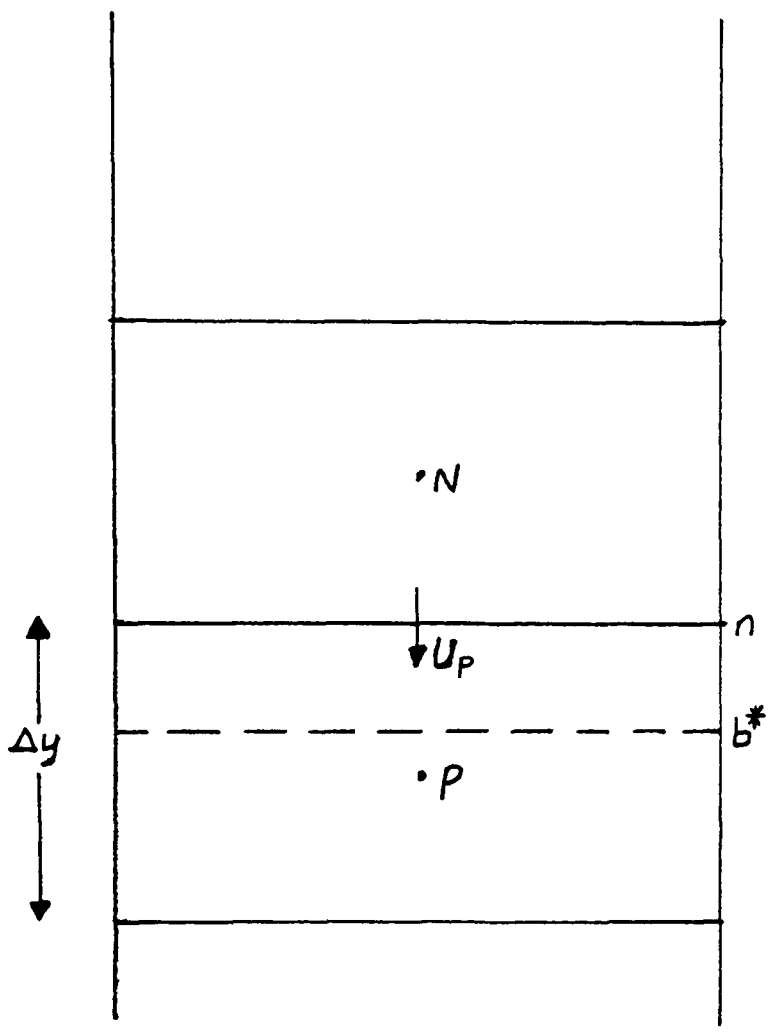

Figure 4.7 The sediment cell

The concentration between the boundary b^* and cell interface n will be the initial concentration S_{BB}. This is the value used for cell P when calculating U_p and concentrations at node N. This once again

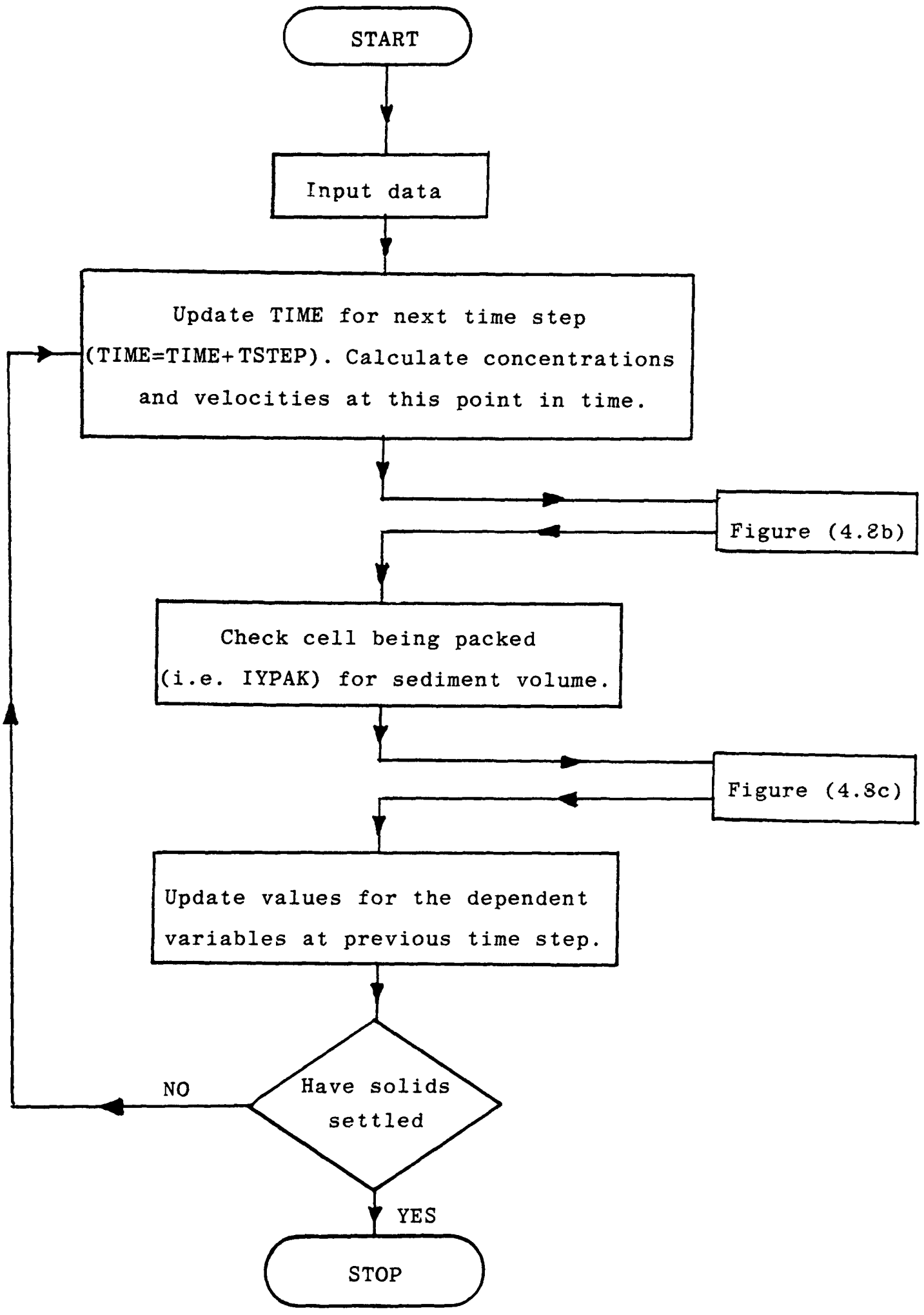

Figure 4.8a Overall solution procedure

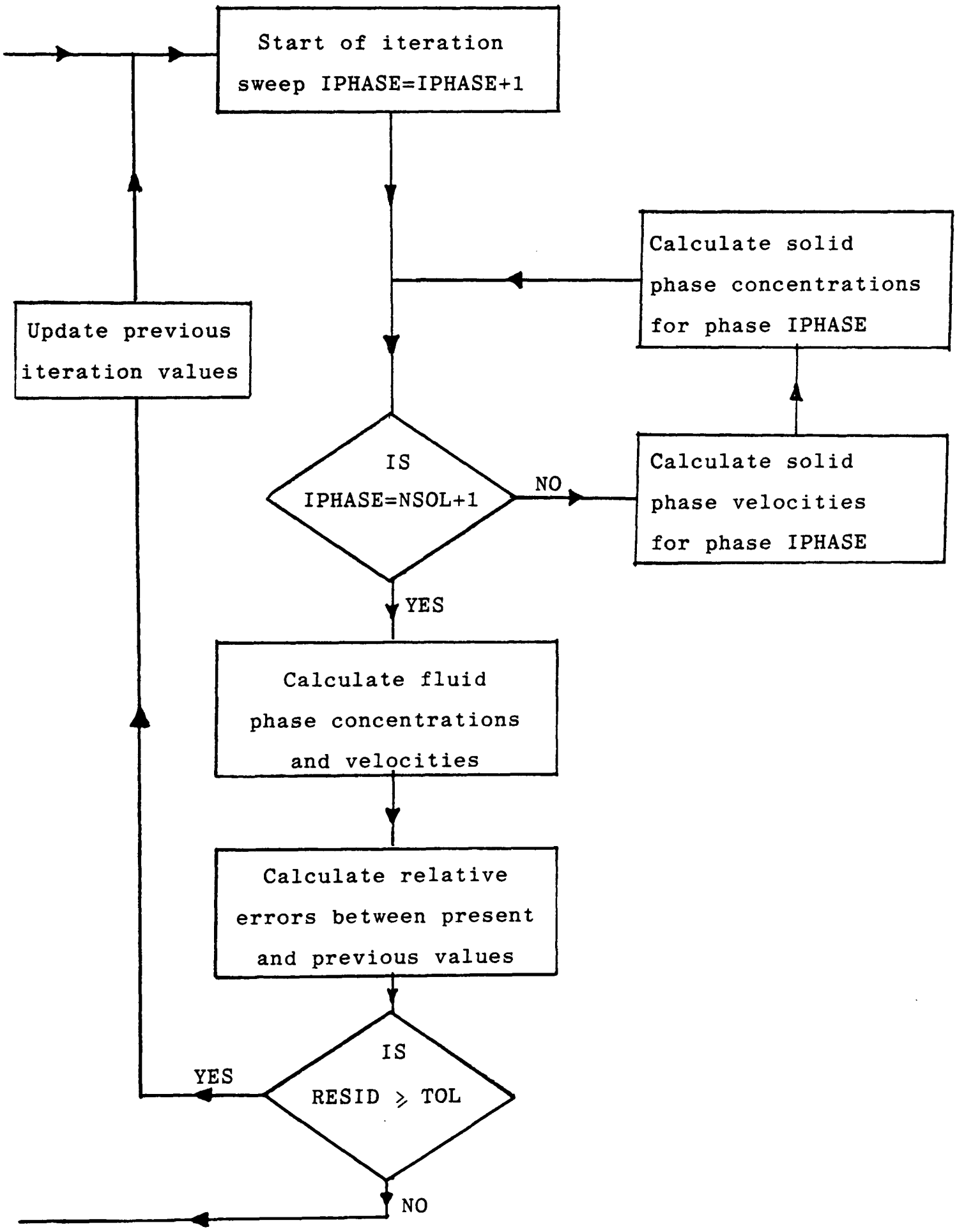

Figure 4.8b Iteration cycle

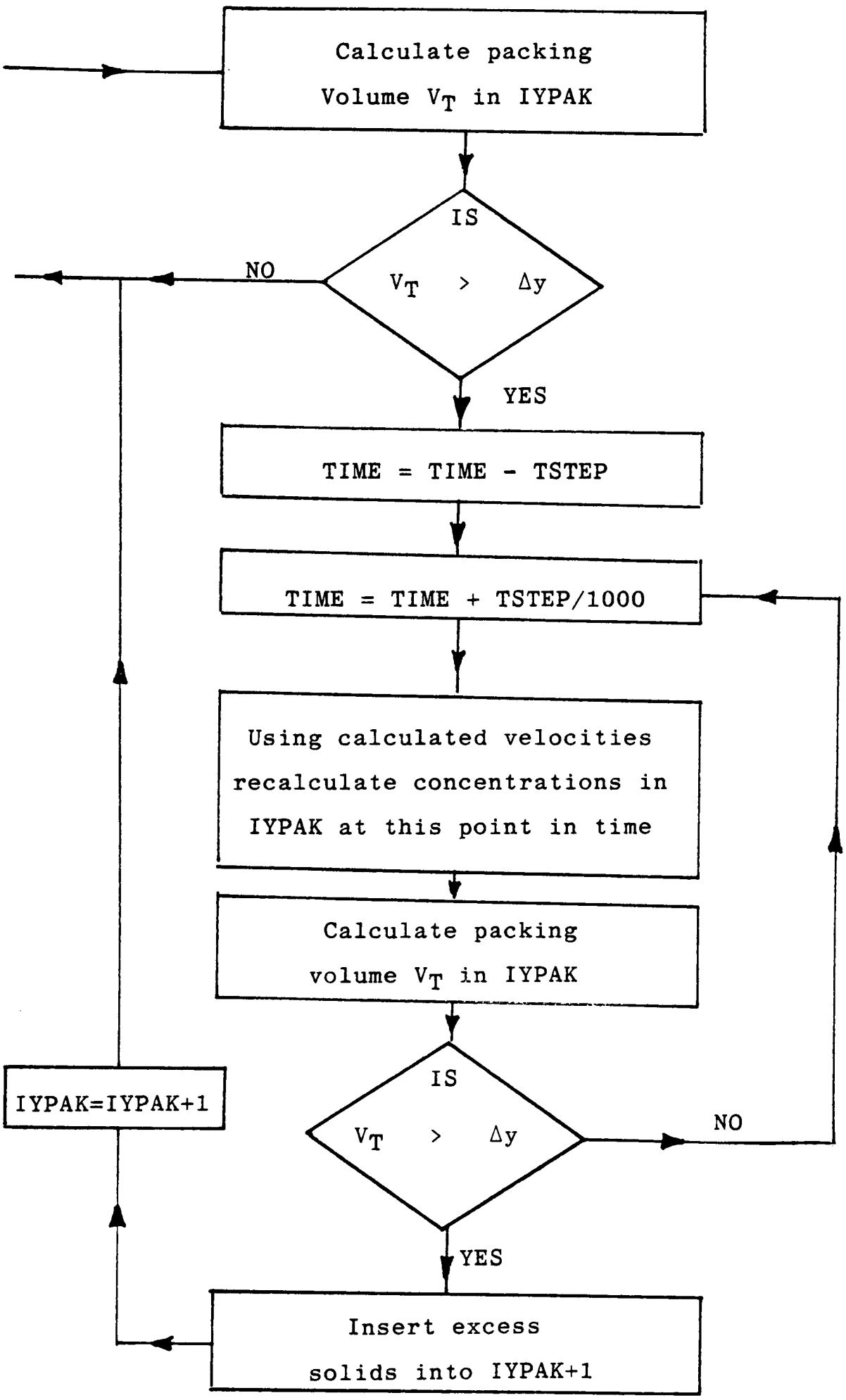

Figure 4.8c Packing cycle

avoids a concentration gradient forming due to ignoring the sediment boundary. When the cell becomes packed the concentrations are adjusted so that

$$V_T = \Delta y. \tag{4.32}$$

and the excess solids are inserted into the cell above. If the hydraulic diameter, see section (4.4.2), for the packed cell is greater than the diameter of the smaller particles then these may still flow into the cell until the hydraulic diameter becomes to small.

4.6 Comparisons with Holdich data

Concentration profiles have been obtained by Holdich, see Holdich (1983), for Ballontini undergoing settlement in water. The experimental procedure uses electrical conductivity techniques and a perspex tube of height 48cm and internal diameter 7·7cm. Unfortunately no size distribution was obtained for the Ballontini, but the material was carefully sieved between 45μ and 75μ and a mean particle diameter of 55μ was observed (by Microscopy). Data was gathered for seven experiments where the initial solids concentrations are 0·1, 0·15, 0·2, 0·25, 0·3, 0·35 and 0·4.

For this study it is essential to obtain a size distribution so that the multiphase effect can be observed. To enable this a Schumann distribution, see Schumann (1940), is used. This is given by:

$$Y = \left[\frac{X}{K}\right]^M \tag{4.33}$$

where Y is the cumulative fraction undersize represented by all

particles of size between 0μ and $X\mu$. K is the maximum particle size for which Y is unity and M is a constant near unity. The Ballontini is broken down into 2,3 and 5 phases by dividing the size range into equal parts. The concentrations for each phase is obtained by letting M equal 0·8, 1·3 and 1·55 for 2,3 and 5 phases respectively, see tables 4.1, 4.2 and 4.3.

The density of the Ballontini used was calculated using a density bottle to be 2865 Kg/m^3.

Comparisons between the experimental data obtained by Holdich and the model predictions at 1,2,3 and 5 phases are given in Figures 4·9-4·15. It can be seen that particle segregation occurs in all experiments due to the concentration gradients observed. The degree of segregation is higher at lower concentrations although at high concentrations it is still present. This obviously necessitates the use of multiphase techniques as the one phase predictions fail to predict the general settling profile. Although the model predicts the profiles better by increasing the number of phases used, it seems to underestimate velocities at 0·1 solids concentration and overestimates at 0·35 and 0·4. This is probably due to:

1) Use of the Schumann distribution to obtain initial phase concentrations.
2) Observed mean diameter of 55μ being in error.
3) Errors in experimental data.
4) The empirical correlations used for fluid-particle and particle-particle interactions being in error at these concentrations.

		Total Solids concentration						
Phase	Diameter(μ)	0·1	0·15	0·2	0·25	0·3	0·35	0.4
One	67·5	0·0288	0·043	0·0576	0·072	0·0864	0·1008	0·1153
Two	52·5	0·0712	0·107	0·1424	0·178	0·2136	0·2492	0·2847

Table 4.1 Concentrations and diameters for two phase mixtures.

		Total Solids concentration						
Phase	Diameter(μ)	0·1	0·15	0·2	0·25	0·3	0·35	0·4
One	70	0·033	0·05	0·066	0·082	0·1	0·115	0·13
Two	60	0·02	0·03	0·04	0·05	0·06	0·07	0·08
Three	50	0·047	0·07	0·094	0·118	0·14	0·165	0·19

Table 4.2 Concentrations and diameters for three phase mixtures.

		Total Solids concentration						
Phase	Diameter(μ)	0·1	0·15	0·2	0·25	0·3	0·35	0·4
One	72	0·025	0·038	0·05	0·063	0·075	0·088	0·1003
Two	66	0·019	0·029	0·038	0·048	0·058	0·068	0·0772
Three	60	0·013	0·020	0·027	0·033	0·04	0·046	0·0531
Four	54	0·009	0·013	0·018	0·022	0·026	0·03	0·0351
Five	48	0·034	0·05	0·067	0·084	0·101	0·118	0·1343

Table 4.3 Concentrations and diameters for five phase mixtures.

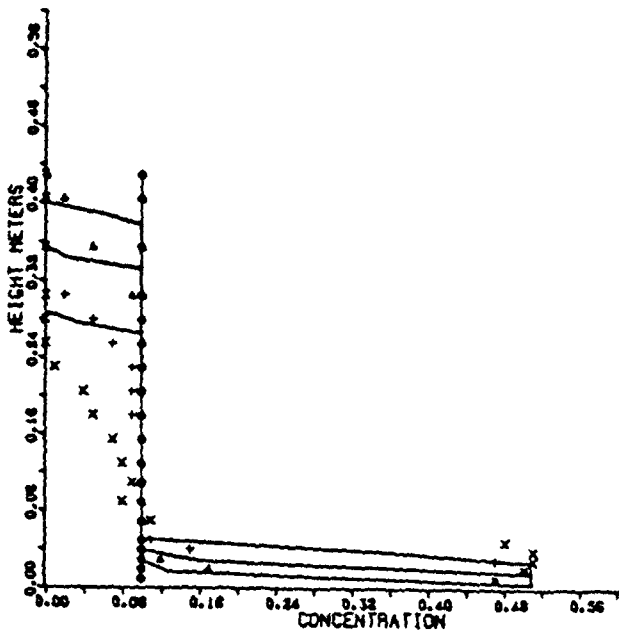

One phase

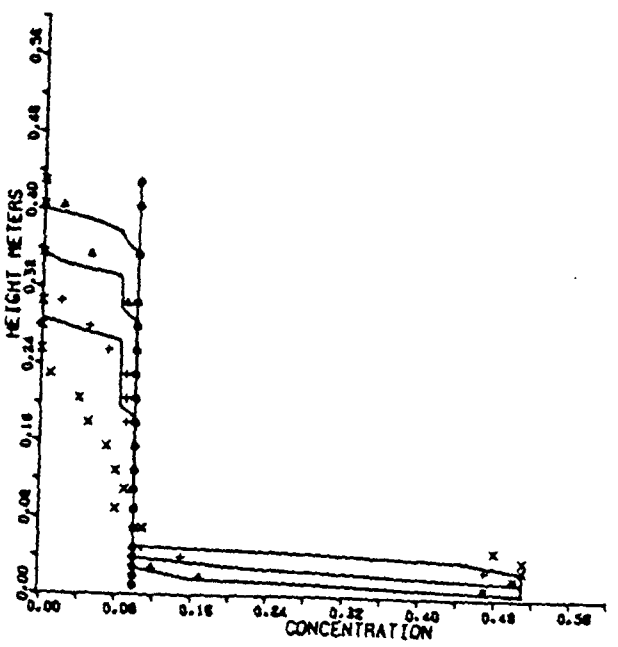

Two phases

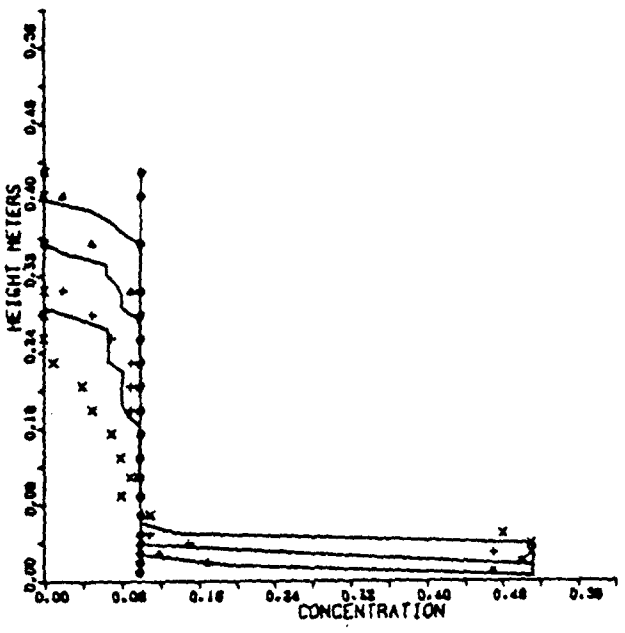

Three phases

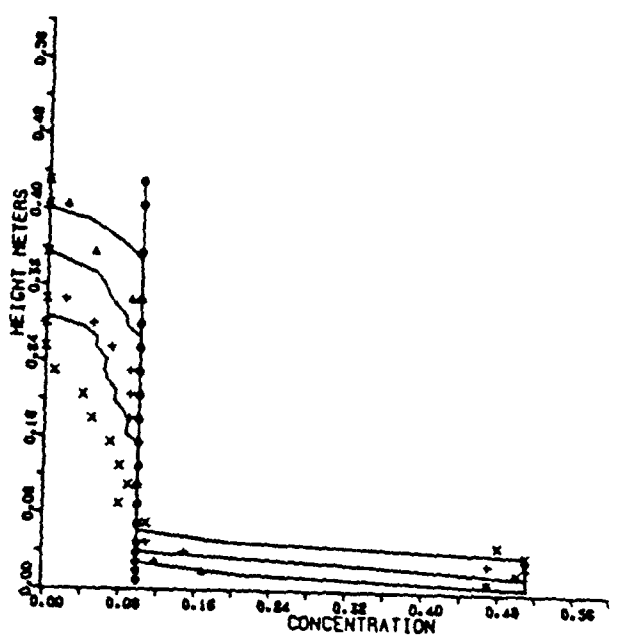

Five phases

Experimental Data

- ● Initial concentrations
- ▲ 36 secs
- \+ 1 run 12 secs
- x 2 mins

Figure 4.9 Comparisons with Holdich data at 90% porosity

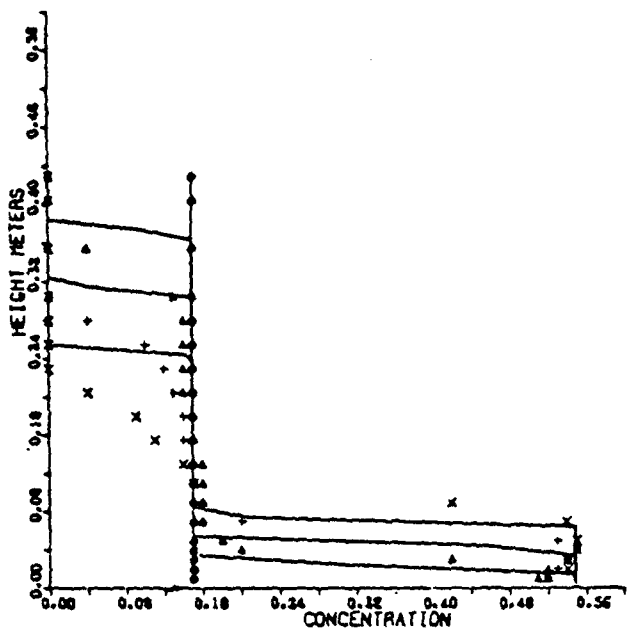

One phase

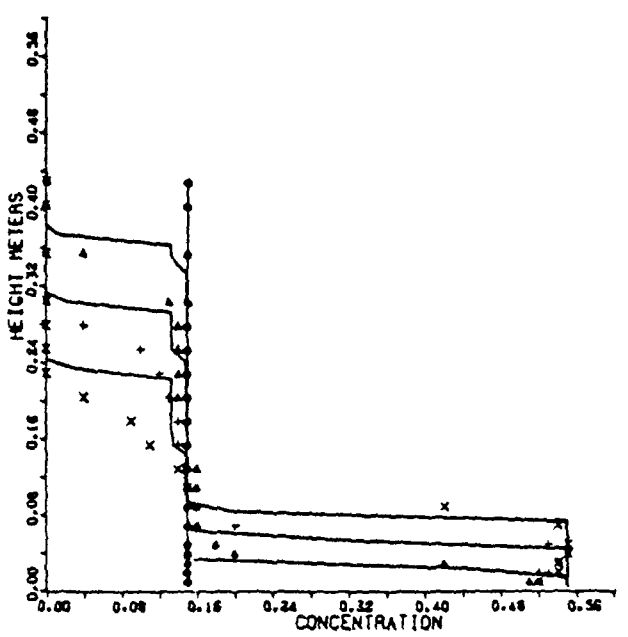

Two phases

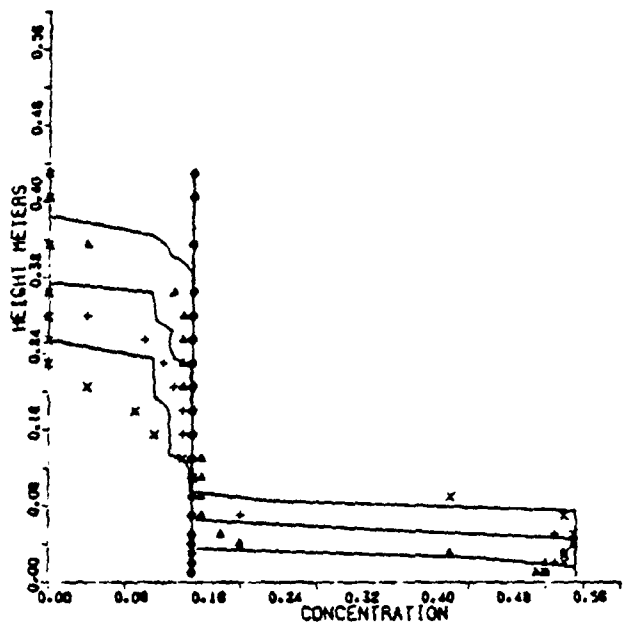

Three phases

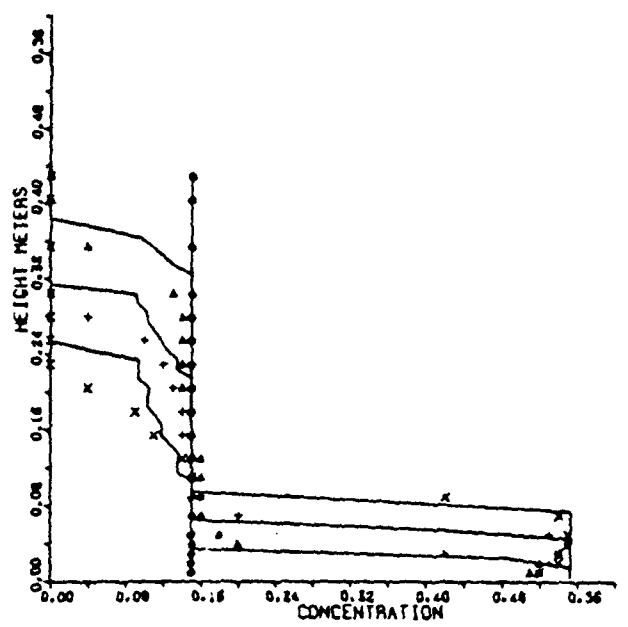

Five phases

Experimental data

- ● Initial concentrations
- ▲ 1 min
- \+ 2 mins
- x 3 mins

Figure 4.10 Comparisons with Holdich data at 85% porosity

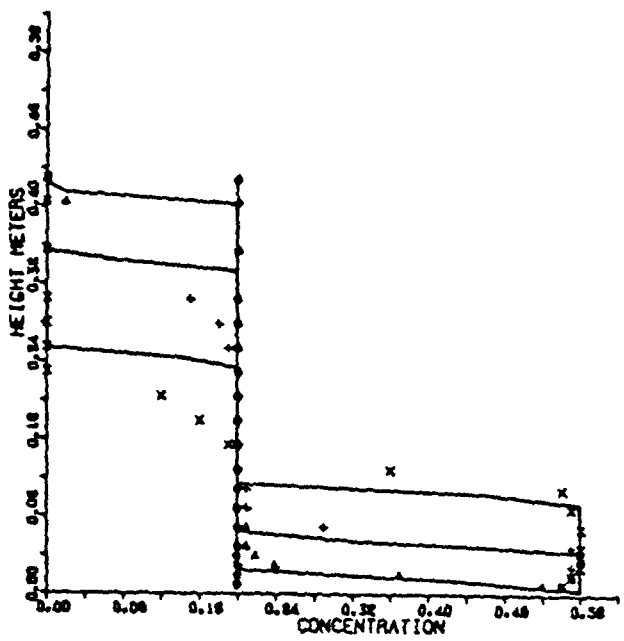

One phase

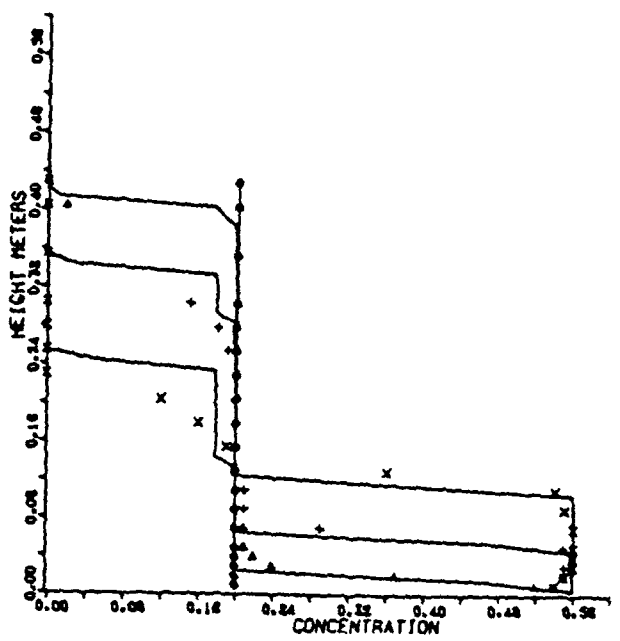

Two phases

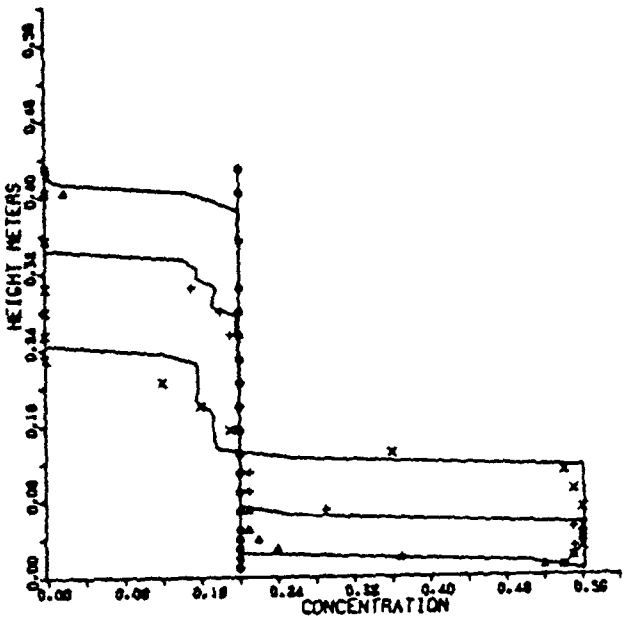

Three phases

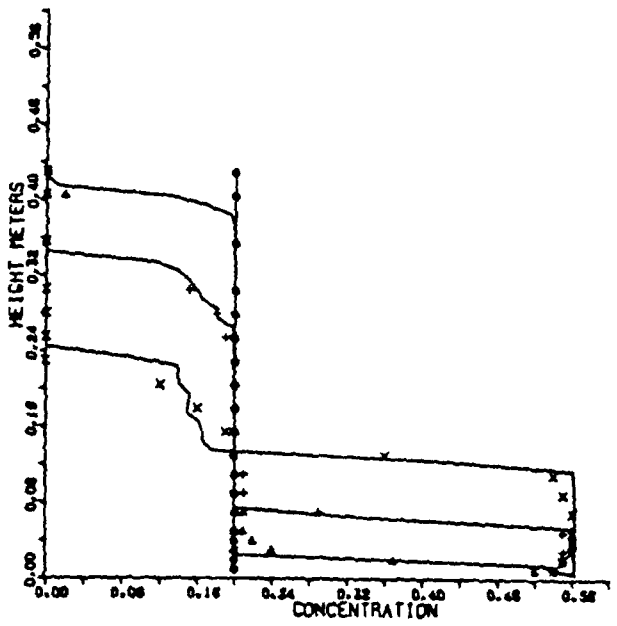

Five phases

Experimental Data

- ● Initial concentrations
- ▲ 36 secs
- \+ 2 mins
- x 4 mins

Figure 4.11 Comparisons with Holdich data at 80% porosity

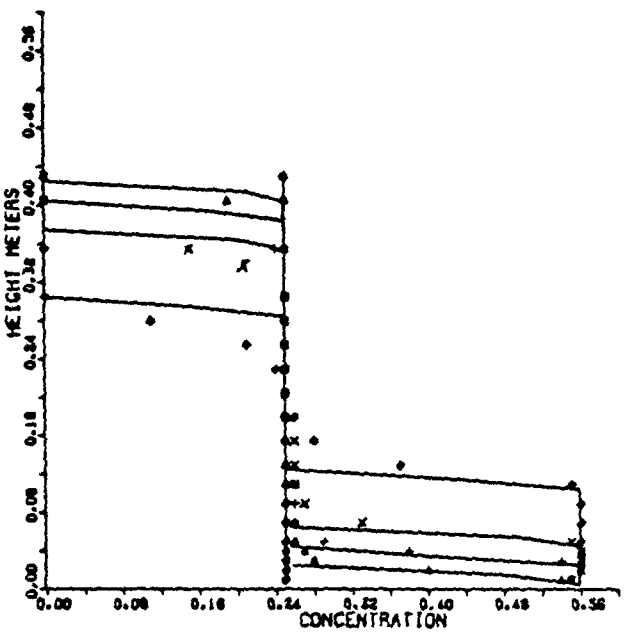

One phase

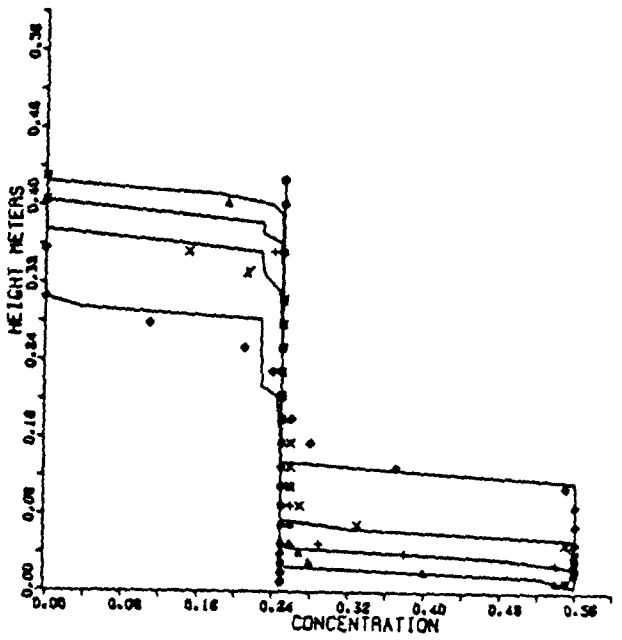

Two phases

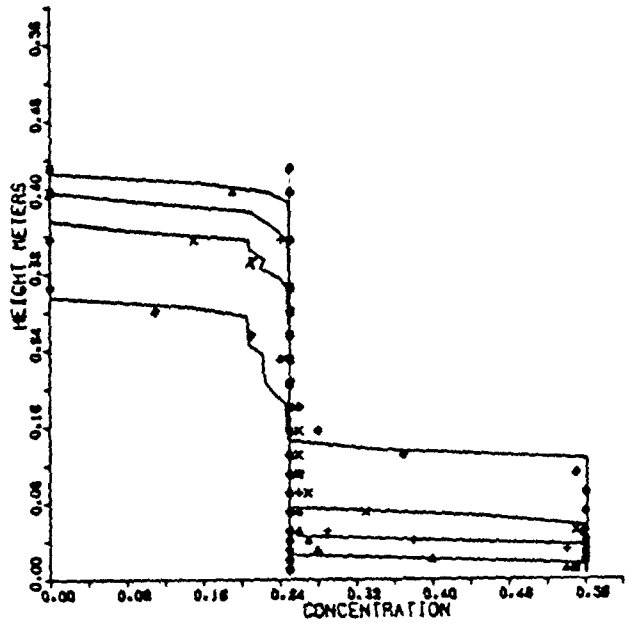

Three phases

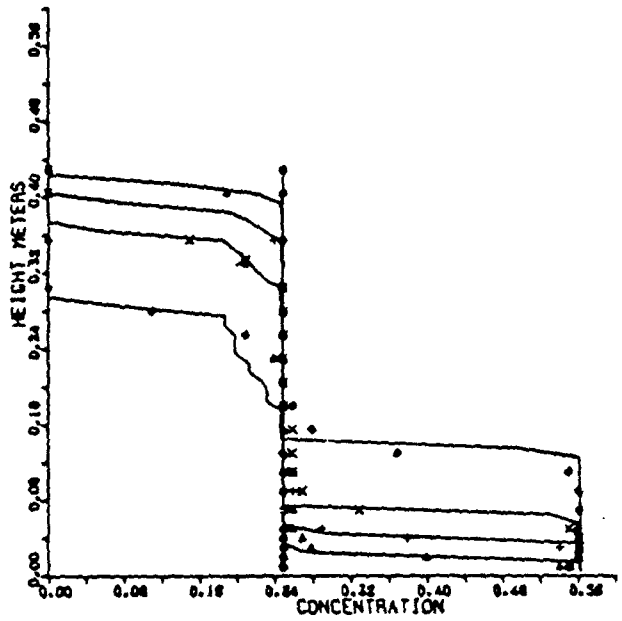

Five phases

Experimental data

- ● Initial concentrations
- ▲ 36 secs
- \+ 1 min 12 secs
- x 2 mins
- ◆ 4 mins

Figure 4.12 Comparison with Holdich data at 75% porosity

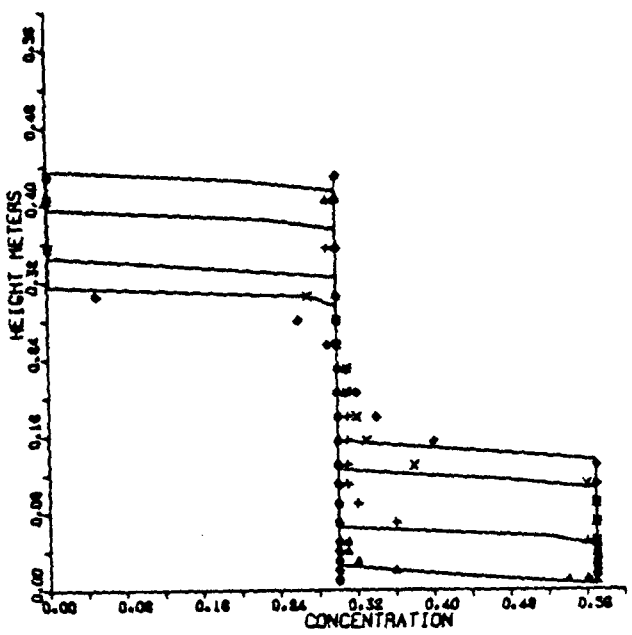

One phase

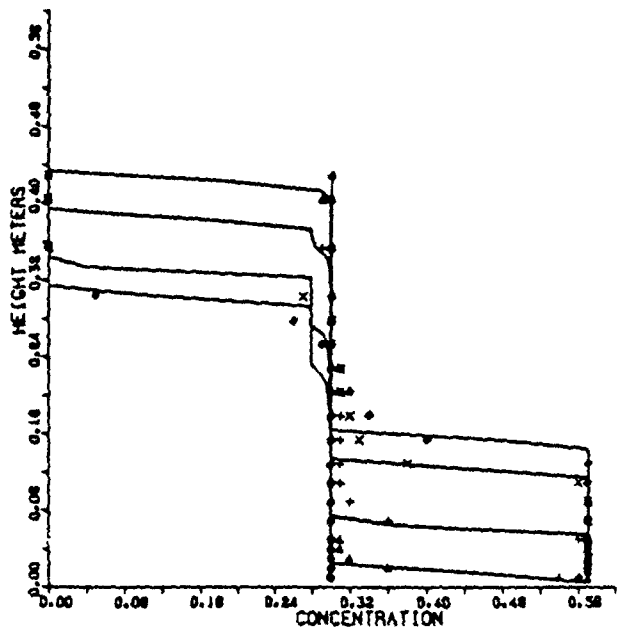

Two phases

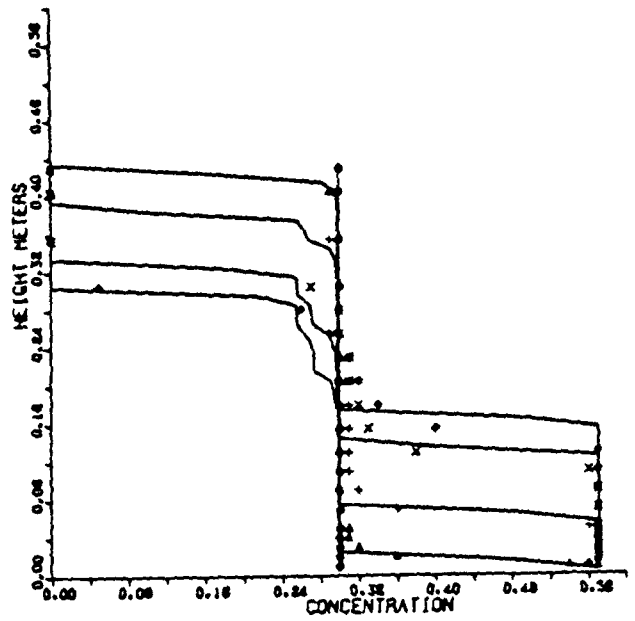

Three phases

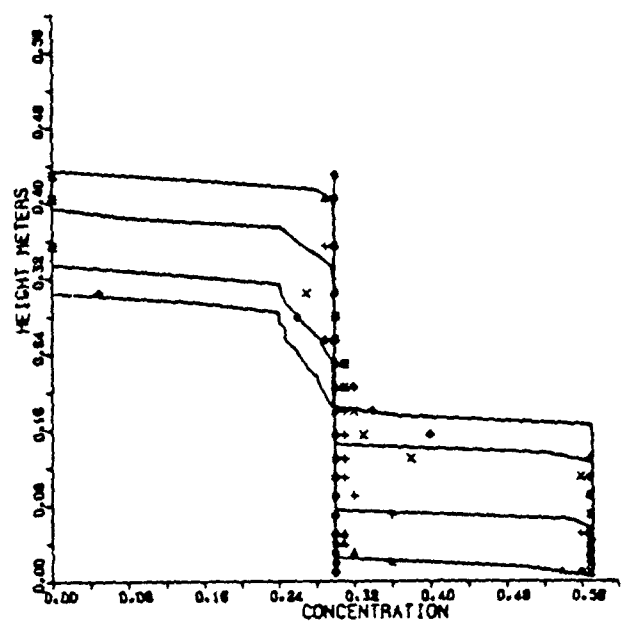

Five phases

Experimental data

- ● Initial concentrations
- ▲ 30 secs
- \+ 2 mins
- x 4 mins
- ◆ 5 mins

Figure 4.13 Comparisons with Holdich data at 70%

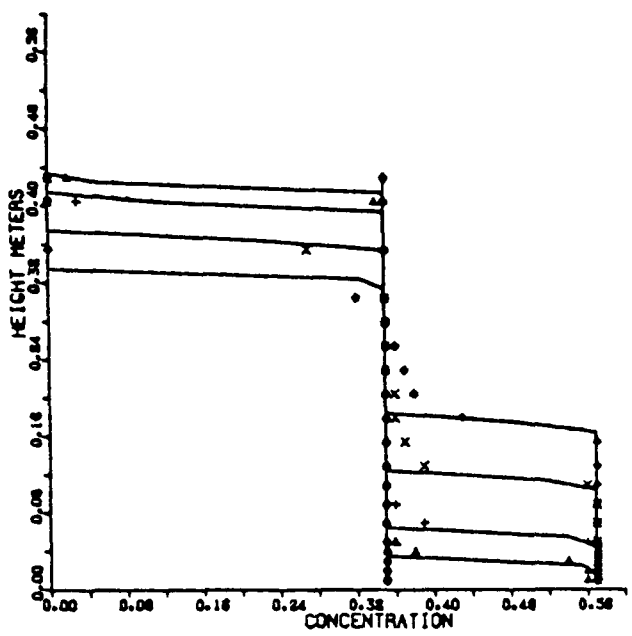

One phase

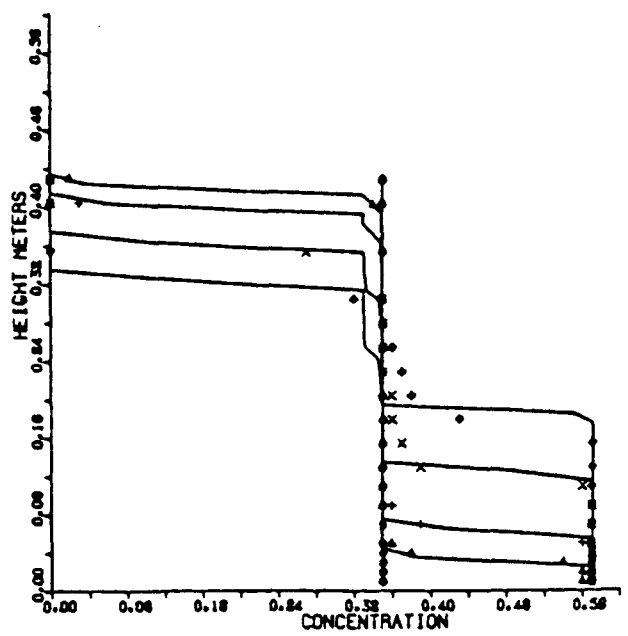

Two phases

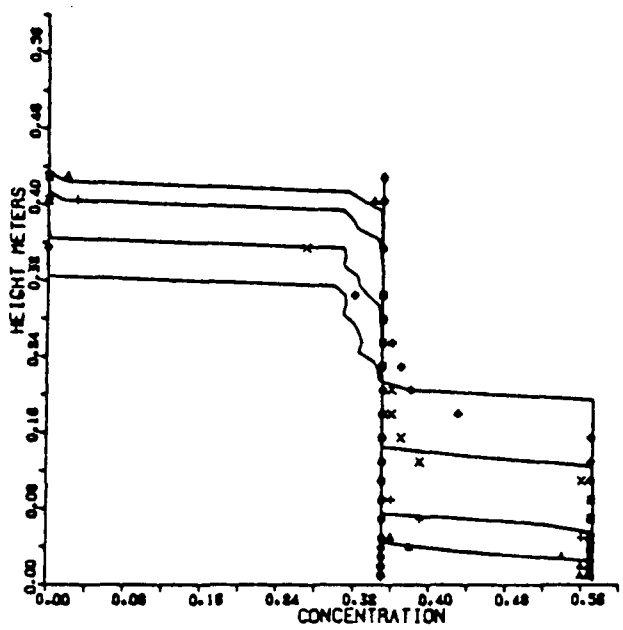

Three phases

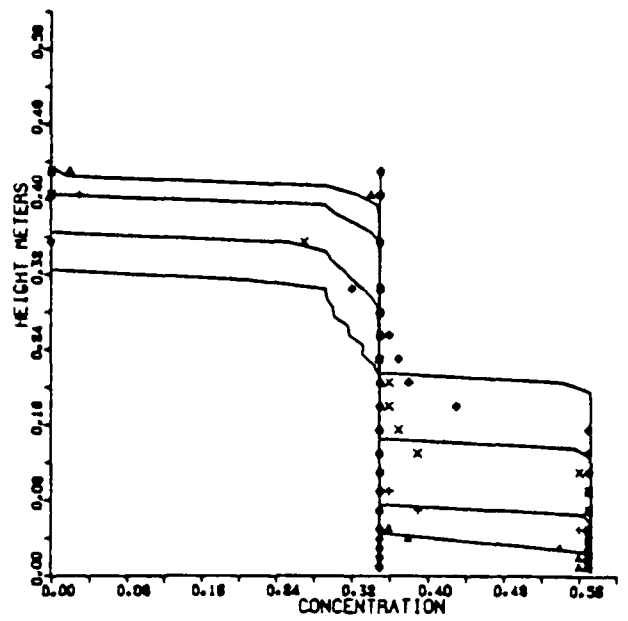

Five phases

Experimental data

- ● Initial concentrations
- ▲ 1 min
- \+ 2 mins
- x 4 mins
- ♦ 6 mins

Figure 4.14 Comparison with Holdich data at 65% porosity

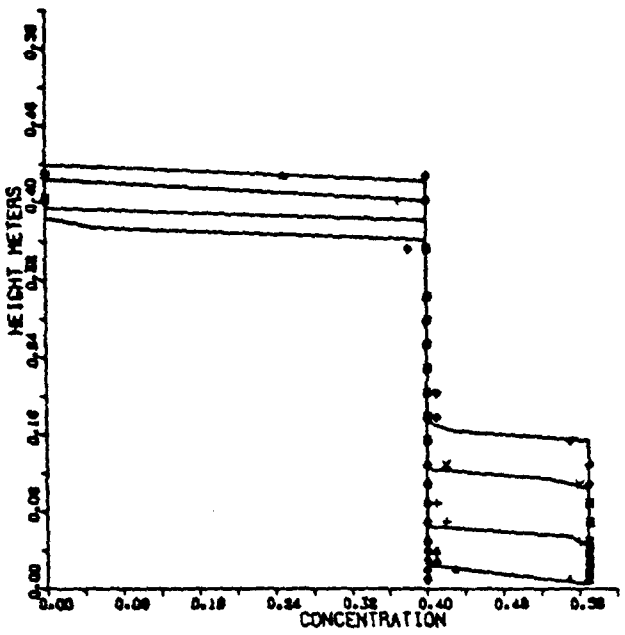

One phase

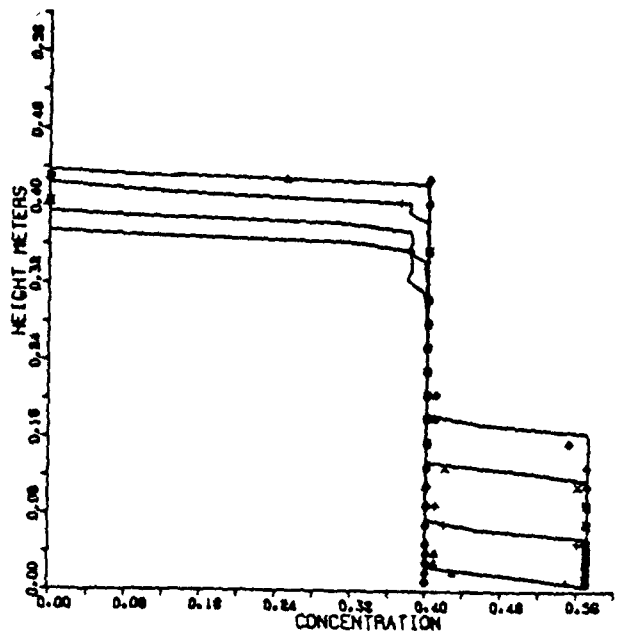

Two phases

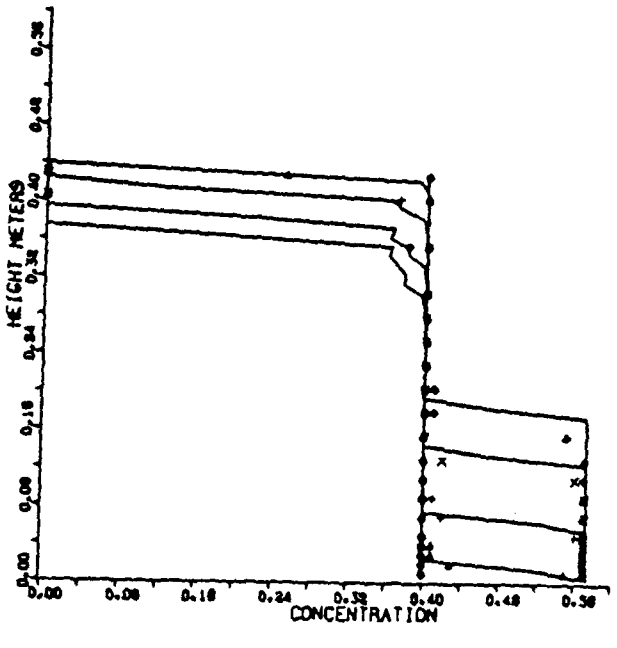

Three phases

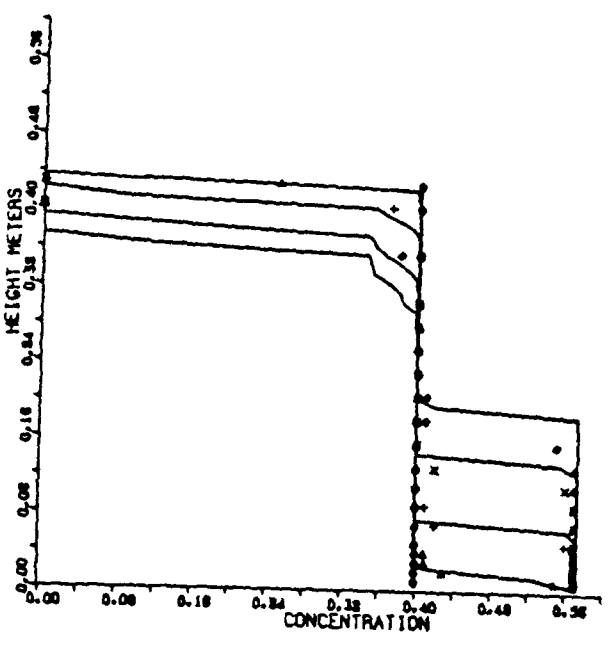

Five phases

Experimental data

- ● Initial concentrations
- ▲ 30 secs
- \+ 2 mins
- x 4 mins
- ♦ 5 mins

Figure 4.15 Comparison with Holdich data at 60% porosity

The concentrations observed in the sediment ranged from 0·58 for the 60% porosity experiment to 0·5 for the 90% porosity experiment. This is due to variation in the packing arrangement where the 60% porosity experiment settled much slower with a more ordered packing structure being observed. For this set of data the packing model used values of $E(d_i)$ to be the observed maximum concentration. In all cases the calculated hydraulic diameter was less than the smallest particle phase size, thus prohibiting particle movement into the sediment.

4.7 Comparisons with Experimental Data

Experimental data has been gathered for a number of one, two and three phase particulate mixtures undergoing batch sedimentation, see chapter two. These experiments measured the changes in slurry density above a certain height during the settlement of an initially uniform suspension. The above numerical model predicts concentrations at different points throughout a suspension. From these concentration profiles the slurry density above a transducer is calculated by:

$$\rho_h = \frac{\sum_{i=T}^{NY} \rho_m \, \Delta y_i}{h} \qquad (4.34)$$

where T is the cell containing the transducer and NY is the top cell. h is the height of mixture above the transducer and Δy_i is the volume of cell i containing a particulate mixture of density ρ_m, see equation (4.8). The volume Δy_T is not the volume of the cell containing the transducer but the volume between the transducer and the north face of the cell. Using the numerical model and equation (4.34) comparisons between density profiles obtained in chapter two and those predicted using the proposed model can be made.

For all the numerical simulations the values of the collision coefficients α_{ij} and e_{ij} are taken as one, which represents head on elastic conditions between each of the particulate phases, see Nakamura (1976). The voidage of each phase when packed alone, $E(d_i)$, is taken as 0·38 for Glass and Copper spheres which represents a random packing structure. The value of $E(d_i)$ for quartz, which is angular, is taken as 0·4, see Cross (1985). The sediment is checked for further compaction by calculating the hydraulic diameter.

Also compared with the experimental data is the model by Selim (1983), see chapter one, which presents the state of the art at the present time. The following plots represent these comparisons as well as concentration profiles of each particulate phase predicted by the proposed model.

4.7.1 One phase comparisons

For solid particulates represented by a unique size, density and shape factor the numerical model is used where the collision term K_{ij} is zero and further densification of the sediment is ignored due to the presence of only one solid phase.

Comparisons of both the Selim model and the proposed model with experimental data have been made, see figures (4.16-4.26). The outstanding feature in all these comparisons is the closer fit to the experimental data for the proposed model. The general trend seems to be that the Selim model over predicts the settling velocity of the particulates. This in turn gives greater density changes over time than those observed. The greater deviations between the proposed model and the experimental data during the later part of the experiments is due to segregation effects. This is because the particle size used to

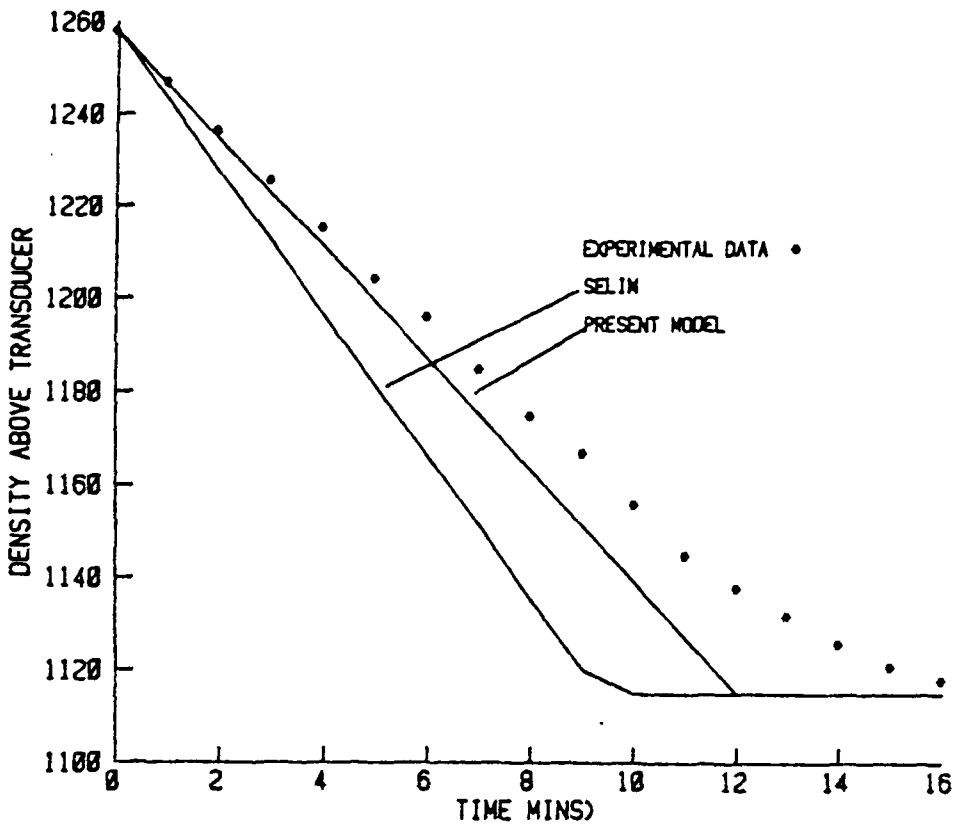

Density profile

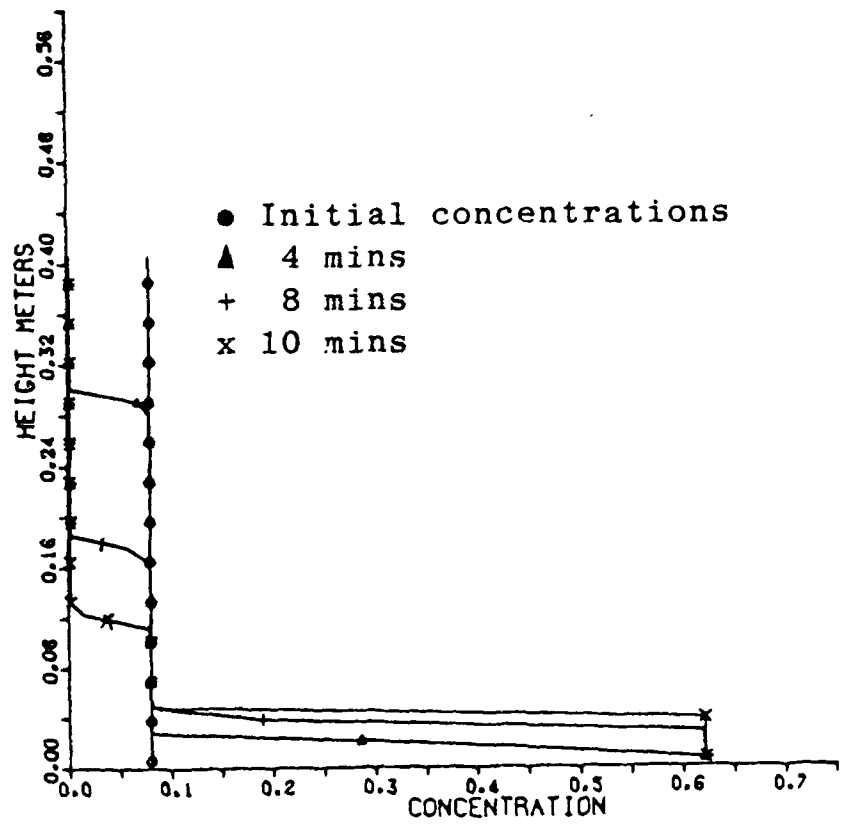

Glass (lead) 120μ

Figure 4.16 Density and concentration profiles for One Phase Exp one.

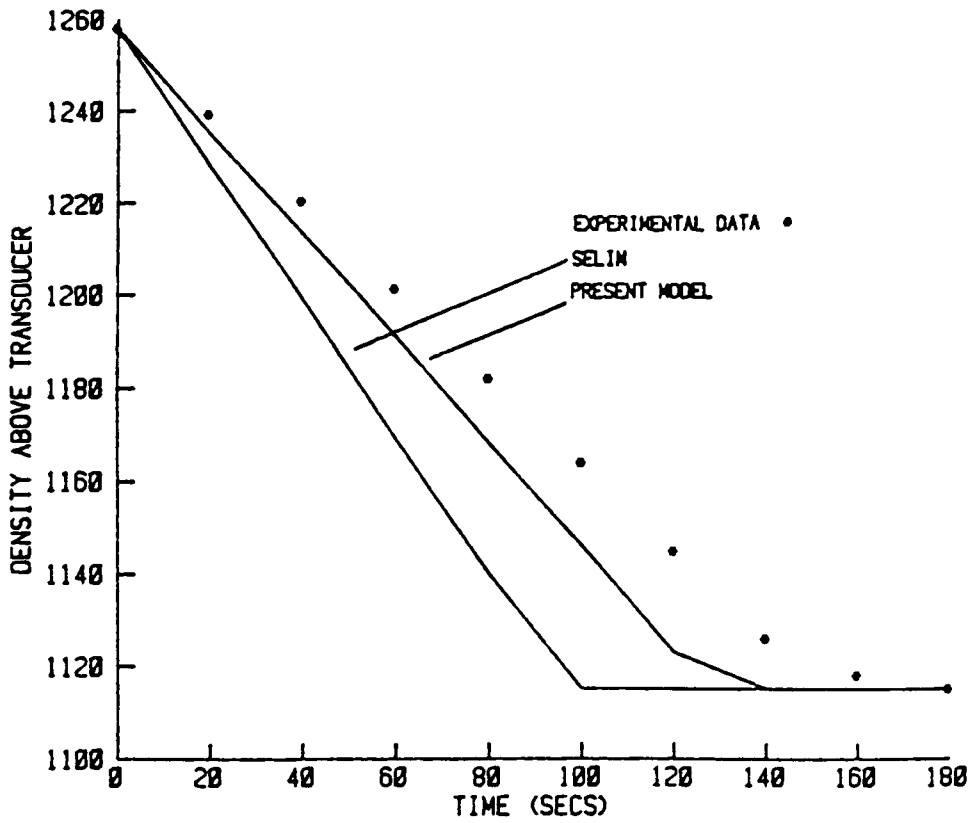

Density profile

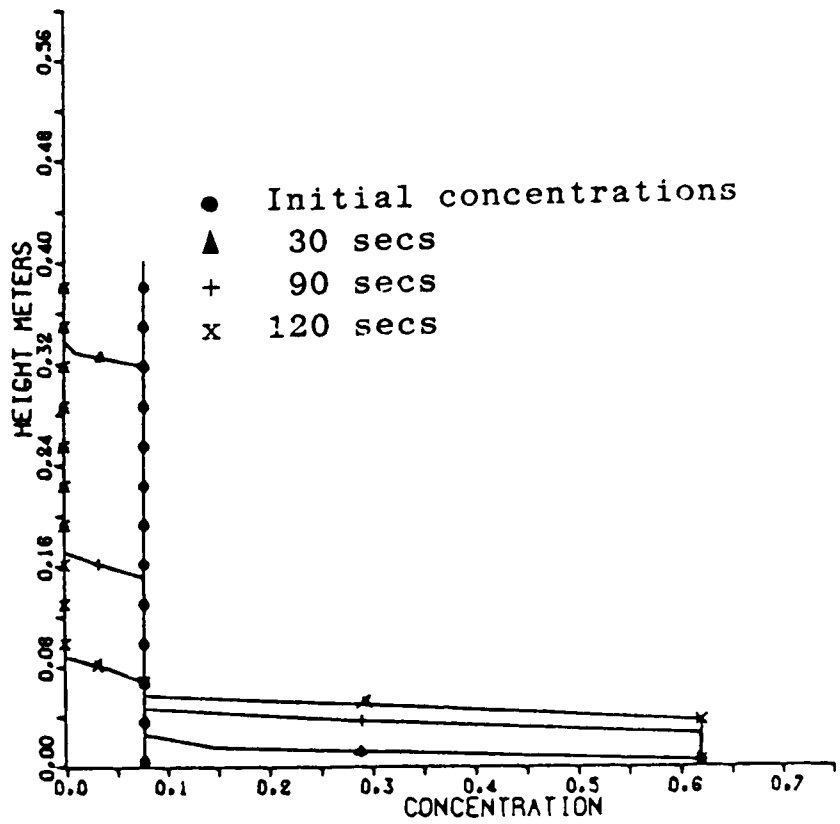

Glass (lead) 275μ

Figure 4.17 Density and concentration profiles for One phase Exp two.

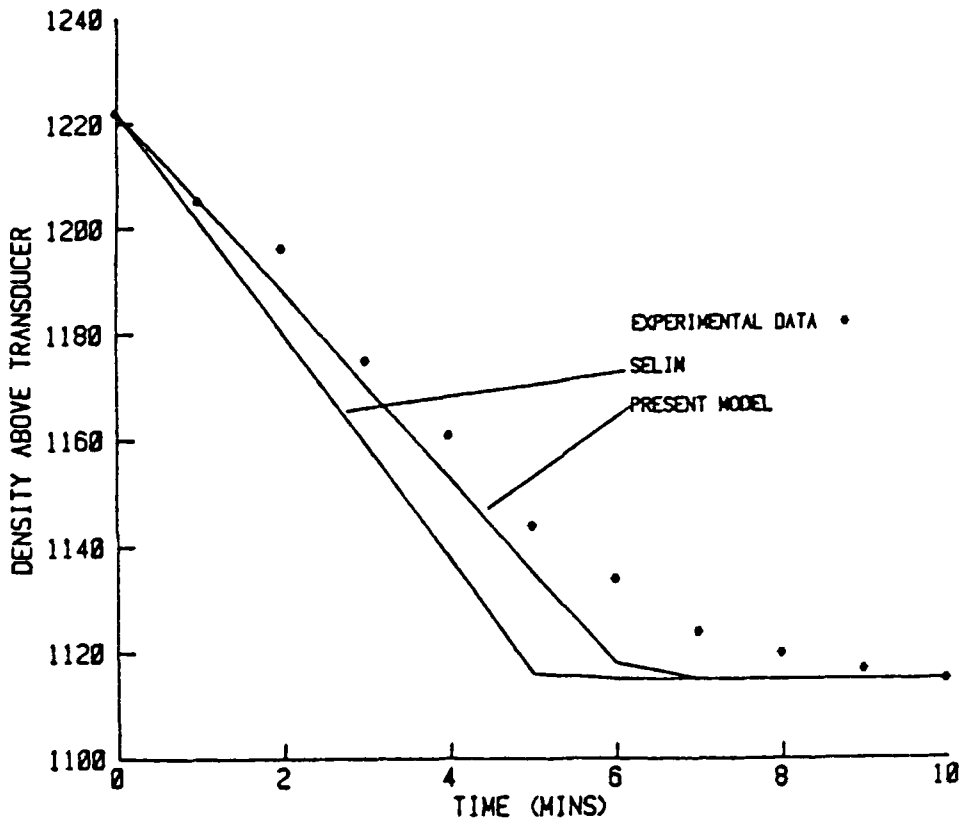

Density profile

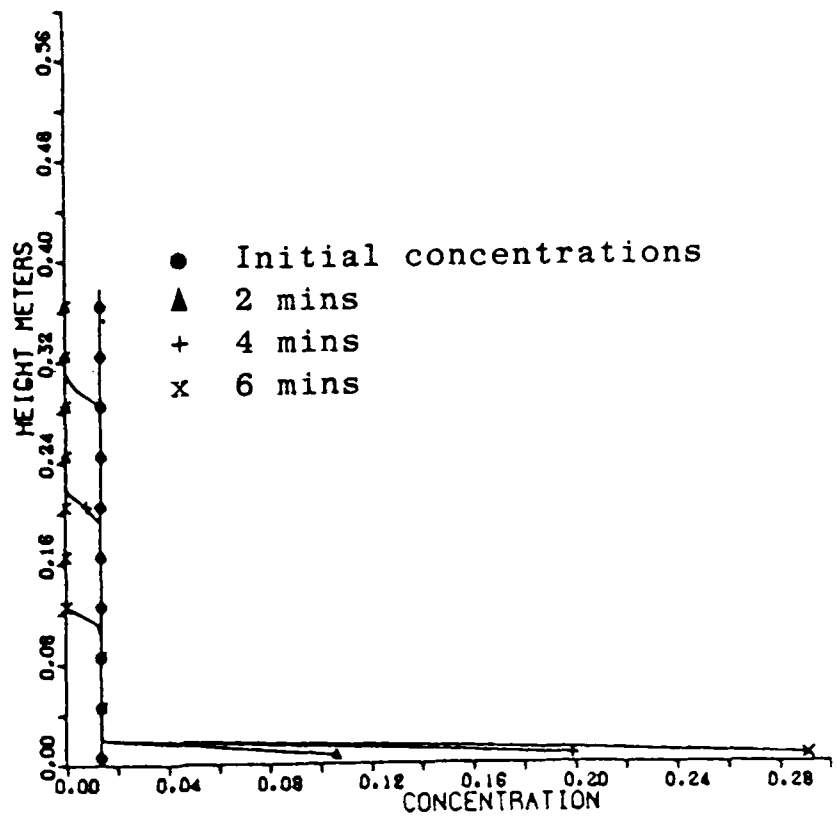

Copper 56.5μ

Figure 4.18 Density and concentration profile for One phase Exp three.

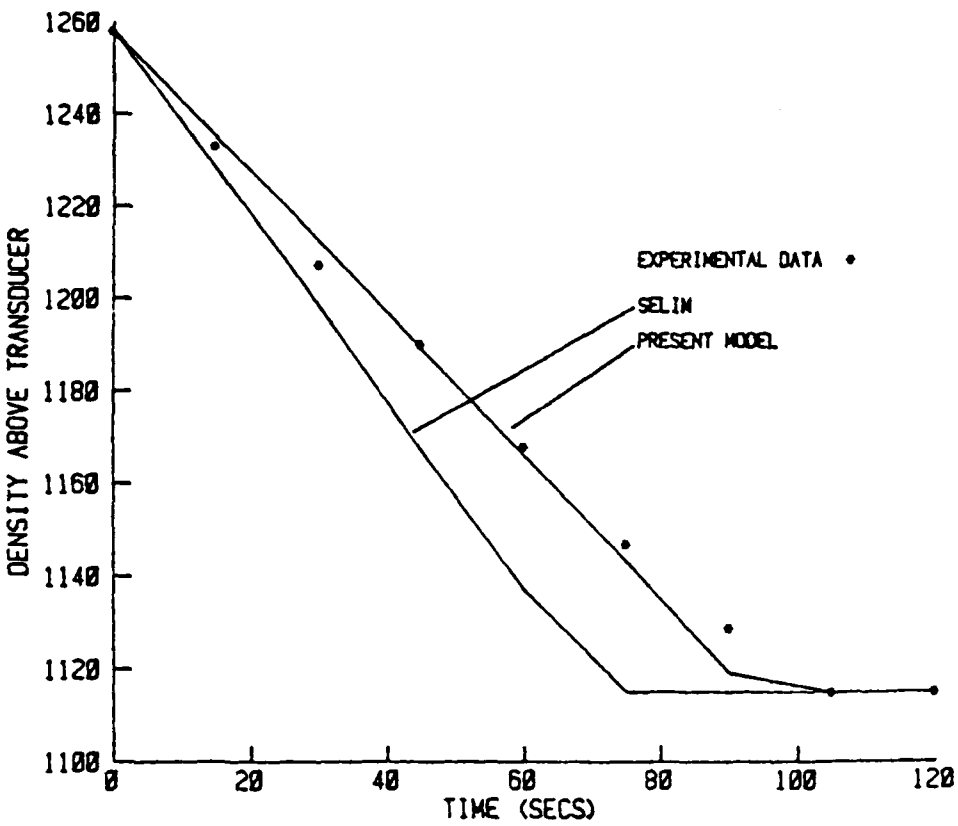

Density profile

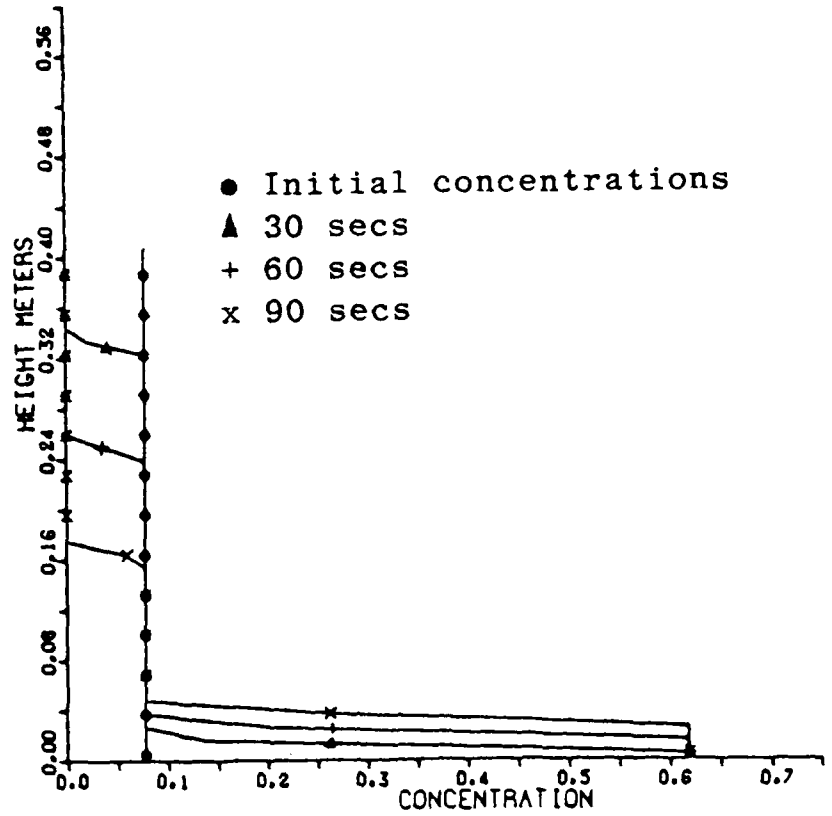

Glass (lead) 275μ

Figure 4.19 Density and concentration profiles for One phase Exp four.

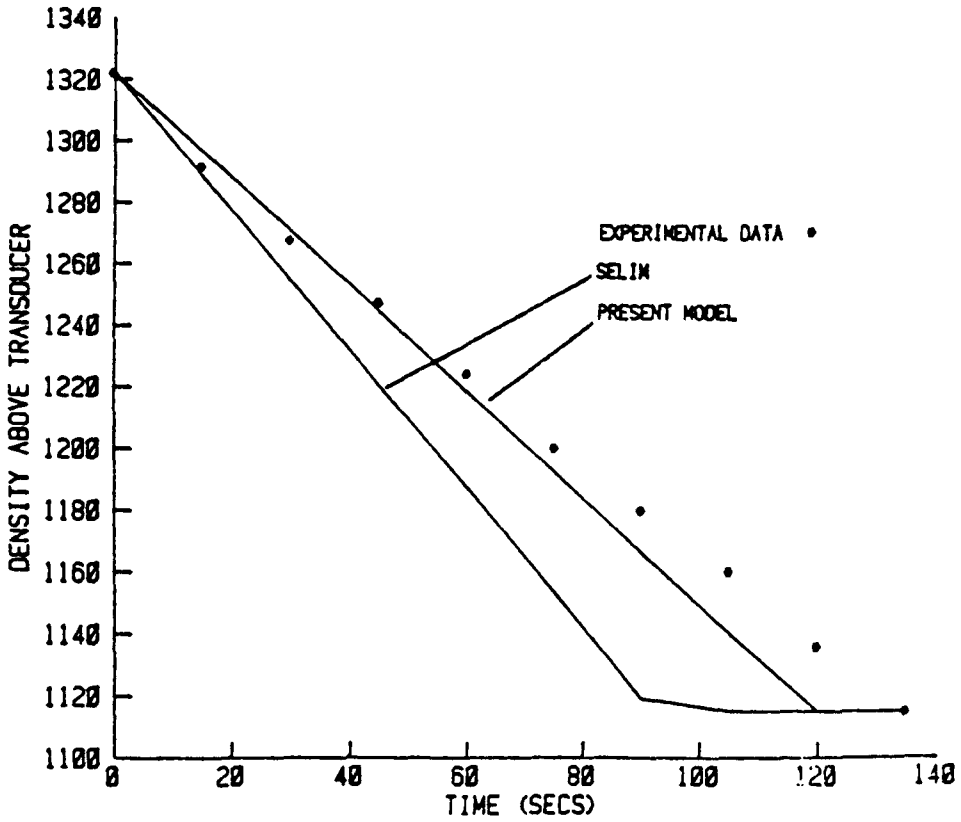

Density profile

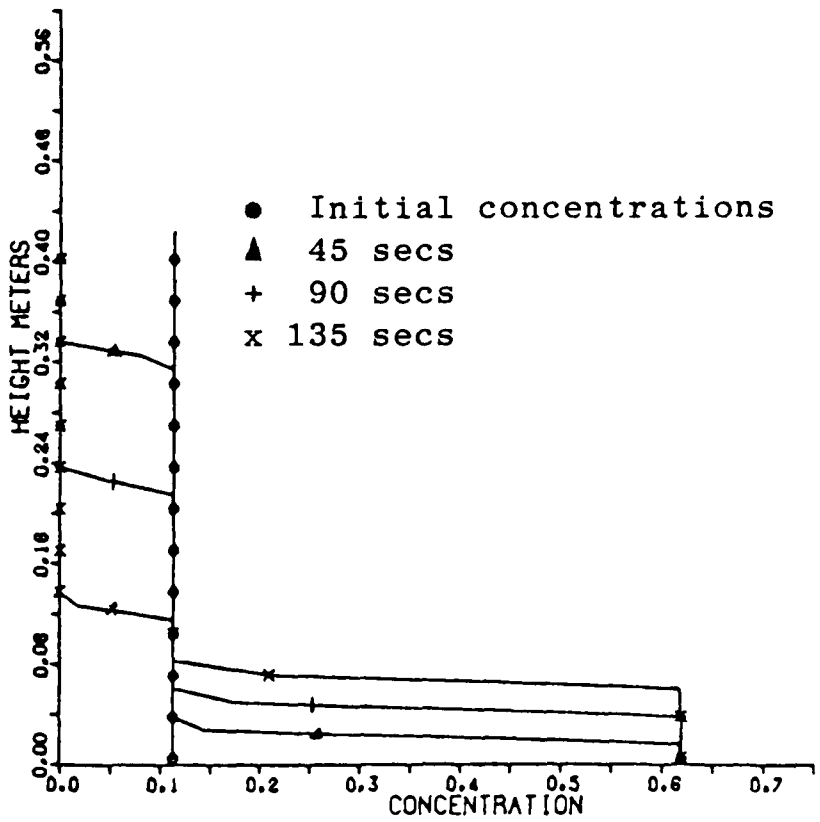

Glass (lead) 275μ

Figure 4.20 Density and concentration profiles for One phase Exp five.

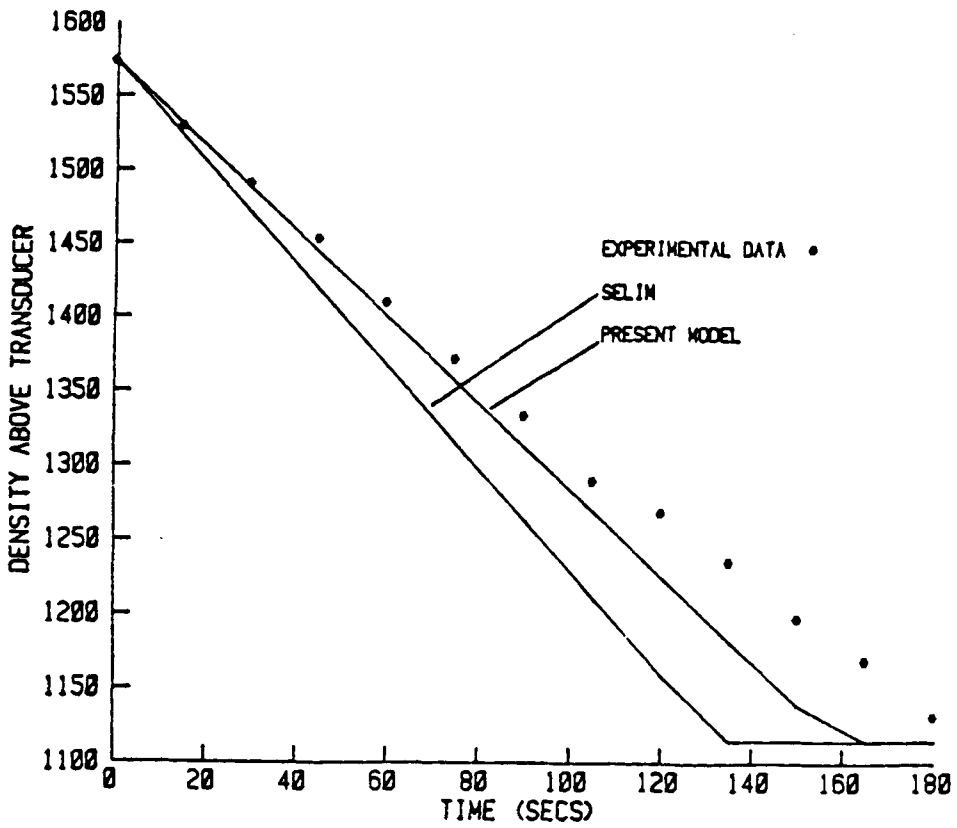

Density profile

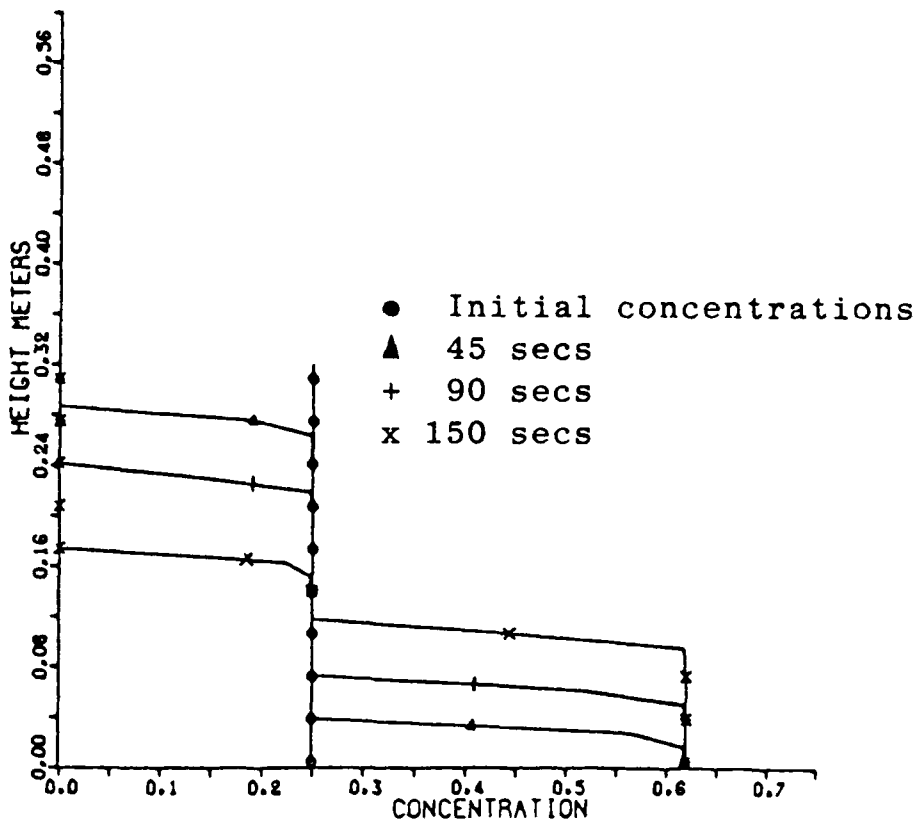

Glass (lead) 275μ

Figure 4.21 Density and concentration profiles for One phase Exp six.

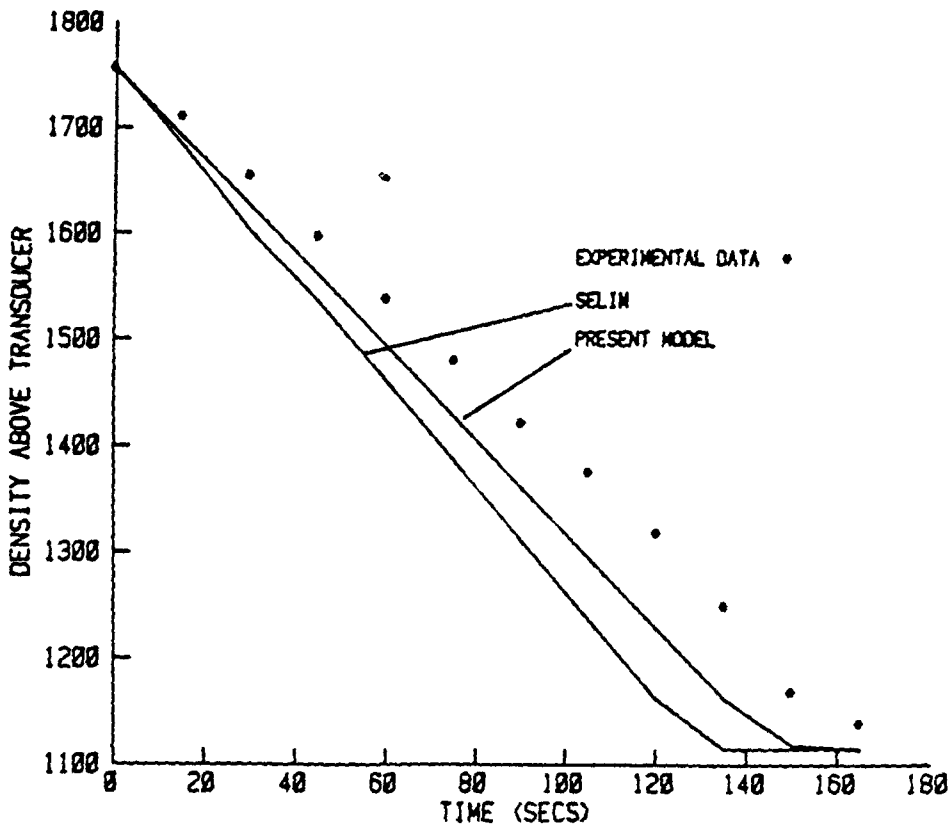

Density profile

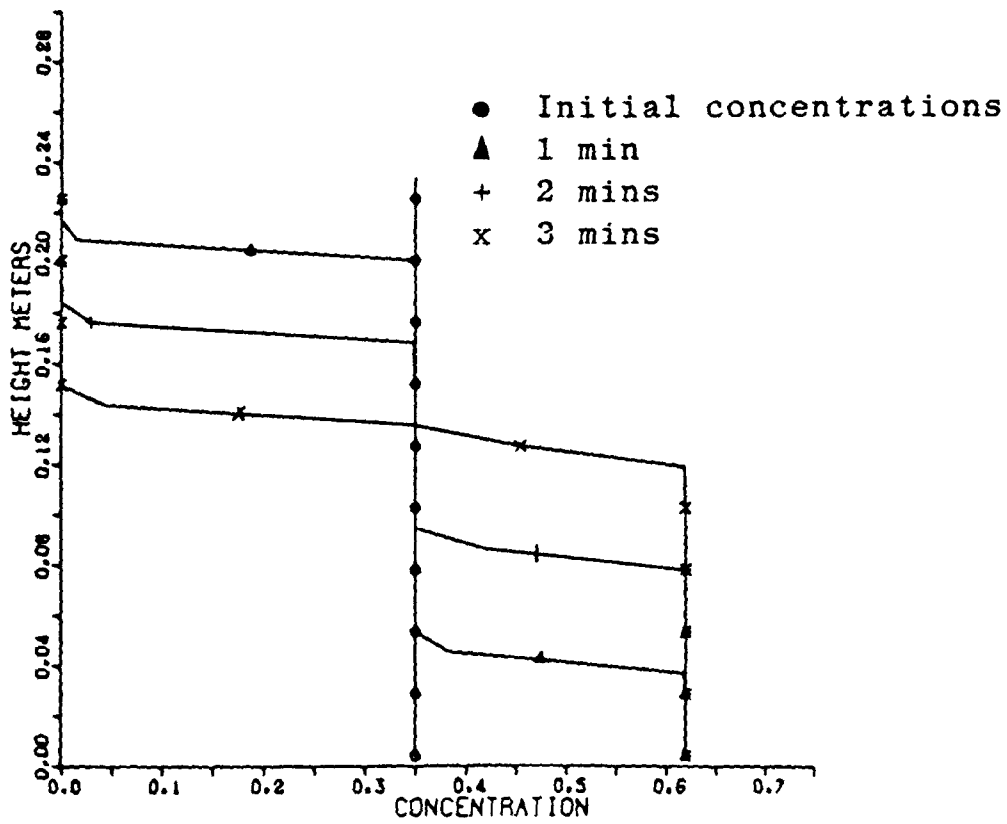

Glass (lead) 275μ

Figure 4.22 Density and concentration profiles for One phase Exp seven.

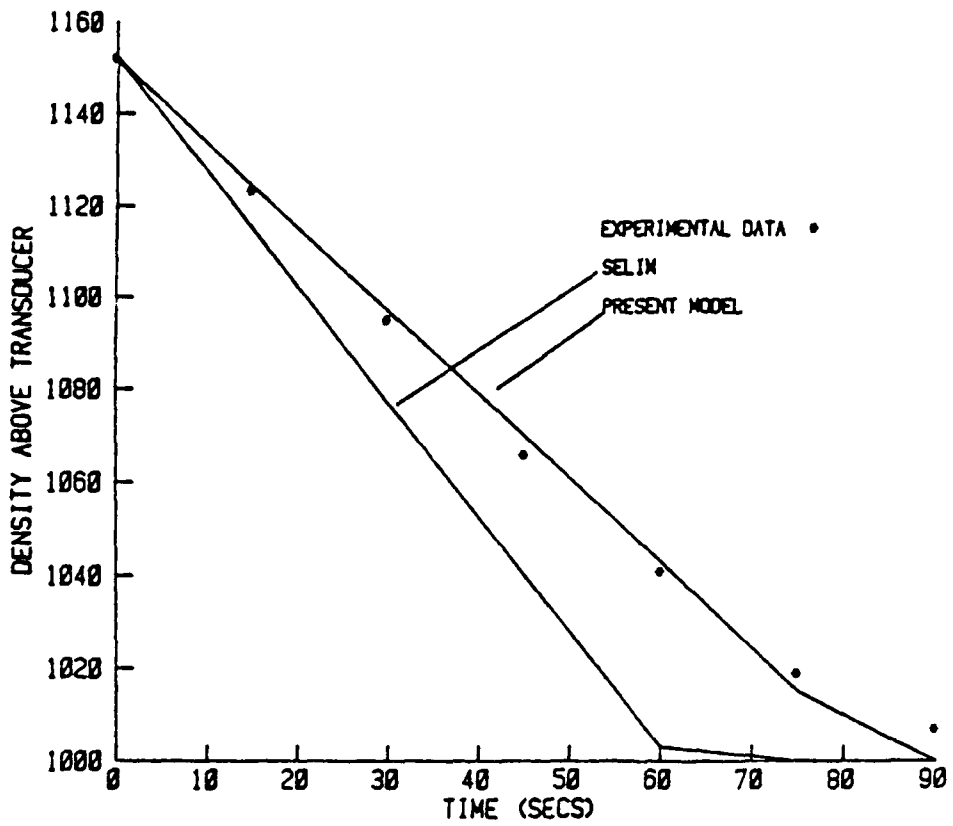

Density profile

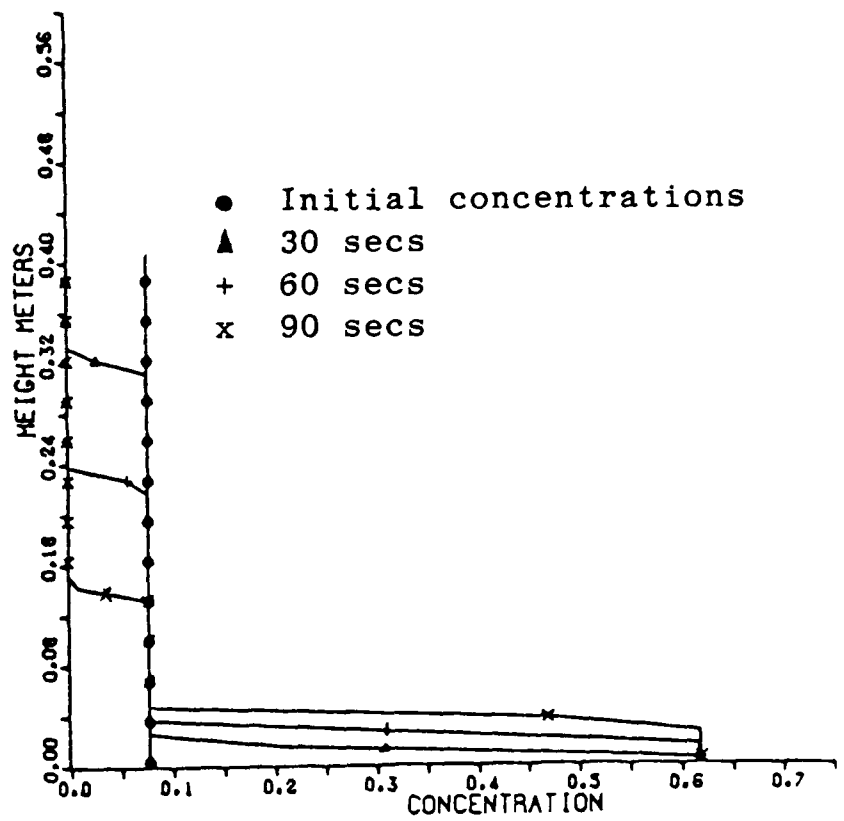

Glass (lead) 76.5μ

Figure 4.23 Density and concentration profiles for One phase Exp eight

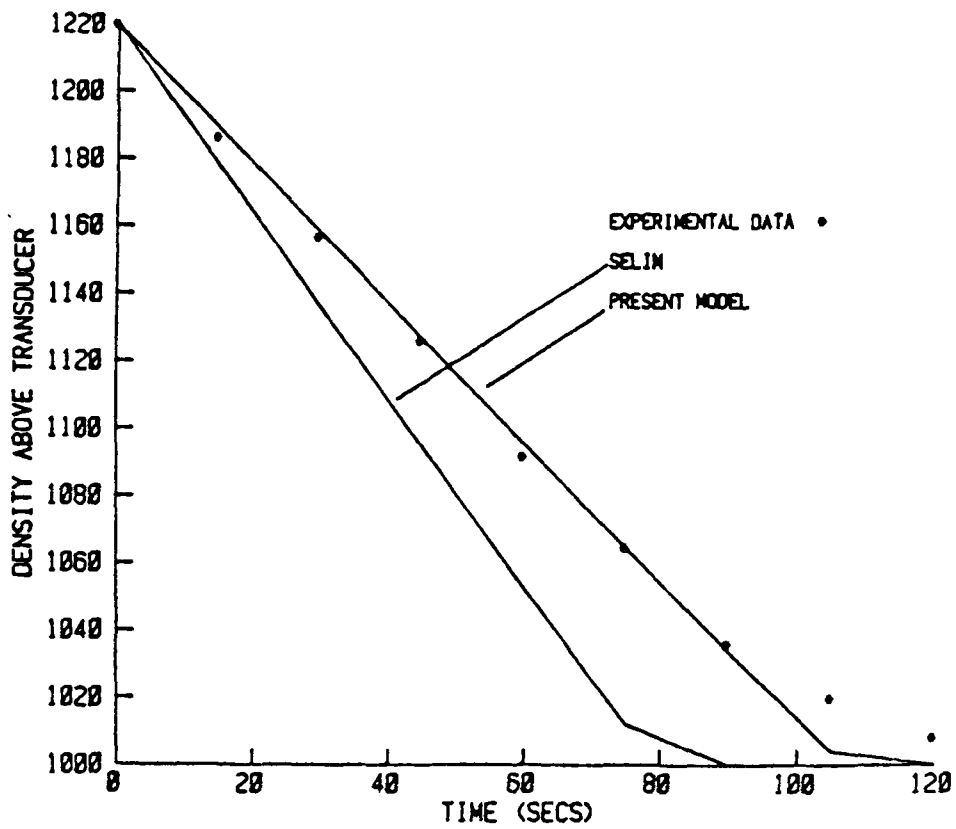

Density profile

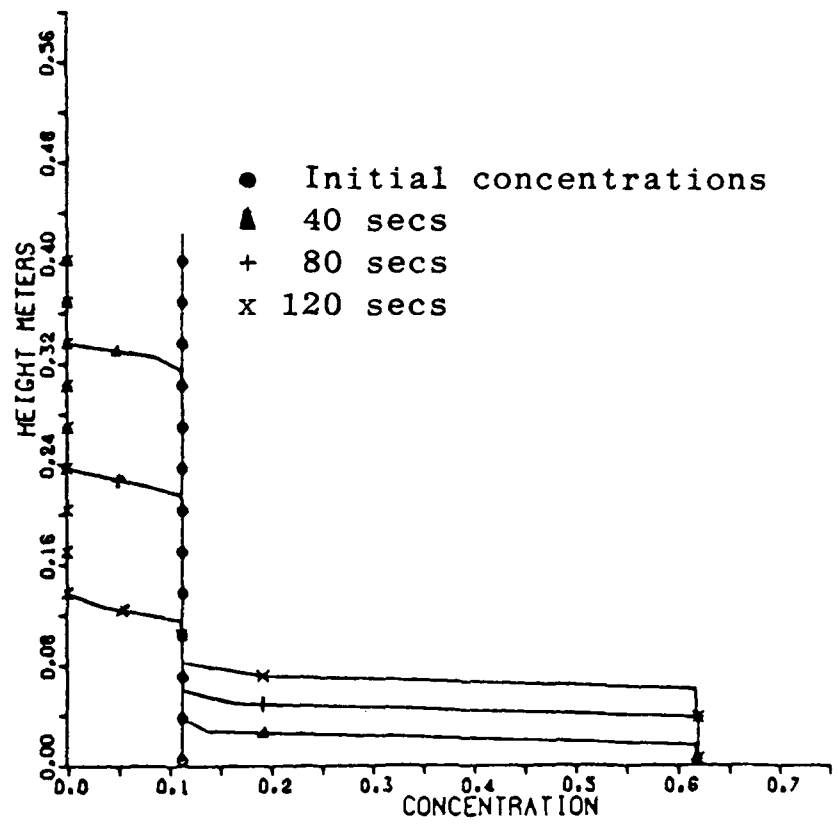

Glass (lead) 76.5μ

Figure 4.24 Density and concentration profiles for One phase Exp nine.

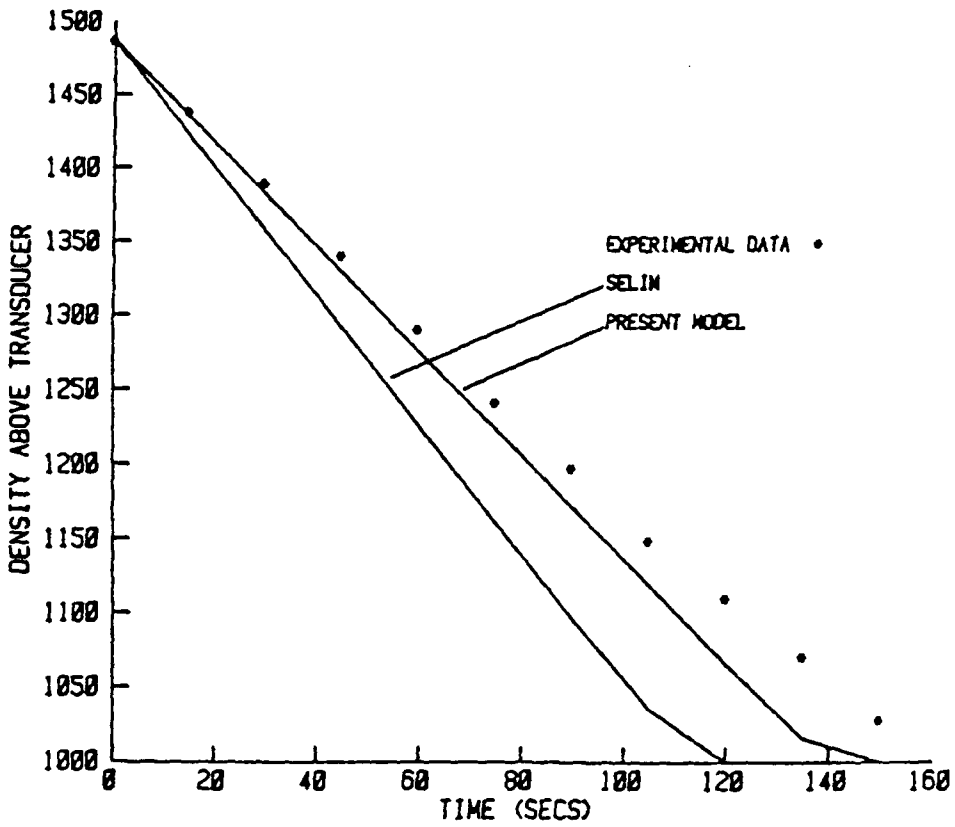

Density profile

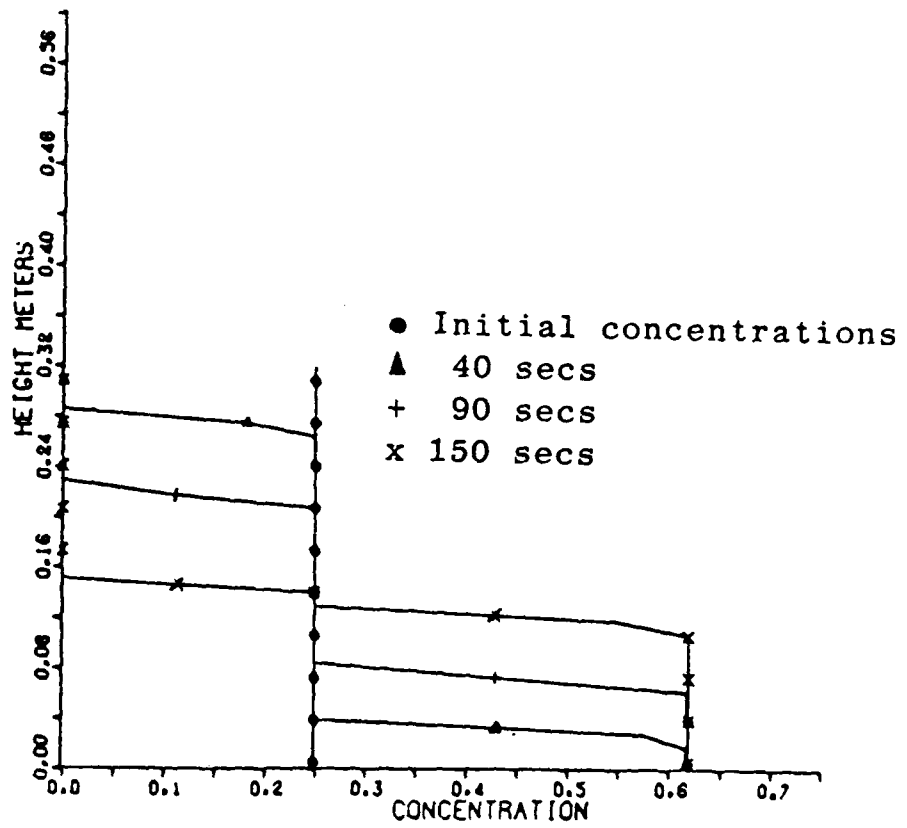

Glass (lead) 76.5μ

Figure 4.25 Density and concentration profiles for One phase Exp ten.

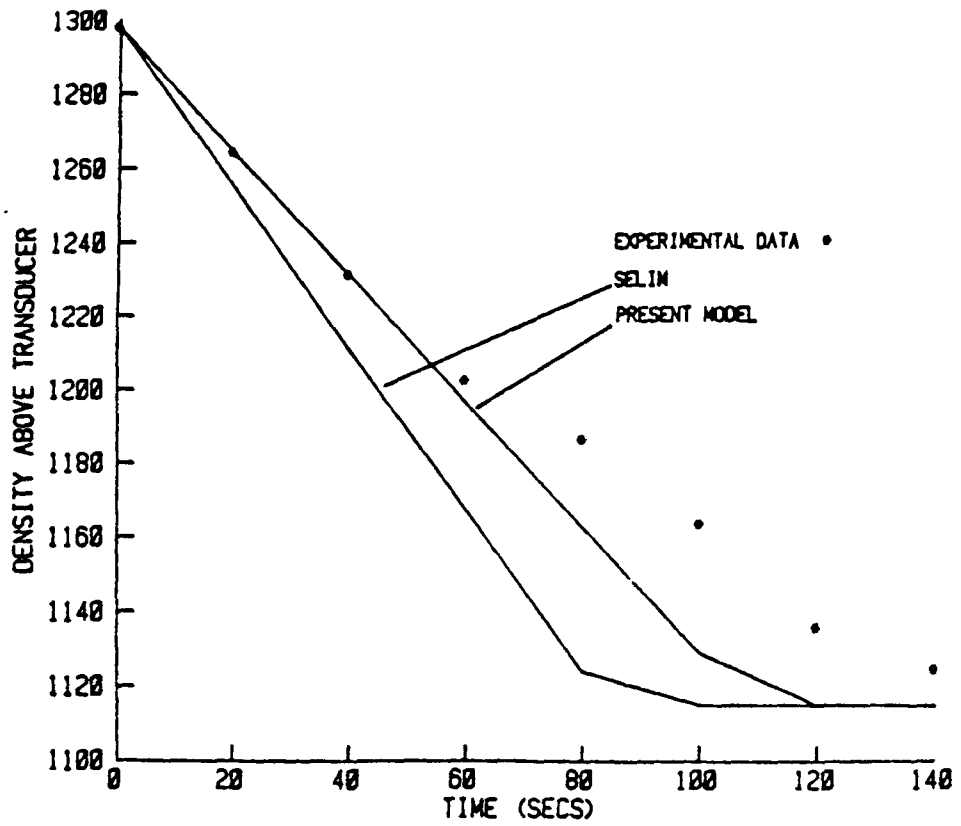

Density profile

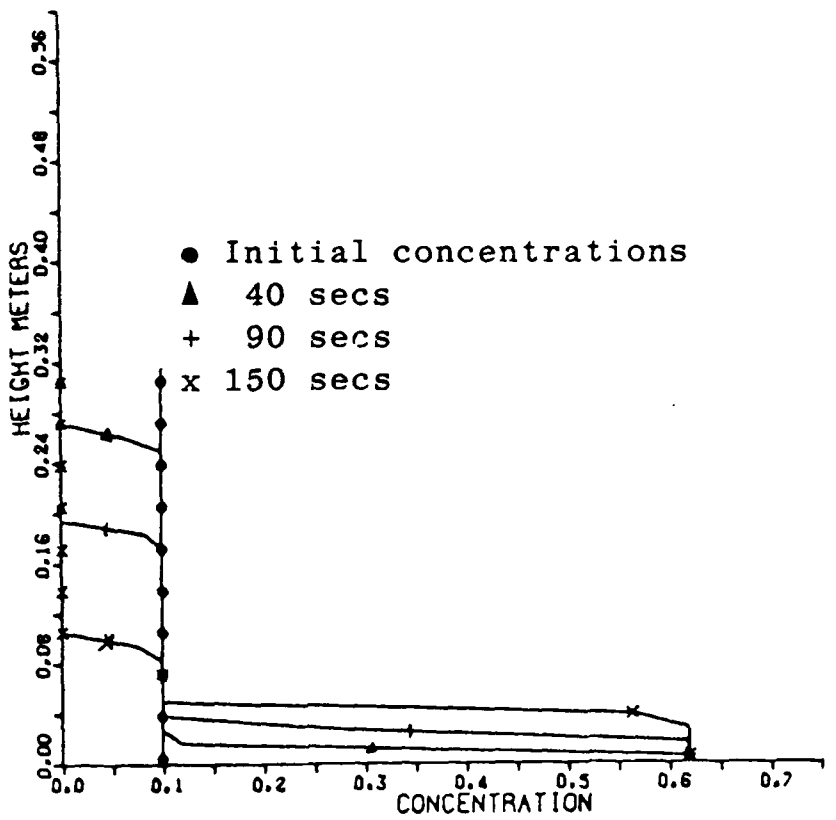

Glass (lead) 220μ

Figure 4.26 Density and concentration profiles for One phase Exp eleven.

represent the solids phase is the mean aperture size of the sieves used in obtaining the solid particulates, therefore segregation of particulates will occur due to the size range of particulates present.

As observed in the comparisons with the Holdich data the proposed model over predicts settling velocity at higher solids concentrations. But unlike the Holdich comparisons the proposed model still over predicts settling velocity at low concentrations although to much lesser extent. This is probably due to the assumptions made about the Holdich data.

4.7.2 Two phase comparisons

A two phase non-flocculated particulate mixture will settle with four distinct zones. These are from the top down:

1) Clear liquid.
2) Slurry containing slowest settling particles only.
3) Slurry containing both particulate phases at their initial concentrations.
4) Sediment.

Comparisons between the proposed model, Selim's model and the experimental data have been made, see figures (4.27-4.35). As with the one phase comparisons the general trend is the same with the Selim model over predicting settling velocities leading to greater density changes than observed. In the comparisons the proposed model restricts particulate settling to a greater extent than the Selim model, this leads to a closer fit with the experimental data.

From the concentration plots the build up of the sediment using the packing model and the formation of a zone containing the slower moving phase only can be observed. The sediment zone for each experiment will contain both particulate phases where the predicted solids

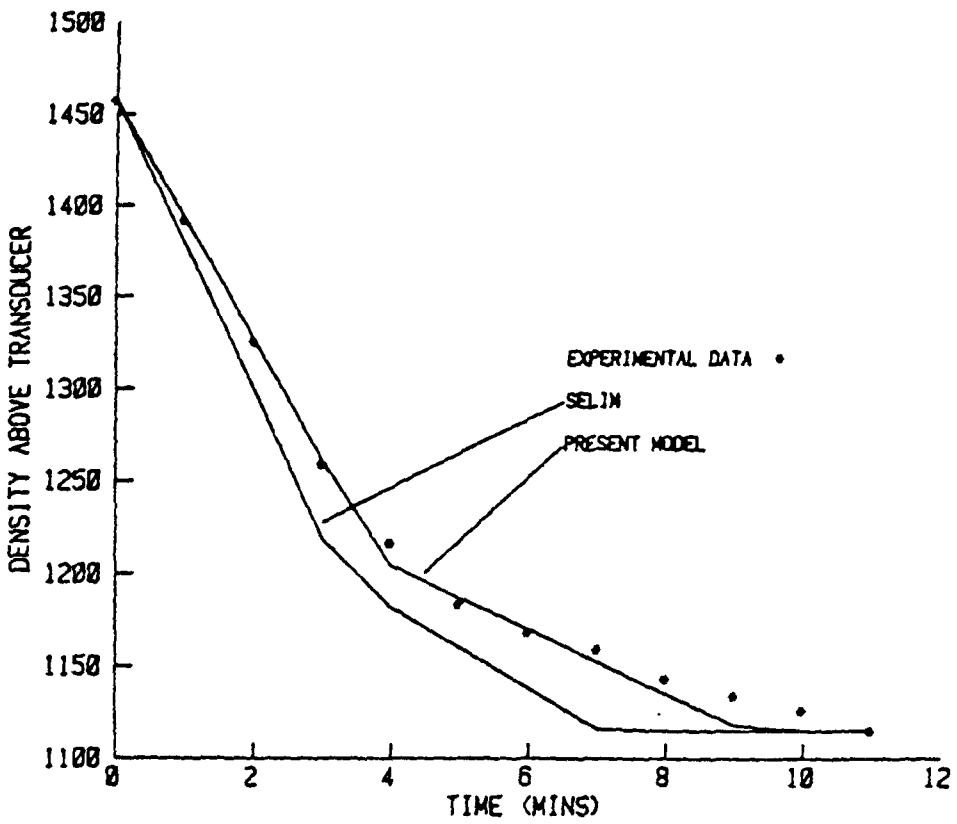

Density profile

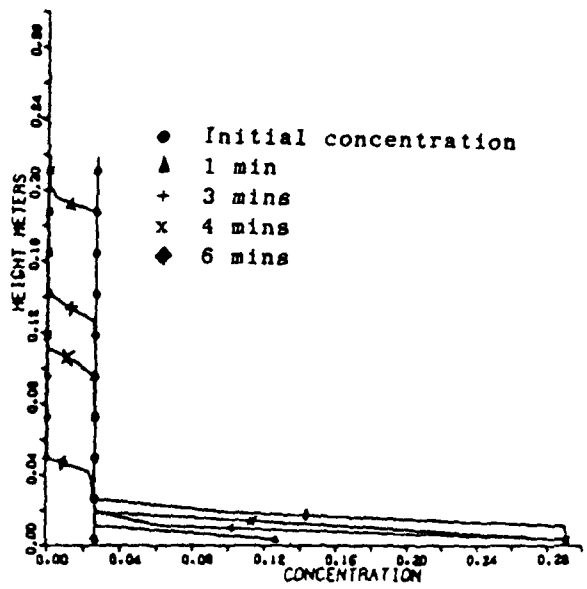

Copper 56.5μ

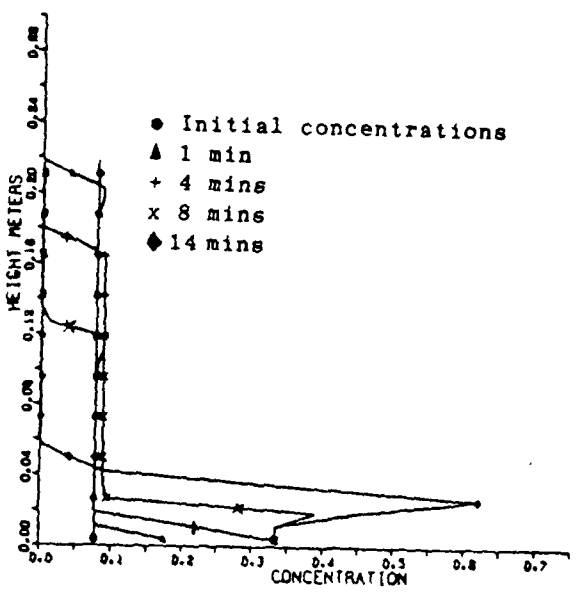

Glass (lead) 76.5μ

Figure 4.27 Density and concentration profiles for Two phase Exp one.

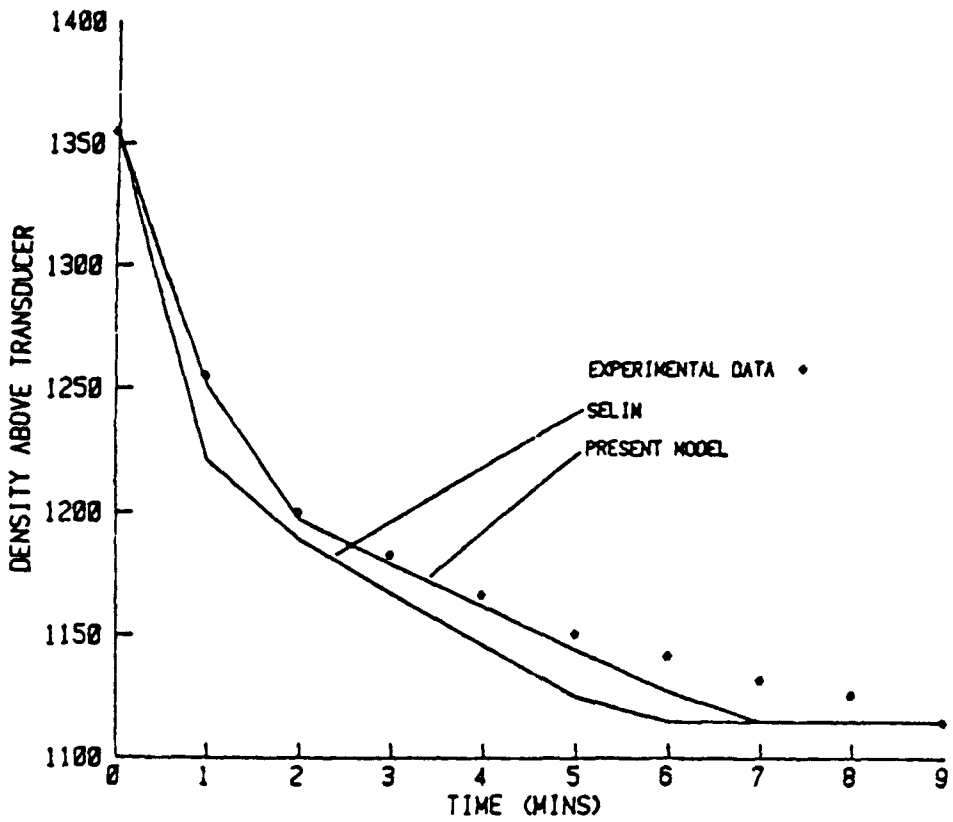

Density profile

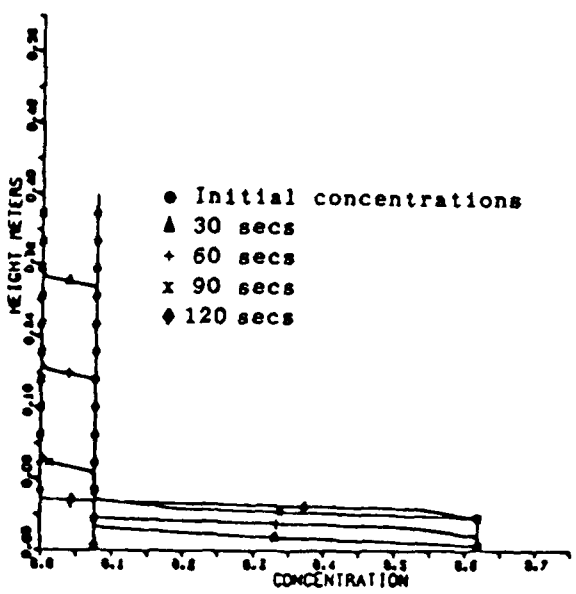

Glass (lead) 302.5μ

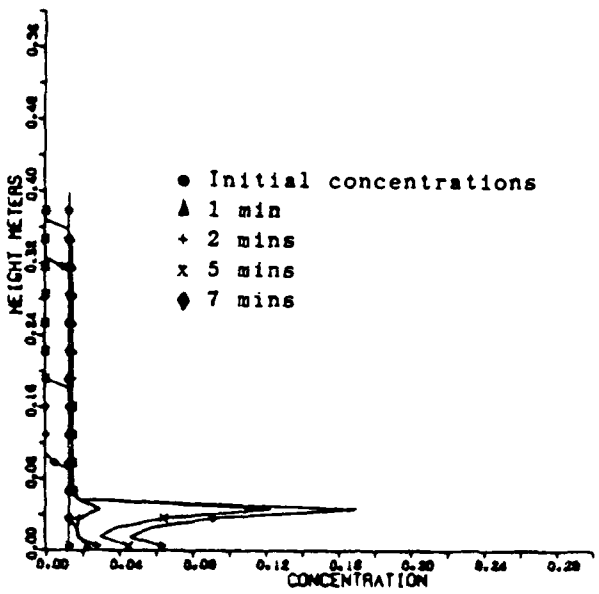

Copper 56.5μ

Figure 4.28 Density and concentration profiles for Two phase Exp two.

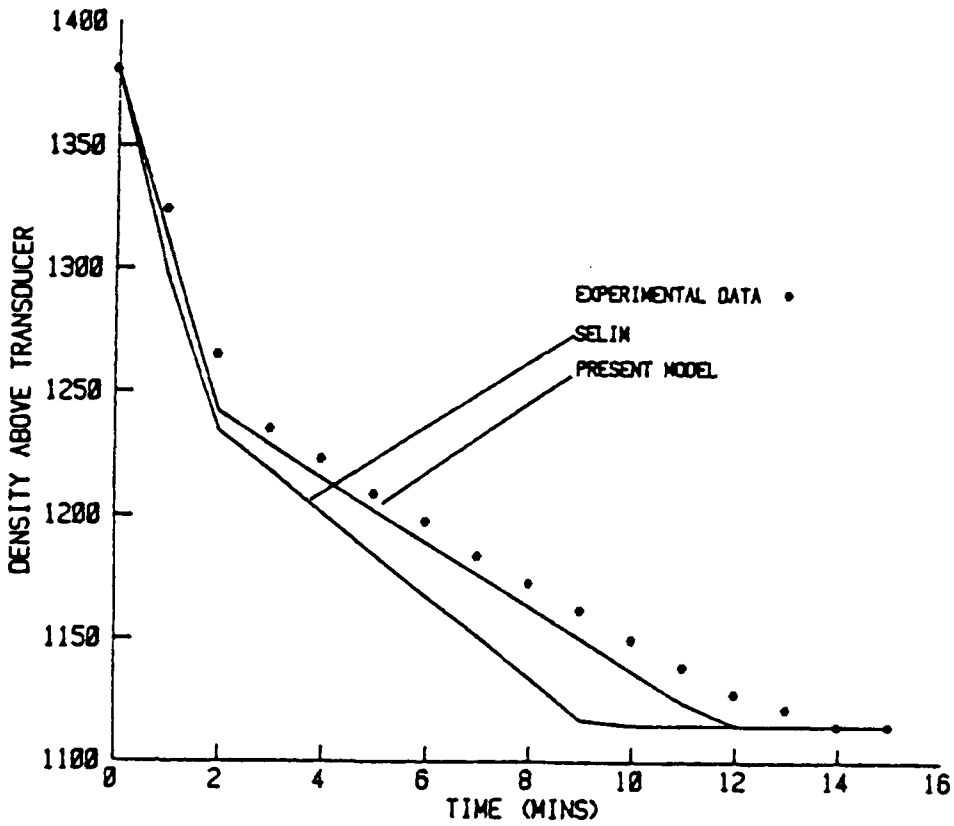

Density profile

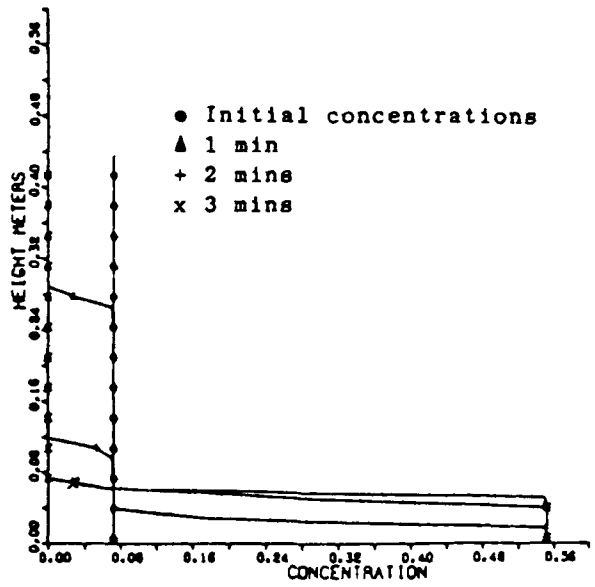

Glass (lead) 327.5μ

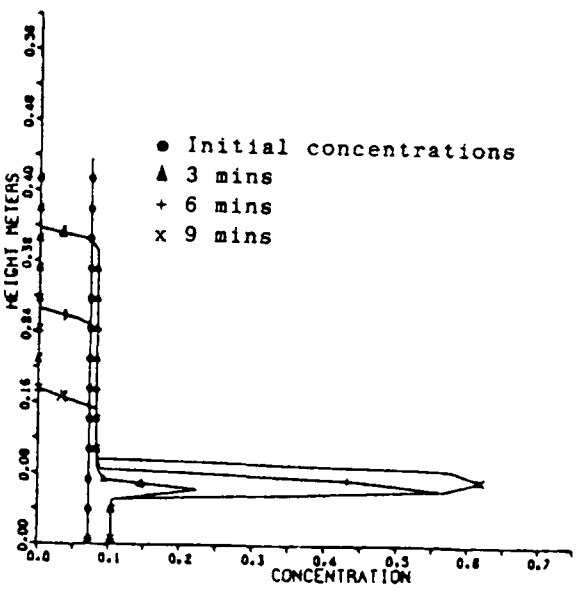

Glass (lead) 120μ

Figure 4.29 Density and concentration profiles for Two phase Exp three.

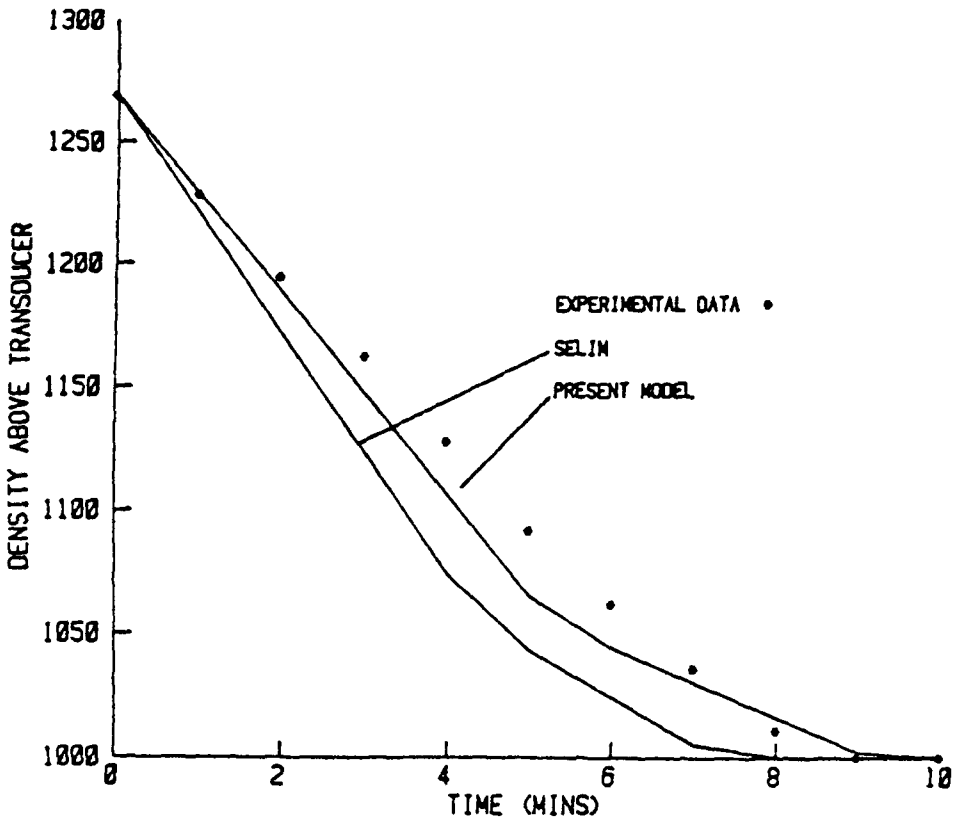

Density profile

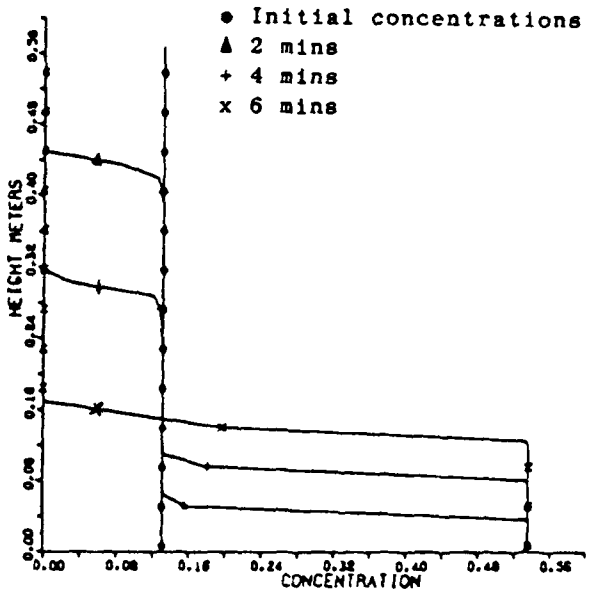

Glass (soda) 69μ

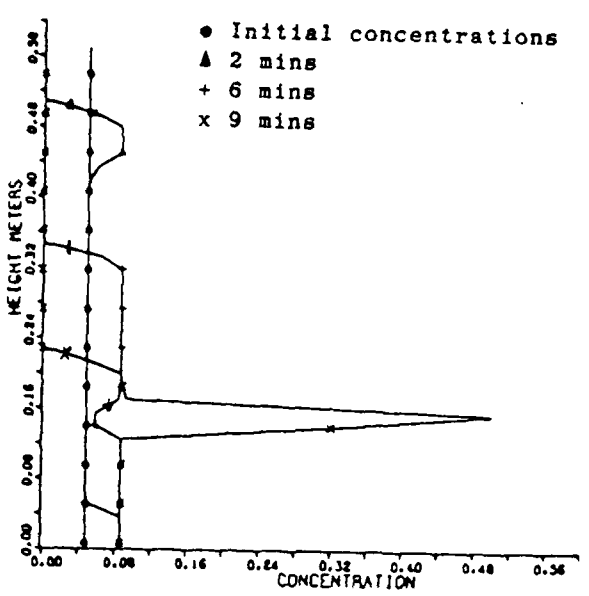

Glass (soda) 41.5μ

Figure 4.30 Density and concentration profiles for Two phase Exp four.

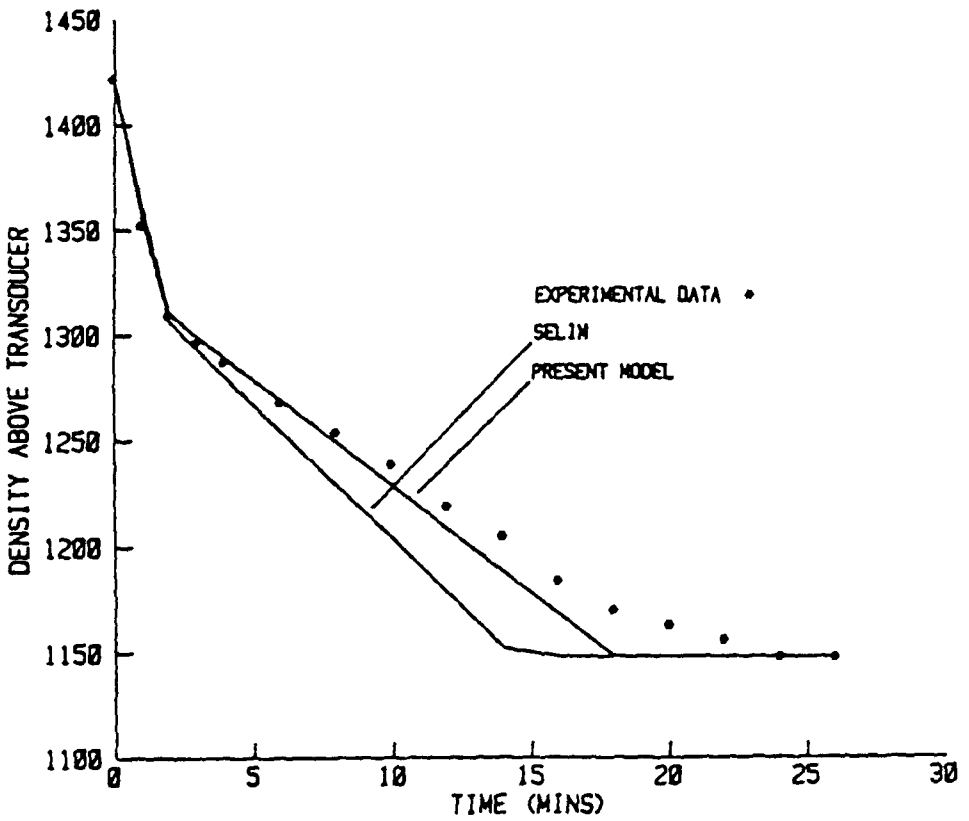

Density profile

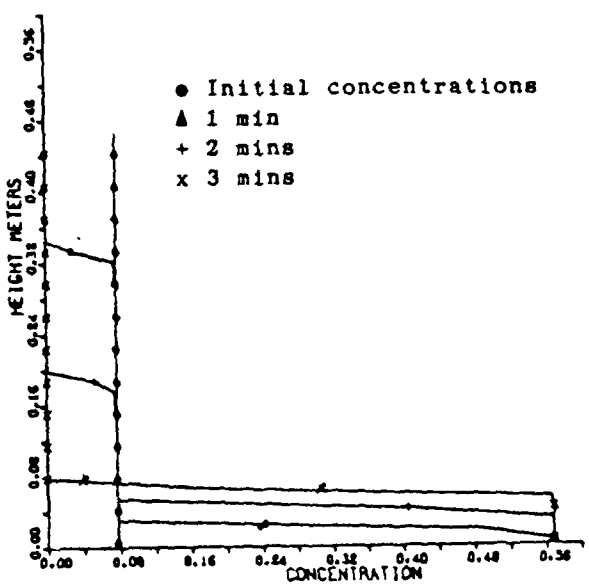

Quartz 200μ

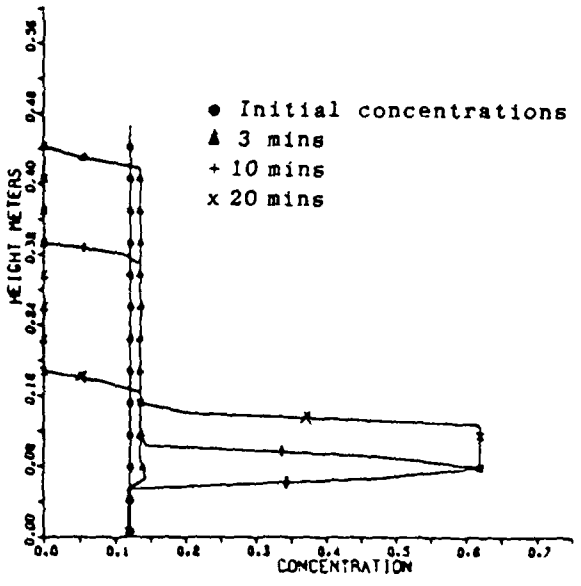

Glass (soda) 60μ

Figure 4.31 Density and concentration profile for Two phase Exp five.

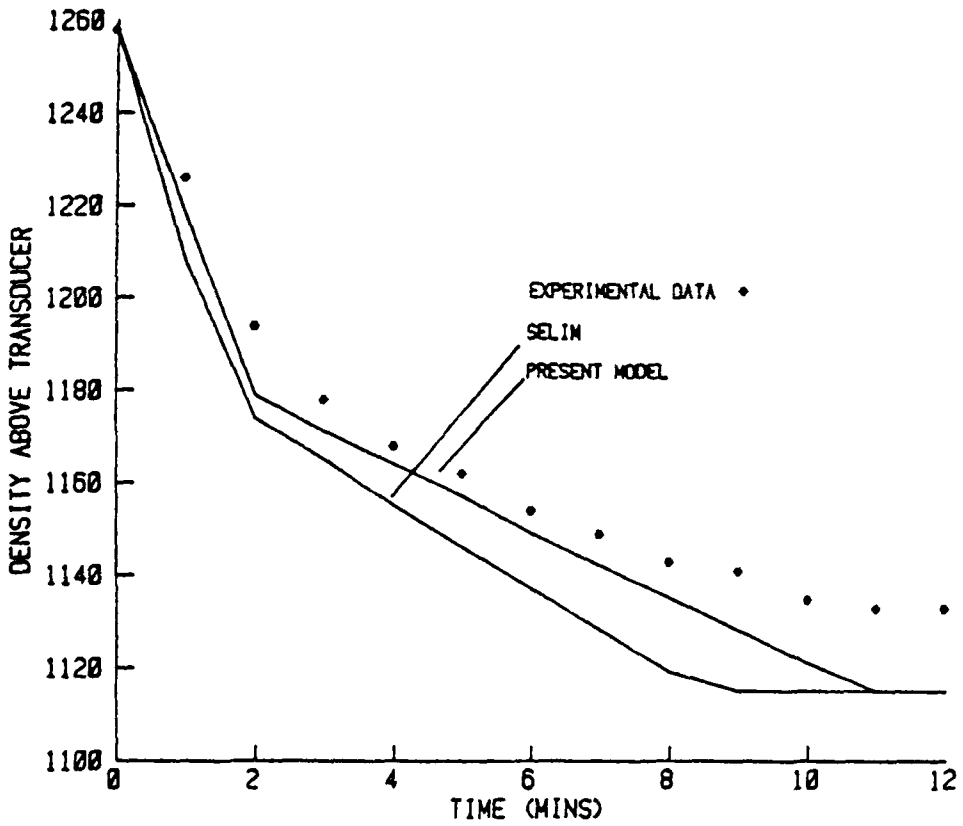

Density profile

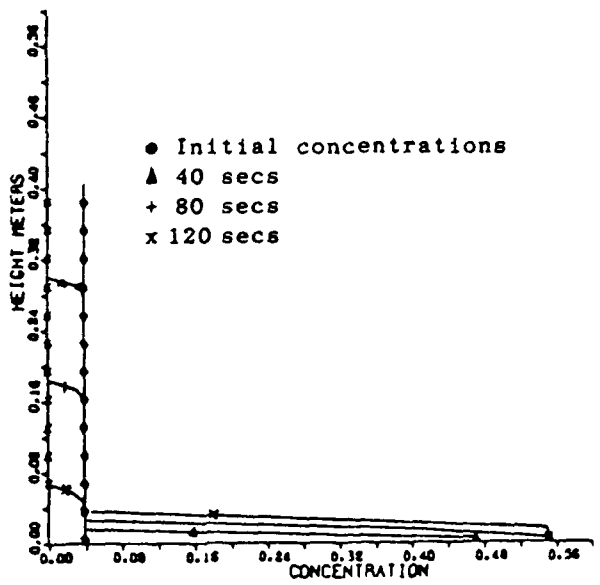

Glass (lead) 275μ

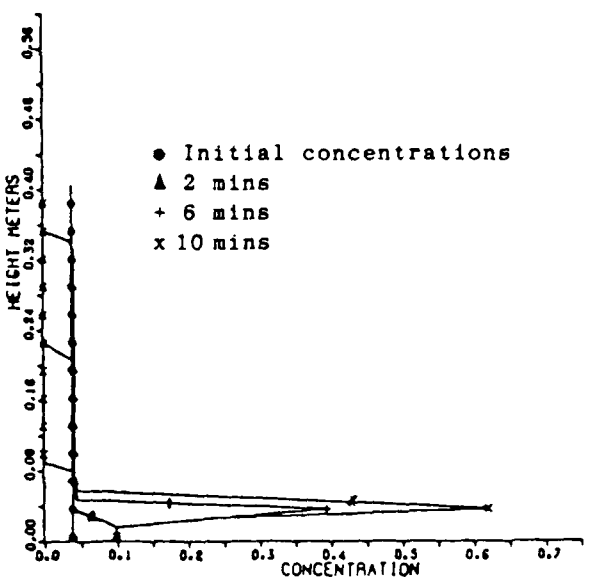

Glass (lead) 120μ

Figure 4.32 Density and concentration profiles for Two phase Exp six.

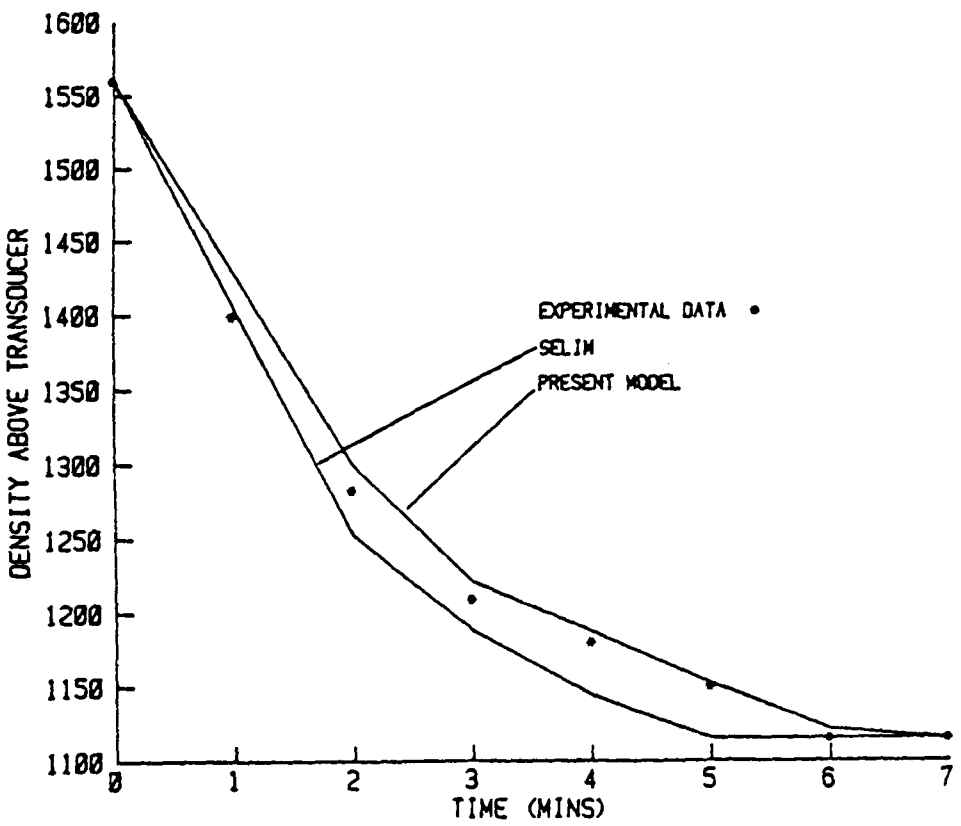

Density profile

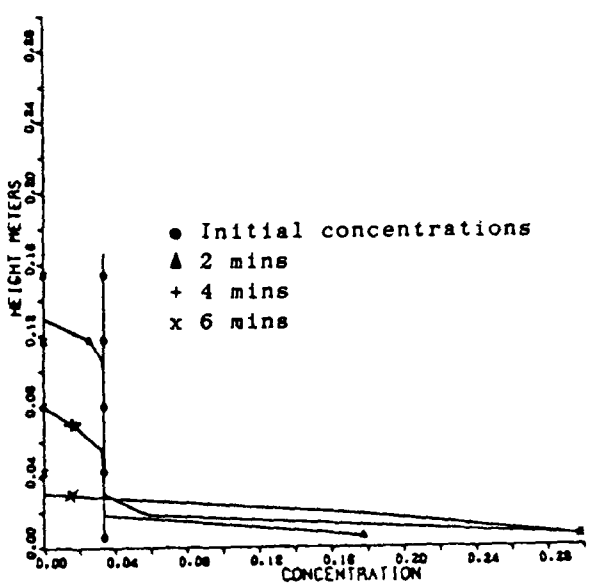

Copper 56.5μ

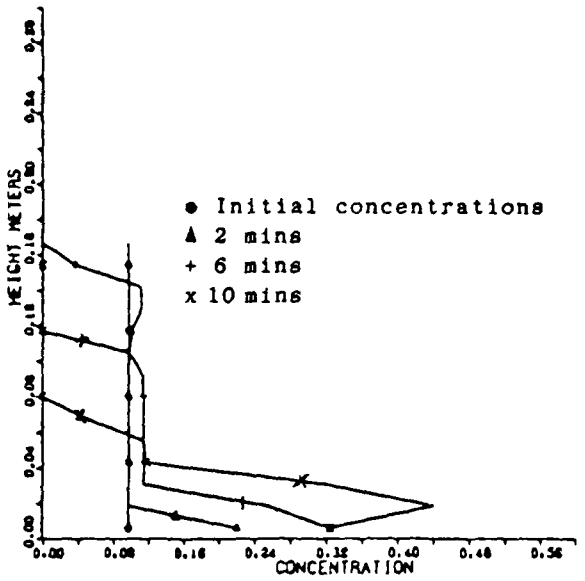

Glass (lead) 76.5μ

Figure 4.33 Density and concentration profiles for Two phase Exp seven.

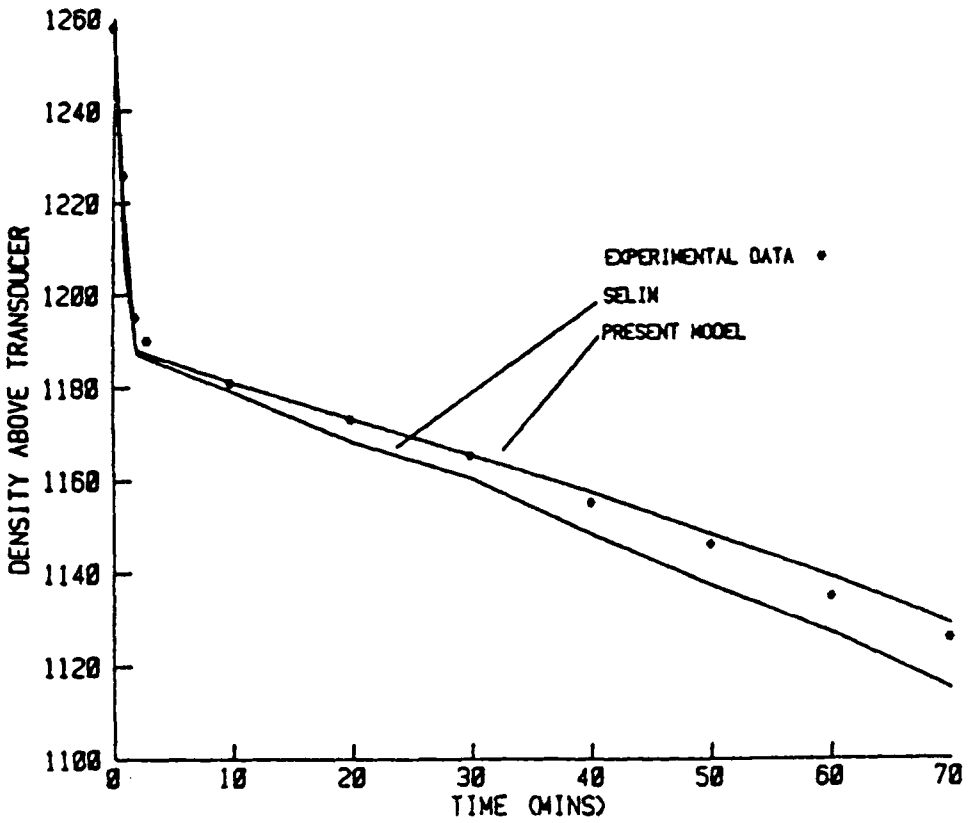

Density profile

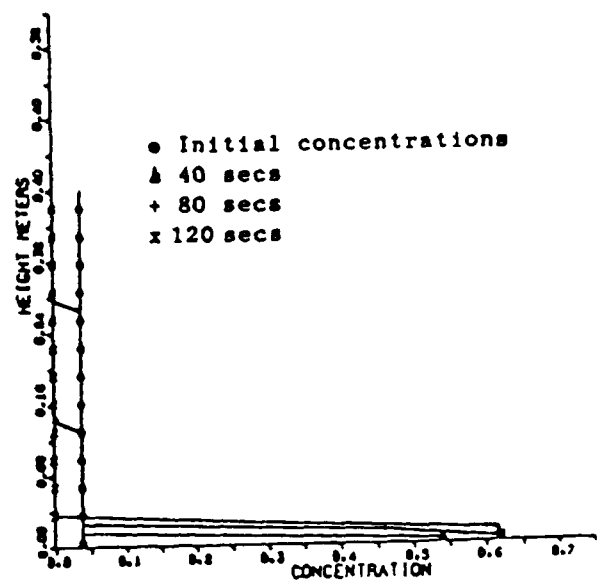

Glass (lead) 302.5μ

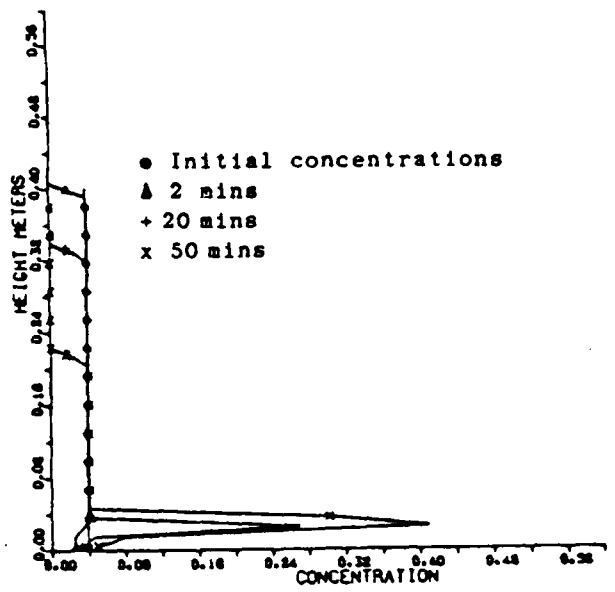

Glass (lead) 41.5μ

Figure 4.34 Density and concentration profiles for Two phase Exp eight.

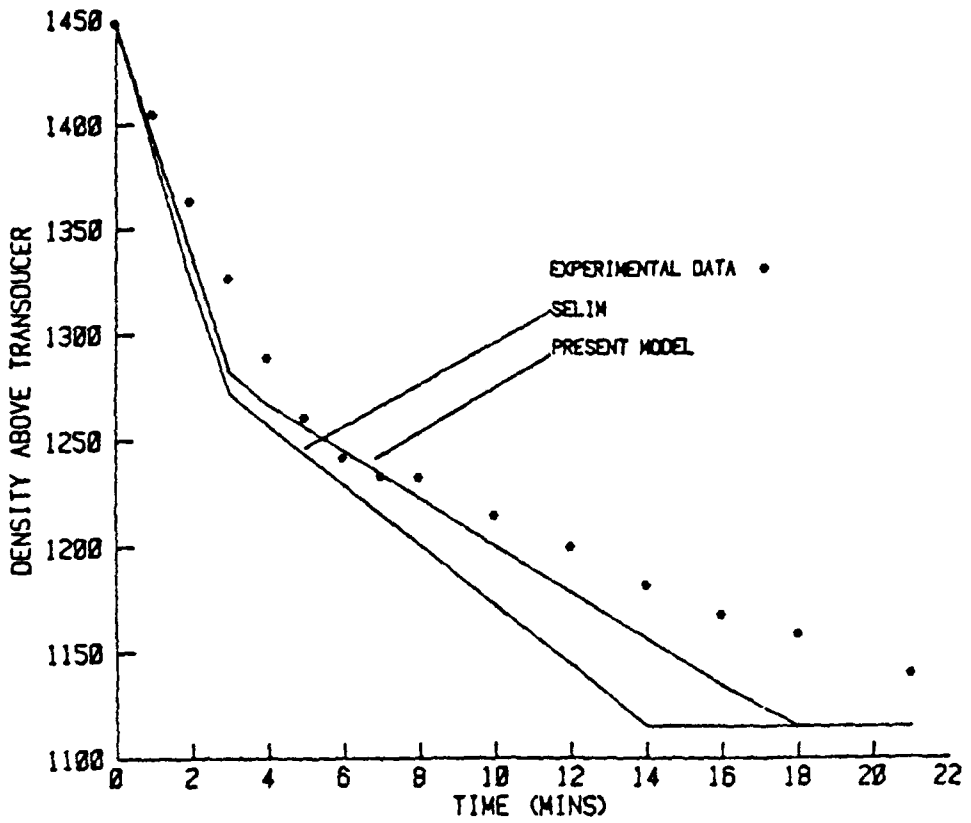

Density profile

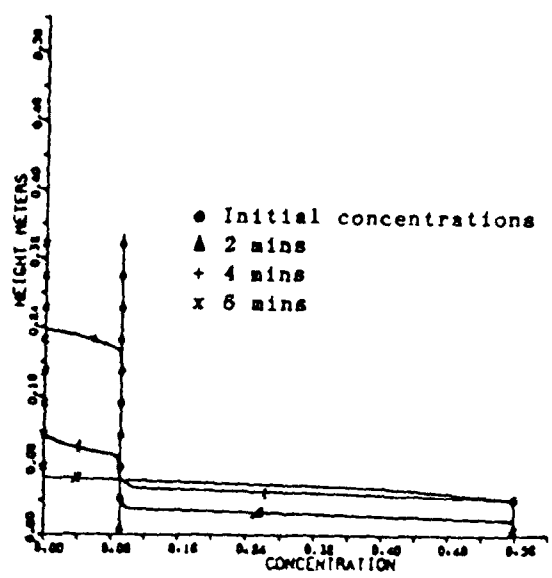

Glass (lead) 220μ

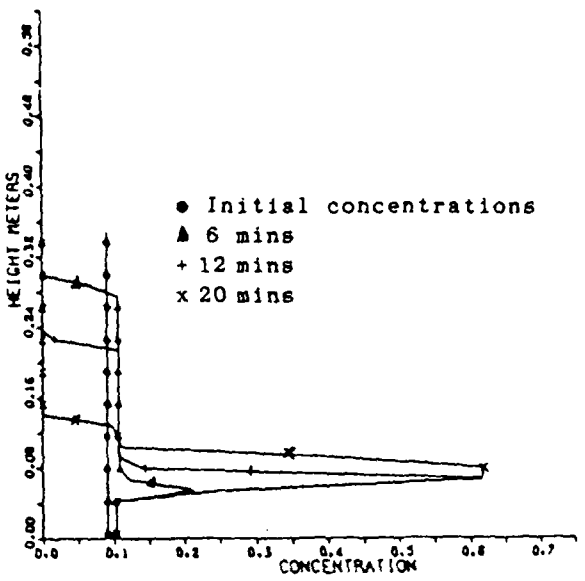

Glass (lead) 76.5μ

Figure 4.35 Density and concentration profiles for Two phase Exp nine.

concentrations of the sediment for each experiment are:

Experiment	Solids concentration	Hydraulic diameter
Exp one	0·622	26μ
Exp two	0·639	100μ
Exp three	0·656	89μ
Exp four	0·624	26μ
Exp five	0·686	43μ
Exp six	0·651	82μ
Exp seven	0·622	26μ
Exp eight	0·645	100μ
Exp nine	0·662	57μ

Table 4.4 Sediment concentrations for two phase runs.

Further densification of the sediment can occur in Exp two and Exp eight as the hydraulic diameter is greater than the diameter of the smallest particulate phases present in these experiments. Although this does not occur for Exp eight until all the larger particles have settled because in the zone where both phases are undergoing settlement at their initial concentratiions the movement of the smaller particles is in the opposite direction (i.e. against gravity), see figure 4.34. This effect was also predicted by Selim and is due to the large drag force exerted on the small particles via the fluid movement. The sediment in Exp two and Exp eight will continue to be packed with smaller particles occupying the voids until the sediment solid concentrations are 0·702 and 0·721 respectively.

4.7.3 Three phase comparisons

Three phase non-flocculated particulate mixtures undergoing sedimentation will settle with five distinct zones. These are from the top down

1) Clear liquid.

2) Slurry containing slowest settling phase only.

3) Slurry containing the two slower settling phases.

4) Slurry containing all three phases at their initial concentrations.

5) Sediment.

Comparisons between Selim's model, the proposed model and the experimental data for the six three phase experiments have been made, see figures (4.36-4.41)

Referring to the density profiles the change in gradient of each profile represents the point at which one of the zones has passed the transducer so that the change in density is now dependent on the rate of fall of the next zone. Selim predicts greater velocities for the largest phase present in each experiment than the proposed model. This will in turn predict greater concentrations for the phases in the two zones above which is why the Selim model underpredicts the change in density for Exp three, Exp four and Exp five. For the other comparisons this has not occurred to such a degree, if at all. The proposed model predicted the movement of the slowest phase, in the zone containing all particulate phases, acting in the same direction as the fluid (i.e. against gravity) for Exp two, Exp three, Exp four and Exp five. This was also predicted by the Selim model except for Exp four where the velocity although very small in magnitude acted in the direction of gravity.

The concentration plots give the formation of the sediment and of the four zones present in the free settling region over time. The sediment zone for three phase particulate mixtures will contain three layers consisting of from the base up:

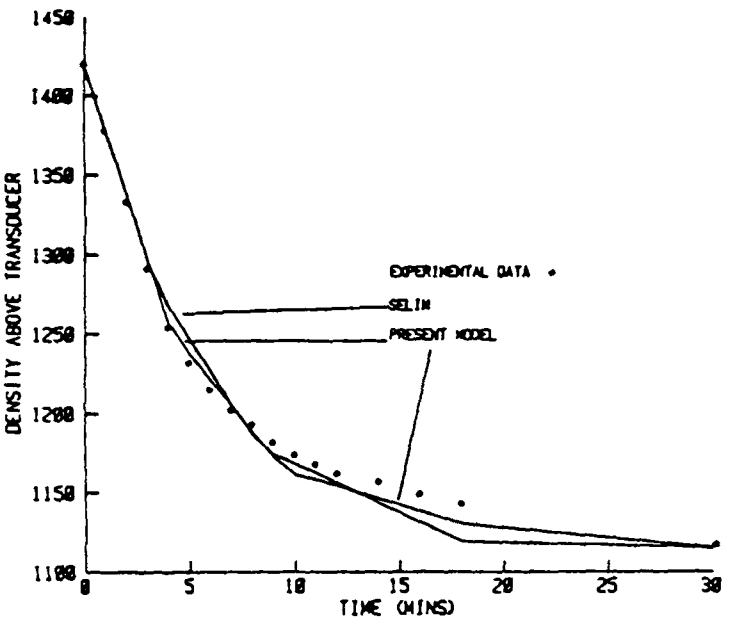

Density profile

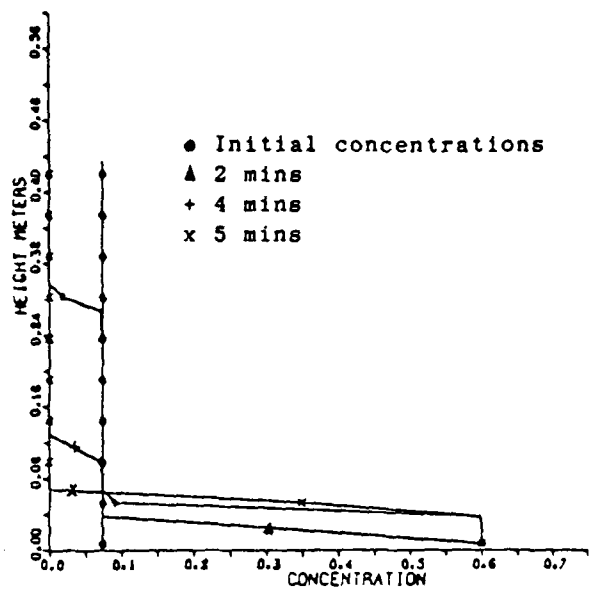

Glass (lead) 220μ

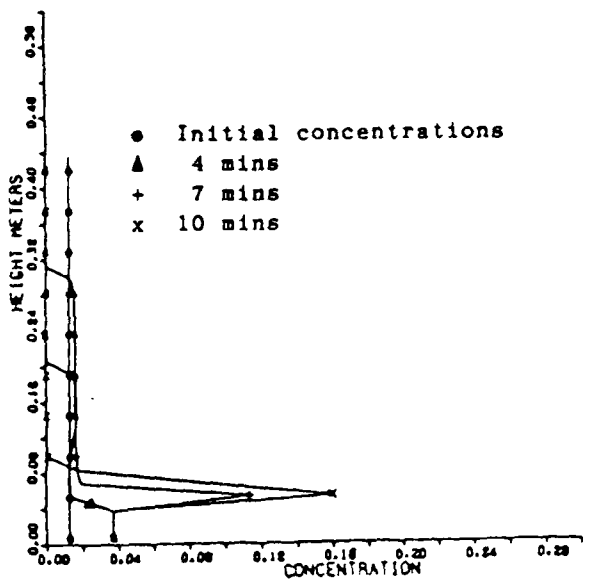

Copper 56.5μ

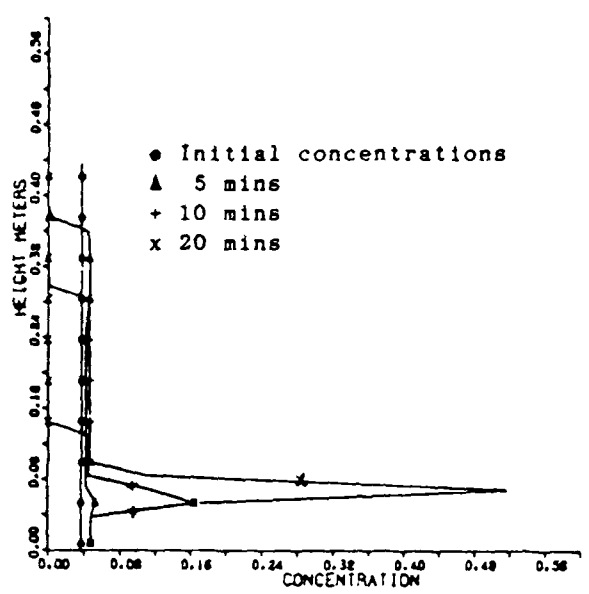

Glass (lead) 76.5μ

Figure 4.36 Density and concentration profiles for Three phase Exp one.

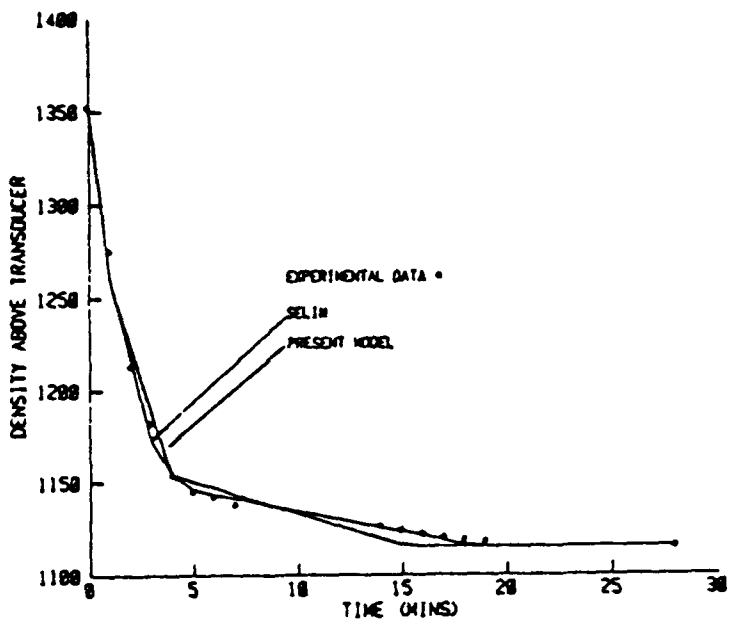

Density profile

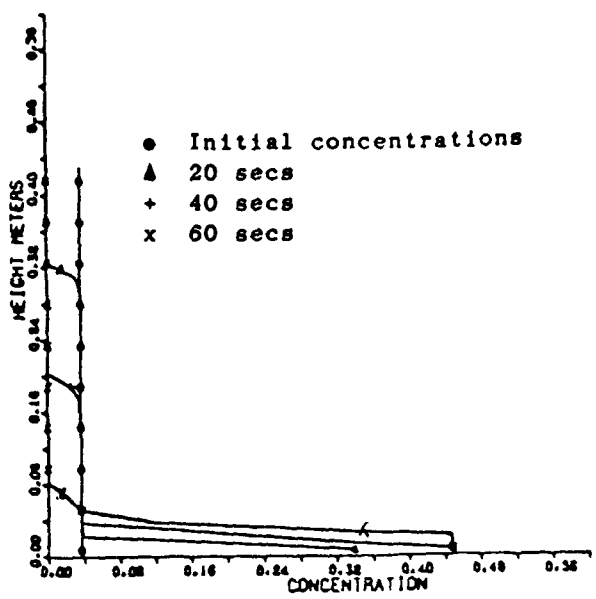

Glass (lead) 462.5μ

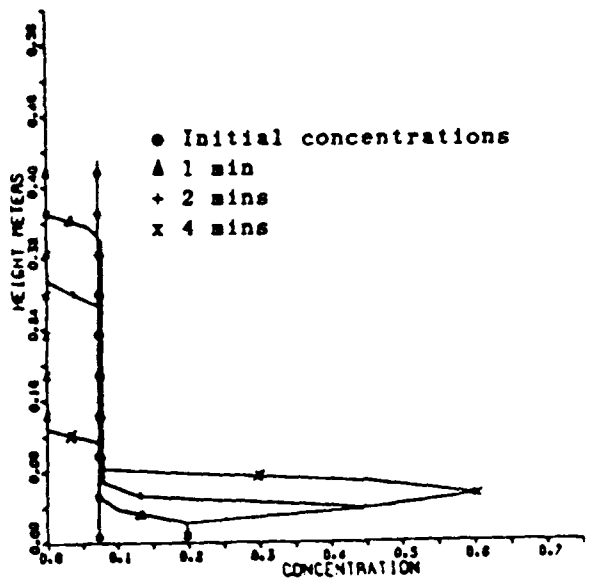

Glass (lead) 200μ

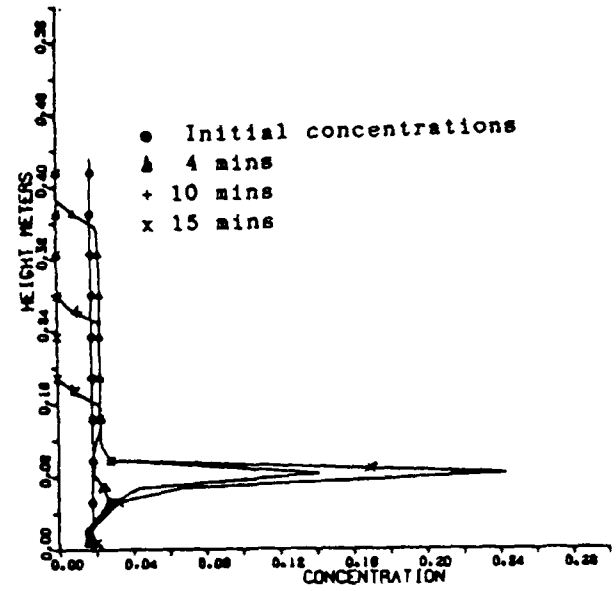

Glass (lead) 76.5μ

Figure 4.37 Density and concentration profiles for Three phase Exp two.

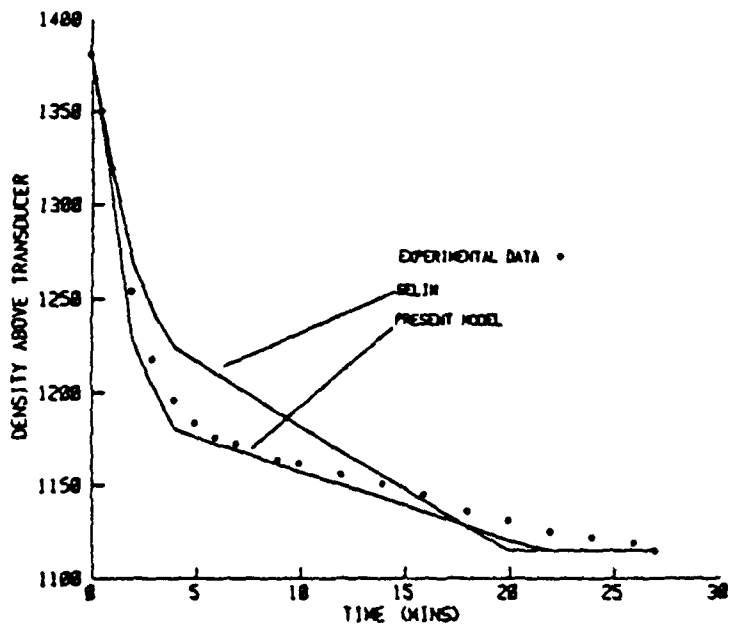

Density profile

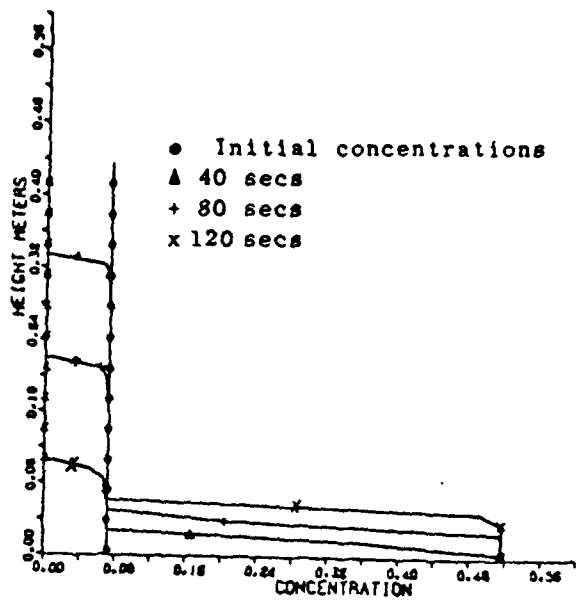

Glass (lead) 327.5μ

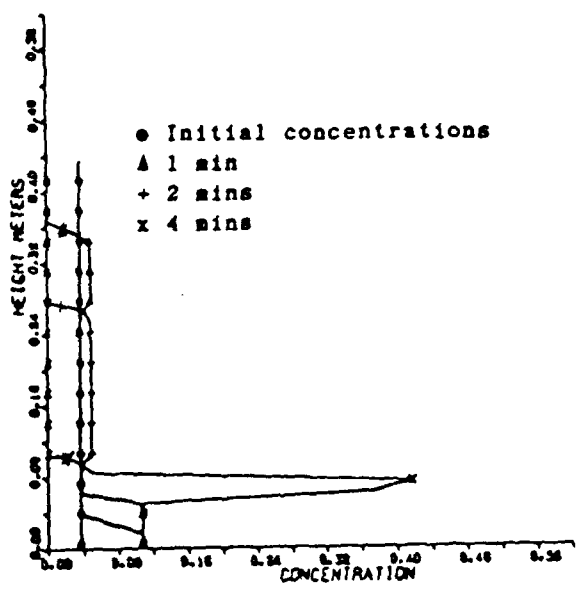

Glass (lead) 200μ

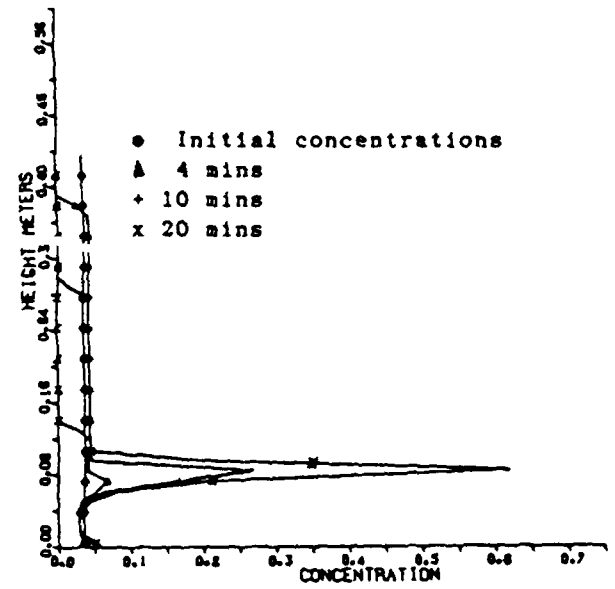

Glass (lead) 76.5μ

Figure 4.38 Density and concentration profiles for Three phase Exp three

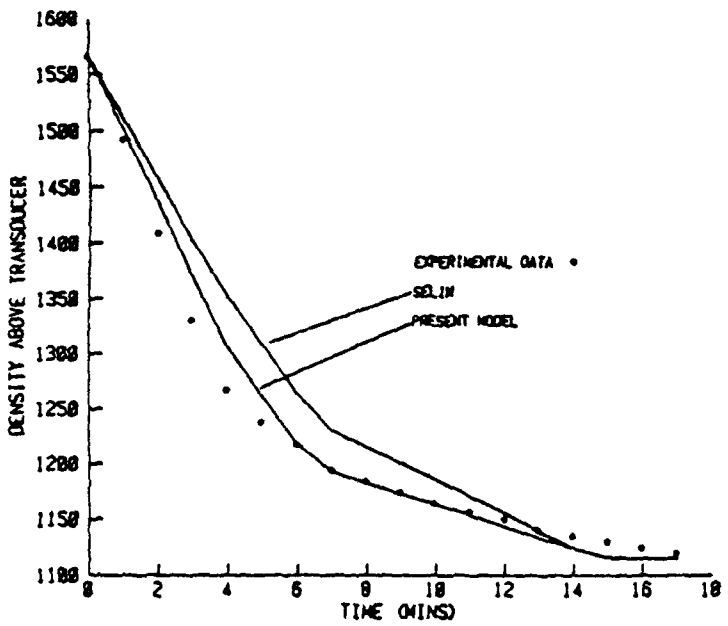

Density profile

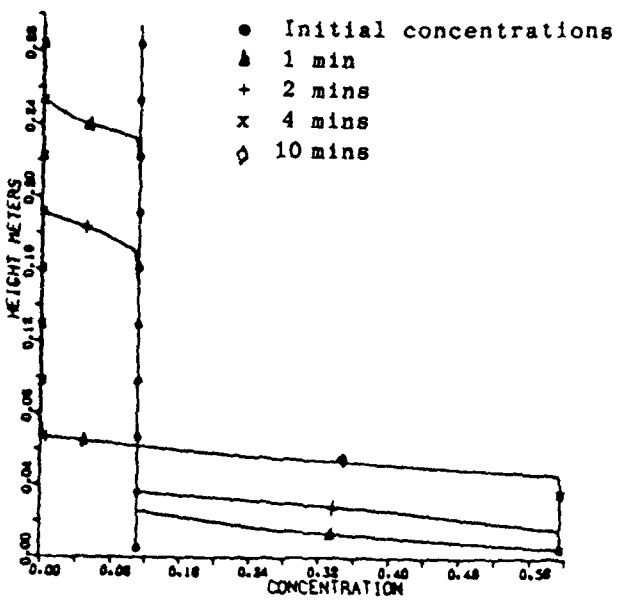

Glass (lead) 220μ

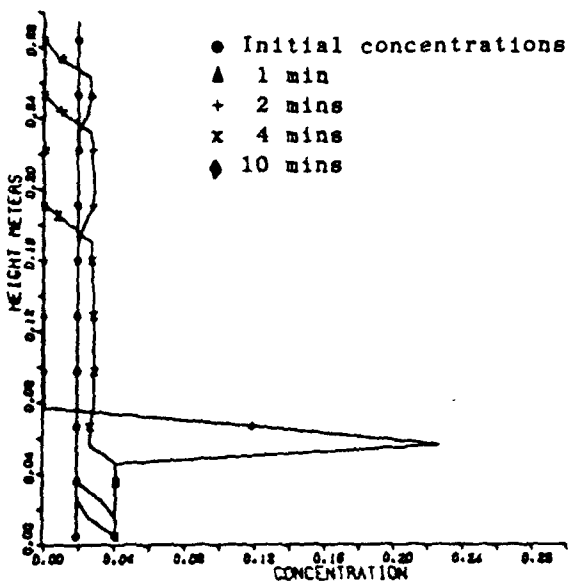

Copper 56.5μ

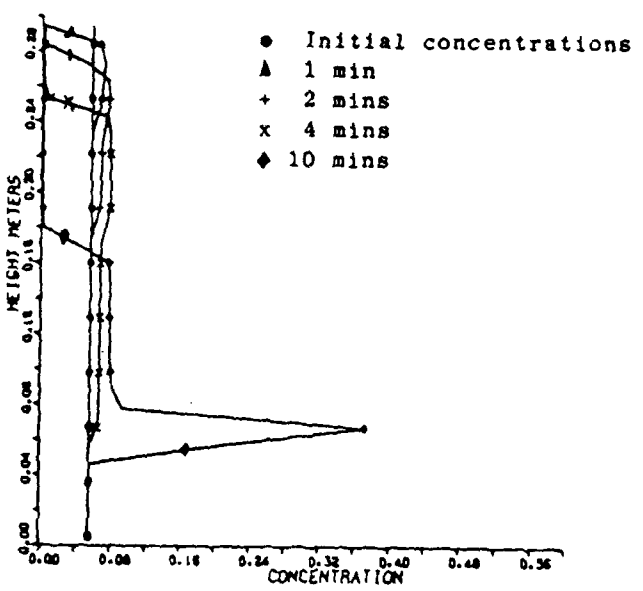

Glass (lead) 76.5μ

Figure 4.39 Density and concentration profiles for Three phase Exp four.

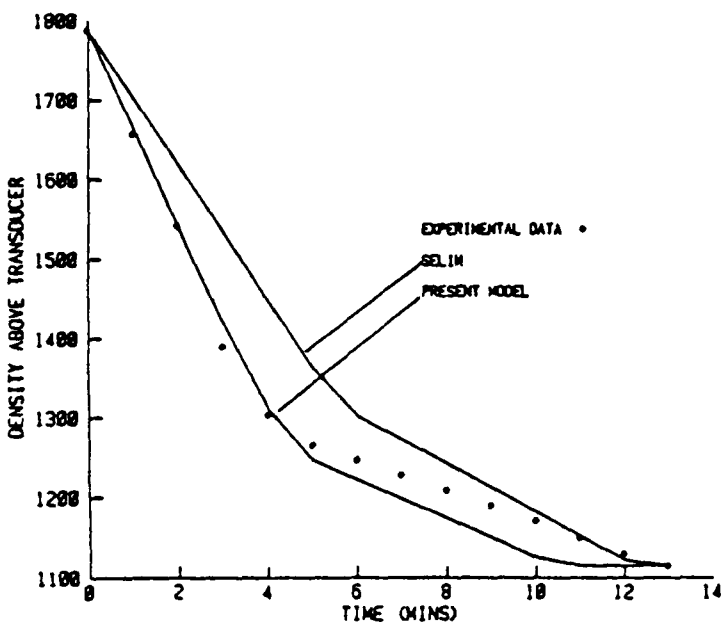

Density profile

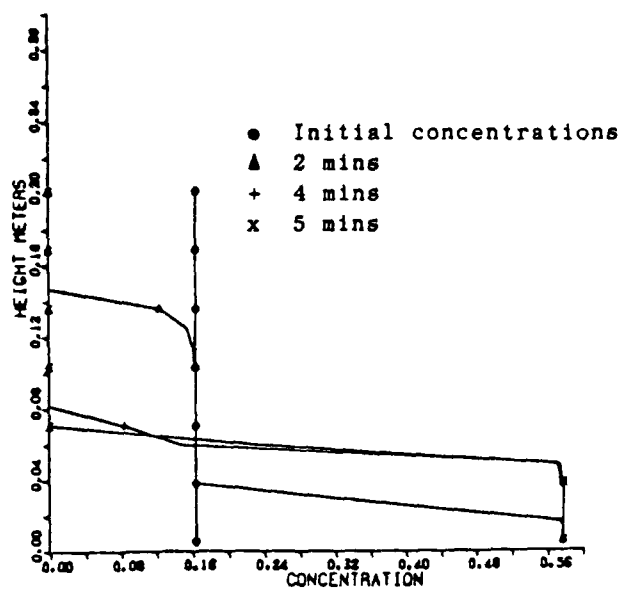

Glass (lead) 220μ

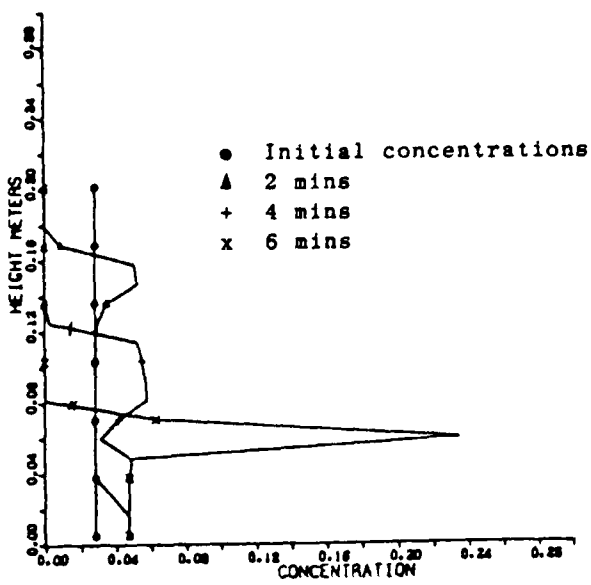

Copper 56.5μ

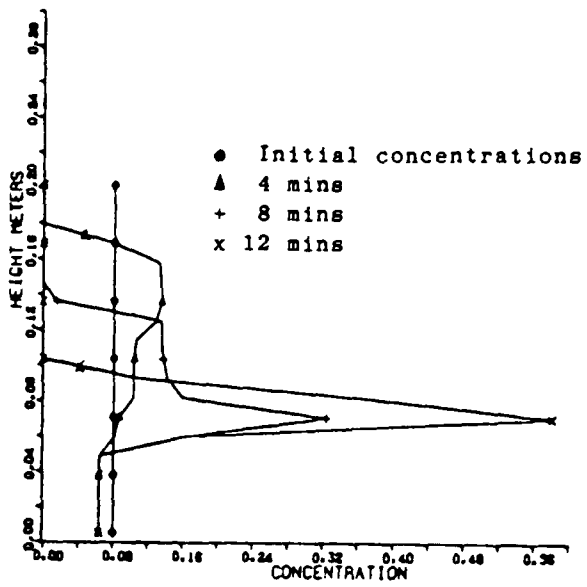

Glass (lead) 76.5μ

Figure 4.40 Density and concentration profiles for Three phase Exp five.

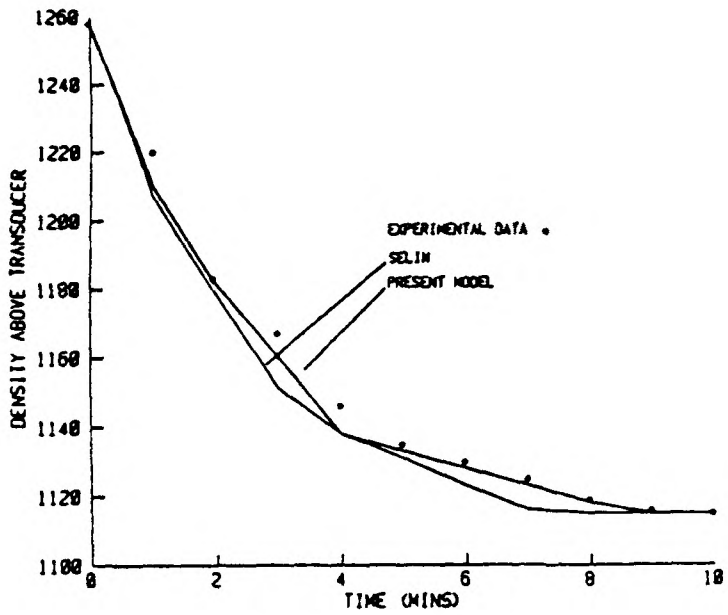

Density profile

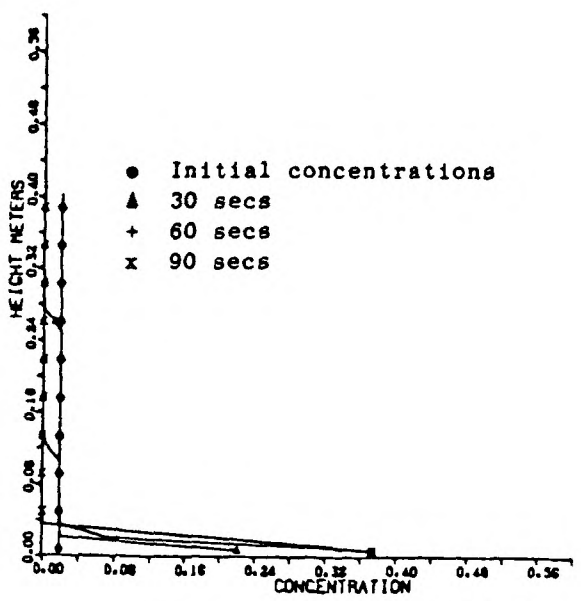

Glass (lead) 362.5μ

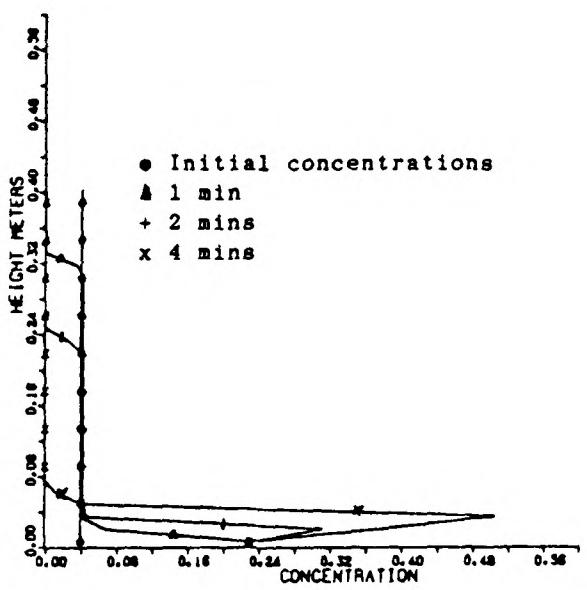

Glass (lead) 220μ

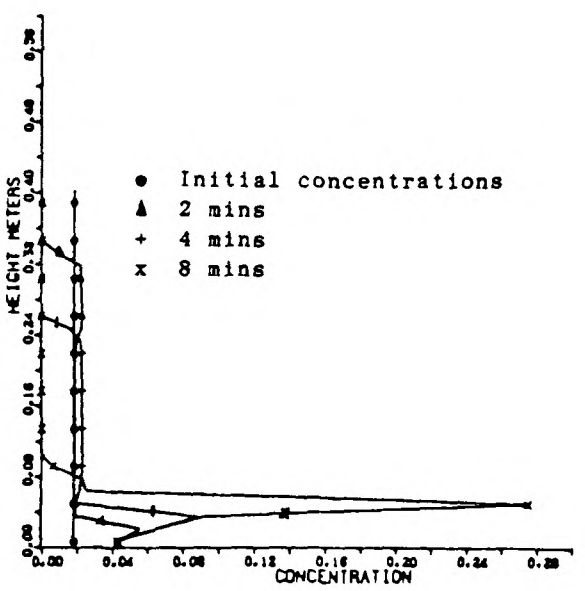

Glass (lead) 120μ

Figure 4.41 Density and concentration profiles for Three phase Exp six.

1) All three phases

2) Two slower moving phases

3) Slowest moving phase only.

The predicted solids concentrations associated with each experiment for the first two layers are:

Experiment	Solid concentration in first sediment layer	D_H	Solids concentration in second sediment layer	D_H
Exp one	0·687	53μ	0·621	29μ
Exp two	0·660	106μ	0·633	72μ
Exp three	0·653	93μ	0·658	50μ
Exp four	0·688	49μ	0·621	24μ
Exp five	0·690	48μ	0·658	30μ
Exp six	0·647	96μ	0·624	78μ

Table 4.5 Sediment concentrations associated with three phase runs.

The solids concentration in the third layer is $(1-E(D_i))$ where $E(d_i)$ is the voidage of the slowest moving phase when packed alone. Further densification of the sediment in the layer consisting of all three phases occurs for Exp two and Exp three only. The hydraulic radius associated with the second layer for each experiment is smaller than the smallest phase present, therefore no more compaction in this layer can occur. The movement of the smallest phases into the first sediment layer for Exp two and Exp three will continue until the solids concentration in this layer is 0·698 and 0·677 respectively.

Although this movement will occur within the structure of the sediment it will not occur from the free settling zone just above the sediment until the zone containing all three phases has disappeared. This is because the movement of the smallest particles in this zone is in the opposite direction to the other phases.

CHAPTER FIVE

MODELLING A CONTINUOUS GRAVITY THICKENER

5.1 Introduction

The theoretical description of thickening is still very poorly understood. As discussed in chapter one the majority of thickeners are designed using data obtained from laboratory batch tests (i.e. Jar tests) on the slurry to be dewatered. This involves noting the height of the slurry/supernatant liquid interface over time and using material balances with the assumption that settling velocity is dependent on concentration only to estimate the thickener surface area required to give a specified dewatering. It is common knowledge that these design procedures are inadequate and large scale safety factors must be incorporated into the thickener design, Pearce (1977). This is because the use of laboratory batch tests inherently assumes that batch settling is analogous to continuous industrial thickening.

Due to the non homogeneity of the feed it is essential to model an industrial continuous thickener as a multiphase problem. Account of the forces present in the system was considered by Dixon (1977) by incorporating a momentum balance equation for the solids particles which he assumed had the same properties. The following multiphase numerical model has been developed to simulate the performance of a thickener using the same assumptions stated for batch sedimentation, see section 4.1, except assumption (1). Also assumption (2) is an approximation especially where the feed separates into the upflow and downflow streams. Modelling a thickener as a multidimensional, multiphase problem would involve solving pressures for each phase in each direction. At the present time solution procedures cannot solve a problem of this complexity. Therefore a one dimensional model is assumed so that the multiphase effects can be analysed. It is also assumed that particles do not settle at the underflow and overflow streams.

5.2 Governing Equations

The governing equations describing the thickening process are essentially the same as for batch sedimentation, see chapter four, except account must be taken of the following:

1) Feed
2) Underflow
3) Overflow
4) Upflow
5) Downflow.

The above streams and flow influences can be incorporated into the batch model by making appropriate adjustments to the governing equations and boundary conditions.

5.2.1 Solid phase equations

Associated with each solid phase is a continuity and momentum equation. The momentum equation is the same as used for batch sedimentation, see equation 4.2. The influence of the upflow and downflow effects on the particles is taken into account via the fluid velocity in the drag term. The presence of the feed is incorporated into the continuity equation which is adjusted as follows:

$$\frac{\partial}{\partial t}(\rho_i S_i) + \frac{\partial}{\partial y}(\rho_i S_i U_i) = \dot{M} \qquad (5.1)$$

where

$$\dot{M} = \frac{\rho_i T_F S_F}{Q\ \Delta y} \quad \text{at feed} \tag{5.1a}$$

$$= 0 \qquad \text{elsewhere} \tag{5.1b}$$

T_F and S_F are the volumetric flow rates and concentrations associated with the feed. $Q\ \Delta y$ is the volume of the control volume representing the feed where Q is the surface area.

5.2.2 Fluid phase equations

Associated with the fluid phase is the fluid continuity equation and the concentration balance equation. For a thickener the concentration balance equation is the same as used in batch sedimentation, see equation (4.9). As with the solid phases the fluid continuity equation is adjusted to incorporate the feed streams:

$$\frac{\partial}{\partial t}(\rho_f F) + \frac{\partial}{\partial y}(\rho_f F V) = \dot{N} \tag{5.2}$$

$$\dot{N} = \rho_f \frac{T_F F_F}{Q\ \Delta y} \qquad \text{at feed} \tag{5.2a}$$

$$= 0 \qquad \text{elsewhere} \tag{5.2b}$$

F_F being the volumetric fluid concentration of the feed stream.

As the solids and fluid phases are incompressible the density terms can be eliminated from equations 5.1 and 5.2. Combining the resulting equations gives the total volumetric balance equation for a thickener

$$\frac{\partial (FV)}{\partial y} + \sum_{i=1}^{NSOL} \frac{\partial}{\partial y}(S_i U_i) = \dot{V} \tag{5.3}$$

where

$$\dot{V} = \frac{T_F}{Q\ \Delta y} \qquad \text{at feed} \qquad (5.3a)$$

$$= 0 \qquad \text{elsewhere} \qquad (5.3b)$$

5.2.3 Boundary Conditions

Boundary conditions must be given at the underflow and overflow outlets (i.e. Y=1 and Y=NY respectively). Due to the assumption that particulate settling does not occur in the underflow or overflow then the following boundary conditions will apply:

$$U_i(i=1\ldots,NSOL),\quad V = -\frac{T_u}{Q_1} \quad \text{at underflow (i.e. Y=1)} \qquad (5.4a)$$

$$= \frac{T_o}{Q_{NY}} \quad \text{at overflow (i.e. Y=NY)} \qquad (5.4b)$$

Also the concentrations at these boundarys are the same as calculated at the underflow and overflow control volume nodal points. Therefore at the boundaries

$$\frac{dS_i}{dy} = 0 \qquad (5.4c)$$

5.3 Control Volume representation

The thickener domain is divided into a number of control volumes, see figure 5.1. Because of the non-uniform shape of the thickener and the area to be modelled, see figure 3.1, control volumes of different surface area are applied at the feed well outlet and around the conical section at the base. The surface area of each control volume is given

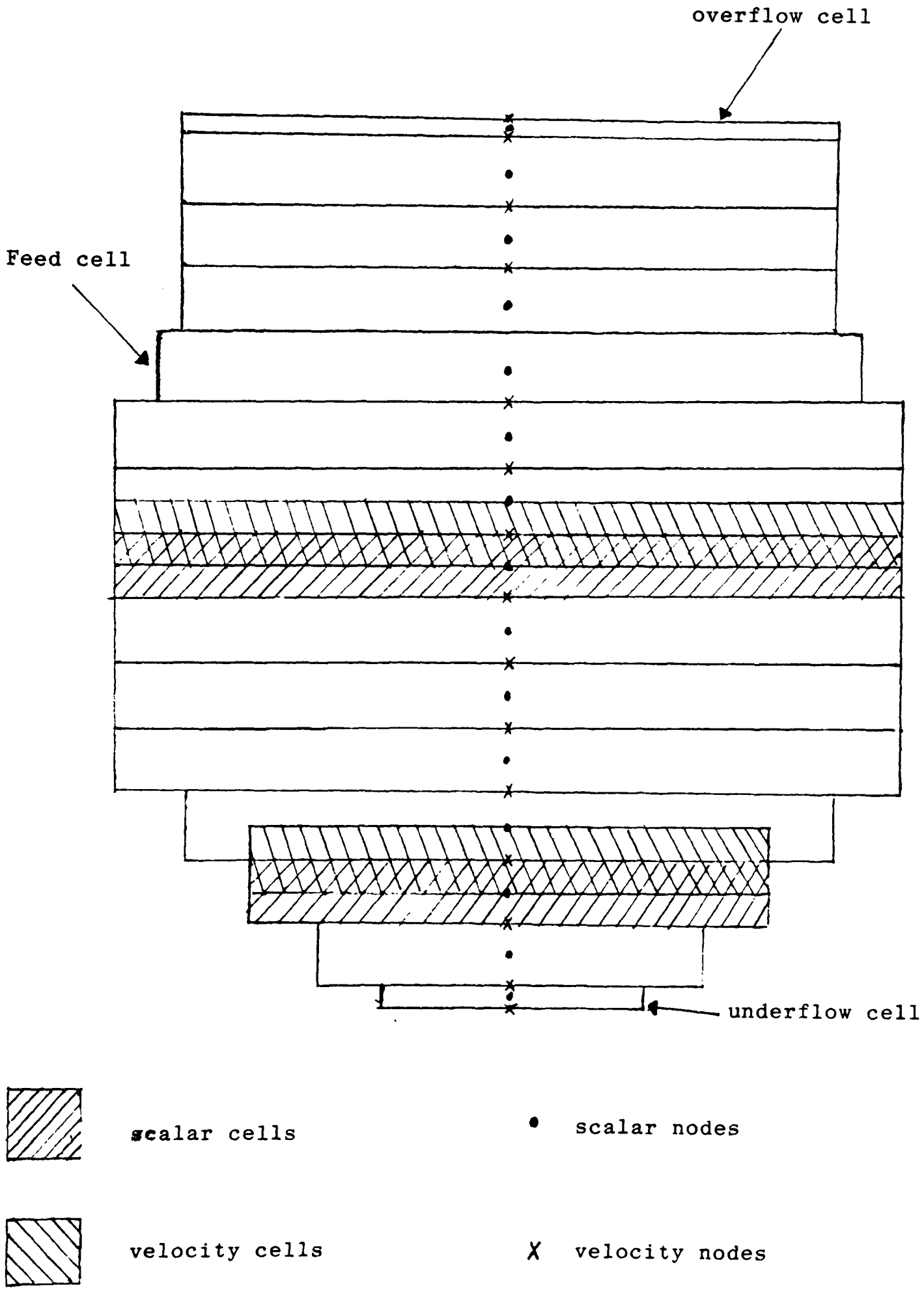

Figure 5.1 Control volume specification for a thickener

by:

$$Q = \pi R^2 \tag{5.4}$$

where R is the radius of the control volume. The value of R for all cells below the feed cell and above the cell containing the top of the conical section is given by

$$R = \frac{TDIAM}{2} \tag{5.5}$$

where TDIAM is the diameter of the thickener. The value of R for all cells above the feed cell is given by

$$R = \frac{TDIAM - WDIAM}{2} \tag{5.6}$$

where WDIAM is the diameter of the feed well. This ensures that only the area outside the feed well is modelled. For control volumes within the conical section (not applicable for flat bed thickeners) down to and including the underflow cell, see figure (5.2c), the value of R is given by

$$R = \frac{TDIAM}{2} - \frac{\Delta y}{TAN(\theta)} \tag{5.7}$$

The control volumes containing the feed outlet and the top of the conical section, see figures (5.2a) and (5.2b), involve calculating the volume of the thickener at these locations which is to be modelled. This volume will correspond to the volume of the cells representing these locations. For the feed cell this volume is:

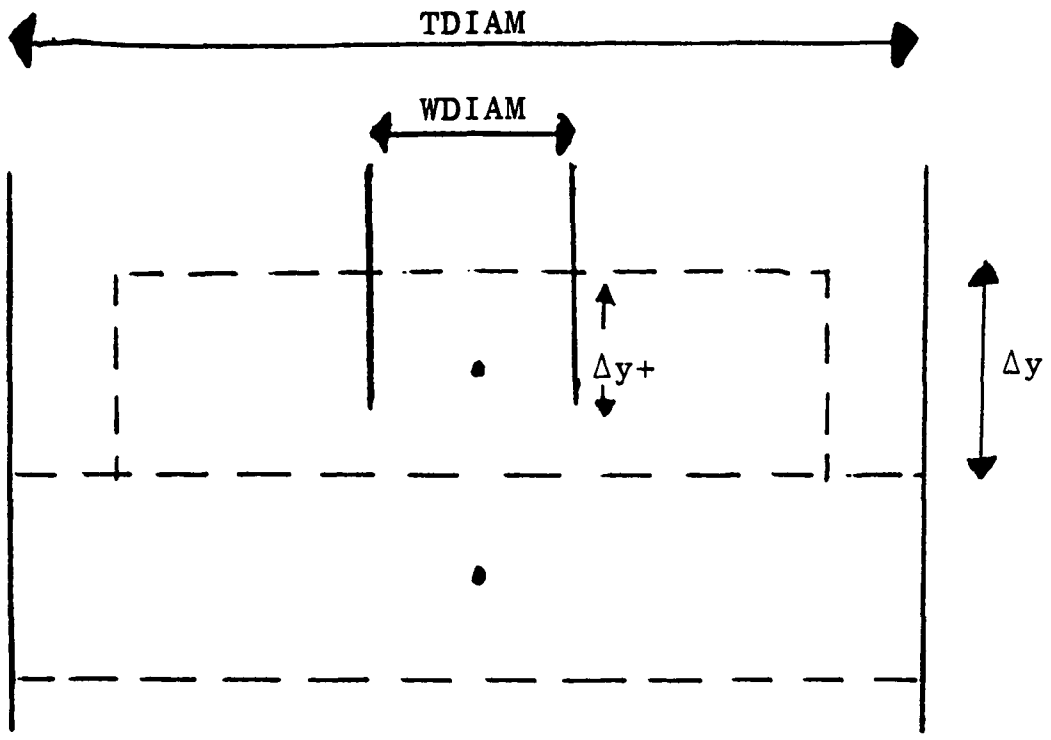

Figure 5.2a Control volumes around the feed well

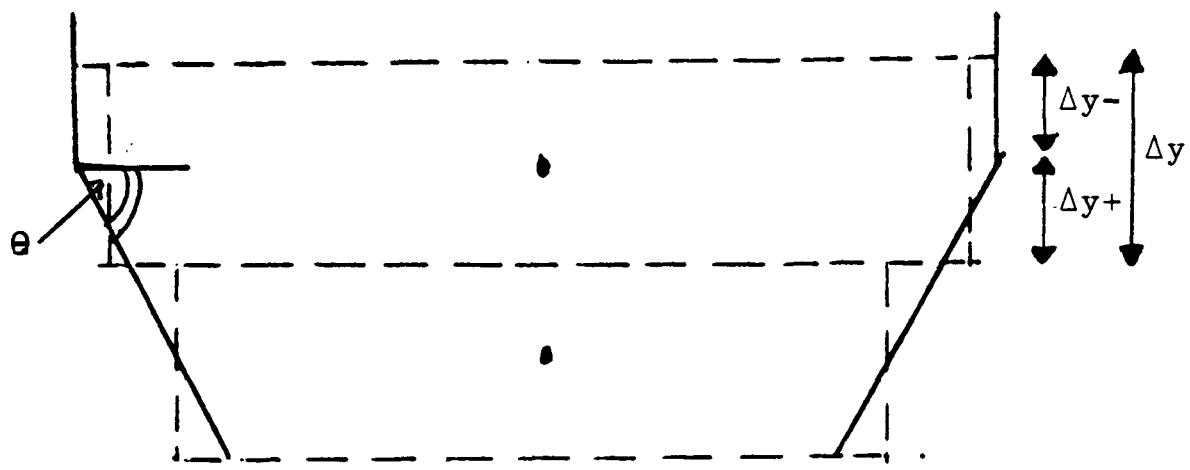

Figure 5.2b Control volumes at top of conical section

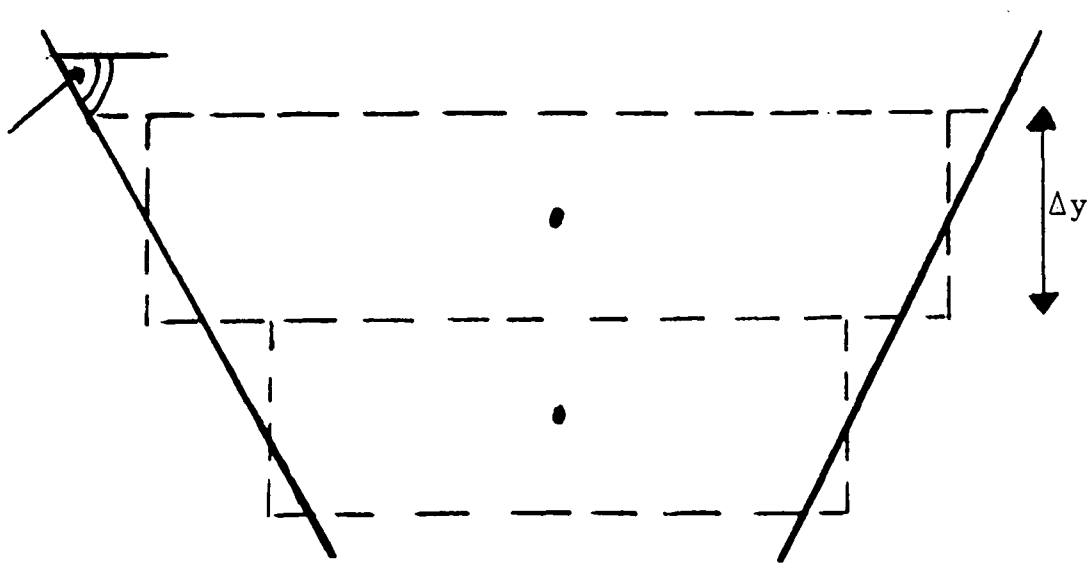

Figure 5.2c Control volumes within the conical section

$$VOL = \frac{\pi}{4} (TDIAM)^2 \Delta y - \frac{\pi}{4} (WDIAM)^2 \Delta y_+ \qquad (5.8)$$

This again ensures only the volume outside the feed well is under consideration. The volume of the cell containing the top of the conical section is:

$$VOL = \frac{\pi}{4} \left[TDIAM - \frac{\Delta y_+}{TAN(\theta)} \right]^2 \Delta y_+ + \frac{\pi}{4} (TDIAM)^2 \Delta y_- \qquad (5.9)$$

The surface area of these two control volumes is calculated via:

$$Q = \frac{VOL}{\Delta y} \qquad (5.10)$$

5.4 Discretised equations

The governing equations are discretised using the techniques outlined in chapter four, see section 4.3, to give discretised equations of the form (4.12).

Consider the control volumes in figure 5.3. It can clearly be seen that the difference in the surface area of some control volumes will effect the inflow and outflow contributions. To incorporate this effect the following variables are calculated:

$$A_1 = \frac{Q_N}{Q_P} \qquad (5.11a)$$

$$A_2 = \frac{Q_S}{Q_P} \qquad (5.11b)$$

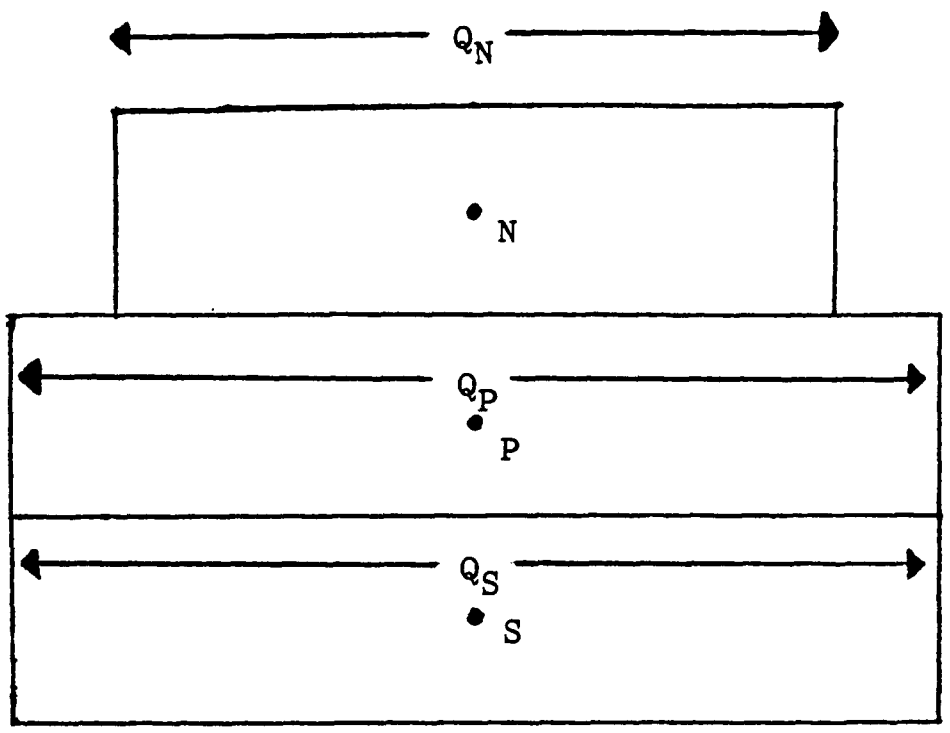

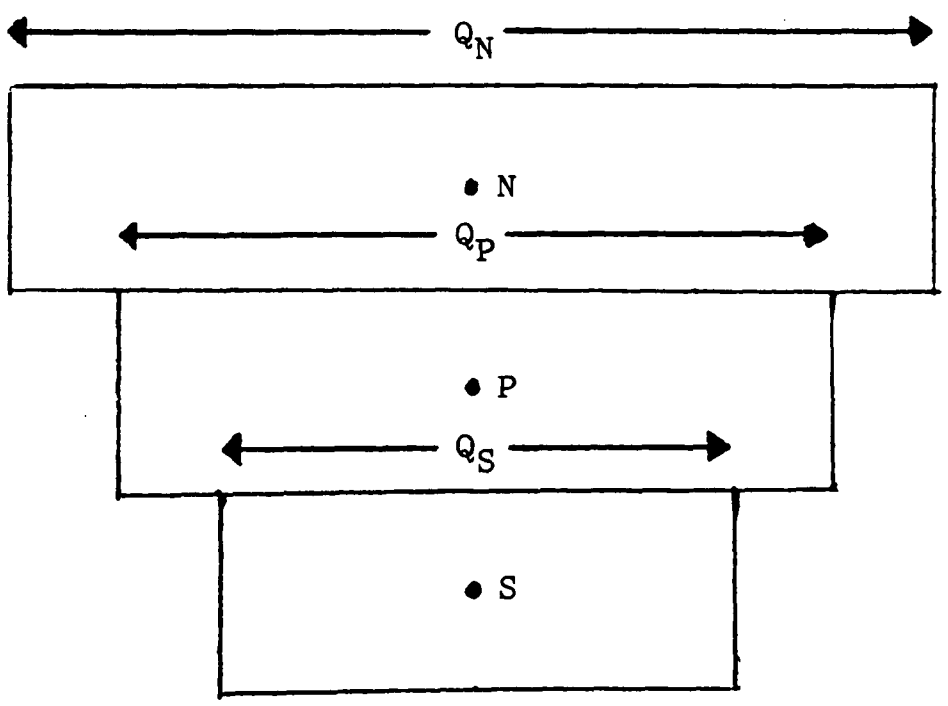

Figure 5.3 Surface Areas associated with control volumes

Now if

$$A_1 \geqslant 1 \qquad \text{then} \qquad A_1 = 1 \tag{5.11c}$$

$$A_2 \geqslant 1 \qquad \text{then} \qquad A_2 = 1 \tag{5.11d}$$

Therefore A_1 and A_2 represent the proportions of the dependent variable Φ that can flow across the north and south faces of the control volume respectively.

Because of the source terms associated with the continuity equations at the feed as well as the different surface areas of the control volumes the discretised equations will contain different coefficients for all the governing equations except the concentration balance which remains the same, see equation (4.16).

5.4.1 Solid phase continuity

The continuity equation (5.1) is integrated over the scalar control volumes. This results in equation (4.12) where Φ is the solid concentration S and:

$$AN = [-U_p, 0] A_1 \tag{5.12a}$$

$$AS = [U_S, 0] A_2 \tag{5.12b}$$

$$AP = \frac{\Delta y}{\Delta t} + [U_p, 0]A_1 + [-U_S, 0]A_2 \tag{5.12c}$$

$$b = \frac{\Delta y}{\Delta t} S_p^{OLD} + \dot{X} \tag{5.12d}$$

where

$$\dot{X} = \frac{T_F S_F}{Q_P} \qquad \text{for feed cell} \tag{5.12e}$$

$$= 0 \qquad \text{elsewhere} \tag{5.12f}$$

5.4.2 Solid phase momentum

The momentum equation of each solid phase is integrated over velocity control volumes. The coefficients associated with equation (4.12), where Φ is the solid velocity U, are the same as for batch sedimentation see section 4.3.2. The only difference is due to the different surface areas associated with some control volumes. Considering the inflow contributions these become:

$$AN = AN^* A_1 \tag{5.13a}$$

$$AS = AS^* A_2 \tag{5.13b}$$

where AN^* and AS^* are the values given in section 4.3.2. The new values of AN and AS given by equations (5.13a) and (5.13b) are used to calculate AP in the usual manner.

5.4.3 Total volumetric balance

Equation (5.3) is integrated over scalar control volumes to give a discretised equation of the form (4.12) where Φ is the fluid velocity v. The coefficients associated with equation (4.12) are given by equations (4.18) except the source term b which is given by:

$$b = \sum_{i=1}^{NSOL} \left\{ \mathbb{I}-(S_i)_N \ (U_i)_p, 0 \mathbb{I} - \mathbb{I}(S_i)_p \ (U_i)_p, \dot{0} \mathbb{I} \right\} + FLOW \qquad (5.14)$$

where

$$FLOW = - \frac{T_u}{Q_p} \quad \text{if cell is below feed cell} \qquad (5.14a)$$

$$= \frac{T_o}{Q_p} \quad \text{for feed cell and above} \qquad (5.14b)$$

The terms given by equations (5.14a) and (5.14b) represent the downflow and upflow velocity effect, where Q_p is the surface area of the appropriate control volume.

5.5 Solution procedure

In modelling a continuous gravity thickener the following information is required:

1) Volmetric flow rates of the feed (T_F) and the underflow (T_U). The overflow volumetric flow rate is then calculated via:

$$T_O = T_F - T_U \qquad (5.15)$$

2) Dimensions of the thickener which include:

- Diameter of thickener.
- Depth of thickener from slurry surface to the underflow outlet.
- Conical angle associated with a conical base thickener.
- Distance from underflow outlet at which conical section begins.
- Depth of feed well from slurry surface to feed well outlet.
- Diameter of feed well.

3) Volumetric concentrations of each solids phase present in the feed (S_F).

Given the above information the model predicts:

1) Clarity of overflow.
2) Solid concentration in underflow.
3) Distribution of solids throughout the thickener.

If weight concentrations (C_i) and mass flow rates (W) are given instead of volumetric concentrations (S_i) and flow rates (T) then volumetric values are calculated via:

$$S_i = \frac{\rho_m}{\rho_i} C_i \tag{5.16}$$

$$T = \frac{W}{\rho_m} \tag{5.17}$$

where the pulp density (ρ_m) is given by equation (4.8) or

$$\rho_m = \frac{\rho_f}{\left[1+\rho_f \sum_{i=1}^{NSOL} \frac{C_i}{\rho_i} - \sum_{i=1}^{NSOL} C_i\right]} \tag{5.18}$$

Using the dimensions of the thickener a one-dimension control volume representation is set up, see figure 5.1. Unlike batch sedimentation the operation of a continuous gravity thickener is a steady state process. The model assumes initially that the thickener is full of water only. The effect of the feed and underflow streams are modelled by solving the dependent variables S_i, U_i (i=1...,NSOL), F and V

throughout the thickener over time until a steady state solution has been obtained. The upflow and downflow effects are directly incorporated into the "total volumetric balance" equation which is solved for the fluid velocity. These flow effects will be felt by the solid particles via the drag term in the momentum equations which have the fluid velocity incorporated within them.

The discretised equations are solved using the same procedure as for batch sedimentation, see section 4.5, with the following adjustments:

- Due to the overall slurry movement, the boundaries associated with each phase and the sediment are not monitored, Although the packing model is still used to check what cells become packed.

- If a cell becomes packed then the velocities associated with that cell are set to the upflow or downflow velocity at that cell depending on the location of the cell

$$U_i \ (i=1,NSOL), \ V = -\frac{T_u}{Q} \quad \text{if cell is below feed cell.} \qquad (5.19)$$

$$= \frac{T_o}{Q} \quad \text{if cell is feed cell or above.} \qquad (5.20)$$

- The solution procedure stops when a steady state solution has been obtained. If the total solids mass in the thickener as well as the dependent variables do not change significantly between two time steps then steady state has been achieved. The mass of solids in a control volume is given by

$$TMASS = \sum_{i=1}^{NSOL} S_i \rho_i Q \Delta y \qquad (5.21)$$

combining the mass present in each control volume will give the total solids mass in the thickener.

5.6 Comparison with experimental data

The data gathered at the mineral processing plant, see chapter three, has been used in validating the above model. The fluid phase in each thickener is water and the density and viscosity values used are those at room temperature. Therefore

$$\rho_f = 1000 \text{ Kg/M}^3$$

$$\mu_f = 0{\cdot}001 \text{ Kg/MS}.$$

For each of the three thickeners the underflow and overflow scalar nodes are situated 3cm from the thickener base and slurry surface respectively. The thickener domain is divided into nineteen control volumes with the cells between the underflow and overflow cells being of uniform size. All information needed to simulate each thickener is available except the depth of the feed well which is assumed to be approximately a third of the thickener height. The voidages $E(d_i)$ associated with the packing model are taken as 0·4 for each of the materials under investigation. The experimental data consists of mass flow rates and concentration profiles by weight. The model uses equations (5.15), (5.16) and (5.17) to convert the input data into volumetric terms and outputs concentrations as weight fractions.

5.6.1 Galena Thickener

The Galena thickener is a flat bed thickener containing Galena and small quantities of Barytes and Fluorite. The volumetric flow rates of the feed, underflow and overflow are calculated from the mass concentrations of each material present in these streams as well as their mass flow rates. Therefore:

$$T_F = 0{\cdot}003364 \ M^3/S$$

$$T_U = 0{\cdot}002016 \ M^3/S$$

$$T_O = 0{\cdot}001348 \ M^3/S.$$

The domain of the thickener, see figure 3.11, is divided into control volumes whose surface areas are:

distance of scalar node from underflow (M)	surface area of control volume (M^2)
1·64	38·8
1·56	38·8
1·47	38·8
1·38	38·8
1·29	38·8
1·20	38·94
1·11	39·59
1·02	39·59
0·92	39·59
0·83	39·59
0·74	39·59
0·65	39·59
0·56	39·59
0·47	39·59
0·37	39·59
0·28	39·59
0·19	39·59
0·10	39·59
0·03	39·59

Table 5.1 Surface areas associated with Galena thickener.

The depth of the feed well below the slurry surface was taken to be 0·5m. The size distribution of the Galena, Barytes and Fluorite present in the feed are assumed to be the same and are given in figure 3.12. By using the average particle diameter and the presence of the three materials we are modelling a three phase problem, see table 5.2a. The size distribution is split into two and three equal parts giving a six and nine phase (A) problem where the concentrations of the phases belonging to any one of the materials are equal, see tables (5.2b) and (5.2c). The diameters of each phase correspond to the central location of each split section from the size distribution. Therefore the diameters in the six phase model corresponds to the 75% and 25% undersize points in figure 3.12. Comparing the model using three, six and nine phase (A) data against experimental data, see figure 5.4, it can be seen that representing the feed distribution in greater detail enables closer comparisons with the experimental solids concentration profile throughout the thickener to be made. The underflow concentration is predicted in all cases but for each run no solids are present in the overflow. To incorporate smaller particles into the model the size distribution was split into three parts consisting of the smallest 5% with the other 95% being split into two equal parts, see table (5.2d). Nine phase (B) predicts the overall solids profile with a greater degree of accuracy than the other comparisons. Solids are also present in the overflow, see table (5.4a) and (5.4b), which consists of Barytes and Fluorite only, although chemical analysis of the overflow predicted a quantity of Galena as well as Barytes and Fluorite being present. The quantities of each material present in the underflow compares favourably with the values given by chemical analysis. The reason no Galena is present in the overflow is probably due to:

Phase	1	2	3
Concentration (WT%)	53·23	2·91	4·88
Diameter (μ)	38	38	38
Density (Kg/M^3)	7500	4500	3100

Table 5.2a Three phase data for Galena Thickener

Phase	1	2	3	4	5	6
Concentration (WT%)	26·615	26·615	1·455	1·455	2·44	2·44
Diameter (μ)	69	21	69	21	69	21
Density (Kg/M^3)	7500	7500	4500	4500	3100	3100

Table 5.2b Six phase data for Galena Thickener

Phase	1	2	3	4	5	6	7	8	9
Concentration (WT%)	17·743	17·743	17·743	·97	·97	·97	1·627	1·627	1·627
Diameter (μ)	81	38	15	81	38	15	81	38	15
Density (Kg/M^3)	7500	7500	7500	4500	4500	4500	3100	3100	3100

Table 5.2c Nine phase (A) data for Galena Thickener

Phase	1	2	3	4	5	6	7	8	9
Concentration (WT%)	25·284	25·284	2·662	1·382	1·382	·146	2·318	2·318	·244
Diameter (μ)	71	23	4	71	23	4	71	23	4
Density (Kg/M^3)	7500	7500	7500	4500	4500	4500	3100	3100	3100

Table 5.2d Nine phase (B) data for Galena Thickener

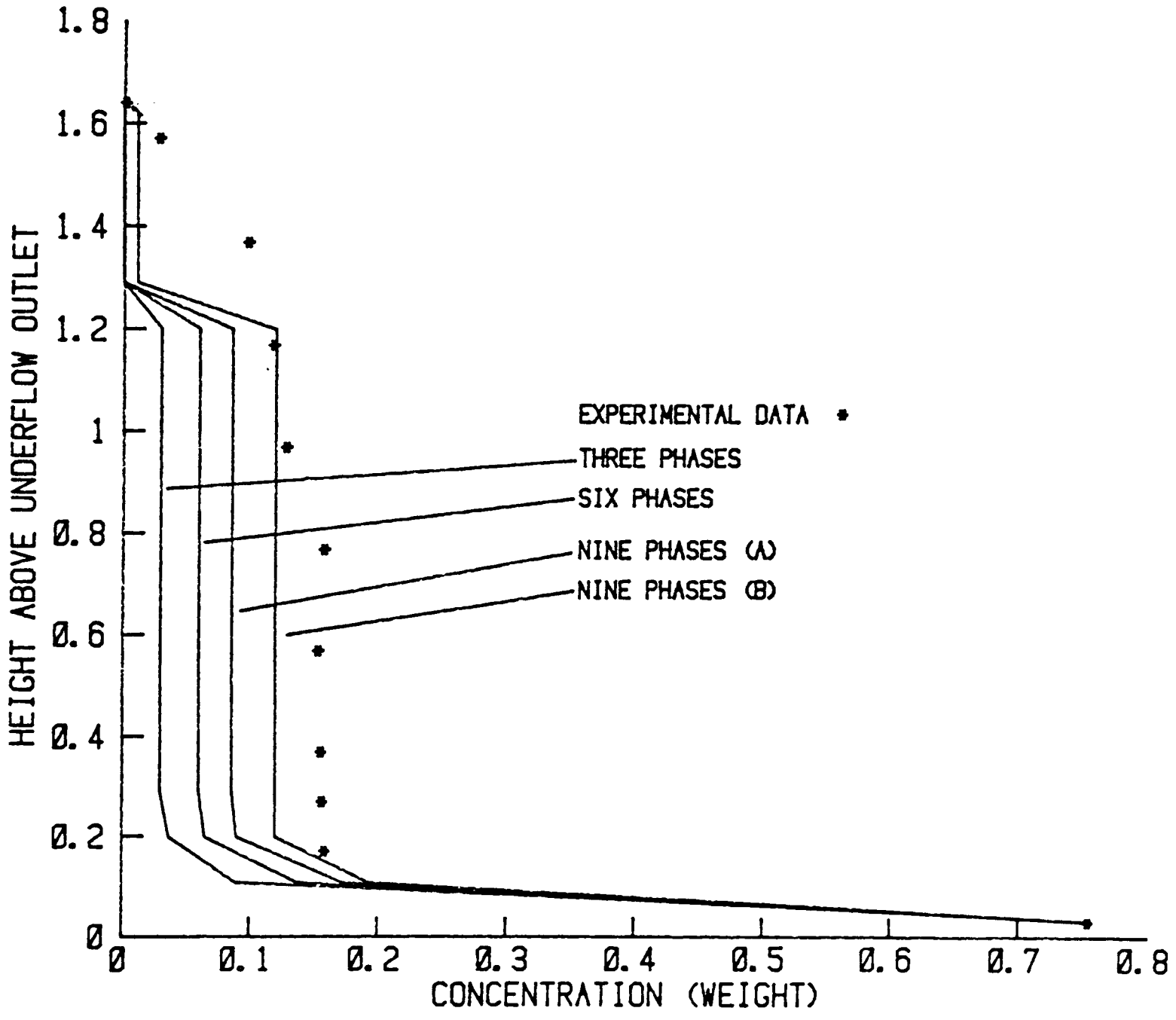

Figure 5.4 Comparisons between model and experimental data for Galena thickener

Distance from	Galena			Barytes			Fluorite		
underflow (M)	71μ	23μ	4μ	71μ	23μ	4μ	71μ	23μ	4μ
1·67	0·0	0·0	0·0	0·0	0·0	0·16	0·0	0·0	0·42
1·64	0·0	0·0	0·0	0·0	0·0	0·16	0·0	0·0	0·42
1·56	0·0	0·0	0·0	0·0	0·0	0·47	0·0	0·0	0·69
1·47	0·0	0·0	0·0	0·0	0·0	0·46	0·0	0·0	0·68
1·38	0·0	0·0	0·0	0·0	0·0	0·46	0·0	0·0	0·68
1·29	0·0	0·0	0·0	0·0	0·0	0·46	0·0	0·0	0·68
1·20	0·4	3·3	6·0	0·04	0·3	0·3	0·11	0·9	0·56
1·11	0·4	3·3	6·0	0·04	0·3	0·3	0·11	0·9	0·55
1·02	0·4	3·3	6·0	0·04	0·3	0·3	0·11	0·9	0·55
·92	0·4	3·3	6·0	0·04	0·3	0·3	0·11	0·9	0·55
·83	0·4	3·3	6·0	0·04	0·3	0·3	0·11	0·9	0·55
·74	0·4	3·3	6·0	0·04	0·3	0·3	0·11	0·9	0·55
·65	0·4	3·3	6·0	0·04	0·3	0·3	0·11	0·9	0·55
·56	0·4	3·3	6·0	0·04	0·3	0·3	0·11	0·9	0·55
·47	0·4	3·3	6·0	0·04	0·3	0·3	0·11	0·9	0·55
·37	0·4	3·3	6·0	0·04	0·3	0·3	0·11	0·9	0·55
·28	0·4	3·3	6·0	0·04	0·3	0·3	0·11	0·9	0·55
·19	0·41	3·4	6·0	0·04	0·3	0·3	0·11	0·9	0·56
·10	0·78	6·4	7·5	0·09	0·7	0·4	0·34	2·46	0·61
·03	31·4	31·4	3·3	1·72	1·72	0·14	2·8	2·8	0·2
0	31·4	31·4	3·3	1·72	1·72	0·14	2·8	2·8	0·2

Table 5.4a Solid concentrations (weight %) throughout Galena Thickener for Nine phase (B)

Distance from underflow (M)	Galena 71μ	Galena 23μ	Galena 4μ	Barytes 71μ	Barytes 23μ	Barytes 4μ	Fluorite 71μ	Fluorite 23μ	Fluorite 4μ
1·67	·347-04	·347-04	·347-04	·347-04	·347-04	·347-04	·347-04	·347-04	·347-04
1·61	-·117-01	-·136-02	-·797-05	-·662-02	-·719-03	·118-04	-·405-02	-·418-03	·210-04
1·52	-·117-01	-·134-02	-·731-05	-·652-02	-·708-03	·121-04	-·399-02	-·411-03	·212-04
1·43	-·117-01	-·134-02	-·733-05	-·652-02	-·708-03	·121-04	-·399-02	-·411-03	·212-04
1·34	-·117-01	-·134-02	-·733-05	-·652-02	-·708-03	·121-04	-·399-02	-·411-03	·212-04
1·25	-·107-01	-·122-02	-·302-05	-·593-02	-·637-03	·148-04	-·359-02	-·365-03	·232-04
1·15	-·102-01	-·122-02	-·712-04	-·565-02	-·665-03	-·543-04	-·341-02	-·406-03	-·464-04
1·06	-·102-01	-·122-02	-·715-04	-·565-02	-·666-03	-·546-04	-·342-02	-·407-03	-·466-04
0·97	-·102-01	-·122-02	-·715-04	-·565-02	-·666-03	-·546-04	-·342-02	-·407-03	-·466-04
0·88	-·102-01	-·122-02	-·715-04	-·565-02	-·666-03	-·546-04	-·342-02	-·407-03	-·466-04
0·79	-·102-01	-·122-02	-·715-04	-·565-02	-·666-03	-·546-04	-·342-02	-·407-03	-·466-04
0·70	-·102-01	-·122-02	-·715-04	-·565-02	-·666-03	-·546-04	-·342-02	-·407-03	-·466-04
0·61	-·102-01	-·122-02	-·715-04	-·565-02	-·666-03	-·546-04	-·342-02	-·407-03	-·466-04
0·52	-·102-01	-·122-02	-·715-04	-·565-02	-·666-03	-·546-04	-·342-02	-·407-03	-·466-04
0·43	-·102-01	-·122-02	-·715-04	-·565-02	-·666-03	-·546-04	-·342-02	-·407-03	-·466-04
0·33	-·102-01	-·122-02	-·715-04	-·565-02	-·666-03	-·546-04	-·342-02	-·407-03	-·466-04
0·24	-·102-01	-·122-02	-·715-04	-·565-02	-·666-03	-·546-04	-·342-02	-·407-03	-·466-04
0·15	-·972-02	-·116-02	-·698-04	-·536-02	-·633-03	-·535-04	-·321-02	-·385-03	-·460-04
0·06	-·481-02	-·582-03	-·526-04	-·227-02	-·281-03	-·434-04	-·101-02	-·140-03	-·391-04
0	-·509-04	-·509-04	-·509-04	-·509-04	-·509-04	-·509-04	-·509-04	-·509-04	-·509-04

Table 5.4b Solid velocities throughout Galena Thickener for Nine phase (B)

- Greater breakdown of size distribution needed to incorporate even smaller particles into the model.

- One dimensional assumption.

- Errors in experimental data.

- Flocculation, where Galena has agglomerated with other material lowering the overall density.

Also the poor comparison with experimental data above the feed well outlet is due to the assumed feed well depth.

The total mass of solids at steady state and the time it takes to reach steady state as well as the computing time for each run is:

Run	Solids mass in Thickener	Time to reach steady state	CPU time
Three phase	6932 Kg	3 hours 30 mins	67 secs
Six phase	8393 Kg	4 hours	23 mins
Nine phase (A)	9725 Kg	5 hours	32 mins
Nine phase (B)	11710 Kg	12 hours	50 mins

Table 5.3 Steady state details and computing time for Galena thickener.

5.6.2 Fluorite Thickener

The fluorite thickener is a conical base thickener containing fluorite only. The volumetric flow rates of the feed, underflow and overflow are:

$$T_F = 0{\cdot}01246 \ M^3/S$$
$$T_U = 0{\cdot}0055 \ M^3/S$$
$$T_O = 0{\cdot}00696 \ M^3/S$$

The thickener domain, see figure 3.6, is divided up into control volumes whose surface areas are:

distance of scalar node from underflow (M)	surface area of control volume (M^2)
2·94	174
2·83	174
2·66	174
2·49	174
2·32	174
2·16	174·2
1·99	174·8
1·82	174·8
1·65	174·8
1·49	174·8
1·32	174·8
1·15	174·8
0·98	174·8
0·81	165·6
0·65	113·2
0·48	66·3
0·31	31·8
0·14	9·9
0·03	2·1

Table 5.5 Surface areas associated with Fluorite thickener.

The depth of the feed well below the slurry surface is taken to be 0·87m. The fluorite size distribution for the feed is split equally into two, five and ten parts and particle diameters for each phase are estimated, see tables (5.6a), (5.6b), (5.6c) and (5.6d). Comparing the model predictions at steady state with the obtained experimental data, see figure (5.5), it can be seen that although the underflow is predicted in all cases the greater break down of the feed does not predict the experimental data. The fact that the one and two phase runs give better predictions is probably because flocculation is playing a major role in this thickener creating bigger particles (i.e. flocs)

Phase	1
Concentration (WT%)	29·53
Diameter (μ)	53

Table 5.6a One phase data for Fluorite Thickener

Phase	1	2
Concentration (WT%)	14·81	14·81
Diameter (μ)	102	21

Table 5.6b Two phase data for Fluorite Thickener

Phase	1	2	3	4	5
Concentration (WT%)	5·926	5·926	5·926	5·926	5·926
Diameter (μ)	154	87	53	27	7

Table 5.6c Five phase data for Fluorite Thickener

Phase	1	2	3	4	5	6	7	8	9	10
Concentration (WT%)	2·963	2·963	2·963	2·963	2·963	2·963	2·963	2·963	2·963	2·963
Diameter (μ)	171	136	102	77	61	46	32	21	11	4

Table 5.6d Ten phase data for Fluorite Thickener

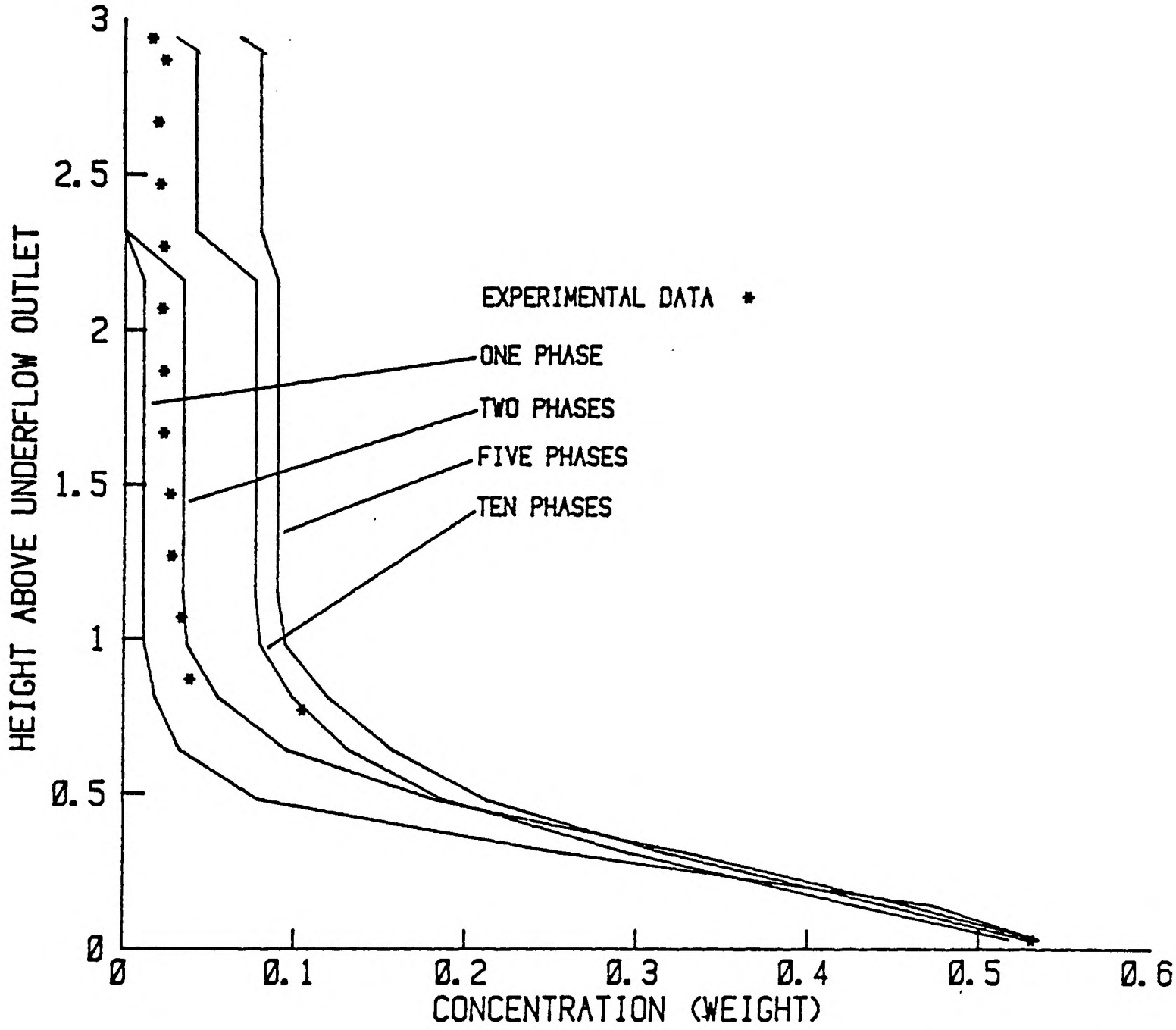

Figure 5.5 Comparisons between model and experimental data for Fluorite thickener

inside the thickener. The ten and five phase runs predict particles in the overflow consisting of the smallest phase only.

The total mass of solids at steady state in the thickener and time it takes to reach steady state as well as computing time for each run is:

Run	Solids mass in thickener (Kg)	Time to reach steady state	CPU time
One phase	7691 Kg	3 hours	52 secs
Two phase	17530 Kg	5 hours 38 mins	2 mins 47 secs
Five phase	44640 Kg	1 day 2 hours	105 mins
Ten phase	35517 Kg	20 hours 44 mins	189 mins

Table 5.7 Steady state details and computing time for Fluorite thickener.

The greater mass present in the thickener at five phase is due to small particles of size 7μ being caught in the upflow whereas for ten phase particles of size 4μ are caught in the upflow but their concentration is much smaller due to the greater break down of the feed.

5.6.3 Barytes Thickener

Like the fluorite thickener this is a conical base thickener containing Barytes only. Unfortunatley, concentration profiles down the thickener could not be obtained but the model has been used to give predictions of solids distribution throughout the thickener for one, two, five and ten phases where the size distribution of the feed, see figure 3.9, is split evenly with particle diameters representing each phase being calculated in the usual manner, see tables (5.9a),(5.9b),(5.9c) and (5.9d). The volumetric flow rates of the feed, underflow and overflow are:

$$T_F = 0{\cdot}004596 \ M^3/S$$
$$T_U = 0{\cdot}002310 \ M^3/S$$
$$T_O = 0{\cdot}002286 \ M^3/S.$$

Phase	1
Concentration (WT%)	33·119
Diameter (μ)	28·5

Table 5.9a One phase data for Barytes Thickener

Phase	1	2
Concentration (WT%)	16·5595	16·5595
Diameter (μ)	48	16

Table 5.9b Two phase data for Barytes Thickener

Phase	1	2	3	4	5
Concentration (WT%)	6·6238	6·6238	6·6238	6·6238	6·6238
Diameter (μ)	74	42	28·5	18	9

Table 5.9c Five phase data for Barytes Thickener

Phase	1	2	3	4	5	6	7	8	9	10
Concentration (WT%)	3·312	3·312	3·312	3·312	3·312	3·312	3·312	3·312	3·312	3·312
Diameter (μ)	85	63	48	37·5	32	26	21	16	12	6

Table 5.9d Ten phase data for Barytes Thickener

The thickener domain, see figure 3.8, is divided into a number of control volumes whose surface areas are:

Distance of scalar node from underflow (M)	Surface area of control volume (M^2)
3·89	44·82
3·75	44·82
3·53	44·82
3·30	44·82
3·08	44·93
2·86	45·60
2·63	45·60
2·41	45·60
2·19	45·60
1·96	45·60
1·74	45·60
1·51	45·60
1·29	45·60
1·07	45·60
·84	45·60
·62	45·60
·39	40·49
·17	11·88
·03	1·78

Table 5.8 Surface areas associated with Barytes thickener

The depth of the feed well below the slurry surface was assumed to be 0·92m. Comparisons between the model and experimental data, see figure 5.6, show that increasing from five to ten phases does not make a significant difference in the solids profile although for ten phases the 6.2μ phase does incorporate itself in the upflow stream but over-estimates the amount of solids present in the overflow. The solids concentration in the underflow is predicted accurately by each run.

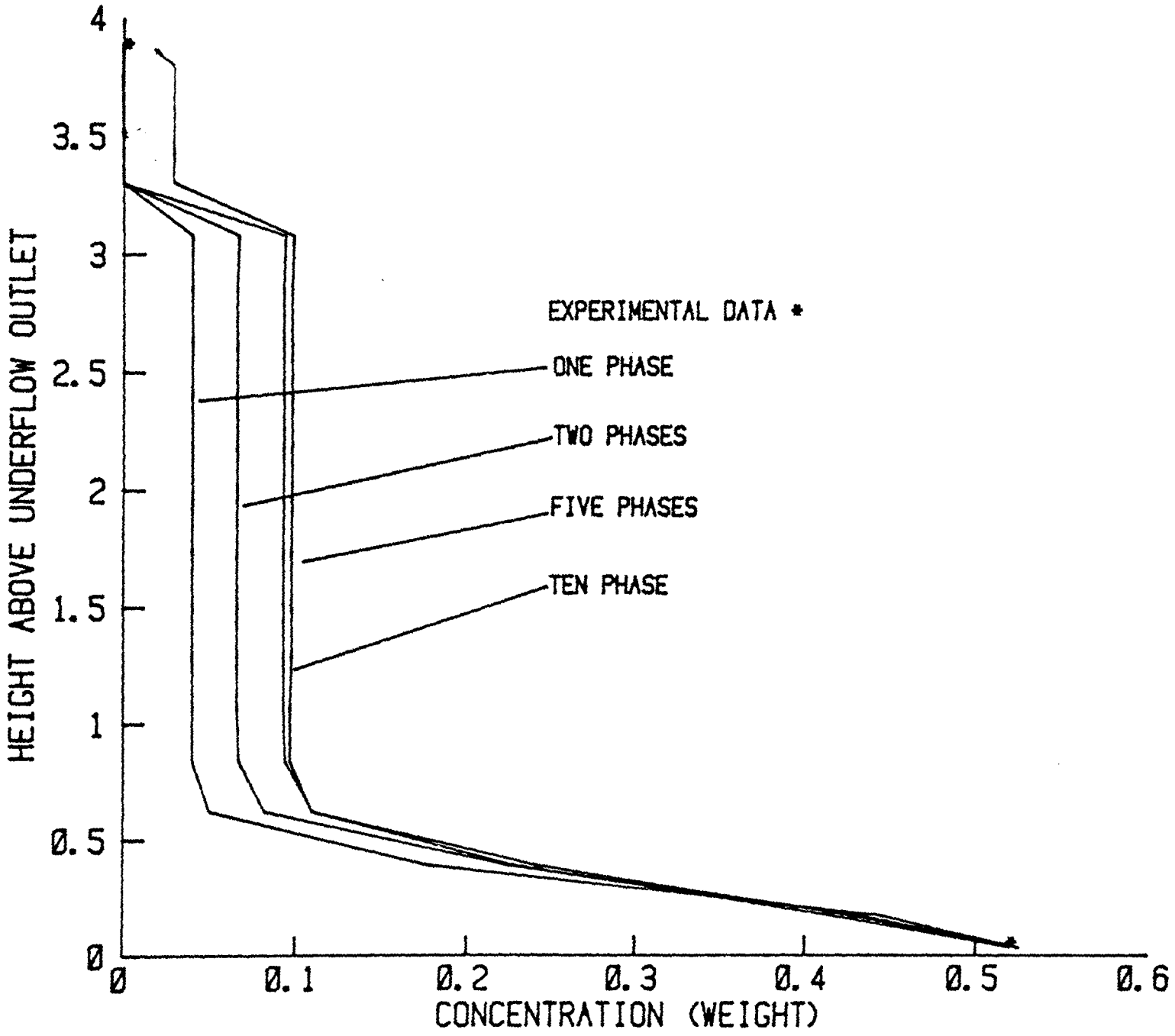

Figure 5.6 Comparisons between model and experimental data for Barytes thickener

The total mass of solids at steady state and time it takes to reach steady state as well as the computing time for each run are:

Run	Solids mass in thickener (Kg)	Time to reach steady state	CPU time
One phase	8867 Kg	4 hours 11 mins	2 mins 4 secs
Two phase	13021 Kg	7 hours 6 mins	9 mins 34 secs
Five phase	16960 Kg	12 hours 24 mins	46 mins 17 secs
Ten phase	18282 Kg	1day 1 hour	224 mins

Table 5.10 Steady state details and computing time for Barytes thickener

CHAPTER SIX

A NUMERICAL MODEL FOR FLOCCULATED BATCH SEDIMENTATION

6.1 Introduction

The major method of increasing the efficiency of solid/liquid separations is through the use of aggregating or agglomerating chemical additives known as flocculants or coagulants. Both these additives produce small clusters of particles (plus enclosed fluid) called flocs. Coagulants are used to break down the repulsive forces around the particles enabling the attractive London-van de Waals forces to dominate. Flocculants form bridges bonding the particultes together, see Wills (1985). Particulate mixtures in which either of the above effects are occurring will be referred to as flocculated mixtures.

Like non-flocculated mixtures two regions will form during the settlement of particulates in a flocculated mixture, see figure 6.1, these are:

1) Free settling region
2) Sediment region.

The free settling region will consist of discrete particles settling at different velocities due to their differences in density and/or size and shape. These particulates will collide and form flocs which can grow in size, due to further collision, until a maximum stable size is reached. The weight of the particulates and flocs in the free settling region is borne solely by hydraulic forces. As the flocs and particulates settle they will pack from the base up and form the sediment region. The solids concentration at which this occurs is known as the compression point and depends on the structure and concentrations of the flocs and particulates present. Within the sediment the flocs lose their individual identity but the attractive/bonding forces between the particles form a particulate structure which can be broken down when the weight of particulates above becomes too great for these forces to support. This leads to a sediment which is compressible.

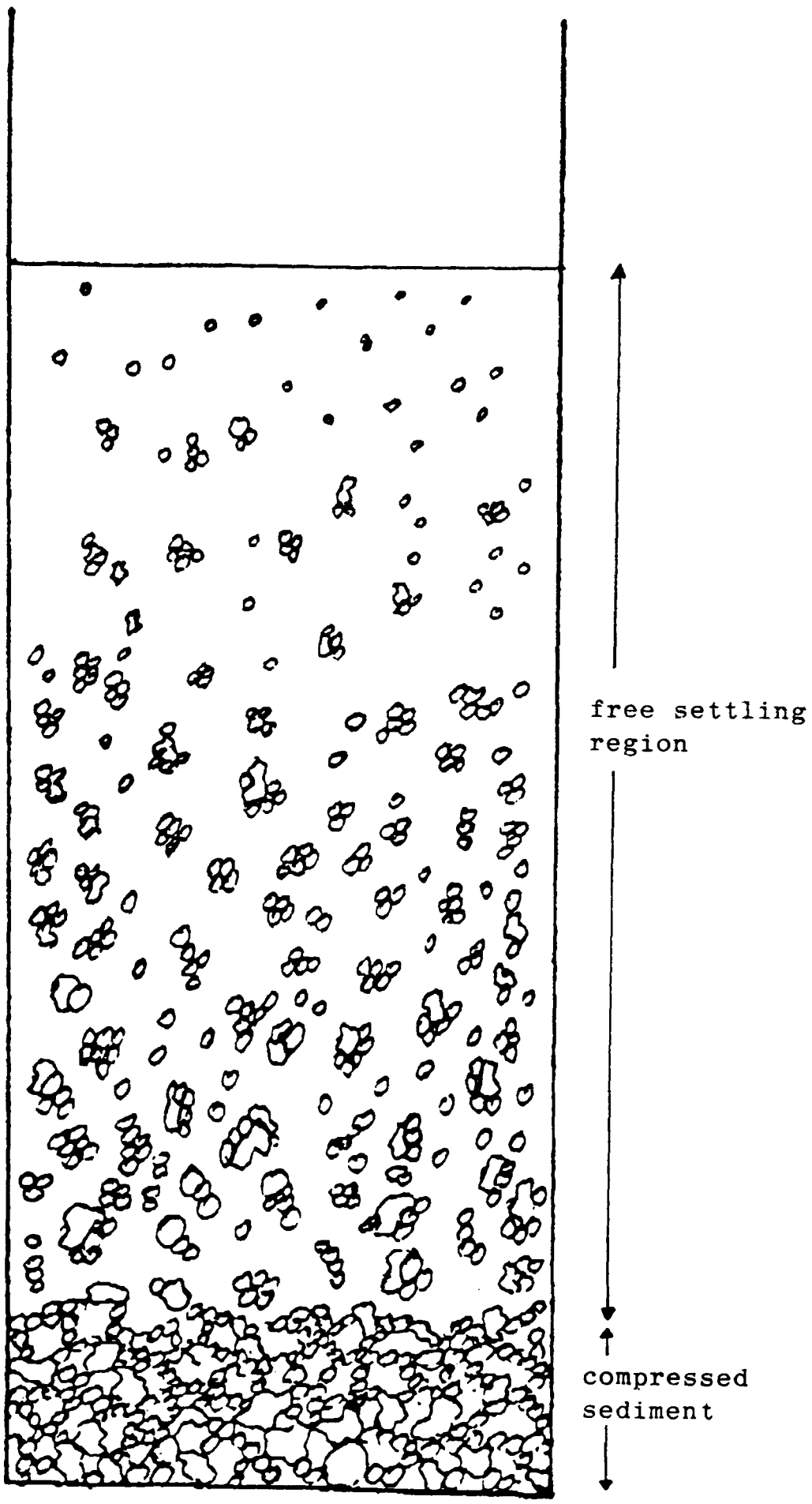

Figure 6.1 Region associated with flocculated suspensions.

The following multiphase numerical model has been developed to simulate the settling process associated with flocculated particulate mixtures. This model is an extension of the non flocculated model with the same assumptions, see Chapter four. One extra assumption is made that the density of the solids making up the flocs is constant.

6.2 Floc build up in free settling region

The build up and movement of flocs in the free settling region can be monitored by assigning a continuity and momentum equation to each floc phase. The free settling region will initially contain only primary particles and these will form flocs due to collisions and the attractive/bonding forces present, see figure 6.2.

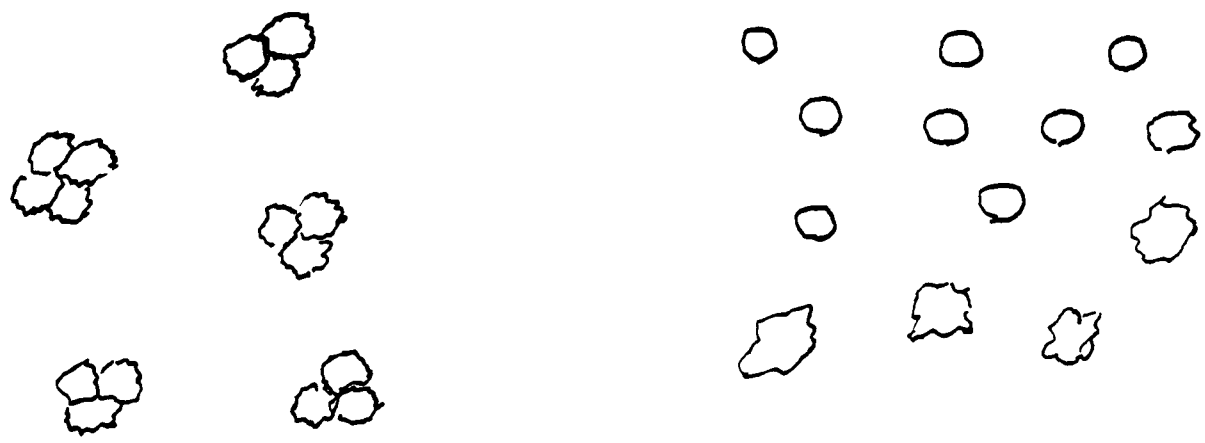

Figure 6.2 Solids present in free settling region.

Like each primary particulate phase the floc phases will be distinct via their size, density and shape. The density of a floc must take into account the enclosed fluid which is assumed to be stationary as well as the solids present in the floc. The build up of flocs can be incorpor-

ated into the model by making appropriate adjustments to the continuity equations. These adjustments are based on the following population balances.

6.2.1 Smoluchowski population balances

The flocculation of particles in a liquid depends upon the collisions between particles, caused by their relative motion. Smoluchowski (1917) developed population balances which have been used to model such phenomena. The relative motion can be due to Brownian movement or by external forces acting on the particles such as gravity. Two types of floccu- lation can occur, these are:

1) Perikinetic flocculation
2) Orthokinetic flocculation.

Perikinetic flocculation is due to the Brownian movement causing collisions. This form of flocculation becomes important for particles in the sub-micron range only, see Moir (1980). Orthokinetic floccu- lation is due to velocity gradient, caused by external forces. The following analysis is only concerned with orthokinetic flocculation due to gravity. Smoluchowski assumed that all particles and flocs are spheres and that all collisions resulted in the formation of flocs (i.e. rapid flocculation). Consider figure (6.3) where particles i and j are undergoing sedimentation. Ignoring the viscous effects encountered when particles move closer together, particles i and j will collide if the distance between their paths of motion x satisfies

$$x \leq \tfrac{1}{2} d_{ij} \tag{6.1}$$

where

$$d_{ij} = d_i + d_j \tag{6.2}$$

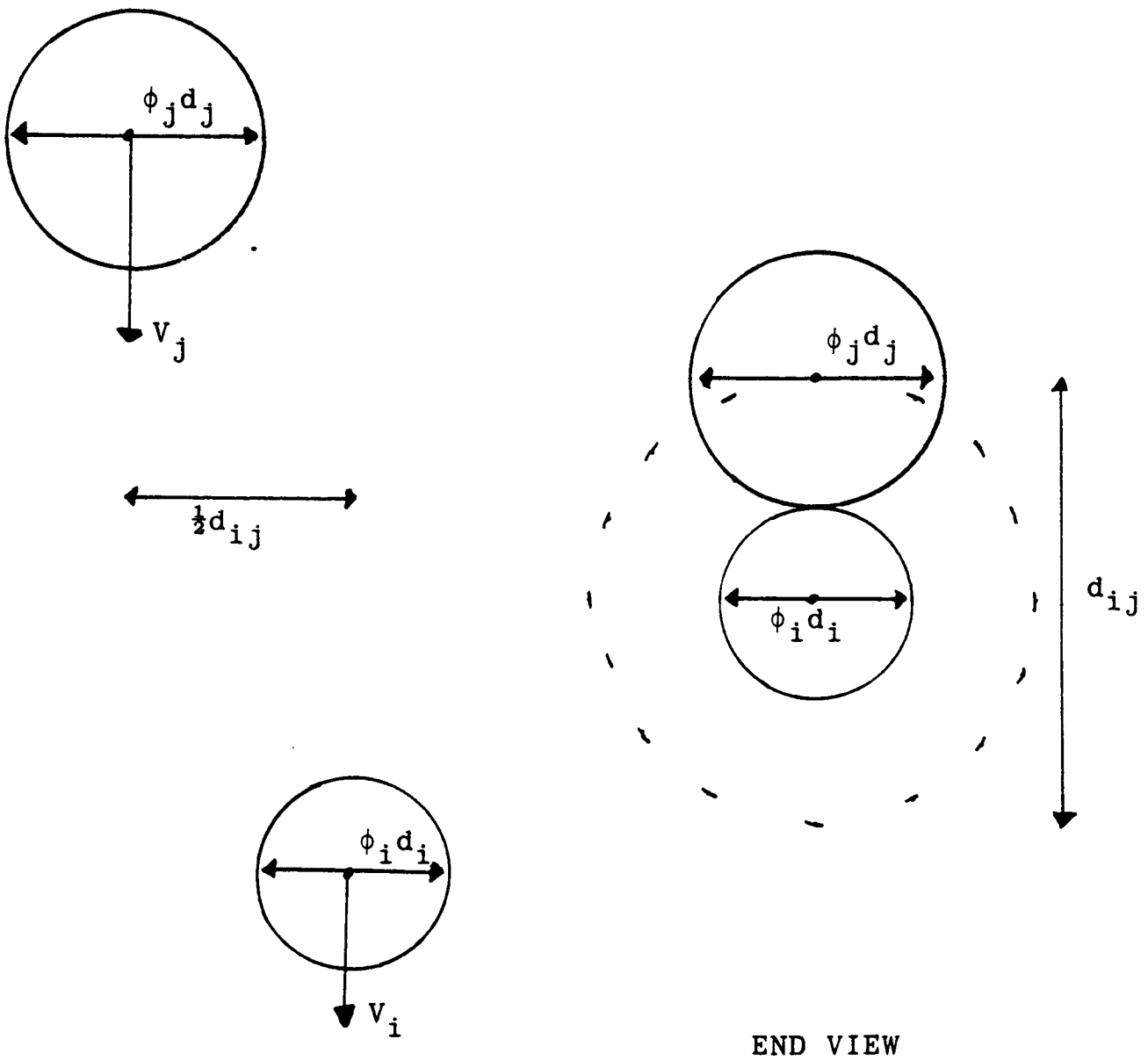

Figure 6.3 Smoluchowski Model

Consider the cylinder of diameter d_{ij} centered on particle i, the volumetric flow rate through this cylinder is given by

$$\frac{dz}{dt} = \frac{\pi}{4} d_{ij}^2 \bar{u} \tag{6.3}$$

where $\bar{u}$ is the relative velocity. If N is the number of particles per unit volume then the rate of collisions of j particles with the i-particle is

$$N_j \frac{dz}{dt} = N_j \frac{\pi}{4} d_{ij}^2 |u_j - u_j| \tag{6.4}$$

The total collision rate between phases i and j per unit volume is given by:

$$N_i N_j \frac{dz}{dt} = N_i N_j \frac{\pi}{4} d_{ij}^2 |u_j - u_i| \tag{6.5}$$

Smoluchowski assumed that when two particles collide they coalesce to form a spherical particle with volume equal to that of the colliding particles. Therefore if collisions between phases i and j result in phase k then equation (6.5) can be rewritten as:

$$\frac{dN_k}{dt} = N_i N_j \frac{\pi}{4} (d_i+d_j)^2 |u_j - u_i| \tag{6.6}$$

Equation (6.6) represent the rate of appearance of particles in phase k, due to collisions between phases i and j. The total rate of change for phase k due to appearance and disappearance, where phase k particles collide with any other particles, is given by:

$$\frac{dN_k}{dt} = \sum_{i+j=k} N_i N_j \beta_{ij} - N_k \sum_{i=1}^{\infty} N_i \beta_{i,k} \qquad k=1...\infty. \tag{6.7}$$

where β is the rate constant given by:

$$\beta_{ij} = \frac{\pi}{4} (d_i+d_j)^2 \, |u_j - u_i| \tag{6.8}$$

Equation (6.7) represents the basic Smoluchowski population balance for coalescence of particulates.

6.2.2 Incorporating floc build up via continuity and momentum equations

Assuming floc breakdown does not occur then the above Smoluchowski equations can be incorporated into the continuity equations as source terms to represent the mass transfer from primary particle phases to and between floc phases. During the sedimentation process primary particles cannot be created as it is assumed that floc breakage does not occur. Therefore only a disappearance term is present in the continuity equations of primary particle phases. Appearance and disappearance terms are present in the continuity equations for floc phases except the largest phase (i=1) which contains only an appearance term. The transfer of particles from one phase to another is modelled on a volumetric basis where:

$$N_i = \frac{6 \, S_i}{\pi(\Phi_i d_i)^3} \tag{6.9}$$

substituting equation (6.9) into equation (6.7) and adding the resulting equation to the continuity equation as a source term gives:

$$\frac{\partial S_k}{\partial t} + \frac{\partial (S_k\ u_k)}{\partial y} = \frac{3}{2}\ (\Phi_k d_k)^3 \sum_{i=NF}^{k+2} \sum_{j=i-1}^{k+1} \frac{S_i S_j}{(\Phi_i d_i)^3 (\Phi_i d_j)^3}\ C_{i,j,k}\ \ \beta_{ij}$$

$$- \frac{3}{2}\ S_k \sum_{i=NSOL}^{2} \frac{S_i}{(\Phi_i d_i)^3}\ \ \beta_{i,k} \qquad (6.10)$$

where

$$\beta_{ij} = \frac{\pi}{4}\ (\Phi_i d_i + \Phi_j d_j)^2\ |u_i - u_j| \gamma_{ij} \qquad (6.11)$$

NF is the number of floc phases present given by:

$$NF = NSOL - NP \qquad (6.12)$$

where NP is the number of primary particle phases and NSOL the total number of solids phases. The γ_{ij} terms represent the probability that if phases i and j collide they will form a floc. For rapid flocculation:

$$\gamma_{ij} = 1 \qquad (6.13)$$

γ_{ij} is dependent on the floc size and the nature of the flocculant/ coagulant being used. $C_{i,j,k}$ represents the fraction of a phase k floc formed between a collision of phase i and j particles (flocs). This is given by:

$$C_{i,j,k} = \frac{(\Phi_i d_i)^3 (1-E_F(d_i)) + (\Phi_j d_j)^3\ (1-E_F(d_j))}{(\Phi_k d_k)^3 (1-E_F(d_k))} \qquad (6.14)$$

where $E_F(d_i)$ is the voidage associated with a floc. Obviously for primary particles $E_F(d_i)$ is zero as these are discrete particles with no voidage associated with their structure. $C_{i,j,k}$ also predicts what collisions result in a given floc size via:

$$C_{i,j,k} = \text{equation (6.14)} \quad \text{if} \quad |C_{i,j,T} - 1| \text{ is minimum for } T = k \text{ where } T=j-1\ldots,1$$
$$= 0 \quad \text{if} \quad |C_{i,j,T} - 1| \text{ is minimum for } T \neq k. \qquad (6.15)$$

Notice the fraction $C_{i,j,k}$ is present only in the appearance term, as in the disappearance term a collision between a phase k particle (floc) and any other particle (floc) will result in the loss of that particle (floc).

Equation (6.10) is discretised in the usual manner, see Chapter four. The only differences are due to the added source terms, this gives different values for AP and b. The source term is linearised, see Patankar (1980), as follows:

$$SP = -\frac{3}{2} \sum_{i=NSOL}^{2} \frac{(S_i)_p}{(\Phi_i d_i)^3} \beta_{i,k} \qquad (6.16a)$$

$$SC = \frac{3}{2} (\Phi_k d_k)^3 \sum_{i=NF}^{k+2} \sum_{j=i-1}^{k+1} \frac{(S_i)_p (S_j)_p}{(\Phi_i d_i)^3 (\Phi_j d_j)^3} C_{i,j,k} \beta_{i,j}. \qquad (6.16b)$$

The discretised terms for the continuity equations is given by equations (4.13) with the following adjustment to AP and b

$$AP = AP^* - SP\Delta y \qquad (6.16c)$$

$$b = b^* + SC\Delta y \tag{6.16d}$$

where AP^* and b^* are given by equation (4.13c) and equation (4.13d) respectively.

Due to the mass transfer, above; momentum is also transferred between the phases. This effect is incorporated into the model by adding two additional terms to the R.H.S. of equation (4.2). This equation will now take the following form:

$$\frac{\partial}{\partial t}(S_k\rho_k U_k) + \frac{\partial}{\partial y}(S_k\rho_k U_k U_k) = \text{Normal Sources}$$

$$+ \frac{3}{2}\rho_k(\Phi_k d_k)^3 \sum_{i=NF}^{k+2} \sum_{j=i-1}^{k+1} \frac{S_i S_j}{(\Phi_i d_i)^3(\Phi_j d_j)^3} C_{i,j,k}\beta_{i,j}(U_i + U^j)$$

$$- \frac{3}{2}\rho_k S_k \sum_{i=NSOL}^{2} \frac{S_i}{(\Phi_i d_i)^3}\beta_{i,k}\, U_k \tag{6.17}$$

where the first term represents the gain in momentum (ie. for flocs) and the second represents the loss of momentum due to floc formation. This equation is discretised in the usual manner.

6.3 Compression in the sediment zone

When flocs and individual particulates pack the solids concentration is smaller than the solids concentration that would be given if the particulates in the flocs packed individually. This is because of the open tree-like structure of the flocs. When the flocs enter the sediment zone they lose their individual identity and the particulates

in the flocs settle further due to floc collapse. This process of floc collapse gives the appearance of a consolidating sediment. The build up and movement of the sediment zone is incorporated into the batch sedimentation model, see Chapter four, by making appropriate adjustments to the momentum equations and using the packing theory.

6.3.1 Incorporating compression via the momentum equations

The momentum equation for primary particles in the sediment zone is essentially the same as equation (4.2) except for the following;

1) The fluid particle interaction terms F_D is given by equation (4.3b).

2) In the free settling region particulates and flocs are in suspension and therefore contribute to the buoyancy force exerted on the solids. This is incorporated into the gravity term via a mixture density (ρ_m). When the particulates are fully settled the particulates do not contribute to the liquid pressure gradient and therefore the buoyancy in the gravity term is due to the fluid alone where ρ_f is used instead of ρ_m. It is assumed in this study that throughout the sediment region the buoyancy force exerted on the solids is dependent on the mixture density (ρ_m), although this is debatable, see Holdich (1983).

3) In the sediment region the inter-particle forces oppose the motion of the particulates. This is incorporated into the momentum equations by adding the following to the R.H.S. of equation (4.2).

$$\frac{\partial P_s}{\partial y} \qquad (6.18a)$$

where P_s is the internal pressure in the solid network. This is assumed to be directly related to the solids concentration, see Concha (1987); where

$$\begin{aligned} P_s &= Ae^{B(1-F)} \quad \text{for} \quad F \leqslant F_c \\ &= 0 \qquad\quad\ \ \text{for} \quad F \geqslant F_c \end{aligned} \tag{6.18b}$$

and F_c is the voidage associated with the compression point. A and B are constants that depend on the slurry being thickened and are estimated from consolidation tests.

The momentum equation including the solids pressure gradient, equation (6.18a), and momentum transfer effects due to floc formation, is integrated in the usual manner where solids pressures P_s are calculated using equation (6.18b) and stored at scalar nodes.

6.3.2 Incorporating Packing Theory

As the flocs in the free settling zone are treated as particulates then these will have values of $E(d_i)$. The packing theory, see section 4.4, can be used to estimate the concentrations at which the flocs and particulates come into contact which predicts the build up of the compression zone. Further densification using the hydraulic diameter, see section 4.4.2, would be very restricted due to the attractive forces present between particulates. It is assumed that movement of smaller particulates into the sediment structure using the hydraulic diameter does not occur for flocculated mixtures.

6.4 Solution Procedure

The general solution procedure is essentially the same as for non flocculated batch sedimentation with the following changes:

1) Solids concentrations and velocities for floc phases are only calculated in the free settling zone.

2) In the sediment zone the flocs are broken down into the primary particle phases.

3) Solids concentrations and velocities are calculated for primary particles in the sediment zone until a cell becomes fully packed. This is predicted using the packing model with the primary particles.

When a cell becomes packed with flocs and particulates then the solids in this cell are in the sediment region which is compressible. As flocs in the sediment lose their individual identity the solid particulates making up the flocs must be incorporated back into the primary particle phases. Consider a floc phase k, the mass of solids associated with this phase in a cell is given by

$$M_{MASS} = S_k(\rho_k - E_F(\rho_f)\Delta y \qquad (6.19)$$

Summing equation (6.19) over the whole domain gives the total solids mass associated with floc phase k, (i.e. F_{MASS}). Also consider a primary particle phase i the mass of this phase lost due to flocculation is given by:

$$P_{MASS} = \sum_{j=1}^{NY} ((S_i)_j^* - (S_i)_j)\rho_i \Delta y_j \qquad (6.20)$$

where $(S_i)^*$ is the initial concentration of primary phase i. This phase is not incorporated in floc phase k if:

$$C_{i,j,k} = 0 \quad \text{for all} \quad j=i-1\ldots,k+1. \tag{6.21}$$

The equation (6.21) is not valid then when floc phase k is broken down in the sediment some of its solids mass must be incorporated into primary particle phase i. Therefore for a packed cell the amount of solids mass given to primary particle phase i is:

$$I_{MASS} = M_{MASS} \cdot \frac{P_{MASS}}{F_{MASS}} \tag{6.22}$$

The new solid concentrations for phase i are thus calculated via:

$$S_i = S_i + \frac{IMASS}{\rho_i \Delta y} \tag{6.23}$$

Using the above procedure the flocs can be distributed proportionately between the primary particle phases in the sediment.

6.5 Comparisons with Holdich data

Concentration profiles have been obtained by Holdich, see Holdich (1983), for calcium carbonate undergoing settlement in water. Although originally thought to be incompressible this material was found to possess self flocculating characteristics which lead to a compression point at 0·31 solids volume fraction and, therefore, a compressible sediment.

The density of calcium carbonate was calculated using a density bottle to be 2643 Kg/M^3. Using an Andreason pipette Holdich estimated that 88% of particles had a settling diameter, based on Stokes law, in the range 25-35μ. The Andreason pipette has many sources of errors and Holdich

did not state if a dispersent was used in these measurements. The following comparisons have been made between the above model and the Holdich data starting initially with two primary particle phases and one floc phase each with diameters and initial concentrations given below:

Phase	Diameter (μ)	0·1	0·15	0·2	0·25
one	35	0	0	0	0
two	25	0·05	0·075	0·1	0·125
three	20	0·05	0·075	0·1	0·125

Table 6.1 Concentrations and diameters for floc model comparisons

The two primary phases (phases two and three) initially have the total volume of particles split between them. Using the size distribution given by Holdich, comparisons were made between the non-flocculted model and the data. For all cases the model overpredicted the rate of settlement by a large degree. This was thought to be due to errors in using the Andreason pipette. Therefore the above diameters for phases two and three were taken to represent the upper and lower quartiles respectively. The densities and voidages associated with each phase are:-

Phase	Density	$E(d_i)$	$E_F(d_i)$
one	2134	0·38	0·31
two	2643	0·52	0·0
three	2643	0·52	0·0

Table 6.2 Densities and voidages associated with solid phases

where the density of the floc phase (phase one) is given by:

$$\rho_{FLOC} = (1-E_F(d_i))\rho_s + E_F(d_i)\rho_f \qquad (6.24)$$

where ρ_{FLOC} is the floc density and ρ_s is the general solids density. The maximum packing concentration was 0·48. To ensure that the primary particles packed to this value their voidages, when packed alone $E(d_i)$, are set to 0·52. It is assumed that the floc particles, including solids and enclosed water, would pack to a floc concentration of 0·62. Therefore associating a floc voidage, $E_F(d_i)$, of 0·31 would predict a solids concentration corresponding to the compression point of 0·31 as observed by Holdich.

Comparisons have been made for the non-flocculated and flocculated models with the Holdich data at 90%, 85%, 80% and 75% porosities, see figures 6.4-6.7. It is assumed that rapid flocculation occurs between the two primary phases and that the variables relating the internal pressure in the compressible solids network, see equation 6.18, are given by:

$$A = 5\ N/M^2$$
$$B = 10 \qquad (6.25)$$

From the comparisons it can be seen that in all cases the flocculated model gives closer predictions than the non-flocculated model. In all cases phase two completely disappeared in the free settling zone due to collisions with phase three which formed flocs (i.e. phase one). This occurred early in the predictions and the rest of the simulations consisted of modelling phases one and three in the free settling zone and phases two and three in the compression zone. The packing model predicts a cell becoming fully packed with flocs and primary phase three at a solids concentration of 0·34 for all comparisons. This corresponds

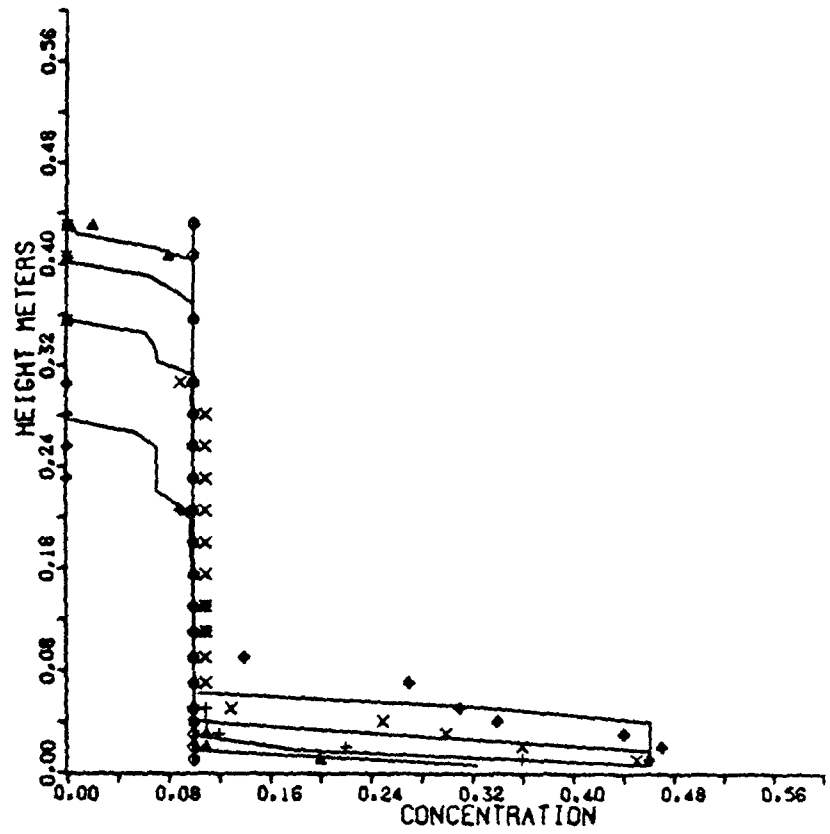

a) Non-flocculated model

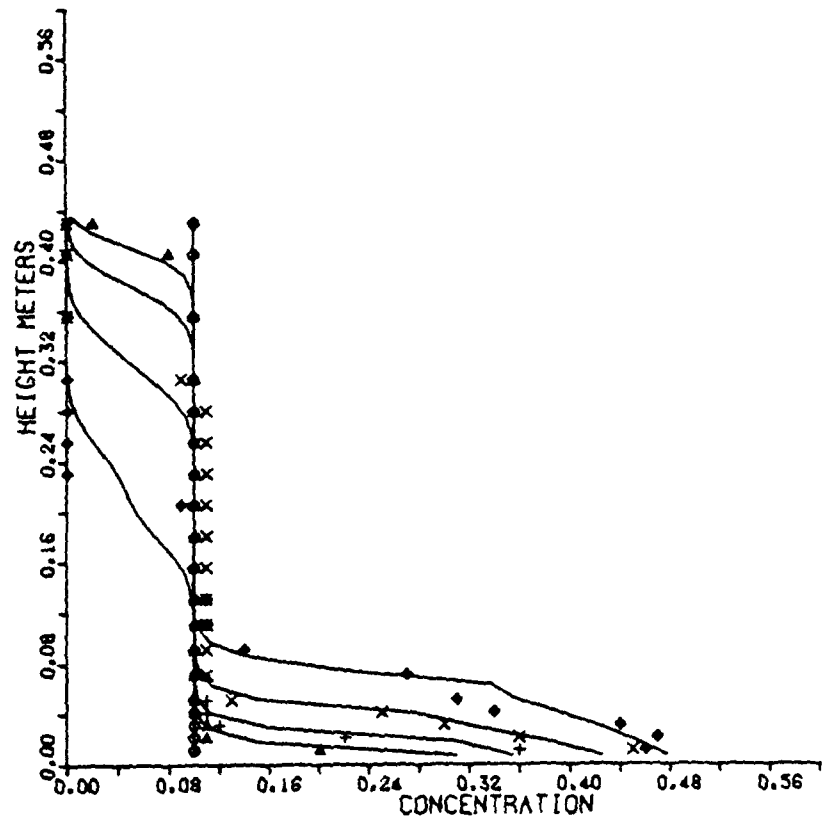

b) Flocculated model

Experimental data

o initial concentrations
▲ 2 mins
\+ 4 mins
x 8 mins
◆ 15 mins

Figure 6.4 Comparisons with Holdich data at 90% porosity.

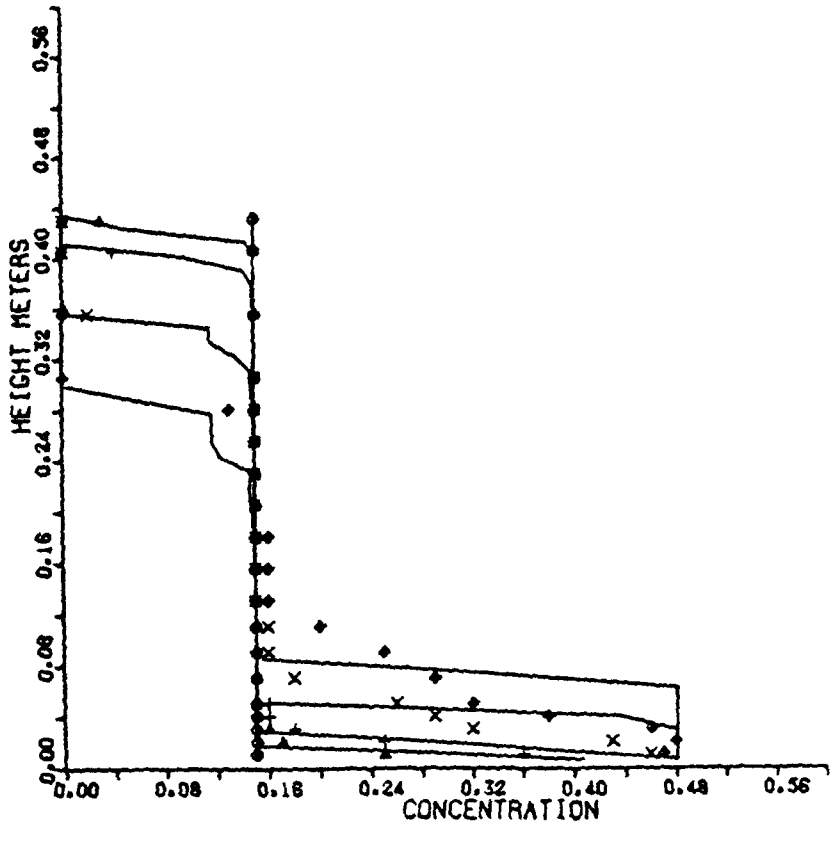

a) Non-flocculated model

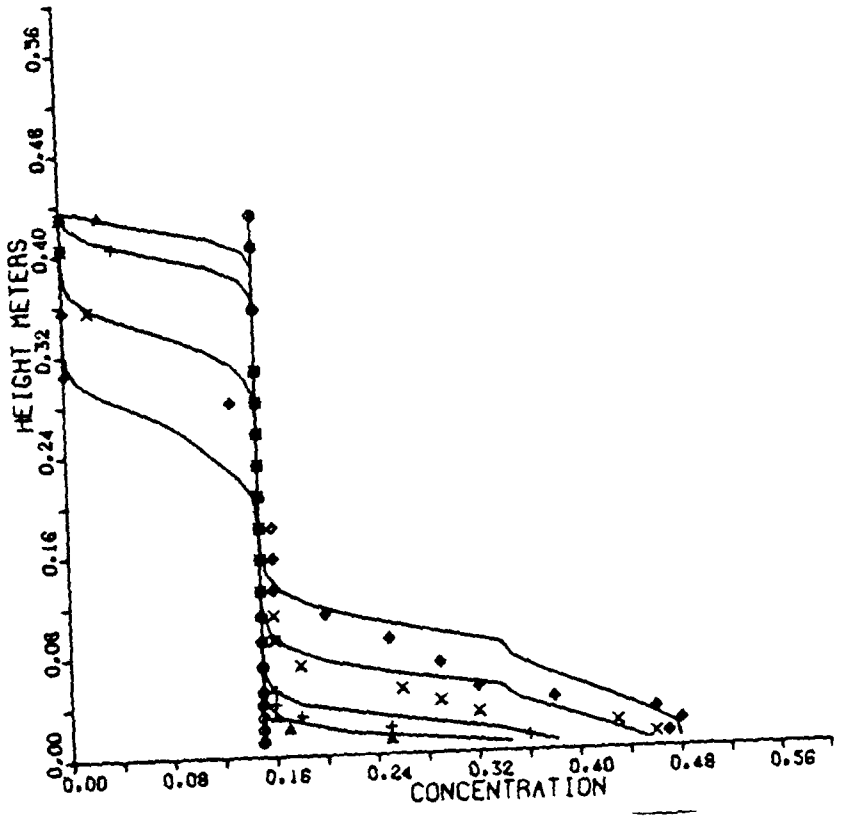

b) Flocculated model

Experimental data

- o initial concentrations
- ▲ 2 mins
- \+ 4 mins
- x 10 mins
- ♦ 17 mins

Figure 6.5 Comparisons with Holdich data at 85% porosity.

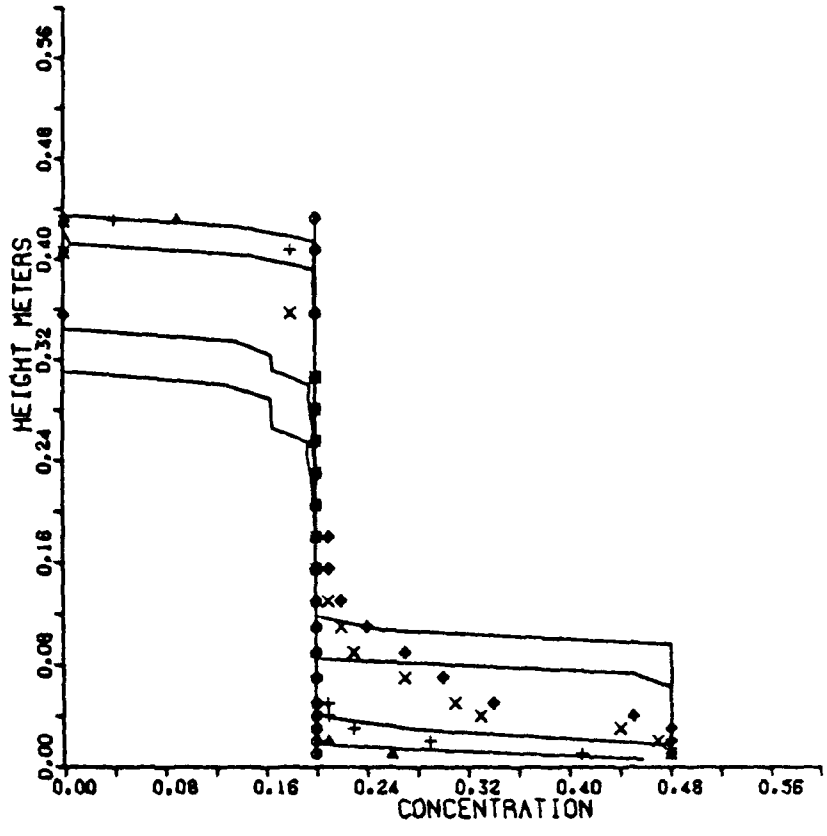

a) Non-flocculated model

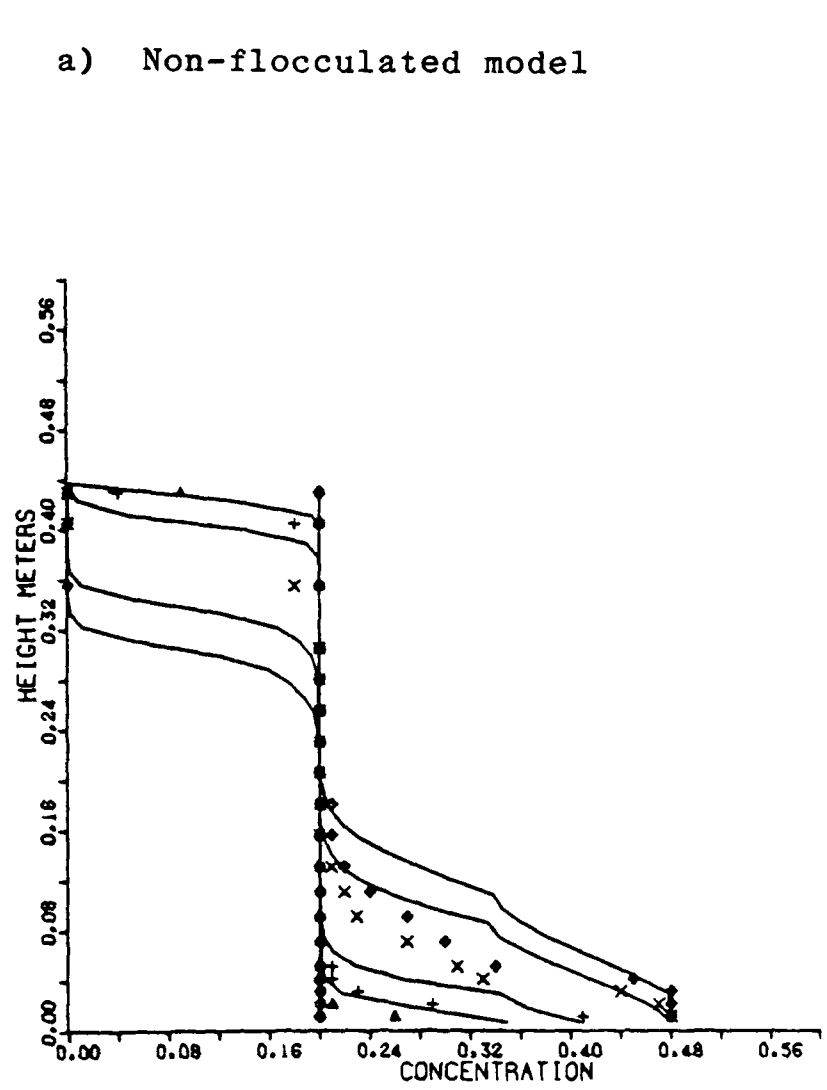

b) Flocculated model

Experimental data

- o Initial concentrations
- ▲ 2 mins
- \+ 5 mins
- x 15 mins
- ◆ 20 mins

Figure 6.6 Comparisons with Holdich data at 80% porosity.

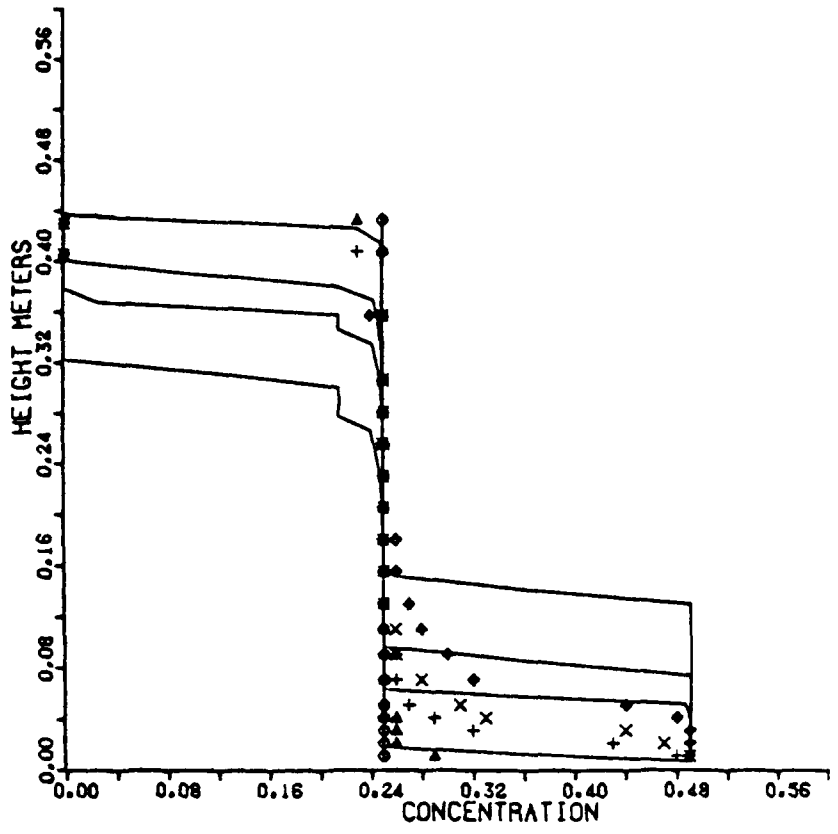

a) Non-flocculated model

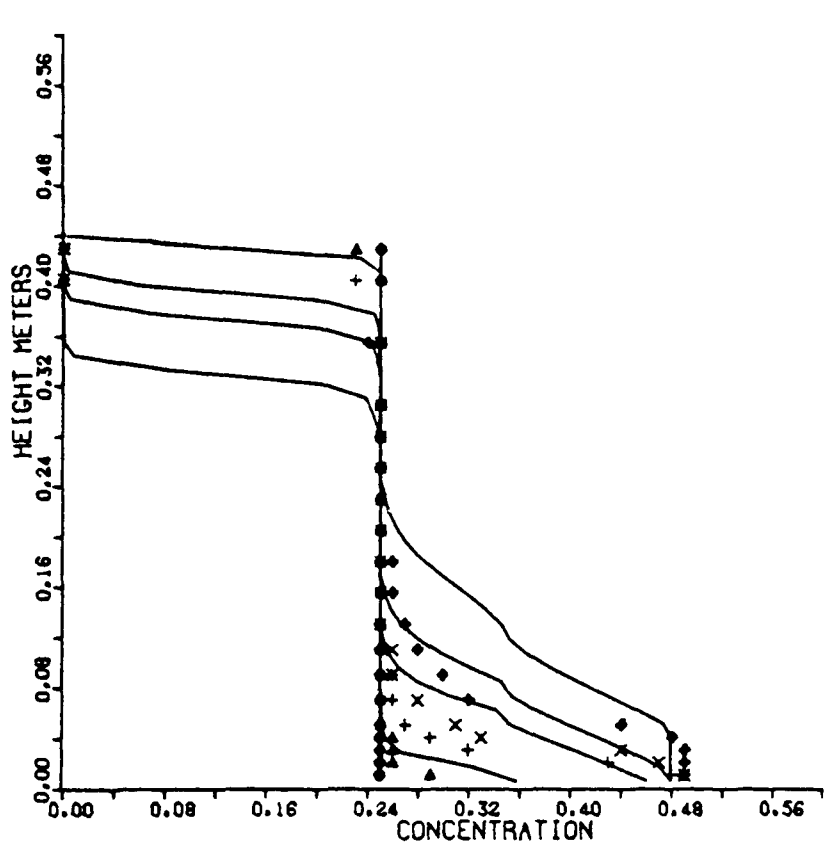

b) Flocculated model

Experimental data

o initial concentrations
▲ 2 mins
\+ 10 mins
x 15 mins
◆ 25 mins

Figure 6.7 Comparisons with Holdich data at 75% porosity.

to the predicted compression point, which is different from the value observed by Holdich due to the presence of primary particles (phase three) as well as flocs in the cell being packed. Because values for A and B in equation (6.18) could not be obtained the guessed values above were used. These values were chosen from a number of different values and are similar in magnitude to the values given by Concha (1987) for flocculated copper tailings. As can be seen reasonable comparisons between model and experimental data are obtained. Although the model predicts the concentration profiles at 90% porosity very well it tends to overpredict velocities as the initial porosity gets smaller. This is probably due to:

1) Errors in experimental data.
2) The empirical correlations used for particle-fluid interaction and the internal pressure being in error.
3) Using a floc size of 35μ as well as assuming rapid flocculation to take place.

CHAPTER SEVEN

CONCLUSIONS

7.1 Experimentation

Experimental work has been undertaken, during the course of this research, to obtain data which could be used to verify the models developed for non-flocculated batch sedimentation and continuous thickening. Previous work on multiphase settling, in batch sedimentation, has consisted of monitoring, visually, the rate of fall of each species present in the system. The use of pressure transducers to measure the density changes during settlement of the particulates represents the sedimentation process in much greater detail. Of the eight pressure transducers available only two could be used down to an accuracy of 0·005 mV on the two pen plotter. Also one of these two transducers became defective at an early date. By lowering the input voltage of 5V, the other six transducers could also be monitored at this degee of accuracy but the deflections obtained on the plotter would be much smaller. This would essentially defeat the objective of obtaining as much accuracy as possible. Clearly the use of at least one transducer is sufficient to monitor density changes above a certain height during sedimentation. Using the appropriate transducers a number of one, two and three phase experiments were carried out using solids and liquids with wide ranging density, sizes and viscosities respectively. As observed by other authors the sedimentation process consists of the formation and settlement of distinct zones. The number of zones present depends on the number of phases in the suspension. This phenomena can clearly be seen on the density/time plots where the change in gradient represents the boundary between two zones passing the location of the transducer. Future experiments of this nature should use a data logger, if available, as this would eliminate errors associated with examining graphical output. Although there are elements of error associated with the above procedure it offers more indepth information on sedimentation than previously obtained.

For continuous thickening, data has been obtained in the form of concentration profiles throughout the thickener. Because of the size of an industrial thickener direct sampling can be undertaken, as disturbance of the operation when obtaining samples will be negligible. It can be seen that each thickener is used well below its critical capacity. No flocculants were added to any of these thickeners, but this does not mean flocculation will not occur as self flocculating characteristics may be present especially with vey small particles. The concentrations throughout the fluorite thickener are constant with an increase near the underflow. The appearance of solids in the overflow and the difference in particle sizes, especially near the underflow, represent the multiphase effects associated with the operation of a thickener. The Galena thickener poses a very interesting problem as in this case quantities of other materials are observed. This extends the problem as we now have different densities as well as sizes associated with the solid materials. The concentration profile throughout this thickener is essentially constant with a decrease at the overflow and a increase at the underflow. Further representing the multiphase effects are the average particle sizes measured at the sample locations. The smaller particles being at the overflow and the larger ones at the underflow. For the Barytes thickener no concentration profiles could be obtained but the multiphase effect can still be observed by noting the presence of solid material in the overflow.

7.2 Mathematical Modelling

A mathematical model has been developed to simulate the flow of non-flocculated particles in a host fluid, see Chapter four. This model was extended to predict thickener performance as well as model flocculation in batch sedimentation, see Chapters five and six. These three modes of the model are available in Fortran 77 code which was

implemented on Norsk Data machines.

For non-flocculted batch sedimentation the model was compared with experimental data consisting of concentration profiles and density profiles. In both cases the results are encouraging and for the comparisons with the data consisting of density profiles the proposed model gave closer comparisons than did a model developed by Selim (1983). This is primarily due to a greater representation of the forces present in the system and the use of the Barnea correlation for the hindered settling function in the proposed model. Also unique with the proposed model is its ability to predict the build up of the sediment region using a modified version of packing theory.

The performance of an industrial thickener for non flocculated material can be predicted using an extension of the non-flocculated batch sedimentation model. The main difference between the two models being the influence of the streams associated with each thickener as well as the two dimensional domain of a thickener. Although some horizontal movement will be present in the thickener it is assumed that this will be negligible and therefore the one dimensional assumption is valid. The actual domain of the thickener is incorporated into the discretised equations using the surface areas of the control volume interfaces. The model has been validated against data obtained on three industrial thickeners. The comparisons are encouraging, especially for the Galena thickener, and the use of multiphase techniques is clearly emphasised.

Modelling the settlement and compaction of flocculated suspensions has gained considerable importance during the last decade. This is due to the increasing use of flocculants in solid/liquid separations. The non-flocculated batch sedimentation model has been extended to simulate

the build up of flocs in the free settling region and the compaction of these flocs in the sediment region. Even though some variables relevant to the model were not available in the experimental data; comparisons between the model and this experimental data using valid values for the unknown variables was encouraging. The use of multiphasee techniques is once again clearly valid in modelling the settlement of flocculated suspensions.

This research has shown experimentally and mathematically that the use of multiphase techniques in modelling sedimentation and thickening is essential in obtaining satisfactory predictions. With regards to non-flocculated batch sedimentation future work would involve obtaining better terms for the hindered settling function and the solid-solid interaction value. This is also the case for the flocculated mode of the model where the dependence of solids pressure on solids concentration may need to be validated further. Also more detailed experimental data is needed to validate the flocculated model further. This data must contain values for the variables associated with the solids pressure term as well as the packing theory. Also if rapid flocculation is not present then the probability of floc formation is required. At present the model for thickener performance is a valid tool with regards to process control on non-flocculated pulps. An extension to this model would be to incorporate flocculation as outlined in Chapter six into its framework. Also an extension to two dimensions would enable greater precision to be made, especially around the feed entrance.

Overall it is clear that much work is still needed; but it is hoped that the work outlined in this thesis will enable future research to follow the same reasoning and thus lead to a greater understanding of thickening and sedimentation.

APPENDIX

The following footnote will further explain why pressure in the solid momentum equation is essentially given by the buouancy term which is dependent on the mixture density.

As the flow within the particulate systems under investigation was assumed to be one dimension then the need to solve for pressure is eliminated as this is dependent on the local suspension density (ie. hydrostatic pressure) and is incorporated into the momentum equation via the buoyancy term. This obviously simplifies the solution procedure considrably as we need only solve for solids concentration and velocity as well as the fluid concentration and velocity.

The numerical performance of the model predictions in chapter four is encouraging. The number of cells used in modelling this system was thirty for all experiments except one phase "exp-seven", two-phase "exp-one" and "exp-seven" as well as three phase "exp-five" which used twenty cells. The time step used for all comparisons was one second and the model ran fairly fast for all comparisons (ie. less than 3 minutes) except for two-phase "exp-eight" which required 8 mins cpu time due to the large size differences between the two phases. Although uniform grids were used the ability to use non-uniform grids is present in the codes.

NOMENCLATURE

AN, AP, AS	Contributions from nodal positions N,P and S.
b	Source term
$C(d_i)$	Co-ordination number
C_D	Fluid-Solid drag coefficient
$C_{i,j,k}$	Fraction of floc phase (k) formed between phases (i) and (j)
d_i	Diameter of solid phase (i) particle
d_{ij}	Combined diameter of phase (i) and (j) particles
D_H	Hydraulic diameter
$\bar{d}$	Average particle diameter
$E(d_i)$	Voidage of a packing consisting of phase (i) particles only
E_M	Voidage of a notional shell
C_{ij}	Coefficient of restitution
$E_F(d_i)$	Floc voidage
$F_{N,P,S}$	Fluid volumetric concentrations at nodes N,P and S
F	Fluid volumetric concentration
$F_{F,U,O}$	Volumetric fluid concentrations of feed, underflow and overflow
F_D	Fluid-solid friction factor
$f(d_i)$	Number fraction of solid phase (i)
g	Gravity constant
h	Height of slurry above a transducer
H	Hindered settling correlation
IYPAK	Cell being packed with solid particulates
IPHASE	Solid phase under investigation
K_{ij}	Interaction coefficient between solid phases (i) and (j)
$\dot{M}$	Mass flow rate of solid phase (i) into the feed cell
M_i	Mass of solid phase (i) in system
N	Total number of particulates

$\dot{N}$	Mass flow rate of fluid phase into feed cell
NSOL	Total number of solid phases present
$\bar{n}$	Number of hypothetical shells
n	North face of a cell
NF	Number of floc phases present
NP	Number of primary (non-floc) phases present
P	Hydrostatic pressure
P_s	Solids pressure
Q	Surface area
R_e	Reynolds number
RESID	Residual
S_i	Solids volumetric concentration for phase (i)
S^{OLD}	Solids volumetric concentration at previous time step
S_{INT}	Solids volumetric concentration at an interface
SC, SP	Constant and coefficient, respectively, in the linearised source term
S	South face of a cell
$S_{N,P,S}$	Solids concentration at nodal points N, P and S
S_F	Solids concentration in feed for phase (i)
TIME	Total time passed
TSTEP	Time step
TMASS	Total mass of solids present in the system
TOL	Tolerance
t	Time
$T_{,F,U,O}$	Volumetric flow rates of feed, underflow and overflow
U_i	Solid phase (i) velocity
$U_{N,P,S}$	Solid phase velocity at nodal points N, P and S
V	Fluid phase velocity
V_F	Volume of fluid in system

V_M	Volume of slurry present
V_{INT}	Initial voltage
V_{FIN}	Final voltage
V_T	Total volume of a particulate packing
$V_M(d_i)$	Volume of a notional shell
$V_S(d_i)$	Volume of solids of size d_i
$V_C(d_i)$	Space allocated to a particle of size d_i
$V_{N,P,S}$	Fluid velocity at nodal points N,P and S
$\dot{V}$	Volumetric flow rate
y	Vertical distance

GREEK

α	Contribution of variable stored at nodal point P
α_{ij}	Coefficient of restitution between phases (i) and (j)
β	Contribution of variable stored at nodal point S
β_{ij}	Collision rate constant between phases (i) and (j)
Δy	Increment of distance
Δt	Increment of time
γ_{ij}	Probability of flocs forming between phases (i) and (j)
μ_f	Laminar viscosity of the fluid phase
π	pi: (eg.3·141593)
ρ_i	Density of solid phase i
ρ_B	Bulk mixture density above a transducer
ρ_s	Solid density
ρ_f	Fluid density
ρ_m	Mixture density for model
ρ_h	Slurry density above a transducer
Φ	Volumetric shape factor
$\Phi_{N,P,S}$	Dependent variable at nodal points N,P nd S
Φ^*	Value of dependent variable at previous iteration

Mathematical symbols

$[a,b]$ Maximum of a or b

REFERENCES

AKERS R J (1974)

"Sedimentation techniques - a review", Inst Chem Eng, Symposium series No.41, H1-H14.

ADORJAN L A (1975)

"A theory of sediment compression", Proc XIth Int Min Proc Congr, Cagliari, Paper 11.

BARNEA E, MIZRAHI J, (1973)

"A Generalised approach to the fluid dynamics of particulate systems", Chem Eng J, Vol 5, pp.171-184.

BHATT J I (1986)

"Cluster formation during sedimentation of dilute suspensions", Separation Sci and Tech, Vol 21, No 9, pp.953-967.

BIRD R B, STEWART W E, LIGHTFOOT E N (1960)

"Transport Phenomena" : Published by Wiley International.

CHANDLER J L (1983)

"Dewatering by Deep Thickeners without Rakes", Filtration and Separation, March/April.

CHAKRAVARTI A, DELL C C (1968)

"The behaviour of highly flocculated suspensions in batch tests", Powder Tech, Vol 3, pp.287-295.

COE H S, CLEVENGER G H (1916)

"Methods for determining the capacities of slime settling tanks", Trans A.I.M.E., Vol 60, pp.356-384.

CONCHA F, BUSTOS M C (1987)

"A modification of the Kynch Theory of sedimentation", A.I.Ch.E.J, Vol 33, No.2, pp.312-315.

CROSS M et al (1985)

"Optimal design methodology for Composite Materials with Particulate Filters", Powder Tech, Vol 3, pp.27-36.

DAVIES R (1968)

"The Experimental Study of Differential Settling of Particles in Suspension at High Concentrations", Powder Tech, Vol 2, pp.43-51.

DAVIES R, ACRIVOS A (1985)

"Sedimentation of Noncolloidal Particles at Low Reynolds Numbers", Am Rev Fluid Mech, Vol 17, pp.91-118.

DELL C C, KELEGHAN W T (1973)

"The Dewatering of polyclay Suspensions", Powder Tech, Vol 7, pp.189.

DICK R I, EWING B B (1967)

"Evaluation of Activated Sludge Thickening Theories", J.San.Engng.Dev, Proc ASCE, No 95, pp.9-29.

DICK R I (1972)

"Gravity Thickening of Sewage Sludge", Water Pollution Control, Vol 71, No 4.

DIXON D C (1977)

"Momentum-Balance Aspects of Free-Settling Theory", Sep.Sci, Vol 12, No 2, pp.171-203.

DIXON D C (1978)

"Momentum-Balance Aspects of Free-Settling Theory, 3-Transient Compression Resistance", Sep.Sci, Vol 13, No 9, pp.753-766.

FITCH B (1975)

"Current Theory and Thickener Design - Compression Theory", Filtration and Separation, Vol 12, pp.480-489.

FITCH B (1983)

"Kynch Theory and Compression Zones", A.I.Ch.E, Vol 29, No 6, pp.940-947.

GARSIDE J, AL-DIBOUNI M R (1977)

"Velocity-Voidage Relationships for Fluidization and Sedimentation in Solid-Liquid Systems", Ind.Eng.Chem, Proc.Des.Dev, Vol 16, No 2, pp.206-214.

GAUDIN A M, FUERSTENAU M C (1962)

"Experimental and Mathematical Model of Thickening", Trans A.I.M.E., Vol 223, No 2, pp.122-129.

GIDASPOW D (1987)

"Hydrodynamics of Fluidization and Heat Transfer : Super Computer Modelling", Appl Mech Rev, Vol 39, No 1, pp.1-23.

GRAY W A (1968)

"Packing of Solid Particles", Published by Chapman and Hall Ltd.

HASSET N N (1969)

"Thickening in Theory and Practice", Min.Sci.Engng, Vol 1, No 1, pp.24-40.

HOLDICH R (1983)

"A Study of the Formatiion of Compressible Compacts in Filtration and Thickening Processes", PhD Thesis, University of Exeter.

KITCHENER J A (1977)

"Flocculation in Mineral Processing", NATO Advance Study Inst Series E27, Scientific Basis of Flocculation, Vol 2, pp.283-328.

KOS P (1974)

"Gravity Thickening of Water-Treatment Plant Sludges", In 94th Annual Conference, A.W.W.A., Boston.

KOS P (1977)

"Continuous Gravity Thickening of Sludges", Prog.Wat.Tech, Vol 9, pp.291-309.

KYNCH C J

"A Theory of Sedimentatiion", Trans Faraday Soc, Vol 48, pp.166-176.

LOCKETT M J, AL-HABBOBY (1973)

Differential Settling by Size of Two Particle Species in a Liquid", Trans Instn Chem Engnrs, Vol 51, pp.281-292.

LOCKETT M J, AL-HABBOBY (1974)

"Relative Particle Velocities in Two-Species Settling", Powder Tech, Vol 10, pp.67-71.

MARKATOS N C, SPALDING D B (1983)

"Computer Simulation of Fluid Flow and Heat/Mass Transfer Phenomena - The Phoenics Code System". School of Mathematics, Statistics and Computing, Thames Polytechnic, London.

MASLIYAH J H (1979)

"Hindered Settling in a Multi-Species Particle System", Chem.Eng.Sci, Vol 34, pp.1166-1168.

MICHAELS A S, BOLGER J C

"Settling Rates and Sediment Volumes of Flocculated Kaolin Suspensions", Ind Eng Chem Fund, Vol 1, nO 1, PP.24-33.

MIRZA S, RICHARDSON J F

"Sedimentation of Suspensions of Particles of Two or More Sizes", Chem Eng Sci, Vol 34, pp.447-454.

NAKAMURA K, CAPES C E (1976)

"Verticle Pneumatic Conveying of Binary Mixtures", Fluidization Technology, Ed.D L Keairns, Hemisphere.

OUCHIYAMA N, TANAKA T (1980)

"Estimation of the Average Number of Contacts Between Randomly Mixed Solid Particles", Ind Eng Chem Fund, Vol 19, pp.338.

OUCHIYAMA N, TANAKA T (1981)

"Porosity of a Mass of Solid Particles Having a Range of Sizes", Ind Eng Chem Fund, Vol 20, pp.66.

OUCHIYAMA N, TANAKA T (1984)

"Porosity Estimation for Random Packings of Spherical Particles", Ind Eng Chem Fund, Vol 23, pp.490.

OUCHIYAMA N, TANAKA T (1986)

"Porosity Estimation from Particle Size Distribution", Ind Eng Chem Fund, Vol 25, pp.125-129.

PATANKAR S V (1980)

"Numerical Fluid Flow and Heat Transfer", Pub Hemisphere.

PEARSE M J (1977)

"Gravity Thickening Theories : A Review", W.S.L. Report, No LR261(MP).

RICHARDSON J F, ZAKI W N (1954)

"Sedimentation and Fluidization : Part 1", Trans Inst Chem Engrs, Vol 32, pp.35-53.

SCOTT K J (1968)

"Thickening of Calcium Carbonate Slurries", Ind Eng Chem Fund, Vol 7, No 3, pp.484-490.

SCHUMANN R (1940)

Sc.D Thesis, Department of Metallurgy, M.I.T.

SELIM M S et al (1983)

"Sedimentation of Multisized Particle in Concentrated Suspensions", A.I.Ch.E J, Vol 29, No 6, pp.1029-1038.

SHIRATO M et al (1970)

"Analysis of Settling of Thick Slurries Due to Consolidation", J Chem Eng of Japan, Vol 3, No 1, pp.90.

SIMPSON D (1988)

"Mathematial modelling and analysis of uncertainty of networks of minimal processing operations", PhD Thesis, School of Mathematics, Statistics and Computing, Thames Polytechnic, London.

SMOLUCHOWSKI von M (1917)

"Drei Vorträge uber Diffusion. Brownische Molecularbewegung und Koagulation von Kolloidteilchen", Z.Physik.Chem 92, pp.129.

STOKES G G (1845)

"On the Theories of Internal Friction in Motion, and the Equilibrium and Motion of Elastic Solids", Trans, Cambridge Phil Soc, Vol 8 pp.287.

TALMAGE W P, FITCH E B (1955)

"Determining Thickener Unit Areas", Ind Eng Chem, Vol 47, No 1, pp.38-41.

TARRER A R et al (1974)

"A Model for Continuous Thickening", Ind Eng Chem, Process Des Develop, Vol 13, No 4, pp.341-346.

TAY JOO-HWA A, HEINKE G (1983)

"Velocity and Suspended Solids Distribution in Settling Tanks", J W.P.C.F, Vol 55, No 3, pp.261-269.

TILLER F (1981)

"Revision of Kynch Sedimentation Theory", A.E.Ch.E, Vol 27, No 5, pp.823-829.

TURNER J, GLASSER D (1976)

"Continuous Thickening in a Pilot Plant", Ind Eng Chem Fund, Vol 15, No 1, pp.23-30.

WILLS B A (1981)

"Mineral Processing Technology", Pergamon, Oxford, 2nd edn.

YOSHIOKA N, et al (1957)

"Continuous Thickening of Homogeneous Flocculated Slurries", Soc Chem Engng, Japan, Vol 2, No 2, pp.47-54.